

Computational fluid dynamics modelling of fluid flow inside fractured reservoirs.

AL-MASHHADANIE, H.A.J.

2021

The author of this thesis retains the right to be identified as such on any occasion in which content from this thesis is referenced or re-used. The licence under which this thesis is distributed applies to the text and any original images only – re-use of any third-party content must still be cleared with the original copyright holder.

**Computational Fluid Dynamics
modelling of Fluid flow inside
Fractured Reservoirs**

Haider Abdulkareem Jasim Al-Mashhadanie

PhD 2021

Computational Fluid Dynamics modelling of Fluid flow inside Fractured Reservoirs

Haider Abdulkareem Jasim Al-Mashhadanie

A thesis submitted in partial fulfilment of the
requirements of the
Robert Gordon University
for the degree of Doctor of Philosophy
(School of Engineering)

September 2021



Computational Fluid Dynamics modelling of Fluid flow inside Fractured Reservoirs

Haider Abdulkareem Jasim Al-Mashhadanie

Supervisory Team:

Principal Supervisor

Dr Sheikh Islam

Second Supervisors

Dr Mamdud Hossain

Dr Mohamed Ghazi Droubi

Dr Gbenga Oluyemi

School of Engineering, Robert Gordon University,
The Sir Ian Wood Building, Riverside East,
Garthdee Road, AB10 7GJ,
Aberdeen, United Kingdom

Dedication

I would like to dedicate my phd thesis to Almighty God "Allah" for his guidance, grace, divine strength, knowledge, for being supreme provider of my needs and his mercy towards me ever since, and through the course, to achieve this project.

Thank you, "Allah", for all this, and I can never thank you enough.

Acknowledgements

I would like to express my deepest gratitude to my principal supervisor Dr Sheikh Islam for his valuable guidance and support throughout the period of this project. Also, I extend my deepest gratitude to the other supervisors Dr Mamdud Hossain, Dr Mohamed Ghazi Droubi and Dr Gbenga Oluyemi. I would like to say to you all, thank you very much for your time, words, kind support, valued guidance and encouragement throughout my PhD programme. It has been a very interesting journey for so many years, and always I will remember our talks and discussions; this has left a big thumbprint in my knowledge and my heart.

I wish to thank all the staff in the School of Engineering, IT department and the Library at Robert Gordon University, for their prompt support and help during this journey: particularly, Professor Ian Steel, Dr Rosslyn Shanks, Kirsty Stevenson, Petrena Morrison and Colin MacLean.

Also, I wish to thank the staff in the Graduate School at Robert Gordon University for their support always, and advice in many levels, particularly, Professor Andrew Lamb, Martin Simpson, Nick Anderson and Andrea MacMillan.

Moreover, I would like to thank my fellow researchers in the Flow Modelling and Heat Transfer Research Group and the School of Engineering Research Hub, particularly, Oluwademilade Ogunesan and Russein Mahon, amongst others. Your words of encouragement and our supporting each other during this long journey and late nights of researching in the Research Hub kept me going. I say thank you all.

I would like to express my sincere appreciation and thankfulness to my work colleagues in Robert Gordon University, particularly, Mrs Christine Buchanan, Mr Terry Knight, Ms Rachel Grant and Mrs Margaret L'Etang, for their unlimited and unforgettable support, advice and encouragement, throughout my studies. I will never forget them, and they will always be in my heart and mind.

Moreover, I wish to express my sincere appreciation to my wife Josephine Crimp for all the support, help, encouragement and patience during my Phd study journey. Your patience and help for all the late night studies and no relaxing weekends will always be remembered in my heart and my mind and I wish to say thank you so very much! You have been super helpful and supportive to me during my Phd journey.

Finally, I would like to express my deepest gratitude and appreciation to my parents, who brought me up and taught me a lot in life: "all blessings from mighty God to their souls"; and as well, my brother Engineer Ahmed Al-Mashhadanie for his encouragement and support in every step during my studies and my life.

Lastly, I would like to raise my hand and pray to the Almighty God "Allah" for all of you, to bless you all, and all your families.

Haider Al-Mashhadanie
September 2021

Abstract

Fractured media exist in most layers of the earth's crust, often dominating bulk properties of subsurface geological formations. Therefore, fractured media are involved in many key engineering sectors that impact humans living on Earth. Fractured formations consist of two distinct media sharing the same location: matrix and fracture, which affect each other's flow. Both have heterogeneous properties, such as anisotropic matrix permeability and rough fracture surfaces; also, fractures have varied orientation angles and exist in fractured formations in either discrete fracture form, or in connected networks with varied angles/patterns. Due to this heterogeneity, most fractured media modelling and studies in the literature have considered assumptions that don't represent flow in realistic conditions.

Thus, this research presents systematic investigations conducted on fractured media by using Computational Fluid Dynamic ANSYS CFD Fluent FVM to investigate fluid flow in many kinds of fractured media. These investigations ranged from simple and widely used fractured geometries to more complex ones, firstly, parallel plates fractures and rough fractures with horizontal orientation inside fractured domains; both fractures were investigated with different fracture surface conditions in these fractured domain models, such as: inclusion and exclusion of the matrix effect on flow; and matrix isotropic/anisotropic permeability's effects on flow, to create most mimicked realistic fractured formation conditions. The results of these models were validated, and compared with current understandings of fractured media model flow in the literature. The outcomes of these models have reflected that parallel plates fractures with single aperture are unsuitable to represent flow in fractured media. As well, that exclusion of matrix in fractured media flow will highly mislead flow calculations in fractured media. Secondly, the results of ANSYS CFD Fluent FVM rough fracture models were used in developing two fracture friction factor models in realistic fractured media conditions (analytical and numerical friction factor models), that account for rough fracture geometry effects and matrix permeability (isotropic and anisotropic matrix permeability along layers of formations along fracture length, and, in two directions of flow X and Y - consider K_x and K_y anisotropic effect on lateral and perpendicular flow of

each layer) on entire fracture domain flow. Friction factor is an important factor for predicting pressure drop ($\frac{\Delta P}{L}$) along fractures, and accordingly on fluid migration in fractured formations. And thirdly, ANSYS CFD Fluent FVM rough fracture network models were created, which included many heterogeneous properties of fracture media such as: many patterns of network orientations, where each model has different inlets and outlets of flow, and matrix effect was included with isotropic and anisotropic matrix permeability. The outcomes of these models have resulted in new and interesting understandings of modelling fractured media, which proved that matrix functionality in fractured media is not only as fluid provider, but it does have major effects on providing and transporting fluids in fractured media. As well, it provided new evidence that modelling a single fracture of fractured media will highly mislead flow calculation.

Keywords:

Fractured reservoirs; Computational Fluid Dynamics; Fracture geometry; Fracture networks; Friction factors; anisotropic matrix; permeability.

Table of Contents

Dedication	IV
Acknowledgements.....	V
Abstract.....	VII
1 Introduction.....	1
1.1 Overview.....	1
1.2 Challenges Of Subsurface Fractured Media.....	2
1.3 Aim And Objectives	6
1.3.1 Aim.....	6
1.3.2 Objectives.....	6
1.4 Thesis Outline	8
1.5 Contributions to knowledge	9
2 Literature Review.....	11
2.1 Reservoir Modelling Overview	11
2.2 Naturally Fractured Formations Overview	12
2.2.1 Natural fracture types	13
2.3 Natural Fractures' Parameters	14
2.3.1 Single fracture parameters	15
2.3.2 Fracture network parameters	15
2.4 Porosity And Permeability Of Fractured Media	17
2.4.1 Porosity	17
2.4.2 Permeability	18
2.4.2.1 Permeability's influence on fractures and matrices	24
2.5 Flow In Fractured Reservoirs	27
2.5.1 Flow in fractures with one aperture size (parallel plates).....	27
2.5.2 Flow in rough fractures with varied apertures (multi-parallel plates fracture geometry).....	31

2.5.3 Summary of flow in fractures with one aperture size (parallel plates) and rough fractures with varied apertures (multi-parallel plates fracture geometry)	38
2.5.4 Multiple fractures (fracture networks) modelling	39
2.5.5 Fluids Imbibition And Invasion Percolation between Fracture and Matrix	47
2.6 Friction Phenomena Overview	50
2.6.1 Flow regimes as Reynolds and Forchheimer equations in fractured formations	54
2.6.2 Friction factor (head loss) formula in systems	58
2.6.3 Friction factor in naturally fractured formations	59
2.7 Summary of the literature review.....	66
3 CFD Methodology	68
3.1 Overview	68
3.2 Fracture Flow Modelling	69
3.3 Computational Fluid Dynamics - ANSYS CFD Fluent FVM Overview	72
3.3.1 Governing equations.....	75
3.4 Boundary Conditions In ANSYS CFD Fluent FVM	77
3.4.1 Pressure inlet boundary conditions	78
3.4.2 Pressure outlet boundary conditions	78
3.4.3 Wall boundary conditions.....	78
3.4.4 Symmetry boundary conditions	79
3.4.5 Interior (face) boundary conditions	79
3.5 Modelling Fractured Media Using ANSYS CFD Fluent FVM	81
3.5.1 Parallel plates fracture	82
3.5.1.1 Parallel plates fracture geometry	83
3.5.1.2 Meshing the geometry	83
3.5.1.3 Simulation set up of parallel plates fracture	86
3.5.2 Rough Fracture - parallel plates fractures with varied aperture heights (regeneration Crandall, Ahmadi and Smith (2010)'s model)	87
3.5.2.1 Geometry of rough fracture	88
3.5.2.2 Meshing rough fractured media geometry	89

3.5.2.3 Simulations set up of rough fracture	91
4 Solution Procedure, Validation And Results Of Parallel Plates And Rough Fractures	92
4.1 Overview	92
4.2 Parallel Plates Fracture Simulations, Results extraction method and validations	94
4.2.1 Grid sensitivity analysis	97
4.2.2 Validation of parallel plates fracture model	98
4.2.3 Parallel plates fracture ANSYS CFD Fluent FVM models with surface boundaries as “impermeable Walls” and “Permeable Interior face”, with isotropic matrix permeability	101
4.2.4 Parallel plates fracture ANSYS CFD Fluent FVM models with permeable surface “Interior faces boundary” with anisotropic matrix permeability: results	
106	
4.2.4.1 Simulation results	109
4.2.4.2 Summary of anisotropic permeability simulations of parallel plates fractures	116
4.3 Rough Fracture Simulations Results and Validations	119
4.3.1 Grid sensitivity analysis	121
4.3.2 Rough Fracture surfaces set up as “Impermeable Walls boundary conditions” with Validation	123
4.3.3 Rough fracture surfaces set-up “Interior faces” permeable boundary conditions with validation	126
4.3.4 Rough fracture ANSYS CFD Fluent FVM models with surface boundaries as “Walls” and “Interior faces”, with isotropic matrix permeability	128
4.3.5 Rough fracture ANSYS CFD Fluent FVM models with permeable surface boundary “Interior faces” with anisotropic matrix permeability results.....	137
4.3.5.1 Simulation results	138
4.3.5.2 Summary of anisotropic permeability simulations of rough fractures models	143
4.4 Comparisons Between Parallel Plates And Rough Fractures	148
4.4.1 Summary of the comparisons between parallel plates fractures and rough fractures	150

4.5 Conclusion.....	154
5 Friction Factor In Fractured Media	157
5.1 Introduction	157
5.2 Extraction Of Friction Factor Value From ANSYS CFD Fluent FVM Models	158
5.3 Friction Factor In A Rough Fracture (Re-generating Crandall, Ahmadi and Smith (2010)'s Paper)	160
5.3.1 Friction factor in rough fracture with fracture's surface boundaries set as impermeable "Walls boundry" with Validation	161
5.3.2 Friction factor in rough fracture with two boundary conditions of fracture surfaces set up as impermeable "Walls boundry" and permeable "Interior faces boundry" with Validation	163
5.3.3 Friction factor in rough fracture with anisotropic matrix permeability and fracture surface boundaries set up as permeable "Interior faces boundary".	166
5.3.4 Summary of friction factor for rough fracture models with surface boundaries set up as impermeable "Walls boundry" and permeable "Interior faces boundry" with isotropic and anisotropic matrix permeability	169
5.4 New Proposed Analytical Model Of Fracture Friction Factor	172
5.4.1 Validation of the new proposed Analytical model of fracture friction factor	181
5.5 A New Friction Factor Numerical Model In Rough Fractures With Anisotropic Permeability, Using ANSYS CFD Fluent FVM Fracture Models	184
5.5.1 Analysis and validation of the new Numerical friction factor model with the previous models, in rough fractures with anisotropic permeability	186
5.6 Conclusion.....	191
6 Fracture Networks	192
6.1 Overview	192
6.2 Fracture Network Scenarios	193
6.3 Fracture Networks modelling	195
6.3.1 Geometry descriptions	195

6.3.2	Fracture network geometries.....	196
6.3.3	Fractal properties of fracture networks.....	198
6.3.4	Meshing fracture networks.....	200
6.3.5	Extracting results from surface lines of ANSYS CFD Fluent FVM fracture network simulations.....	203
6.3.6	Fracture network simulations results	206
6.3.6.1	Fracture network 1 simulation results	207
6.3.6.2	Fracture network 2 simulation results	211
6.3.6.3	Fracture network 3 simulation results	215
6.3.6.4	Fracture network 4 simulation results	219
6.3.6.5	Fracture network 5 simulation results	223
6.3.7	Investigating fracture network 2 model.....	227
6.3.7.1	First Approach.....	227
6.3.7.2	Second Approach.....	231
6.3.7.3	Analysis of pressure contours distribution in Network 2 ..	233
6.4	Comparisons Among Fracture Network Models	235
6.4.1	Results analysis	239
6.5	Comparisons Of Ten Sections Inside Fracture Network Models ..	247
6.5.1	Results analysis	252
6.6	Flow Comparisons Between Rough Fracture Network And Single Horizontal Rough Fracture.....	253
6.7	Flow Comparisons Between Fracture Network Models And Literature Flow Models.....	257
6.8	Conclusions	259
7	Conclusions And Future Work	262
7.1	Conclusions	262
7.2	Recommendations For Future Work	266
8	References	267
9	Appendix 1 – Recreating Rough Fracture From A Fracture Image .	280
9.1	Rough Fracture Geometry Validation.....	286

10	Appendix 2 - Post-processing FLUENT Solver Of Fracture Networks	292
10.1	Fluent set-up.....	292
10.1.1Solution	
	294	

List of Tables

TABLE 2.1 SUMMARIZES THE DEVELOPED MODELS OF FRACTURE FRICTION FACTORS	65
TABLE 3.1 MESH CELLS STATISTICS.....	85
TABLE 3.2 MESH CELLS STATISTICS.....	90
TABLE 4.1 ANSYS CFD FLUENT FVM MODEL’S MESH DETAILS WITH THE AVERAGE VELOCITY VALUES OF THE SECTIONS INSIDE THE PARALLEL PLATES FRACTURE MODELS.....	98
TABLE 4.2 SIX SCENARIOS OF ANISOTROPIC MATRIX PERMEABILITY OF THE SIMULATIONS SET- UP	109
TABLE 4.3 SUMMARISING FLOW RESULTS OF ANSYS CFD FLUENT FVM MODELS WITH ANISOTROPIC PERMEABILITY OF PARALLEL PLATES FRACTURES - AVERAGE VALUES OF FOUR PRESSURE DROPS (5, 100, 1000, 2000) PA	115
TABLE 4.4 ANSYS CFD FLUENT FVM MODELS MESH DETAILS WITH THE AVERAGE VELOCITY VALUES OF THE SECTIONS INSIDE THE ROUGH FRACTURE MODELS	122
TABLE 4.5 SUMMARISING FLOW RESULTS OF ANSYS CFD FLUENT FVM MODELS WITH ANISOTROPIC PERMEABILITY OF ROUGH FRACTURES - AVERAGE VALUES OF FOUR PRESSURE DROPS (5, 100, 1000, 2000) PA	142
TABLE 5.1 SUMMARISING REYNOLDS AND FRICTION FACTORS ADV OF ANSYS CFD FLUENT FVM MODELS’ SIMULATION RESULTS, FOR ISOTROPIC AND ANISOTROPIC PERMEABILITY OF ROUGH FRACTURES	167
TABLE 6.1 FRACTURE NETWORK 1 CALCULATIONS OF APERTURES’ FREQUENCY AND THE STANDARD DEVIATION	199
TABLE 6.2 SUMMARY OF ALL FRACTURE NETWORKS’ CALCULATIONS, SUCH AS: APERTURES’ FREQUENCY (TOTAL SECTIONS), THE STANDARD DEVIATION, (%) FRACTURE/MATRIX AREA IN THE DOMAIN	200
TABLE 6.3 MESH STATISTICS OF FRACTURE NETWORK MODELS.....	203
TABLE 6.4 PERMEABILITY SCENARIOS OF THE MATRIX’S FRACTURE NETWORK MODELS	207
TABLE 6.5 ADV OF X-VELOCITY COMPARISONS BETWEEN THE THREE BOUNDARY CONDITION SET-UPS AND INITIAL MODEL OF NETWORK 2	230
TABLE 6.6 FRACTAL PROPERTIES COMPARISON BETWEEN FRACTURE NETWORK 4 AND SINGLE ROUGH FRACTURE	253
TABLE 6.7 AVERAGE VALUE OF FRACTURE FLOW WITH PRESSURE DROPS (5, 100, 1000, 2000) PA	258

TABLE 9.1 SECTION OF THE MANUALLY AMENDED IMAGE DIGITIZER (X, Y) COORDINATES TABLE BY EXCEL	284
TABLE 9.2 CALCULATIONS OF FRACTURE APERTURE HEIGHT FREQUENCY OF NAZRIDOUST, AHMADI AND SMITH (2006)'S FRACTURE – SECTION D.....	287
TABLE 9.3 COMPARISON OF FRACTURE APERTURE HEIGHT FREQUENCY OF THIS RESEARCH'S FRACTURE WITH NAZRIDOUST, AHMADI AND SMITH (2006)'S FRACTURE	287
TABLE 9.4 STANDARD DEVIATION CALCULATIONS OF THIS RESEARCH'S FRACTURE	289
TABLE 9.5 NORMAL DISTRIBUTION CALCULATION OF THIS RESEARCH'S FRACTURE AND NAZRIDOUST, AHMADI AND SMITH (2006)'S FRACTURE.....	289
TABLE 9.6 CALCULATION OF TORTUOSITY VALUE OF THIS RESEARCH'S FRACTURE GEOMETRY	290

List of Figures

FIGURE 2.1 SCHEMATIC DISTINGUISHING BETWEEN FAULTS AND JOINTS IN FRACTURE FORMATIONS	13
FIGURE 2.2 FRACTURED FORMATIONS STUDY PROCEDURE.....	14
FIGURE 2.3 FOUR FRACTURE NETWORKS, WHERE EACH NETWORK HAS A DIFFERENT DEGREE OF INTERCOMMUNICATION, CLASSIFIED FROM WEAK TO STRONG CONNECTIONS	16
FIGURE 2.4 A: SIMILAR ORIENTATION FRACTURES, B: RANDOM ORIENTATIONS FRACTURES	22
FIGURE 2.5 RESERVOIR LAYERS WITH DIFFERENT THICKNESS AND PROPERTIES, AND CROSS FLOW AMONG THEM.....	22
FIGURE 2.6 FLOW IN A RESERVOIR WITH DIFFERENT LAYERS WITH VARIED PERMEABILITIES	23
FIGURE 2.7 SEPARATED LAYERS IN RESERVOIR FORMATIONS	23
FIGURE 2.8 ANISOTROPIC PERMEABILITY IN MATRIX, HIGH K_x AND MODERATE K_y	24
FIGURE 2.9 VELOCITY PROFILE (POISEUILLE PARABOLIC SHAPE) BETWEEN TWO FIXED PARALLEL PLATES WITH DISTANCE HEIGHT - FULLY DEVELOPED FLOW	28
FIGURE 2.10 LINEAR MODEL FOR FLOW IN A SINGLE FRACTURE	31
FIGURE 2.11 REAL FRACTURED MEDIA	39
FIGURE 2.12 DISORDERED FRACTURE NETWORK MEDIA: FRACTURE (RED) AND PERMEABLE MATRIX (BLUE).....	42
FIGURE 2.13 SKETCHES OF REYNOLDS'S PIPE WITH FLOW REGIMES, A. LAMINAR, B. TURBULENT AND C. TRANSITION	53
FIGURE 2.14 INCLINED PIPE WITH STEADY DEVELOPED FLOW BETWEEN TWO SECTIONS	58
FIGURE 2.15 RECTANGULAR PARALLEL PLATES AND FRICTION RESISTANCE DUE TO SURFACES' SHEAR FORCES ONLY (EXCLUDES VISCOSITY).....	60
FIGURE 2.16 COMPARISONS OF FRICTION FACTORS BETWEEN CFD AND PARALLEL MODEL RESULTS	63
FIGURE 3.1 ITERATIVE LOOP OF CALCULATIONS IN ANSYS CFD FLUENT FVM.....	74
FIGURE 3.2 TWO SEPARATED ZONES WITH AN INTERIOR DOUBLE-SIDED FACE (GREEN COLOUR)	81
FIGURE 3.3 CLARIFIES ADJACENT CELLS AT THE INTERIOR FACE BOUNDARY IN ANSYS CFD FLUENT FVM, AND ZOOM ON CELL'S GRADIENT SCALAR WITH VECTORS OF CELL CENTROID AND CELL FACE.....	81
FIGURE 3.4 CONCEPT OF GOING FROM ROUGH FRACTURE IN NATURE TO PARALLEL PLATES FRACTURE WITH SINGLE APERTURE	82

FIGURE 3.5 FRACTURE CROSS-SECTION VARIATIONS	83
FIGURE 3.6 PARALLEL PLATES FRACTURE WITH SINGLE APERTURE BY ANSYS CFD FLUENT FVM DESIGNMODELER.....	86
FIGURE 3.7 ROUGH FRACTURE, FRACTURE (D) FROM NAZRIDOUST, AHMADI AND SMITH (2006)'S PAPER, FIGURE 2 P. 318	89
FIGURE 3.8 THE FINAL GEOMETRY OF THE ROUGH FRACTURE INSIDE THE MATRIX DOMAIN (THE MATRIX IS GREY, THE FRACTURE IS GREEN)	89
FIGURE 3.9 ROUGH FRACTURE MODEL BY ANSYS CFD FLUENT FVM DESIGNMODELER....	91
FIGURE 4.1 DIAGRAM CLARIFYING THE STRUCTURE OF THE MODELS' RESULTS, VALIDATIONS, AND COMPARISONS AMONG MODELS IN THIS CHAPTER.....	93
FIGURE 4.2 SURFACE LINE INSIDE THE FRACTURE ONLY, TO READ X-VELOCITY VALUES (GREEN COLOUR IS MATRIX, AND BLUE COLOUR FRACTURE)	95
FIGURE 4.3 X-VELOCITY VALUES, INSIDE FRACTURE ONLY, ON THE FRACTURE READING LINE FOR PRESSURE 1000 PA, FRACTURE SURFACES INTERACTING WITH MATRIX (INTERIOR FACE BOUNDARY) WITH ISOTROPIC MATRIX ($K_x=K_y= 2000$ MD)	96
FIGURE 4.4 SURFACE LINE INSIDE THE MATRIX ONLY, TO READ X-VELOCITY VALUES (GREEN COLOUR IS MATRIX, AND BLUE COLOUR FRACTURE)	96
FIGURE 4.5 X-VELOCITY VALUES INSIDE MATRIX ONLY, ON THE MATRIX READING LINES FOR PRESSURE 1000 PA, FRACTURE SURFACES INTERACTING WITH MATRIX (INTERIOR FACE BOUNDARY), WITH ISOTROPIC MATRIX ($K_x=K_y= 2000$ MD)	96
FIGURE 4.6 X-VELOCITY PROFILES INSIDE FRACTURE 581-MICROMETRE 1000 PA WITH THREE MESHES	98
FIGURE 4.7 THE LONGITUDINAL READING LINE IN THE CENTRE OF THE PARALLEL PLATES FRACTURE (MATRIX IS GREEN, FRACTURE IS WHITE)	100
FIGURE 4.8 X-VELOCITY VALUE ALONG THE PARALLEL PLATES IN THE CENTRE OF THE FRACTURE, WITH INLET PRESSURE A: 100 PA AND B: 2000 PA, FRACTURE SURFACES SET AS IMPERMEABLE WALL BOUNDARY, AND MATRIX PERMEABILITY K_x AND $K_y=0.2$ MD (NO FLOW INTERACTION BETWEEN FRACTURE AND MATRIX)	100
FIGURE 4.9 VALIDATION OF X-VELOCITY AND FRACTURE FLOW RATE BETWEEN PARALLEL PLATES FRACTURE ANSYS CFD FLUENT FVM MODEL AND THEORY EQUATIONS. A: X-VELOCITY AT THE VERTICAL SECTION IN 581-MICRON APERTURE WITH PRESSURE 5 PA, AND B: PRESSURE DROP AGAINST FRACTURE FLOW RATE. IN ALL MODELS FRACTURE HAD IMPERMEABLE SURFACES WITH WALL BOUNDARY (NO FLOW INTERACTION BETWEEN FRACTURE AND MATRIX), AND ISOTROPIC MATRIX K_x AND $K_y=0.2$ MD	101

FIGURE 4.10 TOTAL PRESSURE CONTOURS, X-VELOCITY CONTOURS AND VELOCITY STREAMLINE RESPECTIVELY (TOP TO BOTTOM) OF PARALLEL PLATES FRACTURE MODELS, MATRIX PERMEABILITY K_x AND $K_y = 2000$ MD, $P = 1000$ PA, WITH TWO FRACTURE SURFACE BOUNDARIES SET UPS: A. IMPERMEABLE WITH SURROUNDING MATRIX "WALLS BOUNDARY", AND B. PERMEABLE WITH SURROUNDING MATRIX "INTERIOR FACE BOUNDARY" 104

FIGURE 4.11 VELOCITY PROFILES OF PARALLEL PLATES FRACTURE OF 581-MICROMETRE FRACTURE APERTURES HEIGHT, AT THE END JUST BEFORE FRACTURE OUTLET, ISOTROPIC MATRIX PERMEABILITY K_x AND $K_y = 2000$ MD. 105

FIGURE 4.12 PARALLEL PLATES FRACTURE COMPARISONS OF: A. TOTAL FLOW RATE (FRACTURE + MATRIX), B. FRACTURE FLOW RATE AND C. MATRIX FLOW RATE (mm^2/s), BETWEEN IMPERMEABLE "WALLS BOUNDARY" AND PERMEABLE "INTERIOR FACE BOUNDARY" OF FRACTURE SURFACE WITH (K_x & $K_y = 2000$ MD) 105

FIGURE 4.13 COMPARISON OF (% FRACTURE FLOW RATE) OF PARALLEL PLATES FRACTURE BETWEEN PERMEABLE AND IMPERMEABLE FRACTURE SURFACES BOUNDARIES WITH THE MATRIX, ISOTROPIC MATRIX PERMEABILITY K_x AND $K_y = 2000$ MD 106

FIGURE 4.14 COMPARISONS OF TOTAL FLOW RATE (mm^2/s) OF PARALLEL PLATES ANSYS CFD FLUENT FVM MODEL FRACTURES, WITH ISOTROPIC AND ALL ANISOTROPIC MATRIX PERMEABILITY SCENARIOS, WITH PERMEABLE FRACTURE SURFACE BOUNDARIES..... 111

FIGURE 4.15 COMPARISONS OF FRACTURE FLOW RATE (mm^2/s) OF PARALLEL PLATES ANSYS CFD FLUENT FVM MODEL FRACTURES, WITH ISOTROPIC AND ALL ANISOTROPIC MATRIX PERMEABILITY SCENARIOS, WITH PERMEABLE FRACTURE SURFACE BOUNDARIES..... 111

FIGURE 4.16 COMPARISONS OF MATRIX FLOW RATE (mm^2/s) OF PARALLEL PLATES ANSYS CFD FLUENT FVM MODEL FRACTURES, WITH ISOTROPIC AND ALL ANISOTROPIC MATRIX PERMEABILITY SCENARIOS, WITH PERMEABLE FRACTURE SURFACE BOUNDARIES..... 112

FIGURE 4.17 COMPARISONS OF PARALLEL PLATES ANSYS CFD FLUENT FVM MODEL FRACTURES: A. % FRACTURE FLOW RATE AND B. % MATRIX FLOW RATE, WITH ISOTROPIC AND ALL ANISOTROPIC MATRIX PERMEABILITY MODELS, AND PERMEABLE FRACTURE SURFACE BOUNDARIES 113

FIGURE 4.18 NORMALIZED VELOCITY PROFILES OF PARALLEL PLATES FRACTURE AT 581 MICRON SECTION: A. (5) PA AND B. 1000 PA, BETWEEN MODELS WITH ISOTROPIC ($K_x = K_y = 2000$ MD) AND ANISOTROPIC MATRIX PERMEABILITIES ($K_x = 380$ $K_y = 2000$ MD) AND ($K_x = 2000$ $K_y = 380$ MD) 114

FIGURE 4.19 AVERAGE FLOW OF FOUR PRESSURE VALUES (5, 100, 1000, 2000) PA FOR THE FRACTURE AND THE MATRIX IN ANSYS CFD FLUENT FVM PARALLEL PLATES FRACTURE MODELS 118

FIGURE 4.20 SURFACE LINES TO READ X-VELOCITY PROFILES: A; INSIDE THE FRACTURE ONLY, AND B; INSIDE THE MATRIX ONLY (MATRIX IS GREEN, AND FRACTURE IS BLUE)..... 121

FIGURE 4.21 X-VELOCITY INSIDE FRACTURE 240- MICROMETRE APERTURE, 1000 PA WITH FOUR FRACTURE MESHES 123

FIGURE 4.22 ROUGH FRACTURE SIMULATIONS TOTAL PRESSURE AND VELOCITY CONTOURS WITH ISOTROPIC MATRIX PERMEABILITY (K_x & $K_y=2000$ MD) AND $P=2000$ PA WITH ZERO OUTLET PRESSURES, FRACTURE SURFACE BOUNDARIES SET AS IMPERMEABLE "WALLS BOUNDRY". A. TOTAL PRESSURE, B. VELOCITY CONTOURS..... 125

FIGURE 4.23 COMPARISONS OF X-VELOCITY PROFILES OF ROUGH FRACTURE MODELS AT THE 240 MICROMETRE VERTICAL SECTION AT THE END OF FRACTURE, WITH ISOTROPIC MATRIX PERMEABILITIES K_x & $K_y=2000$ MD, AND K_x & $K_y=0.2$ MD, FRACTURE SURFACES SET AS IMPERMEABLE BOUNDARIES "WALLS", WITH TWO PRESSURES: A. 5 PA, AND B. 1000 PA 125

FIGURE 4.24 VALIDATION OF PRESSURE DROP WITH A FRACTURE FLOW RATE BETWEEN THIS RESEARCH'S ANSYS CFD FLUENT FVM MODELS AND NAZRIDOUST, AHMADI AND SMITH (2006)'S MODEL, FRACTURE SURFACES SET WITH IMPERMEABLE BOUNDARIES "WALLS", WITH TWO SETS OF ISOTROPIC MATRIX PERMEABILITIES: K_x & $K_y=2000$ MD, AND K_x AND $K_y=0.2$ MD. 126

FIGURE 4.25 ROUGH FRACTURE SIMULATIONS' TOTAL PRESSURE AND VELOCITY CONTOURS WITH ISOTROPIC MATRIX PERMEABILITY (K_x & $K_y=1000$ MD) AND $P=5$ PA, FRACTURE SURFACE BOUNDARIES SET AS PERMEABLE "INTERIOR FACES": A. TOTAL PRESSURE, B. VELOCITY CONTOURS..... 127

FIGURE 4.26 COMPARISONS OF X-VELOCITY PROFILES OF ROUGH FRACTURE MODELS AT THE 240 MICROMETRE VERTICAL SECTION AT THE END OF FRACTURE 127

FIGURE 4.27 VALIDATION OF PRESSURE DROP WITH A FRACTURE FLOW RATE BETWEEN ANSYS CFD FLUENT FVM ROUGH FRACTURE AND CRANDALL, AHMADI AND SMITH (2010)'S MODELS 128

FIGURE 4.28 ROUGH FRACTURE ANSYS CFD FLUENT FVM MODELS' FLOW COMPARISONS BETWEEN IMPERMEABLE "WALLS BOUNDARY" AND PERMEABLE "INTERIOR FACES BOUNDARY" OF FRACTURE SURFACE BOUNDARIES WITH (K_x & $K_y=2000$ MD) 133

FIGURE 4.29 NORMALIZED VELOCITY PROFILES OF ROUGH FRACTURE ANSYS CFD FLUENT FVM MODELS OF 240 MICROMETERE FRACTURE APERTURE HEIGHT, AT THE END JUST BEFORE FRACTURE OUTLET, ISOTROPIC MATRIX PERMEABILITY K_x AND $K_y= 2000$ MD 134

FIGURE 4.30 COMPARISON OF ROUGH FRACTURE ANSYS CFD FLUENT FVM MODELS' FLOW PERCENTAGES BETWEEN PERMEABLE AND IMPERMEABLE FRACTURE SURFACE BOUNDARIES

WITH THE MATRIX, ISOTROPIC MATRIX PERMEABILITY K_x AND $K_y = 2000$ MD. A. % FRACTURE FLOW; AND B. % MATRIX FLOW.....	134
FIGURE 4.31 VELOCITY STREAMLINES OF ROUGH FRACTURE $P=2000$ PA, ISOTROPIC MATRIX PERMEABILITY (K_x & $K_y = 2000$ MD), WITH FRACTURE SURFACE BOUNDARIES SET AS IMPERMEABLE "WALLS".....	135
FIGURE 4.32 VELOCITY STREAMLINES OF ROUGH FRACTURE $P=2000$ PA, ISOTROPIC MATRIX PERMEABILITY (K_x & $K_y = 2000$ MD), WITH FRACTURE SURFACE BOUNDARIES SET AS PERMEABLE "INTERIOR FACES".....	136
FIGURE 4.33 COMPARISONS OF TOTAL FLOW RATE (mm^2/s) OF ROUGH ANSYS CFD FLUENT FVM FRACTURE MODELS, WITH ISOTROPIC AND ALL ANISOTROPIC MATRIX PERMEABILITY SCENARIOS, WITH PERMEABLE FRACTURE SURFACE BOUNDARIES.....	139
FIGURE 4.34 COMPARISONS OF FRACTURE FLOW RATE (mm^2/s) OF ROUGH ANSYS CFD FLUENT FVM FRACTURE MODELS, WITH ISOTROPIC AND ALL ANISOTROPIC MATRIX PERMEABILITY SCENARIOS, WITH PERMEABLE FRACTURE SURFACE BOUNDARIES.....	139
FIGURE 4.35 COMPARISONS OF MATRIX FLOW RATE (mm^2/s) OF ANSYS CFD FLUENT FVM ROUGH FRACTURE MODELS, WITH ISOTROPIC AND ALL ANISOTROPIC MATRIX PERMEABILITY SCENARIOS, WITH PERMEABLE FRACTURE SURFACE BOUNDARIES.....	140
FIGURE 4.36 COMPARISONS OF ROUGH ANSYS CFD FLUENT FVM MODEL FRACTURES: A. % FRACTURE FLOW RATE AND B. % MATRIX FLOW RATE. ISOTROPIC AND ALL ANISOTROPIC MATRIX PERMEABILITY SCENARIOS INCLUDED, WITH PERMEABLE FRACTURE SURFACE BOUNDARIES	141
FIGURE 4.37 AVERAGE FLOW COMPARISONS OF FRACTURE AND MATRIX IN ANSYS CFD FLUENT FVM ROUGH FRACTURE MODELS OF FOUR PRESSURE VALUES (5, 100, 1000, 2000) PA	147
FIGURE 4.38 FLOW COMPARISONS (mm^2/s) BETWEEN ANSYS CFD FLUENT FVM MODELS OF ROUGH FRACTURE AND PARALLEL PLATES FRACTURE WITH PERMEABLE SURFACES ($K_x=K_y=2000$ MD), WITH PRESSURE DROPS (5, 100, 1000, 2000) PA, PERMEABLE FRACTURE SURFACE BOUNDARIES "INTERIOR FACES"	152
FIGURE 4.39 % FLOW COMPARISONS BETWEEN ANSYS CFD FLUENT FVM MODELS OF ROUGH FRACTURE AND PARALLEL PLATES FRACTURE WITH PERMEABLE SURFACES ($K_x=K_y=2000$ MD), WITH PRESSURE DROPS (5, 100, 1000, 2000) PA	152
FIGURE 4.40 COMPARISONS OF X-VELOCITY AND TOTAL PRESSURE, AT FRACTURE'S TOP SURFACES AND INSIDE MATRIX, BETWEEN ROUGH FRACTURE AND PARALLEL PLATE FRACTURE ANSYS CFD FLUENT FVM MODELS, WITH ISOTROPIC PERMEABILITY ($K_x=K_y=2000$ MD)	

AND $P=2000$ PA WITH ZERO PRESSURE OUTLETS, AND PERMEABLE FRACTURE SURFACE BOUNDARIES	153
FIGURE 4.41 SCHEMATIC DESCRIPTION OF FLOW INTERACTION THROUGH THE ROUGH FRACTURE SURFACE INTERFACE LAYER BETWEEN MATRIX AND FRACTURE	154
FIGURE 5.1 COMPARISON OF ROUGH FRACTURE ANSYS CFD FLUENT FVM MODELS WITH FRACTURE SURFACES SET AS IMPERMEABLE "WALLS BOUNDARY", BETWEEN DIFFERENT ISOTROPIC PERMEABILITIES ($K_x=K_y=0.2$ MD) AND ($K_x=K_y=2000$ MD). A. REYNOLDS NUMBER, AND B. FRICTION FACTOR.....	162
FIGURE 5.2 FRICTION FACTOR VALIDATION AND COMPARISON BETWEEN ROUGH FRACTURE OF ANSYS CFD FLUENT FVM MODEL WITH ISOTROPIC PERMEABILITY ($K_x=K_y=0.2$ MD), FRACTURE SURFACES WERE SET AS IMPERMEABLE BOUNDARY "WALLS BOUNDARY", AND NAZRIDOUST, AHMADI AND SMITH (2006)'S MODEL OF FRICTION FACTOR	163
FIGURE 5.3 COMPARISON OF ROUGH FRACTURE ANSYS CFD FLUENT FVM MODELS WITH FRACTURE SURFACE BOUNDARIES SET AS IMPERMEABLE "WALLS BOUNDARY" AND PERMEABLE "INTERIOR FACES BOUNDARY", WITH ISOTROPIC PERMEABILITY ($K_x=K_y=2000$ MD) A. REYNOLDS NUMBER; AND B. FRICTION FACTOR.....	165
FIGURE 5.4 FRICTION FACTOR VALIDATION AND COMPARISON BETWEEN ROUGH FRACTURE ANSYS CFD FLUENT FVM MODEL WITH ISOTROPIC PERMEABILITY ($K_x=K_y=2000$ MD), FRACTURE SURFACES SET AS PERMEABLE "INTERIOR FACES BOUNDARY", AND CRANDALL, AHMADI AND SMITH (2010)'S MODEL.....	165
FIGURE 5.5 COMPARISONS OF ROUGH FRACTURE ANSYS CFD FLUENT FVM MODELS BETWEEN ISOTROPIC AND ALL ANISOTROPIC MATRIX PERMEABILITY SCENARIOS	168
FIGURE 5.6 AVERAGE FRACTURE FRICTION FACTOR AT FOUR PRESSURE VALUES (5, 100, 1000, 2000) PA, ZERO OUTLET PRESSURE, IN ANSYS CFD FLUENT FVM ROUGH FRACTURE MODELS OF TWO ANISOTROPIC PERMEABILITY SETS	171
FIGURE 5.7 COMPOSITE FORMATIONS WITH VARIED PERMEABILITY	177
FIGURE 5.8 FRICTION FACTOR VALIDATION OF ROUGH FRACTURE BETWEEN THE PROPOSED MODEL (EQUATION 5.28) AND CRANDALL, AHMADI AND SMITH (2010)'S MODEL'S DATA FOR DIFFERENT ISOTROPIC MATRIX PERMEABILITY ($K_x=K_y$) 0.2 MD AND 2000 MD..	183
FIGURE 5.9 VALIDATION OF THE PROPOSED FRICTION FACTOR MODEL WITH ANSYS CFD FLUENT FVM FRICTION FACTOR WITH ISOTROPIC AND ANISOTROPIC PERMEABILITY MATRIX SCENARIOS	183
FIGURE 5.10 FRACTURE FRICTION FACTOR VALUES BY ANSYS CFD FLUENT FVM WITH DIFFERENT SCENARIOS OF MATRIX ISOTROPIC AND ANISOTROPIC PERMEABILITY, WITH BEST FIT REGRESSION LINE	185

FIGURE 5.11 ZOOM ON FRACTURE FRICTION FACTOR VALUES BY ANSYS CFD FLUENT FVM WITH DIFFERENT SCENARIOS OF MATRIX ISOTROPIC AND ANISOTROPIC PERMEABILITY, WITH BEST FIT REGRESSION LINE.....	185
FIGURE 5.12 COMPARISON OF THE FRICTION FACTOR VERSUS REYNOLDS NUMBER BETWEEN THE PROPOSED MODEL (EQUATION 5.29) AND CRANDALL, AHMADI AND SMITH (2010)'S EQUATION	190
FIGURE 5.13 LINEARITY OF THE PROPOSED FRICTION FACTOR VERSUS OTHER FRICTION FACTOR MODELS	190
FIGURE 6.1 FRACTURED DOMAIN IMAGE (THE SELECTED FIVE SCENARIOS ARE MARKED WITH YELLOW CIRCLES AND NUMBER 1 TO 5) (YI AND XING 2018).....	195
FIGURE 6.2 FRACTURE NETWORK GEOMETRIES	198
FIGURE 6.3 NORMAL DISTRIBUTIONS OF FRACTURE NETWORKS	200
FIGURE 6.4 SAMPLES OF FRACTURE NETWORK MESHING AND FACE SIZING ZONES BY ANSYS DESIGNMODELER.....	202
FIGURE 6.5 FRACTURE NETWORK 5 READING SURFACE LINES AND X-VELOCITY PROFILES EXTRACTED FROM ANSYS CFD FLUENT FVM FRACTURE MODELS.....	204
FIGURE 6.6 FRACTURE NETWORK 2 READING SURFACE LINES AND X-VELOCITY PROFILES EXTRACTED FROM ANSYS CFD FLUENT FVM FRACTURE MODELS.....	205
FIGURE 6.7 FRACTURE NETWORK 1 SIMULATION CONTOURS.....	208
FIGURE 6.8 FRACTURE NETWORK 1 VELOCITY STREAMLINES, P=5 PA ISOTROPIC MATRIX PERMEABILITY (K_x & $K_y=2000$ MD), WITH FRACTURE SURFACE BOUNDARIES SET AS PERMEABLE "INTERIOR FACES".....	209
FIGURE 6.9 COMPARISONS OF FRACTURE NETWORK 1 FLOW PERCENTAGES IN FRACTURES AND MATRIX; AS WELL, TOTAL FLOW (FRACTURE + MATRIX) BETWEEN ISOTROPIC AND ANISOTROPIC PERMEABILITY MODELS	210
FIGURE 6.10 COMPARISON OF MATRIX FLOW BETWEEN FRACTURE NETWORK 1 ANSYS CFD FLUENT FVM MODELS WITH ISOTROPIC AND ANISOTROPIC MATRIX PERMEABILITY SCENARIOS, & DARCY EQUATION.....	211
FIGURE 6.11 FRACTURE NETWORK 2 SIMULATIONS CONTOURS.....	212
FIGURE 6.12 FRACTURE NETWORK 2 VELOCITY STREAMLINES, P=100 PA ISOTROPIC MATRIX PERMEABILITY (K_x & $K_y=2000$ MD), WITH FRACTURE SURFACE BOUNDARIES SET AS PERMEABLE "INTERIOR FACES".....	213
FIGURE 6.13 COMPARISONS OF FRACTURE NETWORK 2 FLOW PERCENTAGES IN FRACTURES AND MATRIX; AS WELL, TOTAL FLOW (FRACTURE + MATRIX) BETWEEN ISOTROPIC AND ANISOTROPIC PERMEABILITY MODELS	214

FIGURE 6.14 COMPARISON OF MATRIX FLOW BETWEEN FRACTURE NETWORK 2 ANSYS CFD FLUENT FVM MODELS WITH ISOTROPIC AND ANISOTROPIC MATRIX PERMEABILITY SCENARIOS, & DARCY EQUATION.....	214
FIGURE 6.15 FRACTURE NETWORK 3 SIMULATION CONTOURS	216
FIGURE 6.16 FRACTURE NETWORK 3 VELOCITY STREAMLINES P=1000 PA ISOTROPIC MATRIX PERMEABILITY (KX & KY=2000 MD), WITH FRACTURE’S SURFACE BOUNDARIES SET AS PERMEABLE “INTERIOR FACES”.....	217
FIGURE 6.17 COMPARISONS OF FRACTURE NETWORK 3 FLOW PERCENTAGES IN FRACTURES AND MATRIX; AS WELL, TOTAL FLOW BETWEEN ISOTROPIC AND ANISOTROPIC PERMEABILITY MODELS.....	218
FIGURE 6.18 COMPARISON OF MATRIX FLOW BETWEEN FRACTURE NETWORK 3 ANSYS CFD FLUENT FVM MODELS WITH ISOTROPIC AND ANISOTROPIC MATRIX PERMEABILITY SCENARIOS, & DARCY EQUATION.....	218
FIGURE 6.19 FRACTURE NETWORK 4 SIMULATIONS CONTOURS.....	220
FIGURE 6.20 FRACTURE NETWORK 4 VELOCITY STREAMLINES P=2000 PA ISOTROPIC MATRIX PERMEABILITY (KX & KY=2000 MD), WITH FRACTURE’S SURFACE BOUNDARIES SET AS PERMEABLE “INTERIOR FACES”.....	221
FIGURE 6.21 COMPARISONS OF FRACTURE NETWORK 4 FLOW PERCENTAGES IN FRACTURES AND MATRIX; AS WELL, TOTAL FLOW BETWEEN ISOTROPIC AND ANISOTROPIC PERMEABILITY MODELS.....	222
FIGURE 6.22 COMPARISON OF MATRIX FLOW BETWEEN FRACTURE NETWORK 4 ANSYS CFD FLUENT FVM MODELS WITH ISOTROPIC AND ANISOTROPIC MATRIX PERMEABILITY SCENARIOS, & DARCY EQUATION.....	223
FIGURE 6.23 FRACTURE NETWORK 5 SIMULATION CONTOURS	224
FIGURE 6.24 FRACTURE NETWORK 5 VELOCITY STREAMLINES P=2000 PA, ISOTROPIC MATRIX PERMEABILITY (KX & KY=2000 MD), WITH FRACTURE’S SURFACE BOUNDARIES SET AS PERMEABLE “INTERIOR FACES”.....	225
FIGURE 6.25 COMPARISONS OF FRACTURE NETWORK 5 FLOW PERCENTAGES IN FRACTURES AND MATRIX; AS WELL, TOTAL FLOW BETWEEN ISOTROPIC AND ANISOTROPIC PERMEABILITY MODELS.....	226
FIGURE 6.26 COMPARISON OF MATRIX FLOW BETWEEN FRACTURE NETWORK 5 ANSYS CFD FLUENT FVM MODELS WITH ISOTROPIC AND ANISOTROPIC MATRIX PERMEABILITY SCENARIOS, & DARCY EQUATION.....	227

FIGURE 6.27 CLARIFIES 3 BOUNDARY CONDITIONS OF NETWORK 2, WHICH WERE CHANGED AT THE FAR SIDE (TOP AND BOTTOM) OF THE MATRIX, AND THE STATIC PRESSURE CONTOURS OF THESE MODELS 229

FIGURE 6.28 X-VELOCITY PROFILES OF THE TOTAL DOMAIN OF THE THREE SET-UPS OF BOUNDARIES IN NETWORK MODEL 2, THE READING LINES OF THE TOTAL DOMAIN..... 230

FIGURE 6.29 STATIC PRESSURE CONTOURS FROM ANSYS CFD FLUENT FVM -POST NETWORK 2..... 230

FIGURE 6.30 STATIC PRESSURE TRANSIENT WITH TWO DIFFERENT TIME STEPS 232

FIGURE 6.31 CLARIFIES FRACTURE NETWORK 2 - TWO BEHAVIOURS OF STATIC PRESSURE CONTOUR IN THE SAME DOMAIN 235

FIGURE 6.32 A. TOTAL FLOW (MM²/S) COMPARISONS OF 5 FRACTURE NETWORKS WITH K_X=K_Y=2000, B. AVERAGE VALUE OF TOTAL FLOW (MM²/S) COMPARISONS OF ALL FRACTURE NETWORKS WITH K_X=K_Y=2000 MD, IN FOUR PRESSURE DROPS MODELS (5,100, 1000, 2000) PA , ZERO PRESSURE OUTLET, WITH PERMEABLE FRACTURE SURFACES "INTERIOR FACE BOUNDARY" 236

FIGURE 6.33 A. MATRIX FLOW (MM²/S) COMPARISONS OF 5 FRACTURE NETWORKS WITH K_X=K_Y=2000; B. AVERAGE VALUE OF MATRIX FLOW (MM²/S) COMPARISONS OF ALL FRACTURE NETWORKS WITH K_X=K_Y=2000 MD, IN FOUR PRESSURE DROPS MODELS (5,100, 1000, 2000) PA, ZERO PRESSURE OUTLET, WITH PERMEABLE FRACTURE SURFACES "INTERIOR FACE BOUNDARY" 237

FIGURE 6.34 A. FRACTURE FLOW (MM²/S) COMPARISONS OF 5 FRACTURE NETWORKS WITH K_X=K_Y=2000, B. AVERAGE VALUE OF FRACTURE FLOW (MM²/S) COMPARISONS OF ALL FRACTURE NETWORKS WITH K_X=K_Y=2000 MD, IN FOUR PRESSURE DROPS MODELS (5,100, 1000, 2000) PA, ZERO PRESSURE OUTLET, WITH PERMEABLE FRACTURE SURFACES "INTERIOR FACE BOUNDARY" 238

FIGURE 6.35 % FRACTURE FLOW ONLY OF FRACTURE NETWORKS WITH ISOTROPIC MATRIX PERMEABILITY (K_X=K_Y=2000 MD) 246

FIGURE 6.36 % MATRIX FLOW ONLY OF FRACTURE NETWORKS WITH ISOTROPIC MATRIX PERMEABILITY (K_X=K_Y=2000 MD) 246

FIGURE 6.37 % MATRIX FLOW COMPARISONS AVERAGE VALUE OF ALL FRACTURE NETWORKS IN FOUR PRESSURE DROPS MODELS (5,100, 1000, 2000) PA, ZERO PRESSURE OUTLET, WITH PERMEABLE FRACTURE SURFACES "INTERIOR FACE BOUNDARY", WITH EFFECTIVE PERMEABILITIES OF ALL MATRIX SCENARIOS 247

FIGURE 6.38 TEN SECTIONS INSIDE FRACTURE NETWORK MODELS 249

FIGURE 6.39 TOTAL PRESSURE CONTOURS OF FIVE FRACTURED NETWORK ANSYS CFD FLUENT FVM MODELS WITH $K_x=K_y=2000$ MD, $P=1000$ PA.....	250
FIGURE 6.40 THE TOTAL FLOW TRENDS OF FRACTURE NETWORK MODELS' SECTIONS WITH $K_x=K_y=2000$ MD, $P=1000$ PA	251
FIGURE 6.41 THE TOTAL FLOW HISTOGRAMS OF FRACTURED NETWORK MODEL SECTIONS WITH $K_x=K_y=2000$ MD, $P=1000$ PA	251
FIGURE 6.42 TOTAL FLOW COMPARISON BETWEEN ROUGH FRACTURE NETWORK 4 AND SINGLE ROUGH HORIZONTAL FRACTURE ($K_x=K_y=2000$ MD), AVERAGE VALUES OF PRESSURE DROPS (5, 100, 1000, 2000) PA	256
FIGURE 6.43 % FRACTURE FLOW ONLY, COMPARISON BETWEEN ROUGH FRACTURE NETWORK 4 AND SINGLE ROUGH HORIZONTAL FRACTURE ($K_x=K_y=2000$ MD)	256
FIGURE 6.44 % MATRIX FLOW ONLY, COMPARISON BETWEEN ROUGH NETWORK FRACTURE 4 AND SINGLE ROUGH HORIZONTAL FRACTURE ($K_x=K_y=2000$ MD)	257
FIGURE 6.45 COMPARISONS OF FRACTURE NETWORKS - FRACTURE FLOW ONLY (AVERAGE VALUE) (mm^2/s) WITH $K_x=K_y=2000$ MD, ($P=5, 100, 1000, 2000$) PA.....	259
FIGURE 9.1 SHADOW LINES PARALLEL TO THE FRACTURE SURFACE	281
FIGURE 9.2 ROUGH FRACTURE GEOMETRY, ORIGINAL AND DIVIDED INTO THREE SECTIONS	283
FIGURE 9.3 FRACTURE PROFILE THAT WAS CREATED FROM THE IMAGE DIGITIZER COORDINATES	283
FIGURE 9.4 THE AMENDED FRACTURE'S PROFILE OF THE FIRST SECTION	284
FIGURE 9.5 THE AMENDED FRACTURE'S PROFILE OF THE ENTIRE FRACTURE PROFILE.....	285
FIGURE 9.6 MATCHING THE NEW FRACTURE PROFILE WITH NAZRIDOUST, AHMADI AND SMITH (2006)'S FRACTURE'S PROFILE.....	286
FIGURE 9.7 COMPARISONS OF THIS RESEARCH'S FRACTURE APERTURE HEIGHT FREQUENCY WITH NAZRIDOUST, AHMADI AND SMITH (2006)'S FRACTURE.....	288
FIGURE 9.8 NORMAL DISTRIBUTION OF THIS RESEARCH'S FRACTURE COMPARED WITH NAZRIDOUST, AHMADI AND SMITH (2006)'S FRACTURE.....	289
FIGURE 10.1 EXAMPLES OF FRACTURE NETWORK BOUNDARIES IN SOME OF THE NETWORKS	294

Nomenclature

This is a nomenclature of key terms, Latin and Greek, and common units of measurement. Other terms have been defined directly underneath each equation for easy clarity.

Latin Letters

A	Area	H ₂ O	Water chemical formula
ADV	Average Difference Value	P	Pressure
C ₂	Factor of inertial resistance (1/k)	b	Half fracture height
CFD	Computational Fluid Dynamics	\bar{k}	Average permeability
CT	Computerized Tomography	Kx	Permeability in in-plane (x) Cartesian direction
D	Diameter or fracture aperture	Ky	Permeability in through plane (y) Cartesian direction
F	Forces	L	length
F	Friction factor	Le	Equivalent length (fluid travel distance)
FEM	Finite Element Method	L _i	Segment length
FVM	Finite Volume Method	m	Mass
\bar{h}	Effective Fracture aperture	PDF	Portable Document Format (file type)
h_{avg}	Average heights of fracture apertures	Q	Flow rate
h_{eq}	Equivalent Fracture apertures	Q _f	Fracture flow rate
H _f	Fracture height	Q _m	Matrix flow rate
h_m	Formation height	Q _t	Total flow rate
I _A	Anisotropic ratio of permeability	Re	Reynolds number
JPEG	Joint Photographic Experts Group (file type)	S _i	Source term
JRC	Joint roughness coefficient	\vec{u}	Velocity
k	Permeability	V	Average velocity
N	Frequency	y	Through plane Cartesian axis direction
		x	In-plane Cartesian axis direction
		z	Cartesian axis direction
		∅	Porosity

Greek letters

θ	Angle	∇p	Pressure gradient
Θ	Tortuosity	ΔP	Pressure drops
cos	Cosine angle value	ρ	Density
sin	Sine angle value	μ	Viscosity
σ	Standard deviation	β	Inertial coefficient
μ	Average fracture apertures	ρ	Density
F	Source term of momentum	α	Fracture geometry constant

Units

$^{\circ}$	Angle Degrees in Cartesian axis
%	Percent
cm	Centimetres
cp	centipoise viscosity unit (kg/m.s)
Kg	Kilogram
m	Metre
s	Second (time unit)
mD	Millidarcy (permeability unit)
mm	Millimetres
Pa	Pascal (pressure unit) (kg/m.s ²)
μm	Micrometre or Micron

1 Introduction

1.1 Overview

The global energy map is currently witnessing many challenges, attracting all countries' leaders and scientists to predict and solve its future. There is a strong relation with the nerves of world economic status, causing many ambiguities about the future of energy, affecting global economic growth, price fluctuations and political conflicts. In spite of good development and progress worldwide in renewable energies, hydrocarbons are still the main supply of the world's energy. The consumption of hydrocarbons has been increasing simultaneously with many factors, such as global population growth and economic growth: particularly the accelerated growth of Asia, mainly China and India. On the other hand, the majority of the market's hydrocarbons are supplied from conventional reservoirs, and the majority of them are reported to have declining production; very few new reservoirs have been discovered and are starting to supply the market (Jahani, Haugen and Berge 2015; Bo et al. 2014; Kaldor, Karl and Said 2007). Therefore, it is necessary to search for unconditional resources of hydrocarbon, in the expectation that a third of the world's hydrocarbon consumptions will be supplied from them in near future (Devold 2006).

Most geological formations are fractured, and fractured reservoirs contain approximately 60% of the approved hydrocarbon quantities in the world. They can be classified into conventional reservoirs "naturally fractured reservoirs" and unconventional reservoirs "hydraulically fractured reservoirs". Thus, fractured media is considered one of the main topics in reservoir engineering. Reservoir engineers and geologists invest effort to evaluate fractures' functionality, and highlight any development plan (Abushaikha et al. 2015; Jahani, Haugen and Berge 2015; Geiger, Schmid and Zaretskiy 2012).

As well, fractured media are involved not only in hydrocarbon production and recovery of reservoirs, but have key involvement in other important sectors such as: remediation of environments, hydrology, geohazard mitigation, and geothermal exploitation. Therefore, the ability to predict fluid migration in these formations, and the characterization of transport properties, has motivated massive research endeavour regarding flow in these geological formations (Karpyn and Piri 2007 p. 1).

1.2 Challenges Of Subsurface Fractured Media

Formations' fractures introduce structural discontinuities in rock formation bodies, which impact on fluids' mobilization/migration within it (Karpyn and Piri 2007). Fractures in fractured media vary by size and location, with a scale that ranges from micro cracks measured by micrometre, to large faults measured by kilometres. Fractures have a main function, which is as the hydraulic conductors of fluid, and giving easy pathways to flow in fractured media. They have a main effect on the pattern of fluid flow and on transport process in fractured media, or may act as barriers of fluid to flow in these media, while the matrix is considered as fluid storage (Sahimi 2011; Tiab and Donaldson 2004). Karpyn and Piri (2007) stressed the above and confirmed that fractures control overall rock conductivity, while a porous matrix is fluid storage. Therefore, fractures of fractured media are considered as both a problem and an opportunity in these media, based on the fracture's function. The opportunity side considers fractures' important permeability for fluid flow, giving an easy way for hydrocarbons to flow to wells rather than porosity, while the matrix is the main storage provider of hydrocarbon. However, for the problem side it is the opposite image, and fractures are then considered as obstacles to fluid flow, for example: fracture orientations that are not aligned with flow or pressure gradient directions; fractures that do not connect between inlet and outlet boundaries in formations; fracture networks in fractured formations that have numerous small dead-end zones which will not contribute to flow in fractures; blocked fractures that don't allow fluids to flow; rougher fracture surfaces which cause higher pressure drop; material precipitation on fracture surfaces which block pores of fracture surfaces and isolate fracture/matrix fluid movements; and adsorption of fluids in formations as heterogeneous property effects of fluids on pores' structure scale and affect seepage capacity (Li et al. 2021; Luo et al. 2020; Yin et al. 2017; Rasouli and Rasouli 2012; Sahimi 2011; Karpyn and Piri 2007; Sarkar, Toksöz and Burns 2004; Tiab and Donaldson 2004; Zimmerman and Yeo 2000; Zimmerman and Bodvarsson 1996 pp. 44-45; Golf-Racht 1982). In reservoir engineering, fractures are considered by their effect on fluid flow, while for geologists they are regarded with a different perspective as resulting from paleo-stresses that were applied on media through a history of time (Sahimi 2011; Karpyn and Piri 2007; Sarkar, Toksöz and Burns 2004; Tiab and Donaldson 2004; Golf-Racht 1982).

Modelling, mapping and understanding fluid flow is one of the main challenges in fractured media, due to many reasons: particularly, the complex geometry and the interaction between fractures and surrounding matrices. There are many types of models, such as mathematical, numerical and experimental, that have dealt with fractured media's flow in order to approximate and solve flow issues (Holstein 2007; Karpyn and Piri 2007; Sen 1995). However, in spite of all these models, there remain many challenges that have not been solved, such as: isotropic and anisotropic nature of matrix effects on fractured domain flow; choosing a suitable representation of fracture geometry in modelling fractured media (such as smooth parallel plates fracture with single aperture height, single rough fracture with varied apertures, or fracture network with either single aperture or rough fractures); and fracture/ matrix interactions and fluid movement between fracture and matrix's effects on fractured domain flow. These challenges demand solutions for future developments, in order to fully understand flow in fractured media (Sen 1995). Thus, based on these challenges of flow in fractured media, this research judged that understanding of this fluid flow needed to be improved in order to better understand flow behaviour in fractured media. It was essential that these studies were realistic and based on geometries that mimicked real fractured media conditions, in order to get more accurate visualization and results of fluid flow. This was because many models in the previous literature were based on parallel plates fracture geometry assumptions, which have been used widely either as single fracture or fractured networks in domain modelling, as reported by Luo et al. (2020); Luo, Tang and Zhou (2019); Luo et al. (2018); Lu et al. (2017); Rasouli and Rasouli (2012); Sahimi (2011); Popov et al. (2009); Tiab and Donaldson (2004); Sarkar, Toksöz and Burns (2004); Sen (1995) and Golf-Racht (1982). However, in reality, fractures are not smooth surfaces but have varied shapes and patterns (Sahimi 2011; Tiab and Donaldson 2004; Nelson 2001; Sen 1995; Golf-Racht 1982).

Unexpected behaviour of fractured reservoir production in many fields arose from unclear understanding of fractures' effects on fluid flow. Therefore, there was a need for better characterization of flow in fractured media in various scales, then, a transfer of data findings to bigger scales, which could simulate all fractured media. The current situation of fractured reservoir studies has usually consisted of integrated workflow, and have been multi-disciplinary from different sectors (Bourbiaux et al. 2002). Workflow integration includes many steps, such as: choose a proper model for simulation; model fracture network in the geologically

constrained method; characterise the properties of the fracture network; and simulate flow behaviour of the reservoir (Sarkar, Toksöz and Burns2004).

Pressure is the main drive mechanism that pushes fluids in reservoirs/formations for migration towards oil wells or flow in subsurface layers, known as “draw down pressure”. Draw down pressure is influenced by several factors, such as: permeability, porosity, fluid type (single phase, multi-phase), temperature, etc. As well, it’s good to note that fractured formations consist of two different characterizations, with different media properties, in the same rock formation/ location, which act upon each other: fractures and surrounding matrix (Sahimi 2011, Tiab and Donaldson 2004, Dake 2001; Nelson 2001; Sen 1995; Golf-Racht 1982). Thus, knowing the accurate estimated value of pressure drop along the length of flow inside fractures ($\frac{\Delta P}{L}$) is essential for understanding the migration of fluid (Sahimi 2011; Holstein 2007; Tiab and Donaldson 2004; Sen 1995). There are many factors which affect ($\frac{\Delta P}{L}$), such as: fracture aperture change D , fluid type (single or multiphase fluids), flow regime (laminar, turbulent) and fracture friction factor f_D : equation 1.1 below clarifies it.

$$\frac{\Delta P}{L} = (f_D) \frac{\rho}{2} \frac{v^2}{D} \quad (\text{Darcy-Weisbach equation}) \quad (1.1)$$

(White 2003; Eskinazi 1968)

The factors which determine ($\frac{\Delta P}{L}$) in fractures are challenging, and needed to be addressed and estimated accurately:

- a. Varied fracture apertures along the flow, which mean the fracture’s cross section area is changing at each point along the flow; accordingly, fracture aperture size could abruptly decrease/ increase.
- b. Effective roughness and tortuosity of fracture surfaces along the fracture path. Fracture roughness is an important parameter in determining pressure drop. Vortices are generated along the flow when fluid is in contact with internal fracture surfaces. These rough surfaces change the flow direction into a cyclone circle “vortices or eddies” in that region, which affects fracture flow direction between the bulk flow in the centre of the fracture’s aperture and the fracture surfaces (Briggs, Karney and Sleep 2014).

- c. Velocity changes along the flow at each point due to fracture cross-section area changing.
- d. Pressure changes along the flow at each point inside fracture due to the velocity changing. This means that flow interaction between fracture and surrounding matrix changes too, due to pressure differences between the matrix and fracture (Sahimi 2011; Sen 1995; Saidi 1987).
- e. Matrix properties that surround fracture surfaces, such as permeability and porosity, change along the flow (anisotropic properties), and affect fluid movement between fracture and matrix (Sahimi 2011; Tiab and Donaldson 2004; Dake 2001; Nelson 2001; Sen 1995; Golf-Racht 1982).

Computational Fluid Dynamics (CFD) ANSYS-Fluent FVM is a very efficient tool, and the efficiency of its models have been proven in many difficult researches. It has many positive factors such as: accuracy of models; fast results; and the ability to recreate conditions that might not be possible to create in physical experiments. In addition, the cost is low in comparison with physical models' costs (Suri et al. 2020; Karimzade et al. 2019; Roslin, Pokrajac and Zhou 2019; Chen et al. 2017; Liu, Li and Jiang 2016; Jahani, Haugen and Berge 2015; Schafrik and Millar 2015; Gidaspow, Li and Huang 2013; Geiger, Schmid and Zaretskiy 2012; Rasouli and Rasouli 2012; Rasouli and Hosseinian 2011; Crandall, Ahmadi and Smith 2010; Gustafsson, Westerlund and Hellström 2010; Crandall, Bromhal and Smith 2009; Gu et al. 2009; Petchsingto 2008; Nazridoust, Ahmadi and Smith 2006; Sarkar, Toksöz and Burns 2004). However, in the judgement of this research, in spite of all these benefits of CFD, it has only been used with simplified conditions instead of combining many conditions in one model in modelling fluid flow in fractured media, such as: considered simple fracture geometry in modelling fractured media (for instance, parallel plates fractures with single aperture height instead of rough varied apertures fracture); considered impermeable fracture surfaces and excluded matrix flow contribution in a fractured domain; and assumed isotropic matrix properties that surround fracture surfaces. However, ANSYS CFD Fluent FVM has the ability to include more variables in one model, such as considering anisotropic matrix permeability, rough fracture geometry, and permeable surfaces of fractures that can interact with surrounding matrix. All these variables can affect on each other within one model to envisage fluid flow in fractured media (ANSYS, 2013; ANSYS, 2011).

Thus, in this work, ANSYS CFD-Fluent FVM modelling was used for flow simulations in the methodology, which included mimicked real conditions of fluid flow in fractured formations to investigate both medias' pressures, and accordingly flow inside the fracture and surrounding matrix. As well, it was used to analyse the interactions between fracture and matrix (matrix-fracture interface layer). This modelling included a range of conditions of fractured media: a parallel plates fracture with a single aperture height, rough fracture geometry with varied apertures, and rough fracture networks. The results of these models were compared, to highlight the geometry effects and anisotropic matrix permeability on fractured media flow. In addition, these results were validated with the previous works of ANSYS CFD-Fluent FVM in fractured media that were conducted by [Crandall, Ahmadi and Smith \(2010\)](#); [Nazridoust, Ahmadi and Smith \(2006\)](#) and [Sarkar, Toksöz and Burns \(2004\)](#), and theories from the literature as reported by [Briggs, Karney and Sleep \(2014\)](#) pp. 538-539; [White \(2011\)](#) p. 269; [Douglas et al. \(2005\)](#) p. 326 and [Eskinazi \(1968\)](#) pp. 378, 382.

1.3 Aim And Objectives

1.3.1 Aim

The aim of this study consisted of two parts as following:

1. Investigate fluid flow in fractured media with real formation conditions, through CFD modelling, to understand the flow regime and compare it with the current understandings of the literature.
2. Develop more accurate "fracture friction factor models" that account for pressure drops in fractures of fractured formations, analytically and numerically from the CFD models, which could be used in flow simulators, or in field developments.

1.3.2 Objectives

The following objectives summarize the route map which was followed to achieve the aims of this of this research:

1. Create a parallel plates fracture geometry domain with single aperture by ANSYS CFD-Fluent, using the same properties of real formations as isotropic and anisotropic matrix permeability, to investigate flow/velocity with many fracture surface boundary conditions (interface layer), permeable and impermeable, and validate it.
2. Create a rough fracture geometry domain with varied apertures by ANSYS CFD-Fluent, and use the same properties of real formations, such as isotropic and anisotropic matrix permeability, to investigate flow/velocity with many fracture surface boundary conditions (interface layer), permeable and impermeable, and validate it.
3. Compare the results of flow and velocity of the rough and parallel plates fractures, to have a better vision of flow with both simplified and rough fractures.
4. Calculate friction factor values in rough fractures with different boundaries of fracture surfaces, permeable and impermeable with the surrounding matrix, and make a comparison among them, to distinguish the different outcomes of these.
5. Develop an analytical model of friction factor in rough fractures, which accounts for most of the heterogeneous properties in fractured media in subsurface layers, then, compare it with the previous models and validate it.
6. Develop a numerical model of fracture friction factor from the CFD rough fractures' results, which accounted for formations' heterogeneity, then compare it with the previous models and validate it.
7. Create rough network fracture geometry domains with varied apertures and patterns by ANSYS CFD-Fluent, using the same properties of real formations as isotropic and anisotropic matrix permeability, and investigate flow, particularly (% of flow) in the open fractures and surrounding matrix. Then, compare the results among networks, and compare the results with previous models from the literature.
8. Compare rough fracture network flow, particularly, total flow and % flow of (fracture and matrix) contributions separately, with a single rough fracture horizontal-orientation model, to visualize the differences in results among them.

1.4 Thesis Outline

This thesis is outlined as below:

1. **Chapter 1:** gives a brief overview of fractured media and the challenges to model and estimate flow in the media, which provides brief justifications of this research. Moreover, the aims and objectives of this research are outlined and summarized.
2. **Chapter 2:** offers a detailed and up-to-date literature review. Care was taken to the best efforts of this research to have up-to-date, accurate literatures, from respected resources.
3. **Chapter 3:** presents CFD methodology theories, concepts and all the important information of governing equations employed in this research. As well, it presents the methods of creating rough fracture geometry, and its applications in ANSYS CFD Fluent.
4. **Chapter 4:** presents solution procedures and validations of parallel plates and rough fractures' CFD models, with horizontal orientations. As well, it offers models' validations, then concludes with comparisons of results between these two types of fracture geometries.
5. **Chapter 5:** covers calculations of fracture friction factors of rough fracture. As well, it introduces the method of developing a mathematical fracture friction factor, and developing a new analytical fracture friction factor. It then contains comparisons and validations of these friction models.
6. **Chapter 6:** presents generating and ANSYS CFD-Fluent modelling of rough fracture network geometries and patterns. The results are comparisons among networks of flow and with the previous models from the literature. As well, it offers comparisons of rough fractured network models with rough single horizontal orientation fracture models.
7. **Chapter 7:** presents a main summary of the conclusions and findings of this research, as well as highlighting the main pillar contributions of this research, and offering recommendations for future works.

1.5 Contributions to knowledge

This research has contributed to the industry and literature as following:

1. Two new proposed rough fracture friction factor models were developed and introduced to industry: first, an analytical model applicable until Reynolds number values equal or less (≤ 10); and second, a numerical model suitable to be used until Reynolds number value 3000. Both models account for: permeable fracture surfaces; fracture roughness; tortuosity; and anisotropic matrix permeability that includes two cases: first; different matrix layer permeabilities; and second, for each layer anisotropic matrix permeability in-plane (K_x) and through plane (K_y) in Cartesian directions.
2. This research offered analytical and qualitative data of fluid flow in fractured media, with many fractured media domains, starting with a parallel plates fracture with single aperture, including rough fractures, and up to the most complicated geometry models which were rough fractured media networks, using Computational Fluid Dynamic ANSYS CFD Fluent. The fractured models of this research offer many contributions to knowledge for the industry and the literature, as follows:
 - a) A parallel plates fracture with single aperture height doesn't represent the reality of flow in fractured media, and will highly mislead fracture and matrix flow calculations in fractured domains.
 - b) Rough fracture geometry with varied apertures along the flow will reflect a more accurate estimation of flow in fractured media.
 - c) Matrix interaction with a rough fracture is very important, as matrix flow has a good contribution to flow in fractured media.
 - d) Considering impermeable fracture surfaces will lead to highly underestimating flow in matrix, and overestimating fracture flow.
 - e) Anisotropic matrix permeability effects of in-plane (K_x) permeability and through plane (K_y) permeability have a significant effect on flow in fractured media. Through-plane (K_y) permeability is as important in fractured formations as in-plane (K_x).

- f) Rough fracture networks with realistic patterns will have a better opportunity to represent fractured formation flow calculations. Therefore, a single fracture geometry (parallel plates fracture or rough fracture), horizontal or with angle in Cartesian axis, cannot represent flow in fractured domain conditions and will lead to wrong calculation of flow percentages in fractures and surrounding matrix.
- g) Matrix in rough fractured networks are the main fluid conductor and provider with a reasonable and good matrix permeability value surrounding fractures.
- h) Matrix flow in fractured media reflected non-linear increase in comparison with Darcy law. Therefore, Darcy formula underpredicts matrix flow in fractured domains.
- i) Fractures in fractured network formations can represent barriers of flow instead of facilitators, if a fracture does not pass through the domain.
- j) Thus, fractures' rough geometry, matrix flow consideration, fracture network's pattern and matrix/ fracture interaction as one model have key impacts on the flow percentage of the fractured network domain.

2 Literature Review

2.1 Reservoir Modelling Overview

The process of reservoir simulations consists mainly of firstly, dividing a reservoir into cells, then assigning each cell with the flow properties of the reservoir (permeability, porosity, matrix, etc.). This is considered the most important step as predictions of future production from a reservoir depend on correct estimation of these properties. At the same time, assigning flow properties of fractured reservoirs is the most challenging step. For example, a dual porosity - dual permeability model, which was used for fractured reservoir simulation, consisted of assigning equivalent permeability tensor (Transmissivity) of each grid cell in the beginning of the simulation before the start of production ([Chung 2010](#); [Wu and Pruess 2000](#); [Golf-Racht 1982](#); [Kazemi et al. 1967](#); [Warren and Root 1963](#)). At the production stage, these parameters will be changed with time and new parameters will be available, and an update process is necessary to match with production data; this step called History matching. The main goal of the History matching is to have an accurate model that predicts reservoir production with time, in order to have better images of reservoir forecast, which is useful in many development purposes. The expected model is to give an approximate prediction which matches with the initial predictions; however, in reality, these models are not necessary to give an accurate prediction, and results may be totally different to predictions and effects on production expectations of any field. This may disrupt the development, and create cost and delay for developers. Thus, based on this current situation, it is highly necessary to understand physics and flow behaviour in complex fractured media, in order to reduce the uncertainties and have more accurate models, that can reliably predict flow in fractured media ([Chung 2010](#)).

2.2 Naturally Fractured Formations Overview

The records of geological formations indicate that most of the earth's upper crust is fractured; therefore, natural fracture media are an important topic in many sectors that are related to our lives. One sector is hydrogeologists, who work on modelling and analysing groundwater flow of contamination fluids, such as radioactive waters of nuclear stations, which have become a highly concerning topic internationally. Another is reservoir engineering, due to the massive quantities of crude oil in naturally-fractured formations globally. All these different kinds of fluids reside and flow in naturally fractured formations; however, characterising these formations is difficult due to their complexity. It therefore requires economic planning, a good level of understanding and accurate modelling. (Sahimi 2011 p. 143; Tiab and Donaldson 2004; Sen 1995). There are various definitions of fractures in fracture formations. For instance, from the geo-mechanical view, fractures are the results of ruptures in formations that led surfaces to lose cohesion of particular minerals, which induced the construction of a fracture. If there is a displacement of formation then fractures will be called "Faults", or if there is no displacement then fractures will be called "Joints": Figure 2.1 clarifies this. However, the general definition describes a formation's fractures as displacement discontinuities in rocks, which appear as local breaks in a formation's body, and which are considered the natural sequence of the rock's properties. Thus, fractures may be the result of mechanical failures of the rock's strength. This can be due to many reasons, either natural geological stresses (such as lithostatic pressure changes, tectonic movement, and thermal stresses), or by manmade activities (such as fluid withdrawal from formations, since fluids partially support the weight of the overburdened rocks, high fluid pressure 'Fracturing fluid', and drilling activity).

The main functionality of fractures is as fluid flow carriers, due to the fact that fractures can provide hydrocarbon channel transformers between a reservoir matrix that has the main hydrocarbon quantity and producing wellbore. As well, fluid flow in fractures is an important consideration in structure formations such as dams, etc. Therefore, a formation's fractures can be considered as either fluid flow facilitators or as obstacles, and each case will be depend on a fracture's fractal properties, type, orientation and investigation targets (Tiab and Donaldson 2004; Golf-Racht 1982; Warren and Root 1963).

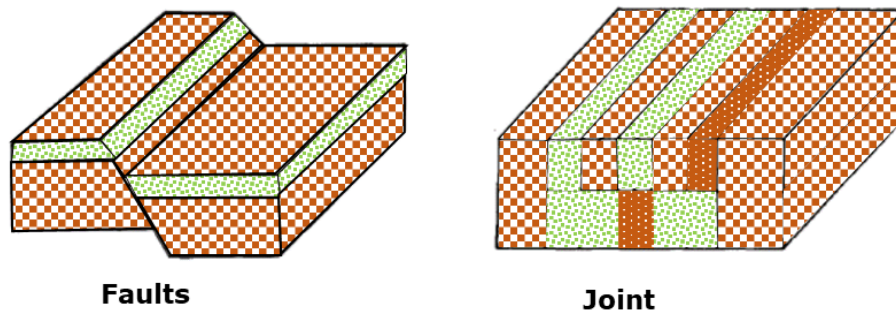


Figure 2.1 Schematic distinguishing between faults and joints in fracture formations

(adapted from Golf-Racht 1982 p. 6)

2.2.1 Natural fracture types

Fracture classification relies on time and patterns at the time of the fracture's creation in a formation. Therefore, fractures can be classified in two ways: geologically; and by reservoir engineering. Geologically, these types of fractures have been classified based on stress/strain conditions, such as extension fractures, shear fractures, and tension fractures, and also other geological paleostress conditions, such as regional fractures, tectonic fractures, and constructional fractures. The fractures that been created due to these stresses are known as "fracture channels or fracture voids", and volumes vary, ranging from only several micrometres (micro fissures) to continental fractures with several thousand kilometres (Tiab and Donaldson 2004). Reservoir engineering classifies fractures as reported by Nelson (1987) into four types of naturally fractured reservoirs, relying on the extent to which fractures have altered the permeability and porosity of the reservoir matrix, as: type 1 reservoirs, where fractures provide all storage of reservoir permeability and capacity; type 2 reservoirs, where fractures add extra permeability to reservoir permeability but matrix already has very good permeability; type 3 reservoirs, where fractures provide the essential reservoir permeability, and the reservoir matrix has negligible permeability but contains most of the hydrocarbons; and type 4 reservoirs, where fractures are filed with minerals, therefore act as barriers for fluid migration. Therefore, in general modelling fractures are treated as flow channels or cracks, and two main properties will be considered: first as the storage capacity for hydrocarbon fluids; and secondly, as fluid transmission or transfer capacity 'fracture conductivity'. These two properties are dependent on a fractures' dimensions, such as length, width, and height. Generally, the volume of fluids in fractured reservoirs is less than 4%,

while a reservoir matrix with “Inter-granular porosity” contains a majority of fluids at around 96-99 % (Tiab and Donaldson 2004 p. 425; Golf-Racht 1982; Warren and Root 1963). Thus, Sahimi (2011) suggested that any modelling or characterization of fractured porous media can usually be divided into three related but distinct parts, as: a single fracture; a network of fractures; and a fractured porous medium.

2.3 Natural Fractures’ Parameters

Fractured formations are very different from conventional formations due to the space variation of fracture characteristics, such as size, orientation and general description, which are complicated and irregular. Therefore, to study any fractured formation a special procedure must be followed. This starts with examining a single fracture’s local intrinsic characteristics, such as: opening (width), size, and nature of fracture. Then it continues with examining the network or multi-fracture’s other characteristics, such as: orientation, distribution, and density or intensity (number of fractures in section). The last step is to generate a bulk unit that consists of fractures and the surrounding matrix, which will be a small model or prototype that reflects fractured information conditions; Figure 2.2 below clarifies this procedure. Thus, each parameter of single and multi-fractures will be clarified briefly in the following sections (Tiab and Donaldson 2004; Nelson 2001; Golf-Racht 1982).

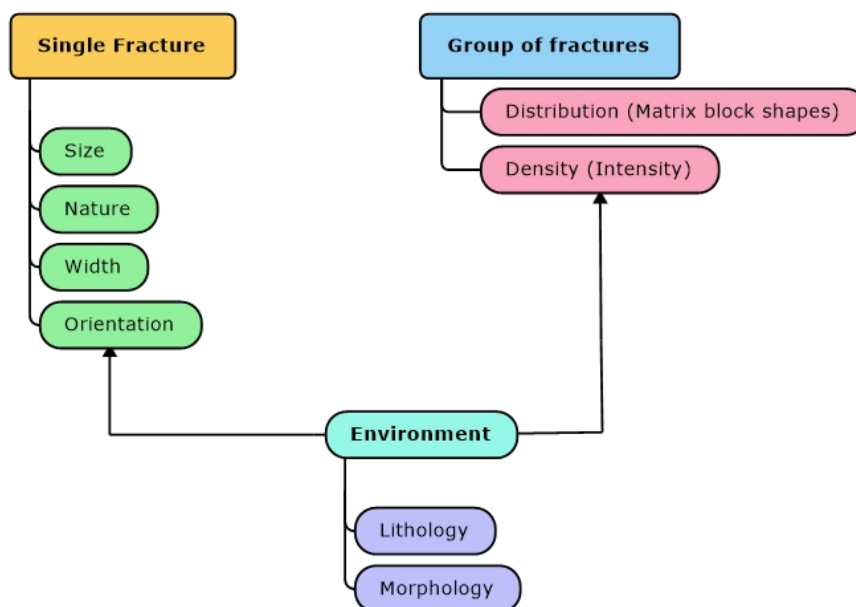


Figure 2.2 Fractured formations study procedure
(adapted from Golf-Racht 1982)

2.3.1 Single fracture parameters

There are many parameters of single fractures, which are briefly clarified here. First, fracture opening, sometimes called fractured width, which is the distance between the fracture's surfaces or walls. This depends on many factors such as: fracture depth in formation, lithological characteristics of the rock, rock type, and nature of stresses in the subsurface/reservoir environs, such as pore/lithostatic pressures. These factors affect fracture width, which generally will be around 10-200 micrometre; the most frequent statistics show a fracture width range of 10-40 micrometre. The measurement of fracture opening is usually carried out in laboratory tests, but as the core of a reservoir/formation is taken from the subsurface into a laboratory, it will result in changes of statistic and pore pressure and lead to rock expansion. Therefore, these opening measurements will not reflect the opening size in real conditions (Golf-Racht 1982). Second, fracture sizes; there are three types of fracture size, based on the relationship between fracture length and thickness of layer. These types are: minor, average and major. Thus, the relation between a fracture's length and rock length determines the type of fracture. Thus, if fracture length is less than a single layer, then it's a minor fracture; it's an average fracture when it passes through many layers; and a major fracture when the fracture length extends significantly, usually tens or hundreds of metres. Third, the fracture orientation parameter describes a single fracture with its surrounding environment in subsurface layers, to help identify fracture direction in relation with a desired study. Single fracture orientation is usually determined by the original forces / stresses that created the fracture in formation (Nelson 2001; Golf-Racht 1982). Fourth and last, fracture nature (morphology) represents the state of a fracture under general observation, which is an important factor as it will indicate fracture porosity and permeability of a fracture. It can usually be observed by core test / well logs. Fracture morphology can be classified into many types, but the most common are: opening (closed, joint); fracture walls (smooth, rough); and filling (fracture filled/closed with minerals or particles) (Nelson 2001 p. 37; Golf-Racht 1982).

2.3.2 Fracture network parameters

Fracture network parameters describe a group of fractures in formations which can be briefly classified as follows. First, fracture distribution; in fractured media this will be controlled generally by the type of stresses that caused these fractures to be generated in these domains (Golf-Racht 1982). Ruhland (1973) clarified that

fracture network distribution can be homogenous when it has a equivalent system or continuous intercommunication, and similarly, when a fracture network system is interrupted and separated by the matrix (no intercommunication). In between these two cases there are varied degrees of intercommunication, where one fracture system is predominant and another is interrupted. Figure 2.3 presents four kinds of fracture networks, with different values of fractured intercommunication. Second, fracture density reflects the degree of fracturing in any particular rock; in other words, it represents the ratios of fractures to the remaining bulk of rock. This ratio can be calculated in many methods, such as: volumetric fracture density, area fracture density, and linear density. Third, matrix blocks among fracture network; a fracture network in a reservoir formation could be distributed in various directions, which divide the bulk unit of matrix into various sizes; each one will be called a matrix block. Each matrix block will be trapped with surrounding fractures, and they will be hydrodynamically separated, even if there are contact points among these matrix blocks (Golf-Racht 1982). Matrix blocks can be defined by volume, shape, and height, and the shapes are irregular in real fractured formations; however, for the sake of simplifying calculations they are reduced to simplified geometry volumes. There are various shapes introduced which have descriptive shapes, and can be classified to geometric dimensions of each block to facilitate calculations (Ruhland 1973). Saidi (1987) p. 53 stressed that matrix block geometry plays a major role in evaluating the recovery of fractured media, particularly in determining block size and distribution.

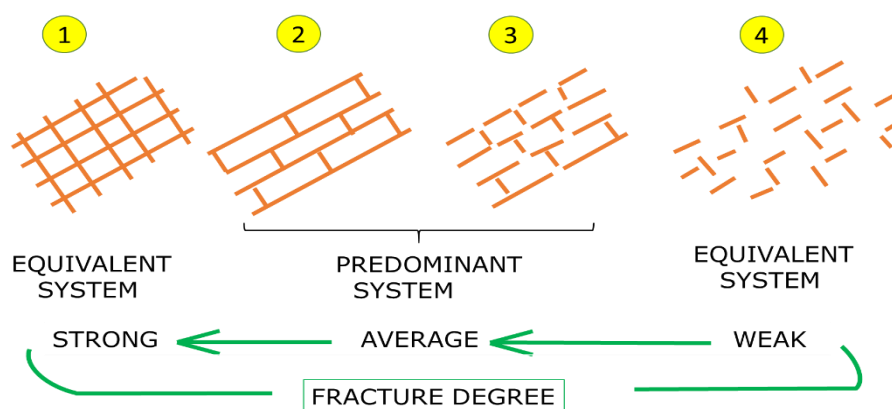


Figure 2.3 Four fracture networks, where each network has a different degree of intercommunication, classified from weak to strong connections
(Adapted from Ruhland 1973 p. 95)

2.4 Porosity And Permeability Of Fractured Media

In any reservoir that contains hydrocarbons, or any fluid flow in subsurface layers of earth crust, knowledge of porosity and permeability are essential before questioning other concerns, such as fluid amount, fluid types, fluid rates and estimations of fluids recovery. These two properties have major effects on flow in subsurface layers or reservoirs. Porosity represents the void spaces in rock bulk volume, and permeability represents rocks' measured ability to transmit fluids through (Tiab and Donaldson 2004 p. 116). Fractured medias / reservoirs are considered unconventional formations or reservoirs. Therefore, modelling, examining and analysing fluid flow in fractured media requires special care and attention to the evaluation of the main formation properties, ie. porosity and permeability, of both fractures and matrix-fracture systems. These properties are not considered similar to the standard (or classic) conventional formations or reservoirs, which can be described only among grains of matrix - matrix interactions (Golf-Racht 1982, Saidi 1987). Thus, the general description of these two properties in fractured formations is highlighted as following:

2.4.1 Porosity

Porosity in fractured reservoirs/media can be divided into two types of porosity systems: the first type is primary porosity, which represents void spaces among grains of matrix due to varied sizes and shapes of grains; and the second type is secondary porosity, which represents void spaces among a fracture's surfaces. Porosity is usually represented as a percentage value out of bulk rock volume. (Nelson 2001 p. 83; Golf-Racht 1982 p. 147).

Interpreting reservoir/formation data does not recognize the potential of recovery reduction, and may mislead reserve estimations, due to the adverse interactions between these two porosity systems in one formation. The interaction complexities between these two porosity systems make early calculations of reserve estimations or recovery factor much more complex than conventional reservoirs/formations. Thus, it's necessary at an early stage to study matrix/fracture interactions, to analyse and illustrate flow rates between matrix and fractures in response with overall fluid pressure gradients. These analyses can be achieved by many methods, for example observing thin sections of fracture planes, and analysing a

whole core. In some cases, the interaction between these two properties are good, however in others the interaction is inhibited by other factors, such as fracture mineralization participation, and etc. (Nelson 2001).

Thus, total porosity in fractured reservoirs/formations represents total void spaces in rocks, and can be observed from different methods of laboratory tests, then simply calculated by adding the two porosity systems. It's good to note that secondary porosity is usually much less than first porosity, at around 0.1 % to 5 % of bulk volume of rocks. The following equations 2.1 and 2.2 clarify this. (Tiab and Donaldson 2004 p. 502; Golf-Racht 1982 p. 148).

$$\phi_t = \phi_m + \phi_f \quad (2.1)$$

$$\phi_t = \phi_f + \phi_m = \frac{V_{pf}}{V_{bt}} + \frac{V_{pm}}{V_{bm}} = \frac{V_{pf}}{V_{bt}} + \frac{V_{pm}}{(1-\phi_f)V_{bt}} \quad (2.2)$$

Where: ϕ_t = total porosity, ϕ_f = fracture porosity, ϕ_m = matrix porosity, V_{pf} = volume voids of the fracture, V_{bt} = total bulk volume of the rock, V_{pm} = volume voids of matrix, V_{bm} = Matrix bulk volume only

(Tiab and Donaldson 2004 P504, Golf-Racht 1982 p. 148)

2.4.2 Permeability

Permeability represents rocks' ability to transmit fluids, and it depends on the effective porosity of the rock. This has many factors affecting it, such as grain shape, grain size, grain distribution, grain packing, cementation among grains, and the existence of fractures (Donaldson and Tiab 2004 p. 100; Dake 1978). One of the standard and most famous mathematical tools was developed by the engineer Henry Darcy in 1856, describing his work in the municipality of Dijon (France) to provide a water source (fountain) for the city. Darcy introduced a formula as equation 2.3 that connects water flow rate through a sand filter. This later became a theoretical base with applications for many scientists and engineers for further development in several fields. Darcy formula introduced a hydraulic conductivity which refers to "absolute permeability" with 100% saturation of a single fluid, which can be applied in conventional formations and reservoirs (Brown 2002). However, later it was developed by other scientists and engineer to include many phases. In many cases in formation media, there are many phases of fluids together in one formation, so permeability is called "effective permeability". To

calculate the ratio of a fluid phase permeability, it can be calculated by a ratio of effective permeability to the absolute permeability in that rock. For example, water and oil $K_{ro} = K_o/K$, K_{ro} will be called a "relative permeability" of oil in rock. (Chery and de Marsily 2007 p. 37; Tiab and Donaldson 2004 p. 100; Dake 1978).

$$Q = \frac{A \cdot K}{\mu} \frac{(\Delta P)}{L} \quad (2.3)$$

Where: K = matrix permeability, A = cross sectional area of matrix, μ = fluid viscosity, L = matrix length and (ΔP) = pressure gradient (Chery and de Marsily 2007)

Fractured media are unconventional formations, and permeability may generate some confusion due to the different systems in one formation. Therefore, to avoid such confusion, permeability has been classified into two types: primary permeability, which refers to matrix permeability, and secondary permeability, which refers to fractures (Donaldson and Tiab 2004 p. 101). As these two permeabilities are located in the same system, and interacting with each other, the definition is more specific in fractured media; matrix permeability, fracture permeability, and system permeability as (fracture-matrix) together (Golf-Racht 1982). There are many methods to determine these permeabilities in fractured media, which are based on the formation's properties, such as low or high matrix permeability surrounding fracture surfaces etc. However, below will be highlighted the common methods to calculate permeability that are related to this research, such as: fracture permeability; matrix-fracture permeability as a system affecting on each other; and anisotropic matrix permeability layers in formations, to clarify the effects of anisotropic matrix permeability on fracture and matrix flow, as investigated in the following chapters.

Sarkar, Toksöz and Burns (2004) pp 5-6 stressed that flow in real fracture formations suffers from rough walls and variable apertures, and that flow in saturated fractures tends to follow the path of least resistance, which is referred to as the biggest fracture aperture in a block. Therefore, for a group of fractures, height can be replaced with a term " h_{eq} ", then fracture permeability can be calculated as equation 2.4. Moreover, for inclined fractures, permeability magnitudes are in the direction of macroscopic gradient of pressure, and are

affected by a reduced factor of cosine value of the angle (θ) in comparison with a horizontal fracture in same direction; [equation 2.5](#) presents this.

$$K_{ff} = \frac{h_{eq}^2}{12} \quad (2.4)$$

$$K_{ff} = \frac{h_{eq}^2}{12} (\cos \theta) \quad (2.5)$$

Where: K_{ff} = fracture permeability of a block, h_{eq} = equivalent fracture aperture

In a fractured formation where the matrix has good permeability and porosity, and there are fluids trapped in fractures and surrounding matrix, both media are contributing to flow in one system. This means the fracture and surrounding matrix form a bulk hydrodynamic unit, and the cross-section model is entirely contributing to flow. Thus, system permeability is as [equation 2.6 \(Golf-Racht 1982 p. 158\)](#).

$$K_f = \frac{b^3}{12 h} \quad (2.6)$$

Where b = fracture height, h = total formation height

The total permeability of a matrix-fracture formation can be clarified as the summation of both permeabilities as [equation 2.7](#). Thus, total permeability will rely on the direction of flow in formations, because any change in flow direction will lead to a change in K_f and K_m , in the case of anisotropic matrix permeability (K_h, K_v) ([Golf-Racht 1982 p. 158](#)). K_t can be calculated from many methods, such as core analysis parameters and from well test data. As rocks' permeability is affected by flow direction, therefore, fracture orientations have a major effect on flow, especially when fractures have similar patterns of orientation. However, when fractures show random orientations, then, K_t value will not have a major effect by changing flow direction in relation to K_f changes. [Equation 2.8](#) clarifies calculation of K_t from core analysis, [Figure 2.4](#) presents directional flow effects ([Golf-Racht 1982 p. 159](#)). [Donaldson and Tiab \(2004\) p. 539](#); [Hidayati, Chen and Teufel \(2000\)](#); and [Saidi \(1987\) p. 81](#) have clarified that if fracture and matrix contribute to flow, as pressure drops in a reservoir due to production, this will lead to an increase of the vertical orientated stress axis due to depletion. This leads to a decrease of matrix and fracture porosity. Thus, effective permeability of the system may be obtained as [equation 2.9](#).

$$K_t = K_f + K_m \quad (2.7)$$

$$K_t = \frac{Q \cdot \mu \cdot L}{A \cdot \Delta P} \quad (2.8)$$

$$K_e = \sqrt{K_{\max} \cdot K_{\min}} \quad (2.9)$$

Where: K_m = matrix permeability, K_f = fracture permeability in formations, Q = flow rate, μ = viscosity, A = cross section area, ΔP = pressure drop among desired points, K_e = formation's effective permeability, K_{\max} = maximum permeability that is parallel to fracture plane (usually $K_{\max}=K_f$), K_{\min} = minimum permeability that is perpendicular on fracture plane (usually $K_{\min}=K_m$). Thus, [equation 2.9](#) can be rearranged as [equation 2.10](#).

$$K_e = \sqrt{K_f \cdot K_m} \quad (2.10)$$

[Donaldson and Tiab \(2004\) p. 539](#)

In layered reservoirs, where each layer has different matrix permeability, flow can be classified as either a crossflow reservoir or a reservoir without crossflow among formation matrix layers ([Donaldson and Tiab 2004 p. 469](#)). Crossflow reservoirs have multiple layers with different thicknesses and varying properties, such as permeability and porosity. These layers in some formations are communicating hydrodynamically at contact planes, leading to fluid cross flow amongst these layers ([Olarewaju and Lee 1990](#), [Bourdet 1985](#)). As well, even if each layer has different properties in horizontal and vertical directions, but can be simplified and modelled as isotropic ([Gao and Deans 1988](#)). [Figure 2.5](#) clarifies this condition. [Russell and Prats \(1962\)](#) investigated these formations further and concluded that flow equations in formations can consider "Kt", which represents a summation of permeability in layers, or (permeability-thickness) "kh"; [equation 2.11](#) below clarifies this model. When reservoir layers' properties are changing along the flow, it is considered as a composite reservoir (vertical layers and flow pass horizontally through) as [Figure 2.6](#) below. The effect of horizontal direction changing in reservoirs has particular importance due to the effect on reservoirs' performance and the required development in fields. Therefore, it is necessary to classify layers of different zones and permeabilities, and each layer has isotropic permeability ([Earlougher 1977](#)). In such a system, the total pressure drop is the summation of each layer's pressure drop, therefore, the average permeability of such a system is as [equation 2.12](#) ([Donaldson and Tiab 2004 p. 476](#)). On the other hand, if

reservoirs have no crossflow among formations layers are interbedded, or separated by impermeable layers such as silt laminations and shales, these separation layers prevent cross flow amongst the reservoir formation layers. Therefore, volumetric flow rate will be equal to the summation of flow rate in each layer. Thus, the equivalent permeability for parallel layers is as [equation 2.13](#) and [figure 2.7](#) below (Donaldson and Tiab 2004 p. 471).

$$(kh)_t = \sum_{i=1}^n (kh)_i \quad (2.11)$$

$$\bar{K} = \frac{\sum_{i=1}^n L_i}{\sum_{i=1}^n \left(\frac{L_i}{K_i}\right)} \quad (2.12)$$

$$\bar{K} = \frac{\sum_{i=1}^n k_i \cdot h_i}{\sum_{i=1}^n h_i} \quad (2.13)$$

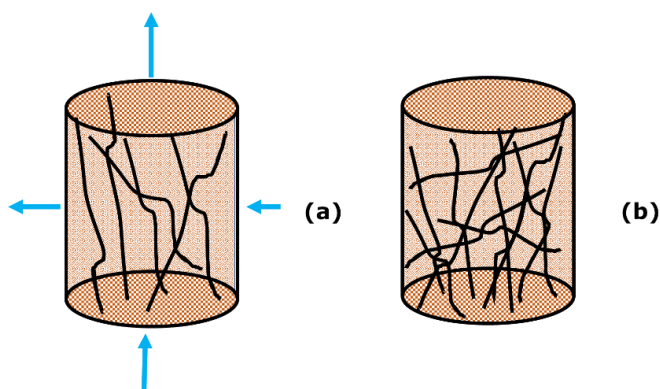


Figure 2.4 a: similar orientation fractures, b: random orientations fractures (adapted from Golf-Racht 1982 p. 159)

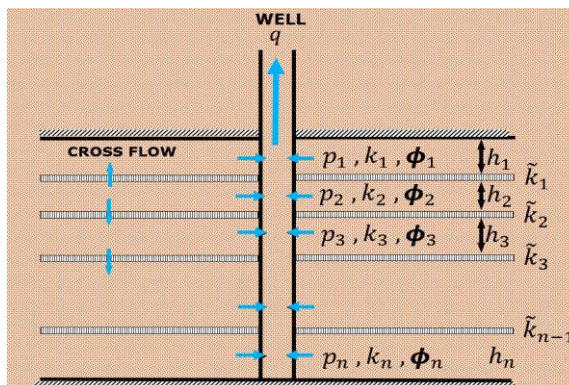


Figure 2.5 Reservoir layers with different thickness and properties, and cross flow among them (adapted from Gao and Deans 1988)

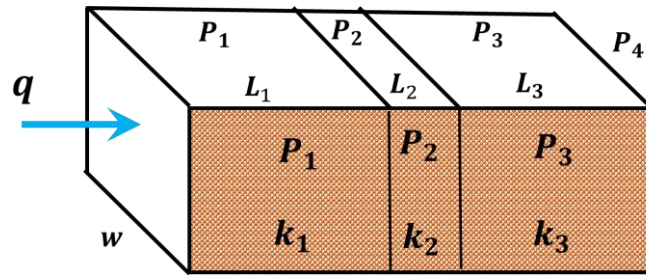


Figure 2.6 Flow in a reservoir with different layers with varied permeabilities
(adapted from Tiab and Donaldson 2004 p. 475)

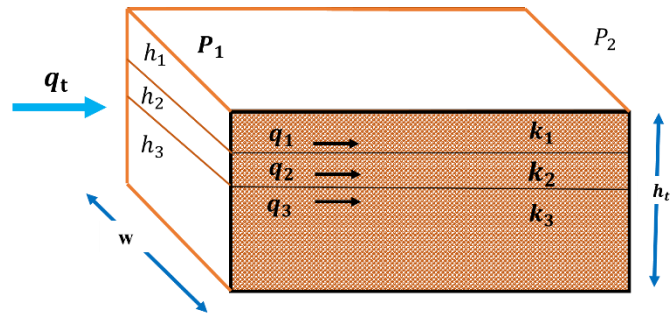


Figure 2.7 Separated layers in reservoir formations
(adapted from Tiab and Donaldson 2004 p. 471)

In each formation layer, there are measured irregularities of a matrix's permeability, in parallel and vertical directions in bedding plane, which is called "anisotropic permeability"; if permeability is assumed to be similar in all Cartesian directions, this is known as "isotropic permeability". For instance, if rocks consist of large flat grain pieces, and are sorted with longest direction, this will lead high K_x and moderate to low K_y ; Figure 2.8 presents this case (Chery and de Marsily 2007 p. 37; Tiab and Donaldson 2004 p. 103; Dake 1978; Hutchinson, Dodge and Polasek 1961 p. 227). The impact of anisotropic permeability on reservoir fluid flow is significant as it affects natural hydrocarbon recovery, water-flooded reservoirs and etc. The majority of reservoirs and subsurface layers are anisotropic; even in reservoirs that are classified as homogeneous, K_x is usually different than K_y . However, in most with a steady state of flow, equations require a single permeability value only. Therefore, it's necessary to recombine or estimate permeability variations of formations, to be in an equivalent average value. This will lead to either loss or gain of permeability in any desired direction, and the averaging of permeability is always less than highest permeability in any direction. Thus, with this kind of anisotropic permeability system, an anisotropic index (I) was introduced to measure the level of heterogeneity in formations, as equation 2.14 when (I)=1 will correspond to isotropic permeability conditions (Di Fratta et al. 2016; Lang, Paluszny and Zimmerman 2014; Tiab and Donaldson 2004 p. 162; Golf-Racht 1982 p. 52; Hutchinson, Dodge and Polasek 1961).

$$I = \frac{K_x}{K_y} \quad (2.14)$$

Where: IA= anisotropic index, K_x and K_y= horizontal and vertical permeabilities respectively in Cartesian coordinates (Lang, Paluszny and Zimmerman 2014).

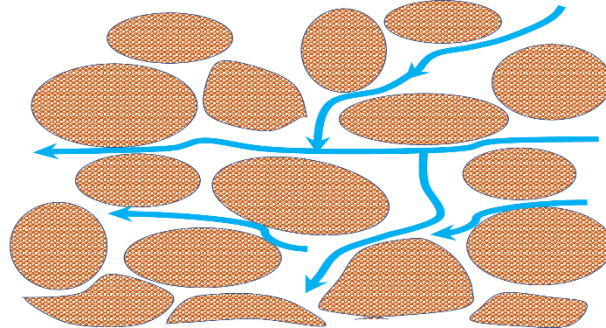


Figure 2.8 Anisotropic permeability in matrix, high K_x and moderate K_y (adapted from Tiab and Donaldson 2004 p. 103)

2.4.2.1 Permeability's influence on fractures and matrices

Saidi (1987) p. 81 clarified that in fractured reservoirs it's common that vertical permeability is higher than horizontal permeability, due to many factors. The higher effects of formations overburden pressure on horizontal fractures, which leads to aperture reductions and resistance of vertical fracture to such pressures, and there are also solid material depositions in horizontal fractures. Thus, horizontal permeability plays a main role in fluid flow towards a well. Lei et al. (2015) stressed that fractured reservoirs consist of fracture and matrix, and fractures' distribution are complex with strong anisotropy. Therefore, permeability values of fractured formations rely very much on the measured direction. Therefore, in general, the permeability that is parallel to fractures is greater than the perpendicular direction. As well, a permeability tensor model was developed, based on comparison between experimental and numerical simulations, for a model with varied fracture angles. Hidayati, Chen and Teufel (2000); Parsons (1966); and Scheidegger (1963) stressed that when horizontal and vertical permeabilities are varied, and flow direction is toward a well, then radial permeability "K_r" is the outcome of both horizontal and vertical permeabilities. This can be expressed as equation 2.15, when measured permeability is in the same direction of velocity vector. On the other hand, if pressure buildup direction is in the same direction of permeability, then, (K_a) can be calculated by equation 2.16

(Saidi 1987 p. 82; Parsons 1966). Ingham and Pop (2005) p. 367 stressed that permeability and fluid transport in porous media are in close relation with detailed geometries of matrix pores, such as pore scale, tortuosity, connectivity, and shape. This relation is not easy to obtain from macroscopic parameters such as porosity. Andersen and Zhou (2020) presented an experimental study to predict relative permeability of immiscible fluids in porous media, and clarified the effects of saturations, spatial pressure gradients of a sample core, and stressed the importance of accurate relative permeabilities on reliable decisions and predictions at field scale.

$$\frac{1}{K_r} = \frac{\cos^2\theta}{K_v} + \frac{\sin^2\theta}{K_h} \quad (2.15)$$

$$K_a = K_v \cos^2\alpha + K_h \sin^2\alpha \quad (2.16)$$

Where: θ = the angle between flow direction (towards observed well) and max permeability axis, K_v and K_h = permeabilities aligned with Y and X Cartesian axis respectively, α = the angle between pressure gradients in formations and max permeability axis.

Di Fratta et al. (2016) tested anisotropic permeability to investigate the effects of the angle between horizontal and vertical permeabilities on observing the effective permeability of the medium and flow. When flow direction is not orientated with any principle permeabilities, then, the effective permeability can be observed as equation 2.17 below. In addition, it was shown that the most critical angle (θ) is the worst case of unidirectional permeability (45°), which leads to the highest errors.

$$K_{\text{eff}} = \frac{K_1 K_2}{K_1 \sin^2\theta + K_2 \cos^2\theta} \quad (2.17)$$

Lang, Paluszny and Zimmerman (2014) stressed that flow in fractured media as a response of hydraulic head gradient is varied heterogeneously through a domain, due to many factors. First, within factures, flux varies locally along the flow due to conductivity, connectivity, and fractures' height and orientations, and second, flux in matrix relies on matrix permeability properties. Thus, two flux conditions are in one medium, which will result in a probability of fracture networks to allow pressure gradients to exist in individual blocks. However, there is always some

flow occurring due to the response of the fracture-matrix. [Yang et al. \(2019\)](#) developed a new fracture permeability model for high-dip angles in the southern Junggar Basin (NW China) of coalbed methane reservoirs. This work stressed that the geological structure of fractured formations has a key effect on variations of regional permeabilities, and to find a general model to describe permeability in such formations is very difficult. [Wang et al. \(2020\)](#) presented a model of pore networks from SEM images in order to have a better permeability prediction of formations. In this work, it was stressed that 2D models are sufficient for permeability calculations, particularly when using Darcy law as it will cancel the third dimension "width". [Ju et al. \(2019\)](#) stressed that the permeability of rough fractures can be determined by considering two factors: standard deviation and average aperture. [Su et al. \(2019\)](#) experimentally studied rough fractures (not including matrix effect) and developed a new correlation of intrinsic fracture permeability. It was confirmed that fracture permeability is proportional to mean aperture size, which is affected by the confining stresses on a fracture. [Roslin, Pokrajac and Zhou \(2019\)](#) studied cores of coals collected from Southern Qinshui Basin (China), and fracture permeabilities were calculated by using CFD open source "Palabos" and Darcy's law, then, compared with an analytical equation of Poiseuille flow between parallel plates. Fracture surfaces were considered as impermeable solid walls "walls Boundary" with the surrounding coal matrix, and fracture apertures were considered as the average value over certain fracture length. This study shows that obtaining the permeability from simulations is comparable to the analytical approximation of analytical Poiseuille flow.

[Al-Yousef \(2005\)](#) presented an analytical solution for measuring anisotropic permeability of core samples, and stressed that permeability is one of the most important properties in reservoir rocks, as it highly affects fluid flow in these formations. [Rasouli and Rasouli \(2012\)](#) stressed the importance of permeability in fractured formations: particularly, that matrix permeability will increase formation connectivity when it's a higher permeability value. As well, permeability will increase with fracture aperture heights. It was stressed that fracture permeability will dominate formation permeability when a fracture's height is more than one tenth of the formation height. Moreover, it was shown that in fractured formations, permeability is partially in the matrix and partly in the fracture, and when overburden stresses are high and fracture apertures reduce significantly, then

most of fluids will be immigrated through the matrix. Therefore, matrix permeability is a very important consideration in fractured formation.

2.5 Flow In Fractured Reservoirs

As mentioned in the above sections, fractured reservoirs / formations are very heterogeneous. Therefore, in different time stages, scientists and engineers have tried their best with the available tools to simplify the heterogeneity, in order to enable a better estimated calculation of this kind of media to be observed. Thus, in the below sections, some of the models are highlighted, starting from the simplest models and continuing into more complicated models that include more variables of the formations. In reservoir engineering, fracture shapes are approximated to regular shapes, such as ellipse, rectangle or square, to match and facilitate the calculation. However, in real life fractures shapes vary, and sizes also depend on the distance from the injecting wellbore, as well as rock properties with other stresses. Fracture sizes are approximated from micrometre diameters to 0.5 cm at maximum (Lake and Clegg 2007; Piri and Karpyn 2007; Valko and Economides 1995).

2.5.1 Flow in fractures with one aperture size (parallel plates)

Flow between two fixed parallel plates, apart by $(2h)$ distance or height, for fully developed laminar viscous flow far from the entrance, with no-slip conditions and with two dimensional (2D) incompressible plane ($\partial/\partial z=0$) is considered. In this situation, the essential flow is axial, and the flow doesn't go through a wall. Thus, X-velocity ($u \neq 0$), while Y-velocity (v) and Z-velocity (w) equal zero ($v=w=0$), and the pressure varies along X-direction. By applying the continuity equation, and substituting the axial velocity value in Navier-Stokes momentum equation of two-dimensions with gravity neglected, this can then be solved for (u), as equations 2.18 and 2.19. Thus, the flow is poiseuille parabolic shape, with negative values and the maximum velocity located at the centre height of the channel between the two fixed plates when ($Y=0$). Equations 2.20 and 2.21 clarify this (White 2011 p.

269; Douglas et al. 2005 p. 326; Zimmerman and Bodvarsson 1996 p. 7; Golf-Racht 1982 p. 299; Eskinazi 1968 p. 378).

$$\frac{\partial u}{\partial x} + \frac{\partial v}{\partial y} + \frac{\partial w}{\partial z} = 0 \quad \left\{ \frac{\partial v}{\partial y} = 0, \frac{\partial w}{\partial z} = 0 \right\} \text{ Continuity equation of Navier-Stokes} \quad (2.18)$$

$$\rho \frac{dV}{dt} = \rho g - \nabla p + \mu \nabla^2 v \quad \text{Momentum equation of Naiver-Stokes} \quad (2.19)$$

$$u_{\max} = - \frac{\Delta p}{L} \frac{h^2}{2\mu} \quad (2.20)$$

$$u = u_{\max} \left(1 - \frac{y^2}{h^2} \right) \quad (2.21)$$

To calculate the flow of the section from the equation ($Q=A.V$), with the area of the parallel plates with ($2h$) height, and the length much bigger than the distance between the plates ($2h$), the Z-coordinates or B-coordinates as Figure 2.9 below are usually much larger (\gg) than the fracture aperture too. This therefore has been assigned in the Figure 2.9 as (∞); therefore, in similar situations, flow will be essentially two dimensional, and equation 2.22 will be the output of these assumptions.

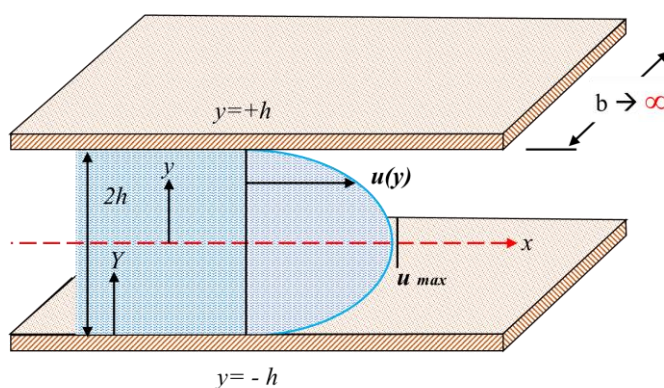


Figure 2.9 Velocity profile (Poiseuille parabolic shape) between two fixed parallel plates with distance height - fully developed flow
(adapted from White 2011 p. 381)

$$Q = \frac{2bh^3}{3\mu} \cdot \frac{\Delta P}{L} \quad (2.22)$$

(White 2011; Eskinazi 1968 p. 382)

Flow in fractured rock is commonly modelled and simplified by assuming that fractures consist of a pair of parallel smooth plates, which excludes surface roughness, and that flow will occur between these two smooth walls along the pressure gradient. As well, in most cases, the surrounding matrix media's flow is ignored and considered solid or impermeable, to adopt a scenario of a very tight formations. This kind of flow in fractures is considered one of the simplest models, and still the most widely used because it's the only actual geometry that has accurate calculation of hydraulic connectivity which yields a "cubic law". Therefore, flow equations were derived from Navier-Stokes equations that describe single phase flow of laminar, un-compressible Newtonian fluids to calculate flow per unit width and average velocity of a rigid parallel plates fracture conduit. These equations are well known as "Cubic law", as it is demonstrated that fracture flow is proportional to the cube of a fracture aperture's height, which is the distance between the two smooth walls, and is considered as a constant value along fracture flow. Thus, based on these assumptions, [equation 2.23](#) below describes it ([Dietrich et al. 2005](#); [Sarkar, Toksöz and Burns 2004](#); [Zimmerman and Bodvarsson 1996 p. 7](#); [Dullien 1992](#); [Bear 1972](#); [Snow 1969](#)). [Holstein \(2007\)](#); [Dietrich et al. \(2005\)](#); and [Golf-Racht \(1982\)](#) stressed that flow through fractures in the early models had been assumed and simplified between a two paralleled surfaces with a fixed aperture which is equal to the mean value of real aperture (rough-walled fracture).

$$T = \frac{\rho g b^3}{12 \mu} \quad (2.23)$$

[\(Bear 1972\)](#)

Where: T = fracture transmissivity relying on (h^3) value; this is therefore considered the core of well known "cubic law", ρ = fluid density, g = gravitational acceleration, μ = fluid viscosity

[Sarkar, Toksöz and Burns \(2004\) p. 4](#) carried out CFD simulation on a parallel plate fracture model. The conditions were: incompressible fluid, and width assumed "1". A comparison between CFD simulations and analytical results was conducted, and the only variable was varying the fracture aperture, and it was found that mean velocity varied by 'h²' and flow rate by 'h³', which is matched with the theory of cubic law. As well, this research studied inclined and impervious surfaces of fractures that are oriented at angles, with respect to the axis of macroscopic pressure gradient embedded in solid slab, and the model was subject to a horizontal pressure gradient axis. The main outcomes of these results were:

pressure and velocity in CFD contour lines have the same orientations and are aligned with a fracture's orientations regardless of pressure gradient direction. It was found empirically that the flow rate decreased by a factor of $\cos \theta$ as [equation 2.24](#) (a similar reduction factor has affected fracture permeability, as clarified in the previous sections which were reported by [Golf-Racht \(1982\) p. 156](#); and [Tiab and Donaldson \(2004\) p. 519](#)). The physical explanation is that the fracture's length increased by an increased factor ($L/ \cos \theta$). [Donaldson and Tiab \(2004\) p. 426](#) stressed the significance of fractures as fluid carriers that extend inside the body of rock and connect it with wellbore, and presented a linear model of velocity and flow of fine and clear slots with units' width; [Figure 2.10](#) presents it.

$$Q = \frac{h^3 \cos \theta}{12 \mu} \left(\frac{\Delta P}{L} \right) \quad (2.24)$$

Where: h = height of fracture, L = fracture length, μ = fluid viscosity, Δp = pressure drop

[Luo et al. \(2018\)](#) introduced a semi-analytical method for calculating the productivity index of a vertical well near one or two discrete fractures. In this study, it was assumed that the reservoir was isotropic, single phase slightly compressible fluid, with constant values of porosity, permeability and thickness. Moreover, fractures were considered as parallel plates fractures with single apertures as a dimensionless value, and represented as flow input. This study clarified the effect of discrete fracture location on the well productivity index and the intersection angle among fractures on pressure behaviour. [Popov et al. \(2009\)](#) stated that an experimental approach for subsurface fractured media is very difficult to conduct with accurate results, due to the complexity of co-existence of porous and open free flow regimes (fractures) with different flow conditions. A mathematical model of flow in fractured media was introduced, called Stokes-Brinkman equations, which accounts for flow in fracture and matrix. Flow in the fracture was assumed as an open channel (parallel plates fracture with a single aperture) and that flow in the matrix obeys Darcy flow. As well, the interface layer between matrix and fracture was considered. Moreover, it was clarified that the interface layer is affected by the components of tangential velocities, which affect various fluid jump (movement) conditions for matrix and fracture. Accordingly, this affects fluid stresses in both media. Fluid jump conditions in the interface layer

are therefore affected by many factors, such as surface structure, flow regime type and fluid properties.

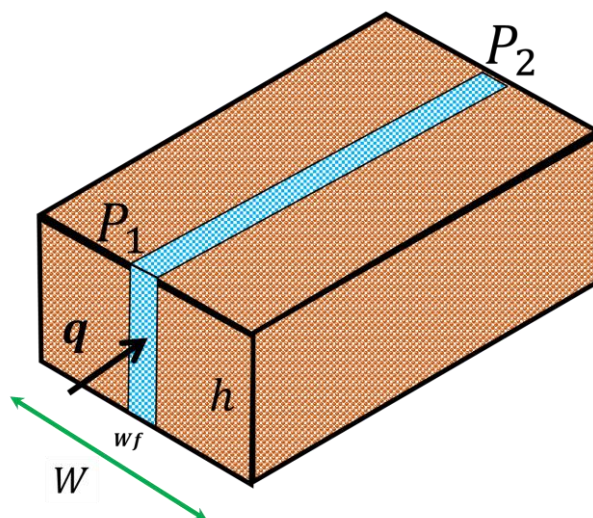


Figure 2.10 Linear model for flow in a single fracture
(adapted from Tiab and Donaldson 2004 p. 427)

2.5.2 Flow in rough fractures with varied apertures (multi-parallel plates fracture geometry)

Petroleum engineers, hydrologists and geo-environmental engineers face huge challenges and difficulties to model and understand fracture morphology characterization, and to investigate fluid flow in fractured media. The main issue usually raised for investigation of fluid flow in fractured media is how geometry complexities affect the flow and properties of fluid transport in fractured media. Many studies have outlined the main challenges in describing fractured media, such as tortuosity characterization, heterogeneity of aperture distribution, and connectivity between fracture/matrix and among a fracture network. Thus, due to this complicated presentation of fractured media, numerical models offer a reasonable representation of fractured media features and an ability to contain fractured aperture variations to model transport properties of fractures (Sarkar, Toksöz and Burns 2004; Keller, Roberts and Blunt 1999). Berkowitz (2002) p. 867 carried out a deep review on flow in fractured media, and stated that a single fracture flow, with parallel smooth plates with a single aperture height, is not adequate for flow description in fractured media; however, using local cubic law (parallel plates fracture with varied apertures) instead is more adequate in conceptual models, and strongly influences quantitative analysis, laboratory and field measurements on fracture flow. Moreover, it was stated that fractures' conductivity differences are expected to be minimal when they are embedded in

permeable or impermeable host rocks, but this still has not received research attention yet. [White \(2003\)](#) introduced an empirical equation to calculate total pressure drop of laminar, viscous fluid flow, for a fracture which consists of many segments (with impermeable surfaces), by the sum of pressure drop in each segment in that fracture, excluding gravity effect. [Equation 2.25](#) clarifies it. As well, as flow rate is constant through a fracture with varied apertures, then pressure drop can be calculated as [equation 2.26](#).

$$\Delta P_i = 12 \frac{\mu L_i V_i}{H_i^2} \quad (2.25)$$

$$\Delta P_i = 12 \frac{\mu L_i Q}{H_i^3} \quad (2.26)$$

Where: ΔP_i = pressure drop, H_i = fracture aperture, L_i = length, V_i = mean velocity of the i^{th} of fracture segments, μ = dynamic fluid viscosity, H = apertures, and $Q = (V_0 H_0 = V_i H_i)$

[Karpyn and Piri \(2007\)](#) carried out experimental work to capture all details of inner fractures geometry with all features by x-ray computed tomography. This imagery was then used in numerical simulations, to investigate the effect of the complex geometry of fluid transports in fracture media, and the interactions between solid walls and fluids inside solid walls of fractures. [Karpyn, Grader and Halleck \(2007\)](#) carried out an experimental approach of two phases fluids through an artificially created fracture of natural Berea sandstone cores. Then, using micro-computed tomography (MCT) to characterize the internal fracture structure, a mapped fracture with varied apertures was created, where each aperture consisted of two parallel plates with a single height. The reason for using this method is to mimic real fracture conditions, by adding more complexity such as varied apertures, in order to create roughness and increase fluid flow tortuosity. This method has added a different approach from two parallel plates for the entire fracture with one aperture height. The outcome stressed the importance and the effect of fracture apertures on fluid distribution inside a fracture, and that flow in rough fracture geometry is typically less than the predicted flow from a parallel plates fracture. [Piri and Karpyn \(2007\)](#) modelled a network of pore fracture slices by using x-ray microtomography scans of a cylindrical Berea sandstone core, to construct detailed conceptual throats and pores of rough-walled fracture apertures. This was done in order to extract exact an inner replica of a fracture's void and inner structure, and

this work stressed that proper characterization of a fracture pore network is essential for accuracy studies. This was investigated further, and the experiment results were validated with X-ray microtomography to study fluid invasion in the fracture domain of two phases of Newtonian fluids. The findings showed that rough fracture geometry, in comparison with parallel plates fractures, exhibits many variations of fracture apertures and surface roughness, which lead to the creation of complex tortuous flow paths. Therefore, to have a better accuracy of reservoir models and representations, it's essential to consider the complex properties of fractures' geometry, and its effects on flow inside fractures. As well, the validation's accuracy indicated that it's an appropriate tool to predict fluid flow in a realistic fracture representation. [Nazridoust, Ahmadi and Smith \(2006\)](#) modelled non-deformable fractures in fractured media BY ANSYS CFD Fluent FVM, with matrix permeability neglected (impermeable fracture walls). The governing equations of incompressible and viscous fluid motion inside fractures with the laminar regime are continuity equations and Navier-Stocks equations. As well, an empirical equation was introduced that is able to calculate pressure drop inside a fracture, by the inclusion of a fracture's tortuosity; this can be defined as the ratio of actual distance that fluid particles travel between two points to the straight-line distance between these same points. The value of tortuosity was considered as an added length to the total length of fractures; as well, a value called "effective fracture apertures" was included, which is the value of average apertures. However, this is a smaller value than the arithmetic average value by a value of the standard deviation. Due to the expectation of the main pressure drop occurring in smallest apertures of fractures, [equations 2.27, 2.28, and 2.29](#) below demonstrate the case. Four different profiles of fractures were used by micro-computed tomography (MCT) method, as created and presented by [Karpyn, Grader and Halleck \(2007\)](#). ANSYS CFD Fluent FVM single-phase Newtonian fluids were used for flow simulation, the tortuosity was considered, and due to the length differences between the top and bottom of fracture boundaries, the average length value of top and bottom fracture was considered as a length of fluid travel. Then, static pressure and velocity magnitude were observed from the simulation for different values of flow rate. The findings were that pressure drop value increased with increasing flow rate. Also, pressure drop increased with high viscosity fluids such as water, and air viscosity differences. From velocity magnitude, it was seen that fluid flow in the mainstream with high speed and smallest aperture dictates the pressure in the fracture. Also, pressure drop is affected inversely by fracture aperture, and linearly with tortuosity. However, the fracture aperture had more

influence than tortuosity, due to the third power of aperture “dependence of cubic law”. Therefore, the equivalent hydraulic aperture should be modified to include the effects of roughness and tortuosity of a rough fracture into parallel plates; this can be done by using a small magnitude of the mean aperture to add more pressure drop. In other words, using an arithmetic mean of apertures is not enough to include roughness and tortuosity of rough fracture, and more reduction of average fracture aperture size by an affective aperture’s method is mandatory, to account for fracture surfaces’ tortuosity and roughness. Thus, it was stressed in this work that parallel plates fractures with varied apertures, considering effective fracture apertures and a factor of tortuosity, would be able to give an appropriate pressure drop estimation in fractures.

$$\theta = \frac{L_e}{L} - 1 \quad (2.27)$$

$$\Delta P = (1 + \theta) \cdot \sum \Delta P_i \quad (2.28)$$

$$\bar{H} = H_{avg} - \sigma \quad (2.29)$$

Where: L_e = actual length between two points, L = straight length between two points, \bar{H} = affective apertures, H_{avg} = arithmetic average aperture, σ = fracture aperture standard deviation

Crandall, Ahmadi and Smith (2010) remodelled Nazridoust, Ahmadi and Smith (2006)’s fractures by ANSYS CFD Fluent FVM and considered the fracture’s tortuosity and affective fracture aperture, but with one modification: it was assumed that the walls of the fractures were permeable with the surrounding matrix, instead of no slip impermeable walls. The findings were: first; the pressure was observed inside the matrix porous media in different positions away from the fracture, and the pressure was linearly decreasing between the inlet and outlet, with marginal differences values. Secondly, the interaction between the fracture and matrix was visible, and fluid does move between fracture and matrix with changing velocity inside an open fracture. Thirdly, the smallest aperture in an open fracture dictates pressure drop and can be considered an effective aperture which has confirmed the finding of Nazridoust, Ahmadi and Smith (2006)’s models. And fourthly, there was an average 10% increase in flow percentage in the open fracture, due to flow movement from matrix to fracture through the fracture/matrix interface layer. This could be increased or reduced based on the fracture profile effect on velocity /pressure and matrix permeability, which

increases flow in a fracture when it's high in comparison with low matrix permeability. As well, in the surrounding porous media where the velocity is at lowest value and high pressure, the fluid moved through the interface layer to the fracture's open space. [Tsang \(1984\)](#) stressed that irregularity of fracture aperture variations, and fracture surfaces asperities, will cause vortexes and tortuosity of flow in rough fractures. Thus, pressure counters of rough fractures don't decrease uniformly as in a parallel plate model. [Dicman, Putra and Schechter \(2004\)](#); and [Lespinasse \(2000\)](#) studied flow in rough fractures. [Lespinasse \(2000\)](#) used finite difference formalisation to study fluid flow in a realistic fracture, with the finding that fluid flow in a rough fracture was heavily affected by two factors: fracture roughness and tortuosity. [Auradou et al. \(2005\)](#); and [Gonzalez-Garcia et al. \(2000\)](#) built a 3D model of intersecting fractures, from a series of sections, to analyse fracture characteristics in systems. Fracture blocks were represented in monodisperse hexagons and randomly oriented, to investigate properties of fracture such as fractures' permeability and fluid velocity. [Auradou et al. \(2005\)](#) proposed an experimental method using transparent splices of a fracture to study fracture flow. Also, a numerical model was presented to capture anisotropy permeability as an outcome of displacement of fracture walls. [Moreno et al. \(1988\)](#) reached the conclusion that parallel plate models (with single aperture) are not suitable to describe fluid flow in fractured media. This case was investigated further by a numerical ANSYS CFD Fluent FVM model by [Petchsingto \(2008\)](#), which compared pressure drop along the length for a parallel plate and a rough fracture. The results were that pressure drop by parallel plates (single aperture height) is much less in comparison with a rough fracture (parallel plates with varied apertures). For the same set-up of CFD model, it was found that pressure drop was 31 pa/mm in the parallel plates model, in comparison with 1520 pa/mm for the rough fracture! The difference is not remotely marginal and could significantly mislead calculations. [Zimmerman and Bodvarsson \(1996\) pp. 1, 21-22](#) studied single-phase flow through rough walled fractures, stressing the derivation of the "Cubic law" as a solution to Navier-Stokes equations for flow between smooth parallel plates fractures. It was stressed that smooth plates fracture geometry is the only amenable treatment for fracture flow challenges. As well, aperture distribution statistics to the effective hydraulic aperture were reviewed, with the conclusion that the effective hydraulic aperture is always less than the mean apertures, by a factor that relies on a ratio between mean aperture value and standard deviation. Moreover, comparisons were conducted among measured values of apertures of fractures from the literature, and hydraulic aperture values

were predicted for some fractures. It was concluded that hydraulic conductivity can be predicted with reasonable accuracy based on two factors: apertures' distribution function and proportion of contact area. [Chen et al. \(2017\)](#) modelled experimentally and numerically by ANSYS CFD Fluent FVM horizontal fractures, with different conceptualized patterns of roughness with Newtonian single-phase fluid and turbulent flow. The shapes of the fracture roughness were investigated with many shapes as rectangular, triangle and trapezoidal. It was clarified that the shape of a fracture's surfaces' roughness and size has an effect on eddies and flow recirculation shape and size. A significant eddy was in rectangular roughness shape; as the angle of fluid entry into the roughness zone is with a 90° angle, while other zones have smaller angles (Figure F6, [p. 186](#) in the journal clarifies this). This has led to a conclusion that non-linear flow becomes higher with increasing asperity height in surfaces, and there is small momentum exchange between fluids in the eddies and fluids of fracture main flow streams. This study shows qualitative effects on different roughness shapes, and requires further quantitative investigation. [Sarkar, Toksöz and Burns \(2004\) p. 6](#) investigated a group of parallel plates fractures with varied apertures, connected in series with the same flow prevailing through each. As well, if this kind of fracture has an orientation different than pressure gradient orientations, then flow affected by a reduced factor $\cos \theta$, which was verified by ANSYS CFD Fluent FVM models with the results, as [equation 2.30](#). As well, it was clarified that low fluid velocity in rough fractures has two main deviations from cubic law, which are: first wall roughness; and distance variations between two faces of fractures' apposite sides along the fracture (fracture aperture abrupt variation). [Yamatomi et al. \(2001\)](#) modelled a single rough fracture with Finite Element method (FEM) with impermeable fracture surfaces, and considered the effect of overburden pressure of fracture displacement. As well, horizontal and sloped fracture orientations were considered. The outcomes were that fluid tortuosity, and average aperture reduction due to the overburden pressure, have a significant effect on flow. As well, in comparison with horizontal orientation fractures, inclined fractures reflected quite different fluid pressure distributions, even with different orientation angles.

$$Q = \frac{h_{eq}^3 \cos \theta}{12 \mu} \left(\frac{\Delta P}{L} \right) \quad (2.30)$$

Where: h_{eq} = equivalent (average) apertures of fracture, L = fracture length, μ = fluid viscosity

[Rasouli and Rasouli \(2012\)](#) modeled two kinds of single fracture in 2D BY ANSYS CFD Fluent FVM with horizontal orientations, embedded in a matrix (permeable fracture surfaces). The first kind were parallel plates fractures with one aperture (two fracture apertures were considered), and the second kind, rough fractures (four fracture profiles were considered). Isotropic matrix permeability, with single phase Newtonian incompressible fluid with a laminar flow regime was considered. The aim of this study was to investigate the fracture and matrix effect of fractured domain flow, fracture roughness, and the effects of applied overburden stress that lead to a reduction of fracture apertures. It's good to clarify that for these two kinds of fractures, there were no connections between them in point of fracture aperture average height, as each kind was used to investigate different findings. The main outcomes of the parallel plates models with a single aperture were that pressure drop was reduced when the fracture aperture height was increased, and the reduction of pressure drop is higher in low matrix permeability for the same fracture aperture. There were similar findings in the rough fracture models; also, that pressure drop reduces more with rougher fracture surfaces, due to the fact that rougher fractures have higher average apertures and more area to accommodate fluids. [Briggs, Karney and Sleep \(2014\)](#) modelled 2D fractures by using numerical simulations of Lattice Boltzmann method (LBM); fracture surfaces set with impermeable walls (no matrix inclusion with fracture flow) were used, and fracture geometries were created by using SYNFRAC software with the same average aperture but with varied fractal dimensions (roughness). It was clarified and confirmed that roughness can affect fracture flow, even with a low Reynolds number. It was observed in velocity streamlines of rough fractures with different Reynolds numbers from 0.6 to 60, that when the fracture aperture experience abruptly changed, it led to a significant change in velocities, which created zones of fluid recirculation, called "eddies or vortexes", that don't contribute to fracture bulk fluids. These recirculation zones became larger and appeared in many places along the fracture flow wherever there were aperture changes (Figure 5 [p. 541](#) in the paper presented these results). [Briggs, Karney and Sleep \(2017\)](#) used the same method, with varied Re from 0.01 to 500, and clarified that these eddies increased in size with increasing fracture roughness, which lowered the hydraulic conductivity of fractures. This is because the eddies' zones were detached (isolated) from fracture bulk flow and, accordingly, reduced hydraulic effective aperture, but the eddies' growth was constrained by fracture main flow rate stream and a fracture's roughness's sharp edges. Similar findings of eddies' creation in fractures were stressed by [Dippenaar and Van Rooy \(2016\) p. 4](#), and [Karimzade](#)

et al. (2019) used ANSYS CFD Fluent FVM and modelled a 3D rough fracture, and stated that formations of eddies in some zones of a fracture, when apertures faced abrupt changes, will cause deviation of flow from the ideal parabolic shape, due to the inertial effects of fluid. It was argued that Navier- Stokes equations can characterize this. Barton and Choubey (1977) were the first to propose the JRC index experimentally, of fractures with rough surfaces between 0 (smooth) and 20 (very rough), of ten profiles with varied roughness by back calculation of shear strength. Tse and Cruden (1979) developed the index and proposed another empirical relation which accounts for fracture roughness. Crandall, Bromhal and Karpyn (2010) and Crandall, Bromhal and Smith (2009) used ANSYS CFD FVM with incompressible single-phase fluid, and modelled six geometries of rough fractures (varied parallel plates apertures). These were obtained from CT image scans of Berea sandstone with six varied meshing cell numbers. Joint roughness coefficients (JRC) were calculated for all fractures, by adapting Barton and Choubey (1977)'s formula to calculate the roughness of rough fractures, then, fracture roughness effects on flow were investigated. The outcomes were that the fracture with smoother surfaces (small JRC) expressed linear decrease in pressure, while the roughest fracture (high JRC) reflected high tortuous flow, with a high degree of non-uniform pressure decrease, and flow channeling 35 times smaller than the smoother fracture. As well, this analysis reflected the ability to verify pressure variations locally (micro-scale) along the flow and overall pressure drops.

2.5.3 Summary of flow in fractures with one aperture size (parallel plates) and rough fractures with varied apertures (multi-parallel plates fracture geometry)

In the literature, for the comparisons between both types of these fractures, it was clarified that the cubic law has significant limitations, due to the fact that the fixed fracture aperture doesn't represent the reality of fractures in fractured media, as in reality fractures have varied apertures and asperities which hinder fracture conductivity for flow. Asperities represent many obstacles of a fracture's fluid flow, which increase tortuosity and fluid channelling of the fluid flow path. However, the cubic law is popular for describing flow in fractures, due to many reasons such as: simple geometry (which leads to an overestimated prediction of fracture flow); simple calculation; and the lack of a realistic or appropriate way to model the real shape of fractures and estimate the flow inside them. There are numerous studies

that raise concern about the applicability of this method, and there are many correction factors which account for estimations of fracture aperture that include fracture roughness and tortuosity of flow (Piri and Karpyn 2007; Nazridoust, Ahmadi and Smith 2006; Sarkar, Toksöz and Burns 2004; Berkowitz 2002 p. 867; Tsang 1987; Witherspoon et al. 1980). Research into rough fractures, called multi-parallel plates fractures in some works, has proven the ability of reflection fractured formation conditions which can optimise and reduce errors in fluid flow prediction and calculation.

2.5.4 Multiple fractures (fracture networks) modelling

Flow simulations of reservoir models represent geological facts of a media's properties (porosity, permeability, etc.), and how they interact with fluid properties (viscosity, fluid type, etc.), to visualise fluid flow. This facilitates better understanding of fluid flow behaviour, which enables researchers/engineers to deal with the fluids in many functions with many media. Modelling entire fractured media as a big scale is the main goal, and the main challenge is the existence of fracture networks. The difficulties of representing fracture networks in modelling are due to challenges such as: fractures have varied orientation angles, which may or may not be coordinated with the flow axis; there are varied fracture apertures and lengths; there are varied shapes; whether they are intersecting with each other at intersecting points or singular fractures; fractures may be located randomly with different locations; and the anisotropic matrix properties that surround fracture surfaces. Figure 2.11 below illustrates an example of a real fractured media image (Sahimi 2011; Sarkar, Toksöz and Burns 2004; Tiab and Donaldson 2004; Nelson 2001 pp. 12, 217; Sen 1995).



Figure 2.11 Real fractured media
(SALMAGUND 2017)

Sarkar, Toksöz and Burns (2004) modelled a parallel plates fracture network with different patterns, rigid and impermeable surfaces (no flow between fractures and matrix), and each fracture having different orientation angles and apertures, by ANSYS CFD Fluent FVM steady state flow (2D) with square shape (0.5 X 0.5) m size. The main findings of these models were firstly, that if any fracture in the network connected between the inlet and outlet of the boundaries even with a small inclination angle with respect to the pressure gradient axis, it will be considered as the least resistant fluid flow path which will carry most of network's flow. Secondly, that the equivalent hydraulic aperture magnitudes value of the network will be close and a bit larger than this least resistance fracture to flow. Thirdly, it's correct to consider that flow in the network is similar to the flow in a fracture with the largest aperture height, because flow in the entire network will be slightly bigger. And fourth, it's a reasonable approach as there are different aperture sizes of fractures in a network; the cubic law of transmissivity is based on the aperture height 'h³'; therefore, 'h' can be replaced with equivalent aperture 'h_{eq}' as [equation 2.30](#). Berkowitz (2002) pp. 864, 868-869 clarified that networks of fractures can be classified geometrically by distributions, orientation, length, density, locations, apertures, and connectivity. As well, these networks are highly heterogeneous due to a broad distribution of fractures, which overwhelmingly govern transport and fluid flow behaviour in a fractured medium. In addition, to deal with a fracture network in any model, models have to account for: many ranges of possible distributions; differing densities; hydraulic characteristics; varied boundary conditions; varied host rock properties; variable fracture apertures for each fracture; and a range of fluid types. Snow (1969) p. 1275 introduced a formula for calculating flow in fractured media, for multi fractures with impermeable parallel plates surfaces geometry and varied aperture heights. If they are along the same direction of hydraulic head gradient, and there is no connection among them, then flow can be extracted as [equation 2.31](#).

$$q = - \frac{2}{3} \frac{g}{\nu} W J \sum b^3 \quad (2.31)$$

Where: J= projection of pressure gradient (I) on conduits planes, W= rock cube size equivalent to fracture's length/width, b= ½ fracture height, ν= kinematic viscosity, g= gravitational accelerations

[Nordqvist et al. \(1992\)](#) stressed that the flow observations in fractured media are very different or uneven, and that the crucial rule is due to the discrete nature of fractures which affects the advective transport. As well, trends and behaviour of flow in fractured rocks were studied by developing a three-dimensional fracture network model as a tool, and a fracture network was developed, with variable apertures, and circular discs distributed independently and randomly in a 3D space. From field observations of fractured rock, it was hypothetically assumed that intersection regions among fractures are the main fluid flow transmissivity regions, which led to the hypothesis that these regions can be considered as equipotential lines. Each fracture was divided with many blocks with varied apertures, with cubic law for each individual fracture, then particles were inserted and traced. From the breakthrough plotted trends, the deservations in fractures were in two scales: small scale due to various apertures and bigger scale due to many available paths of flow in the network. [Yi and Xing \(2018\)](#) carried out a sensitive study of isothermal incompressible fluid flow in three-dimensional disordered fractured network media, generated from a refined image of the rock with permeable matrix with domain size 736x556x10 lattice units; isotropic matrix permeability was considered ($K_x=K_y$), fluid could transfer between matrix and fracture with porosity 0.1, and permeability varied from 0.02 to 0.8 lattice unit. They used the improved Lattice Boltzmann method (LBM) to study flow in a practical and applicable field scale as Representative Elementary volume (REV), because LBM is used widely with pore scale, and requires huge computational resources. Pressure gradient was applied from top to bottom with side walls with non-slip boundaries. The main findings of these simulations were that at low matrix permeability, fractures represent the main fluids pathway with a small amount of matrix fluid contribution. By increasing matrix permeability, matrix fluid contribution in the domain is increased, and fracture flow will be increased too, and there will be more connections among open fractures through the permeable matrix. Flow in open fracture networks is affected by small apertures of fractures, and flow prefers larger apertures. Thus, this study showed that matrix permeability in fractured network media plays an important role to permeate and control fluid flow in fractures, and its effect among fractures. Excluding this matrix effect will lead to wrong and misleading flow estimations. [Figure 2.12](#) clarifies the network.

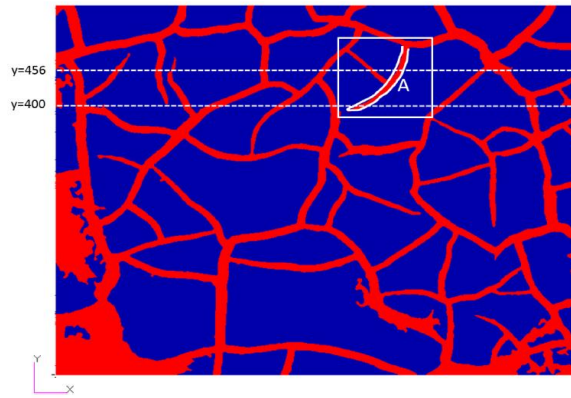


Figure 2.12 Disordered fracture network media: fracture (red) and permeable matrix (blue)

(Yi and Xing 2018), permission for academic reuse from Elsevier Number: 4755050991062)

Ahmadi et al. (2018) experimentally investigated the parallel plates fractures effect, implementing this in a square shape matrix (60 x 60) mm, which was represented by a glass micromodel, with two phase Newtonian fluids (water and oil) to mimic flow in a rough fractured heterogeneous media scenario. Three layers, with varied micro pipe diameters for each layer (200, 250 and 350) micron respectively, represented the matrix, and fractures (with single parallel plates geometry) were fixed with apertures 450 micrometre for all models. Three models were created with the same set-up: one without fractures; another with two separate fractures, each placed with angles of 45° on the flow direction, and the last with two fractures, one perpendicular 90° and one with an angle of 45° on the flow direction. This experiment showed that the fracture and matrix affect and interact on each other during flow in fractured media, due to fracture locations and angles in relation with flow directions, and also the effect of surrounding matrix properties, such as permeability, on flow percentage in the fractured domain. Luo et al. (2020) developed a semi-analytical solution of aquifer flow, based on the Boundary Element Method (BEM) in a 2D model with well pump. This consisted of two types of fractures, discrete (isolated) and connected networks as full domain formations, in order to investigate the behavior of flow between matrix and fracture, and pressure drawdown response in formations. The model's assumptions were: horizontal flow only (no vertical flow); single phase fluid with slight compressibility fracture connectivity was infinite, but with finite (limited) sizes in zones; aquifer resided in the matrix only, and isotropic matrix properties with uniform block size of the formation blocks; and the flow in the matrix and on the edge of fracture-matrix interface was represented by Darcy's law. Moreover, the fractures' geometries were considered as parallel plates fractures with single

apertures. This model's outcomes stressed the effect of the pressure drawdown location (well) in relation to fractures' orientations inside fractured formations, and also that fractures act as main fluid conduits, while the matrix acts as the main fluid supply to fractures. Therefore, only fracture networks transfer fluid to the well, with no matrix contribution to the flow proportion at well. [Lu et al. \(2017\)](#) proposed a semi-analytical model to simulate the transient pressure curves in fractured tight reservoirs by Laplace transform and Stehfest numerical inversion. This model considered stimulated fracture networks, and stressed that a single fracture couldn't represent reservoir conditions. In the developed model, the reservoir was classified into two main regions; firstly, the inner region, which contained artificial main fractures with linear flow and finite hydraulic conductivity, following Darcy's law; and secondly the outer region, which considered flow in natural micro fractures and surrounding matrix, which was assumed is falling under the Warren-Root model with a fixed cube shape and same size micro-fracture apertures surrounding it. This model assumed all the fractures were parallel plates fractures, with single apertures in the network. In the artificial fractures (hydraulic), isotropic properties of reservoir (permeability, porosity), fractures were the main fluid conductors. It assumed the matrix fluid providers as double porosity reservoirs concept with laminar flow, and hydraulic fractures the only fluid conductor to wellbore while natural fractures connect between the matrix and the hydraulic fracture. [Li et al. \(2021\)](#) studied the effect of morphology patterns of fracture networks through modeling micro-networks of fractures of coalbed methane samples. This was done by simulating flow with different pressures, temperatures and isotropic matrix permeability, with simulation method of 2D Lattice Boltzmann method (LBM). The geometries were obtained by optical microscopy nuclear magnetic resonance (NMR), and complexity was characterized by the Box Counting Method (BCM). Network patterns were classified based on the network shape inside the domain, as dendritic, reticular, filamentous and orthogonal. As well, in these networks, a distinction was made in case a fracture of any network connected directly between the inlet and outlet in the domain; this was called a "dominant channel", as the velocity and flow is much larger than other network branches. This study clarified that network pattern shapes, permeability and the existence of a dominant channel have significant effect on flow behavior of the domain, and on domain permeability. The orthogonal pattern reflected the most flow obstacles, while the reticular pattern reflected the most eased flow, whilst dendritic and filamentous patterns were in the middle. This stressed that a network with more connected branches will obstruct flow more than a network

with a simple pattern and less branches. Moreover, this study reflected that any network with higher fracture porosity will increase permeability, and will increase the chance of complicated fluid flow distribution within the domain, which will affect total domain flow. This consolidates the findings of [Wu et al. \(2019\)](#). As well, this clarified the effect of the narrowest fracture aperture on networks, particularly on fracture permeability and flow, as it leads fluid to use different paths and might reduce domain flow. As well, this study confirmed that other numerical simulations such as finite volume method (FVM) have the ability of modeling fracture network patterns with good meshing quality. [Zimmerman and Yeo \(2000\)](#) stressed that fracture networks in fractured formations have numerous small dead-end zones, which will not contribute to flow in fractures, and will lead to error in flow calculations. Instead, it was argued that knowing fracture spacing, and the mean transmissivity of each fracture, gave the ability to use these values to calculate the mean fracture aperture. [Luo, Tang and Zhou \(2019\)](#) developed a semi-analytical method to calculate wellbore pressure and network flow of Z-fold complex fracture network units. In the model, the assumptions were considered as: isotropic properties of porosity and permeability; single phase incompressible fluid with fixed viscosity; and flow in formations followed Darcy's law. Flow in this reservoir type started from the matrix into fractures, then into wellbore through fractures only, and flow could transfer among fractures at intersection points (nodes). Fracture geometries were considered parallel plates fractures with single apertures. This model confirmed that the intersection angle among fracture networks at nodes has an effect on pressure behavior of the domain, and the effect of fracture connectivity, whether high or low, on flow distribution among network fracture units. [Suri et al. \(2020\)](#) modelled a single fracture with varied apertures, with Z-shaped branches by using ANSYS CFD Fluent FVM. Fracture walls were considered permeable with the matrix, and matrix permeability was considered isotropic. Then particle tracking technique in ANSYS CFD Fluent FVM was used to investigate fluid paths with two pressure inlets, 5 and 1000 Pa. The outcome was that a higher-pressure inlet improved flow in the matrix, in comparison with a lower pressure drop, due to the pressure effect on fluid particles that were trapped in pores of the matrix. As well, due to the varied apertures and rapid changes in fracture cross sections, and accordingly in pressure, this led to the creation of eddies in higher velocity sections with low pressure, which drew fluid particles from fracture flow in these areas. These were trapped in fractures, particularly in low inlet pressure, as it left fluid particles in a situation of insufficient momentum to overcome the eddies' forces. [Spence et al. \(2014\)](#) and [Narr, Schechter and](#)

Thompson (2006) stated that fluid flow prediction and movements in naturally fractured reservoirs are highly related to fracture networks' transmissivity and interactions with the surrounding matrix. Hyman et al. (2015) presented Discrete Fracture Network (DFN) modeling, an alternative developed method for generating and simulating flow and transport in 3D fractured media for different scales from millimeters to kilometers. This method is based on Finite Volume solver partial differential codes, and in this study was used to model an example of a fracture network. Fracture geometry shapes were constructed as either lines or planar polygon in 3D, and represented as parallel plates fractures with single apertures. Fracture/matrix interaction was not considered, and fracture intersection points were meshed with triangle shapes, with minimum side triangle length less than fracture apertures, in order to overcome geometry complexity and have a good mesh quality. This work highlighted that fractures with higher aperture heights are less resistant to flow in comparison with smaller fractures. Zou, Jing and Cvetkovic (2017) modeled 3D rough orthogonal fracture network, but excluded the matrix permeability effect by considering fracture surfaces as walls. Single phase Newtonian and incompressible fluid was used, and this was solved with Navier-Stokes equations. This study demonstrated the effects of fracture surfaces' variable apertures and roughness on flow and fluid channeling in fractured formations. As well, it was stressed that the Reynolds equation, and cubic law of flow in a fracture, can predict flow in rough fracture networks with consideration of average aperture. Ishibashi et al. (2012) carried out a similar procedure of 3D modeling of fracture networks, which was conducted by a simulator called "GeoFlow" which considered continuum models. This applied Darcy law of flow in fracture and matrix, and stressed the effects of fracture roughness and flow channeling in a fracture which led to uneven outflow; as well, it confirmed matrix effects and their importance to the domain flow contribution. Liu, Li and Jiang (2016) numerically modeled a 2D discrete fracture network (DFN) with rough surfaces, and impermeable fracture surfaces (matrix effect excluded). This was modeled by ANSYS CFD Fluent FVM to investigate the effects of fracture roughness, aperture height and fracture intersections on DFNs with different pressure drops. This was meshed with triangular cells. The work outcomes were that the non-linear flow regime and hydraulic gradient were affected with rougher fracture surfaces, greater mechanical apertures and a higher number of intersections. As well, surface roughness and fracture intersections were the causes of frictional loss, which requires higher inertial efforts to have significant flow with a high Reynolds number. Moreover, this study observed the creation of

vortices at the fracture intersection junctions, particularly when a fracture had angled orientations. These vortices zones' volumes and numbers were increased with increasing pressure gradients. These intersection junctions in networks had a similar effect on pressure drop as fracture surface roughness. [Popov et al. \(2009\) pp. 226-227, 230](#) modeled a fracture network by using FEM with Stokes-Brinkman equations. The geometry consisted of two fractures crossed with a 45° orientation angle, surrounded with a square shaped matrix with total domain size 0.3×0.3 m, and considered fractures as parallel plates fractures with single apertures of 707 micron (without considering fracture surface roughness). In this study, the matrix was permeable with the fracture, with isotropic permeability. This modeling stated that fracture density (fracture per unit length) and fracture apertures have influence on the effective permeability of the total domain; as well, that the existence of a fracture in fractured media can affect the domain's overall flow substantially. [Zhu et al. \(2020\)](#) stated that in fracture networks, fracture orientation angles (dip angles) have an important effect on a fracture network's flow, fracture permeability and seepage characteristics of a fracture network. In comparison between fracture networks with the same porosity but with different dip angles, as the dip angle increases, the fracture network's permeability decreased. The reason for this permeability decrease is due to the increase of fluid flow resistance, and the maximum dip angle effect is with 45° . As well, a fracture network's permeability increased sharply with increasing the node number (number of intersection points) in the fracture network.

2.5.5 Fluids Imbibition And Invasion Percolation between Fracture and Matrix

As stated by [Yi and Xing \(2018\)](#); [Rasouli and Rasouli \(2012\)](#); and [Crandall, Ahmadi and Smith \(2010\)](#), flow between fracture and matrix and vice versa is affected by abrupt changes of fracture apertures, which results in abrupt changes in pressure/velocity inside a fracture and surrounding matrix, and accordingly, on flow movements between fracture and matrix along the fracture length. Therefore, it's important to highlight briefly the imbibition mechanism between fracture and matrix, through the fracture surface layer (interface layer) that separates them in fractured formations.

[Dietrich et al. \(2005\)](#); [McDonald et al. \(1991\)](#); and [Pruess and Tsang \(1990\)](#) clarified that imbibition and capillary pressure are the main mechanisms of fractured media flow and play a key role in fluid flow, especially with narrow fractures that reach to tens of micrometre in fracture aperture size, and capillary forces play a key part in fluid displacement mechanisms of fracture media, and have been studied by many researchers. [Hughes and Blunt \(2001\)](#) stressed that capillary pressure and viscosity have opposite effects on the flow of fractured media. Capillary pressure flows in narrow channels and drives fluids inside the matrix from a fracture, whilst viscosity drives flow in a more permeable medium, which has a high number of flow channels. Therefore, a new term was developed which is "capillary number", that represents both these driving forces of fluid transfer (capillary pressure and viscosity), applied particularly on the interface layer between matrix and fracture, which denotes forces of viscosity on capillary pressure. [Equation 2.32](#) illustrates it. [Tiab and Donaldson \(2004\)](#); [Berkowitz and Ewing 1998](#); and [Stauffer and Aharony \(1992\)](#) stressed that capillary number values can be altered by two factors: first, increasing the flow rate; and secondly, reducing interfacial forces.

$$N_{ca} = \frac{q\mu}{\gamma} \quad (2.32)$$

Where; q = flow rates per unit area, μ = viscosity of the fluid, and γ = fluids interfacial among pore spaces.

Prues and Tsang (1990) created artificial distribution models of aperture, and assumed the aperture occupancy relied only on local capillary pressure, excluding accessibility. Local capillary pressure was represented by Laplace's equation, which relies on interfacial tension, fracture aperture, and contact angle. The main challenge is fracture aperture (b), because fractures in fractured media consist of varying sizes of aperture. Therefore, determining the capillary pressure of fractured media is not accurate, and usually it has been approximated in many studies (Jahn, Cook and Graham 2008; Tiab and Donaldson 2004). Van Genuchten (1980) proposed many prediction correlations of capillary pressure curves in porous media, and found capillary pressure to be considered as a function of properties of geological formations (pore size, porosity, pore distribution), entry pressure, and saturations. However, Wagner et al. (2001) stressed that the accuracy of capillary pressure predictions relies on many factors, such as porous media types, soil structure, soil texture, and lithologic reservoir formations. Yin et al. (2017) studied coal pore structure by using Nuclear Magnetic Resonance Cytophotometry (NMRC), and clarified that fluid pore structure plays an important role in adsorption of fluids in formations. It was stressed further, that heterogeneous properties of fluids on pores' structure scale affect seepage capacity. As well, formation permeability will be increased when a fluid's heterogeneity has decreased. Roslin et al. (2020) quantified pore distribution in the coal matrix with data analysis by three methods: scanning electron microscopy (SEM) images, nuclear magnetic resonance (NMR) and mercury injection capillary pressure (MICP). As well, the advantages, disadvantages and limitations of each method were highlighted. Ingham and Pop (2005) p. 367 stated that drainage and imbibition of pores' media have a significant effect in predicting fluid percolation.

Reitsma and Kueper (1994) carried out an experiment to predict capillary pressure curves of a rough fracture under various stress loads. These predicted curves were then used to derive the distribution of fractured media apertures. Piri and Karpyn (2007); and Preuss and Tsang (1990) investigated capillary pressure of a rough fracture by modelling the pore-scale network. This modelling incorporated the physics of fluid mechanics into the conceptual geometry of porous media. Many numerical models have used pore scale in modelling, rather than a schematic model in which distribution of aperture is generated artificially. Dullien (1992) built a network model of fractures to mimic fracture networks in real fracture media, consisting of an interconnected network of spaces, to visualise displacement phenomena inside pore scale. Dippenaar and Van Rooy (2016) stated that flow

relation between matrix and fracture is based on fracture as fluid transporter and matrix as fluid provider. As a fracture aperture is much higher than void diameters of interstitial porosity in a matrix, adhesion (the attraction force between water and mineral surfaces) is weak and not dominant in comparison with cohesion (the attraction force between fluid minerals), and cohesion is predominant. This means less capillary flow and more fluid suction into a fracture. As well, as the fracture and matrix face different flow velocities, the non-Darcy conditions generally occur even with low Re value in a fracture, due to the flow tortuosity and fracture surfaces' roughness. [Sahimi \(2011\) pp. 15, 18, 244](#) stressed that a fracture network represents real fractured media, with a fracture or voids surrounded with solid matrix. The inner surfaces of fractures/voids are different, with different roughnesses which consist of different curvature shapes. The pores in these rough surfaces represent the clusters gateway of fluid flow between matrix and fracture, and the continuum percolation theory explains these effects in fractured media, which is an important tool to quantify pore spaces connectivity flow. [Berkowitz \(2002\) p. 856](#) stated that the use of percolation theory in complex subsurface geometry media like fractures networks is important; particularly, in some hydrocarbon wells, it was reported by well test data that only one or two fractures are transferring fluids directly to the well. [Sahimi \(2011\) p. 45](#) confirmed that there are many factors affecting percolation in fractured media, such as fractures' patterns in media, pores' void shapes of the fracture's inner surfaces, fluid properties and etc. [Zimmerman and Bodvarsson \(1996\) pp. 44-45](#) clarified that the percolation limit is relied on as a critical value of inner fracture contact areas with a matrix. [Narr 2011 p. 374](#); and [Narr, Schechter and Thompson 2006](#) stated that fracture connectivity is controlled by an important feature which is fracture permeability, which has been investigated by percolation theory. There are many factors affecting fracture percolation in fractured media, such as: fracture density; size distribution; fractures' orientations; and fracture special distribution (which is related to fractures' intersection and relates to increase fractures' length spanning). However, the effect of fractures' orientation on fractured domain flow, and accordingly on percolation theory, was further stressed. Therefore, in fractured network modeling, fractures' lengths and orientations are important factors to be considered. [Sen \(1995\) pp. 111, 309](#) stated that fluid movement between a matrix and fracture relies on pressure differences between both medias, as both coexist physically in same location; [equation 2.33](#) clarifies it.

$$q_i = \alpha (h_m - h_f) \quad (2.33)$$

Where: q_i = flow rate of matrix/fracture interface layer, h_m = matrix pressure, h_f = fracture pressure, α = parameter for fracture geometry with unit inverse time (1/times).

2.6 Friction Phenomena Overview

Friction can be defined as a tangential resistance force that is generated when the surfaces of materials (such as solid material, or fluids' layers) are physically contacted, either with one surface moving, or both surfaces moving relatively. The value of this force relies on factors based on the conditions of these surfaces, such as: types of material surfaces (liquids, solids); surface roughness; pressure between the surfaces; contact shape; and the velocity of moving surfaces. There are many kinds of friction, based on materials' surfaces and conditions: lubricant friction (fluid separating two solid surfaces); dry friction (solid with solid surfaces); internal friction (material's elements moving due to deformation); fluid friction; and skin friction. This work has focused on two types: fluid friction and skin friction. "Fluid friction" is the result of fluid layers moving on each other relatively. The resistance forces among layers is called viscosity, which is varied based on fluid type; high viscous fluid means it is harder to ease and move, and vice versa for low viscous. "Skin friction" results from fluid motion moving on solid surfaces, due to viscous fluid layers dragging the rough surfaces; this kind of friction relies on solid surfaces' roughness, cross-sectional area, length, and fluid type ([White 2011](#); [Ruina and Pratap 2008](#); [Dullien 1992b](#); [Meriam and Henderson 1992](#); [Swanson 1970](#); [Eskinazi 1968](#)). Friction in closed surfaces, such as pipes or closed channels, will result in pressure drop due to the resistance forces that are generated among fluid layer movements, and between solid surfaces and fluid. These can be measured with a scale called "Friction factor", which represents a ratio of head loss to fluid average velocity in a closed system such as a pipe. "Skin friction factor" represents a ratio of shear stress on solid surfaces to fluid dynamic pressure ([Winterton 2014 chap. 6](#); [White 2011 p. 317](#)).

Historically, the first studies of hydrostatics and hydrodynamics were carried out in eighteenth century by mathematician Daniel Bernoulli. This work, in a textbook in 1738, stated that for incompressible and not viscous fluids, with steady streamlines, energy is conserved through a system (frictionless flow between fluids

and walls and among fluid layers). In 1755, Leonhard Euler completed a derivation of Daniel Bernoulli's work and reached [equation 2.34](#), which is worldwide famous as the "Bernoulli equation"; this is a classic momentum equation similar to Newton's law of incompressible and frictionless fluids, with no energy dissipation to frictions. Therefore, fluids' friction between two points was calculated in that era, of not-advanced calculation, by an empirical formula which was an extension of the "energy equation", as [equation 2.35](#) ([White 2011 p. 169](#); [Brown 2002 p. 3](#)).

$$\left(\frac{P_1}{\rho} + \frac{1}{2} V_1^2 + g Z_1\right) = \left(\frac{P_2}{\rho} + \frac{1}{2} V_2^2 + g Z_2\right) = \text{constant} \quad (2.34)$$

([White 2011 p. 169](#))

$$h_L = \left(\frac{V_1^2}{2g} + h_1 + Z_1\right) - \left(\frac{V_2^2}{2g} + h_2 + Z_2\right) \quad (2.35)$$

([Brown 2002 p. 3](#))

In the 19th century a French mathematician and engineer, Gaspard de Prony, was the first who developed an important equation in hydraulics, which described head loss in pipes and was widely accepted, as [equation 2.36](#). However, these formulas were debated, and were subject to errors due to the exclusion of pipe roughness ([Simmons 2008 p. 1027](#); [Brown 2002 p. 3](#)).

$$h_f = \frac{L}{D} (aV + bV^2) \quad (2.36)$$

Where: h_f = head loss due to friction factor, L = length, D = diameter, V = flow velocity, a & b = empirical factors

In 1839 a German engineer, G.H.L Hagen, carried out experiments about head loss in pipes. Water flow was measured in brass pipes, with the conclusion that there might be two viscous flow regimes; the flow regime was observed changing by increasing flow above certain limits, but the limitations of his work were admitted, and could not be clarified. As well, it was stated that the pressure drop in pipes might be varied as a second power of flow ([White 2011 p. 351](#)). In 1841 Jean Louis Poiseuille introduced an empirical flow formula through the experiment of small diameter capillary tubes, as [equation 2.37](#) below. In spite of the restrictions of this formula, such as low velocity and small diameters, it was one of the first accurate calculations of fluid friction in pipes ([Simmons 2008 p. 1028](#); [Brown 2002 p. 3](#)).

$$Q = KD^4 \frac{h_L}{L} \text{ (Poiseuille's Law)} \quad (2.37)$$

Where: Q= flow, K= empirical coefficient which represents lumps constants with a second order equation for the viscosity, as a function of temperature.

In 1850 a German engineer, Julius Ludwig Weisbach, in the first modern text book to be published on hydrodynamics introduced that the (L/D) affected is proportional on head loss. In 1856, a French civil engineer, Henry Darcy, published a work of design and experiments based on work on Dijon city's water system and fountain during the 1840s. This considered the water flow in internal pipes an important consideration. The intention was to improve the friction coefficient that was developed by Gaspard de Prony. Darcy's results show that friction (head loss) in pipes was due to two factors: pipe diameter and roughness of pipe, as [equation 2.38](#) below. This formula provided a better understanding of friction, as its related friction in pipes to pipe diameter; as well, this scenario applied even with high flow velocities.

$$h_L = \frac{L}{D} \left[\left(\alpha + \frac{\beta}{D^2} \right) V + \left(\alpha' + \frac{\beta'}{D} \right) V^2 \right] \text{ (the Darcy equation of pipe friction)} \quad (2.38)$$

[\(Simmons 2008 p. 1027\)](#)

Where: $\alpha, \alpha', \beta, \beta'$ = friction coefficients

An American engineer, John Thomas Fanning (1837–1911), combined the Darcy and Weisbach formulas to be as [equation 2.39](#); this equation was called "Darcy-Weisbach equation". As well, it's noted that Fanning considered radius rather than the diameter of pipe; therefore, Fanning friction factor is a quarter of Darcy friction factor. In addition, Darcy's work stated that there was a linear relationship between head-loss and flow rate when flow is at a slow speed in small diameter pipes, and the difference of flow regimes in pipes was understood but not quantified. Finally, there was some speculation about the boundary layer of comparisons between smooth and rough pipes. [\(White 2011 p. 356; Simmons 2008 p. 1028; Brown 2002 p. 7\)](#). In 1883 a British engineering professor, Osborne Reynolds, carried out an experiment by introducing a dye into flow inside a pipe to observe flow behavior regimes, as [Figure 2.13](#). The results of this experiment reflected that flow inside a pipe transit from steady into turbulence, and showed that flow change depended on many factors, such as: fluid density, flow velocity, pipe diameter and fluid viscosity. This can be seen as [equation 2.40](#), famously called "Reynolds number", which is a dimensionless value [\(White 2011 pp. 347,](#)

352). Thus, this work classified flow into three regimes, which are: steady and smooth flow "laminar", fluctuating and agitated "turbulent", and in between these two regimes is "transition". (White 2011 p. 347). In 1914 a German professor, Ludwig Prandtl, presented that the thin layers surrounding body surfaces suffer a transition regime from laminar into turbulence, and subsequently, it was confirmed that the body force coefficient was a Reynolds number function "Re". Thus; to conclude, Hagen and Poiseuille started to realize the difference between high and low velocity flow in capillary tubes, whilst Julius Weisbach introduced the effect of (L/D) on head loss; this finding is still effective today. Darcy developed a kernel of truth of the effects of flow velocity, pipe shape (pipe section areas eg. whether circular or rectangular) and surface roughness on friction resistance in pipes. This is particularly important in turbulent flow; however, in his work the flow regimes still were not fully quantified and explained, until Reynolds experimentally fully quantified the occurrence and classified flow speeds into three distinguished regimes in a closed system: laminar, turbulent and transition. (White, 2011 p. 356; Swanson p. 116; Eskinazi 1968 p. 376).

$$h_L = f \frac{L}{D} \frac{v^2}{2g} \quad (2.39)$$

(White 2011 p. 356; Simmons 2008 p. 1028)

$$Re = \frac{\rho}{\mu} v D \quad (2.40)$$

Where: f= a function of (Re, roughness $\frac{\epsilon}{D}$, section shape), v= mean velocity, D= hydraulic diameter, μ = viscosity, ρ = density.

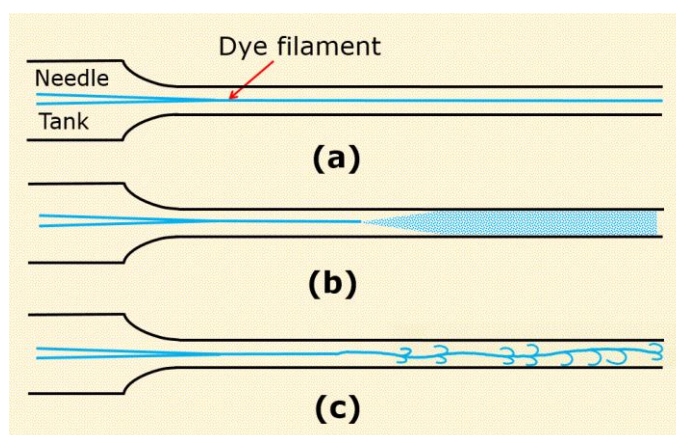


Figure 2.13 Sketches of Reynolds's pipe with flow regimes, a. laminar, b. turbulent and c. transition

(adapted from White 2011 p. 352)

2.6.1 Flow regimes as Reynolds and Forchheimer equations in fractured formations

In most incompressible fluids, density will remain constant. Uniquely, pressure forces will be determined through the balance between inertial forces (the product of mass and acceleration) and viscous forces (the product of shear stresses and area), with exclusion of other forces. Thus, Reynolds number is a dimensionless value and represents the ratio of inertial forces to viscous forces, as [equation 2.41](#) below.

$$\text{Re} = \frac{\text{Inertia forces } (F_i)}{\text{Viscos forces } (F_v)} = \frac{\rho U^2 L^2}{\mu U L} = \frac{\rho L U}{\mu} = \frac{L U}{\nu} \quad (2.41)$$

(Eskinazi 1968 p. 90)

Where: F_p = pressure forces, F_i = inertia forces, F_v = viscosity forces, ρ = fluid density, U = velocity, L = length, μ = viscosity, ν = kinematic viscosity (μ/ρ)

Following Reynolds' classifications of flow regimes in a closed system (such as pipes), as stated earlier, the value can be measured by a scale called "Reynolds number". There are three regimes, which are laminar, transition and turbulence. In each regime, fluid will behave differently, based on the Reynolds number value. When ($\text{Re} < 2,100$), viscous forces are dominant in a system and the flow is laminar flow. This means fluid velocity is low through systems, and fluids move along smooth streamlines, parallel to surfaces. In this flow, fluid flow is virtually constant in time and in any section in system. As well, the pressure drop in a laminar flow system is more than the inertia term. Therefore, friction resistance forces can be described due to the velocity of fluids, and the dimensionless Reynolds number value has been proved experimentally to be the best way to describe flow velocity in any system. When ($\text{Re} > 4000$), the inertia force is dominant and the flow is turbulent flow, which means fluid velocity is high through systems, fluids move randomly, and fluid velocity is varied with time and sections. When ($2100 < \text{Re} < 4000$), this is called transition flow regime; the flow in this region is unpredictable and may have both laminar and turbulent flow in different locations and times in that system ([White 2011 p. 347](#); [Tiab and Donaldson 2004 p. 459](#); [Swanson 1970 p. 116](#); [Eskinazi 1968 pp. 90, 376](#)). To calculate Reynolds number in a pipe of cylindrical shape, the characteristics of length are a pipe

diameter. However, in a parallel plates fracture, the hydraulic radius is equal to $(b/2)$, then Reynolds number is as [equation 2.42](#). The transition between laminar and turbulent flow regimes is $(Re=600)$, which is described as $Re_{critical}$. Moreover, to calculate the Reynolds number for a fracture network, with porous media surrounding and interacting with fractures, porosity and permeability of the matrix is included as [equation 2.43 \(Golf-Racht 1982 p. 305, 310\)](#). Reynolds number relies on two factors: flow rate and viscosity of fluids, as [equation 2.44](#) below. This equation can be applied at any section along a fracture to indicate Reynolds value at that point, and is independent of fracture length ([Nazridoust, Ahmadi and Smith 2006](#)).

$$Re_e = \frac{\rho U 2b}{\mu} = \frac{2b U}{\nu} \quad (Re_{critical} = 600) \quad (2.42)$$

$$Re_e = \frac{5 \times 10^{-3}}{\phi^{5.5}} \frac{U \sqrt{K}}{\mu} \rho \quad (Re_{critical} = 20) \quad (2.43)$$

([Saidi 1987 p. 177; Golf-Racht 1982 pp. 305, 310, 324](#))

$$Re_{\bar{H}} = \frac{Q}{V} \quad (2.44)$$

([Nazridoust, Ahmadi and Smith 2006](#))

Where: U = mean velocity, μ = dynamic viscosity, ρ = density, ν = kinematic viscosity (μ/ρ), b = parallel plates height, ϕ = matrix porosity, k = matrix permeability, Q = flow rate, V = kinematic velocity of fluid

The Forchheimer Model was introduced by Austrian scientist Phillip Forchheimer in 1901, and explains non-linear flow in porous media. Specifically, when flow rate is increased, then pressure loss is transformed from a weak regime to a strong regime of inertia which is called "Forchheimer regime". In this regime, the pressure gradient in porous media is proportional to the square of seepage velocity. Generally, this takes a quadratic relation trend between pressure gradient and seepage velocity; [equation 2.45](#) describes it ([Ma et al. 2018 p. 3; Zhong et al. 2018 p. 3; Dippenaar and Van Rooy 2016; Jambhekar 2011; Sobieski and Trykozko 2011 p. 157; Sen 1995 p. 103; Bear 1972](#)). Since then until now, numerous studies and laboratory experiments in the literature have developed the Forchheimer model, due to the number of certainty and uncertainty issues that the equation faced; it uses empirical verification based on global measurements of velocity and pressure in porous media. Other experiments showed varied results of it, and even Forchheimer has suggested other forms of the equation that are not well known ([Arthur 2018 p. 4; Evans and Civan 1994](#)). [Zhong et al. \(2018\)](#)

p. 3 stated that the Forchheimer formula uses a square root permeability as an equivalent value of length, to enable agreement with linear Darcy law at low velocity. Equation 2.46 clarifies it.

$$-\frac{dp}{dx} = a v + \beta v^2 \quad (2.45)$$

(Arthur 2018 p. 4)

$$-\frac{dp}{dx} = \frac{\mu v}{K} + \beta \frac{\rho v^2}{K^{0.5}} \quad (2.46)$$

(Zhong et al. 2018)

Where: $\frac{dp}{dx}$ = pressure drop in porous matrix, v = velocity, a = coefficient representing a ratio between dynamic viscosity to Forchheimer permeability, β = represent inertial coefficient and fluid density, μ = dynamic viscosity, ρ = fluid density, K = permeability

Following the above, there are many experiments and numerical modeling to investigate the equation: particularly, to calculate more accurately the inertial coefficients β of the Forchheimer formula. This is because it represents a non-linear term which has multiple ambiguities and controversies, with no general agreement; therefore, in most practical application, β value is observed from best fit lines of numerical and experimental data (Arthur 2018; Dippenaar and Van Rooy 2016; Sobieski and Trykozko 2014 p. 321; Jambhekar 2011 p. 15; Sobieski and Trykozko 2011 p. 156; Evans and Civan 1994). Takhanov (2011) studied the validity of the Forchheimer Model and its coefficients in matrix and fractures, and analyzed different formulas that were suggested in the literature, to find Forchheimer coefficient β . This relies on porous medium properties and can be determined through many methods such as laboratory tests and well tests, which have led to many suggested formulas. It was concluded that Geertsma (1974)'s and Pascal and Quillian (1980)'s formulas have good estimations of β values in matrix porous media and fracture media respectively. Equations 2.47, 2.48 and 2.49 below clarify the Forchheimer Model and formulas to find β coefficient.

$$-\frac{dp}{dx} = \frac{\mu v}{K_{fh}} + \beta \rho v^2 \quad (2.47)$$

Where: β = Forchheimer coefficient or non-Darcy flow coefficient (1/m), K_{fh} = Forchheimer permeability (m²) ($K_{fh} \neq K$)

$$\beta = \frac{0.005}{K^{0.5} \phi^{5.5}} \quad (2.48)$$

Where: β = Forchheimer coefficient (1/cm) for porous media, K = permeability (cm²)

(Geertsma 1974)

$$\beta = \frac{4.8 \times 10^{-12}}{K^{1.176}} \quad (2.49)$$

Where: β = Forchheimer coefficient (1/m) for fractures, K = permeability (mD)

(Pascal and Quillian 1980)

Dippenaar and Van Rooy (2016) stated that flow in rock matrix is usually calculated by Darcy's law, as the general assumption of slow flow in subsurface layers. However, if fractures, cavities or high hydraulic gradient exist, then flow in the matrix will be turbulent and Darcy law is not applicable, as the linear relationship between flow rate and pressure drop becomes non-linear. Therefore, in such cases, Forchheimer law is used to explain non-linearity of flow with two parameters: first, "A" linear coefficient, which explains properties of fluid; and second; "B" non-linear coefficient, which explains geometry's effects on the host medium. Equations 2.50, 2.51 and 2.52 illustrate it. Determining "B" parameter is challenging to observe to some extent for different formations, and many studies have suggested different experimental or analytical formulas to observe it.

$$-\Delta P = A Q + B Q^2 \quad (2.50)$$

$$A = \frac{\mu}{K A_h} = \frac{12 \mu}{W e_H^3} \quad (2.51)$$

$$B = \frac{\beta \rho}{A_h^2} = \frac{\beta \rho}{w^2 e_H^2} \quad (2.52)$$

Where: (A, B) = linear and non-linear coefficients, Q = flow, β = Forchheimer coefficient, W = fracture width, e_H = fracture height, K = fracture permeability, μ = dynamic viscosity, ρ = fluid density, A_h = cross sectional area.

2.6.2 Friction factor (head loss) formula in systems

The formula of friction factor is derived, first, by applying the famous Bernoulli equation “continuity equation”, which is a classic linear analysis of momentum. This equation is applicable in closed systems with controlled volume, such as pipes or air ducts, for any cross-sectional shape, such as circular, rectangular and etc., and has been developed and celebrated in many engineering analyses (White 2011 p. 173; Swanson 1970 ; Eskinazi 1968). As well, one can apply the momentum equation of forces in X-direction, to get head loss due to wall shear, gravity and pressure. After rearranging the equation and considering force directions (+ right) (- left), the finding is that head loss is also related to shear stress of solid surfaces, as equation 2.53 and figure 2.14 below. Rearranging the equation 2.53, the finding is that head loss is related to surfaces’ shear stress, and by equalizing $(Z) = L \sin \phi$, the head loss is proportional to h-walls shear stress. This is regardless of the direction of flow, either horizontal/vertical or with angle. As well, it’s proportional to the value (L/d) , as equation 2.54.

$$\sum F_x = \Delta P(\pi R^2) + \rho g (\pi R^2) L \sin \phi - \tau_w (2\pi R) L = \dot{m} (V_2 - V_1) = 0 \quad (2.53)$$

$$\left(\Delta Z + \frac{\Delta P}{\rho g} \right) = h_f = \frac{4 \tau_w}{\rho g} \frac{L}{D} \quad (2.54)$$

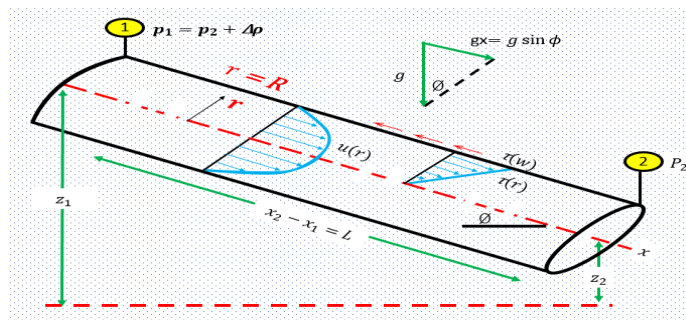


Figure 2.14 Inclined pipe with steady developed flow between two sections
(adapted from White 2011 p. 355)

Thus, equation 2.54 clarifies that the Darcy-Weisbach equation is an effective equation still today, as it states the effect of walls’ roughness, section shape for controlled volume and Reynolds number. It’s good to note that in case the section shape is different, such as rectangle, triangle or square, then it is required to

interpret the average value of wall shear around the perimeter of a section; therefore, it will have a different value of friction factor than a circular shape (White 2011 p. 356). Following this, friction factor was developed based on a section shape of closed systems in relation with Reynolds number (inertial forces/viscous forces). For instance, developed flow in a circular pipe with incompressible steady (laminar) flow, friction factor can be as equation 2.55 below (White 2011 p. 357).

$$f_{\text{laminar}} = \frac{8 \tau_w}{\rho V^2} = \frac{8 \left(\frac{8 \mu V}{D} \right)}{\rho V^2} = \frac{64}{\frac{\rho V D}{\mu}} = \frac{64}{Re} \quad (\text{circular section}) \quad (2.55)$$

(White 2011 p. 357)

2.6.3 Friction factor in naturally fractured formations

Friction behavior has been extensively examined in the 20th century due to its high impact in many sectors, and many experiments have been performed to suit different conditions and cases. However, until now there remain many challenges to estimate the accurate value of friction, due to the complication of calculations and the difficulty to include all ambient conditions of reality in the calculation, particularly in fractured media. Friction factor in fractured media used a similar approach as used in pipes and parallel plates geometries, as a closed and control system, to enable the calculation (Tiab and Donaldson 2004 p. 459). However, the shape mostly considered in describing fractures is parallel plates geometry, and modelled as a series of channels or passages (Nazridoust, Ahmadi and Smith 2006 pp. 316-317; Saidi 1987 p. 169; Golf-Racht 1982 p. 305). As well, it's important to clarify that fracture surfaces in real fractured reservoirs are not flat and polished surfaces, because fracture surfaces (walls) represent the boundaries of mineral grains which were previously joined as one stone (prior to fracturing taking place) (Saidi 1987 p 178). Saidi (1987) p. 169 and Golf-Racht (1982) pp. 306, 310 presented that fracture friction factor in parallel plates geometry with a rectangular cross section area will be as equation 2.56. The differences from a pipe friction factor are due to the difference of parallel plates' hydraulic height, which is (b/2), rather than a pipe diameter. As well, for similar geometry, this work presented empirical friction factor formulas for laminar flow regions, where the height is much smaller than the length for two cases. First, a single smooth parallel plates

fracture, where the finding is that the friction factor is as [equation 2.57](#). Second, for a single rough parallel plates fracture, which included a roughness effect ratio to mimic natural fracture walls, as there's always a degree of roughness on their surfaces, for which the friction factor is as [equation 2.58](#). [Saidi \(1987\) pp. 169-171](#) stated experimentally that head losses due to friction resistance are proportional to the kinetic energy of fluid that flows through a solid conduit with solid surface walls, where viscosity effect is excluded. Therefore, pressure loss will be corresponding to shear forces at conduit surface areas. [Figure 2.15](#) clarifies this case. Moreover, it was stressed that in case the section shape is not clear along the flow, then hydraulic radius can be used instead; this represents as a ratio of cross section area to length of wetted perimeter at that section, multiplied by four. Therefore, for circular hydraulic radius will be ($4 \pi \frac{r^2}{2\pi r} = 2r = \text{Diameter}$) and for rectangular conduit ($4 b.L/2(b+L) = 2b$) by assuming that $b \ll L$.

$$f = \frac{96}{Re} \quad (2.56)$$

$$f = \frac{6}{Re} \quad (2.57)$$

$$f = \frac{6}{Re} \left[1 + 6 \left(\frac{e}{b} \right)^{1.5} \right] \quad (2.58)$$

Where: f = friction factor, Re = Reynolds number, e = average roughness height of surfaces, b = fracture height

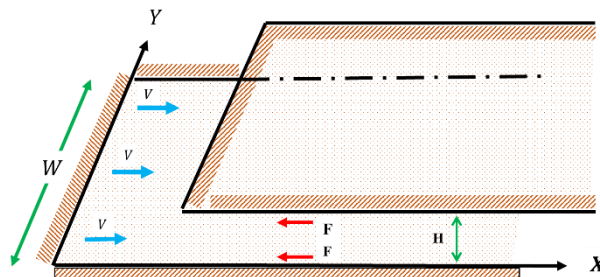


Figure 2.15 Rectangular parallel plates and friction resistance due to surfaces' shear forces only (excludes viscosity)

(adapted from Saidi 1987 p. 170)

[White \(2003\)](#) introduced that pressure drop in fractures represents the pressure drop summations in each segment, and pressure drop in any segment of a parallel plates fracture, with varied apertures and viscous fluid flow, is as [equations 2.59](#) and [2.60](#), and the friction factor coefficient as [equation 2.61](#).

$$\Delta P = \sum \Delta P_i \quad (2.59)$$

$$\Delta P_i = 12 \frac{\mu L_i V_i}{H_i^2} \quad (2.60)$$

$$f = \frac{2 \Delta P \cdot H}{\rho L V^2} \quad (2.61)$$

Where: v = mean velocity, L = fracture length, ρ = density of fluid, μ = fluid dynamic viscosity and H = aperture height between two parallel plates.

[Oron and Berkowitz \(1998\)](#) stated that cubic law of flow in fractures should not be measured on a point to point base, but instead should be measured on a certain range of a fracture's length with average value, and the Re critical value shall be 10. Moreover, it was clarified that a rough fracture with varied apertures has a similar structure of different segments glued together with varied orientations/apertures in each fracture, which consist of numerous corners among them. This will lead to change flow directions and will add additional head loss on flow. [Zimmerman and Yeo \(2000\)](#); [Schrauf and Evans \(1986\)](#) and [Louis \(1969\)](#) stated that flow in fractures can be turbulent with Re greater than 10, as Re will start to reflect non-linearity. As well, Re is not the only factor affecting flow; fracture surfaces' roughness also has an important effect. Therefore, both Re and roughness have a main effect on flow in rough fractures, and should be considered in predicting fractures' flow. [Singh, Singh and Pathegama \(2014\)](#) carried out an experiment on a single fracture created from granite core, to study the effect on flow in rough fractures with applying confining pressure. The outcome was that fracture flow is sensitive to confining pressure and to fracture surface roughness. As well, the Re investigation in this experiment reflected that flow can be turbulent with different values of Re , such as 4 or 10 based on fracture roughness, fracture apertures and fracture flow, which cause large asperities and flow turbulence. There are many developed fracture friction factor models with inclusion of fracture roughness, matrix effect, Reynolds number limit and different methods that have been used to develop it. These were summarised in the [Table 2.1](#) below. Moreover, each model is presented separately to clarify it and distinguish the differences among them. [Masciopinto \(1999\)](#) developed a fracture friction factor model with impervious walls (no flow between matrix and fracture) by a best fit line, which was based on the translations of flow in porous media data. This considered the flow between porous particles as a two parallel plates channel with impervious

porous media particles, and relied on Fanning values of friction factor in laminar ($f=1000/Re$), and for non-laminar relied on the porous media granular data. The values were shifted with $(96/1000)$, as Darcy friction factor was considered equal to four times Fanning friction factor (Darcy friction = 4 x Fanning friction factor). The best fit line was then applied from the observed data. Therefore, this model has no linearity, and can be applied for laminar and non-laminar flow. [Nazridoust, Ahmadi and Smith \(2006\)](#) developed [White \(2003\)](#)'s equations to include the effects of tortuosity and effective fracture aperture on White's equations, due to the expectation of the main pressure drop occurring in small apertures of fractures, as [equations 2.62, 2.63](#) below. As well, four profiles of fractures were modelled in 2D ANSYS CFD Fluent FVM simulations, considering solid impermeable surfaces. From the simulations' results, the friction factor was observed for each fracture by using [equation 2.61](#), then compared with the friction factor equation for laminar flow in a smooth parallel plates fracture ($f=96/Re$). The result of this comparison was that the deviation between the values of these two results increased by increasing Reynolds number values, which suggests that the friction factor of equation ($f=96/Re$) underestimates friction factors in fractures with parallel plates. As well, it was noted that friction factor has non-linear Re dependence when Re is high. Therefore, based on these data, a new friction factor was introduced from a best fit regression line of friction factor, that accounts for the effects of tortuosity and roughness by considering effective fracture apertures which predict friction factor more accurately. With this, as roughness increases, then, friction factor value is increased. [Figure 2.16](#) presents it.

$$f = \frac{2 \Delta P \cdot \bar{H}}{\rho L (1 + \theta) V^2} \quad (2.62)$$

$$f = \frac{2 \Delta P \cdot \bar{H}^3}{\rho L (1 + \theta) Q^2} \quad (2.63)$$

Where: Q= flow rate per unit width ($Q=A.V$) and substituted in [equation 2.70](#), A= fracture sectional area ($\bar{H} \times 1$ unit width), V= mean velocity

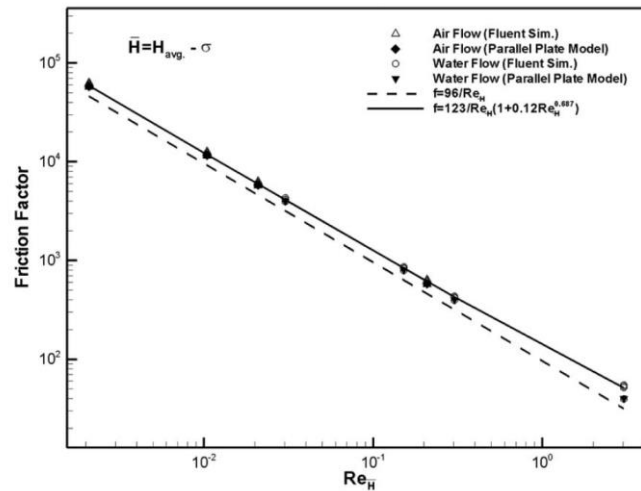


Figure 2.16 Comparisons of friction factors between CFD and parallel model results

- higher friction factor with rougher fracture in comparison with smooth parallel plates ($F=96/Re$)

(Nazridoust, Ahmadi and Smith 2006)

Crandall, Ahmadi and Smith (2010) used the same 2D fracture profiles of Nazridoust, Ahmadi and Smith (2006), and used ANSYS CFD Fluent simulations to model these fractures with inclusion of matrix affects. They assumed fracture walls were permeable, with fluid transfer between matrix and fracture in the same domain. Based on these assumptions, a mathematical model of the friction factor equation was developed, to include matrix affect. This was done by including surrounding isotropic matrix permeability (K), which allows fluid to pass through the fracture walls due to imposed pressure, in addition to the effects of fluid properties and roughness. Thus, the total flow in the domain is the sum of flow in the surrounding matrix and fracture; flow in surrounding matrix was assumed to follow Darcy's law for flow in porous media. As well, a fracture friction factor was calculated from the CFD simulations with different permeability values, and compared with the developed model. It was shown to be well matched, and the friction factor reduced in permeable walls which allow fluid movements into fracture, increasing flow percentage in comparison with impermeable walls. Qian et al. (2011) experimentally studied fracture roughness and average apertures' effects on fracture factor (for not permeable fracture surfaces). This work considered the applicability of local cubic law for flow in a single fracture as a Darcy flow, particularly when Re is greater than 10. A smooth parallel plates fracture was created from plexiglass plates, then another six profiles of rough fractures were created from plexiglass plates; these had a square shaped pattern but with different heights varied from 1 to 6 mm, to create different roughnesses and sharp

corners to represent fracture reality, and were glued on a smooth surface. Fractures were vertically situated, and steady Newtonian fluid was used with open unconfined flow (open to atmospheric pressure). The average apertures and friction factor were calculated. The outcomes of these findings were that flow in rough fractures was affected by fracture apertures and surfaces roughness, and friction factor decreased with a high value of Reynold number (Re) with less rough fracture surfaces, in comparison with the same Re with higher roughness. [Zhang and Nemcik \(2013\)](#) experimentally developed a friction factor model for Darcian and non-Darcian fluid flow, based on two independent variables of Reynolds number and relative roughness of fracture walls (a/eh). It assumed fracture walls were impermeable with no flow between matrix and fracture. Best fit regression was conducted on the data, and it derived friction factor. As well, the proposed predictor of friction factor was compared with parallel-plate ($96/Re$) and [Nazridoust, Ahmadi and Smith \(2006\)](#)'s models. The results were that the new model had better friction factor estimation, due to roughness changing fracture surfaces, when matched with experiment results. This is due to the fact that the parallel plates model underestimated the friction effect, while [Nazridoust, Ahmadi and Smith \(2006\)](#)'s model overestimated it in some values of Re, particularly between Re values 2 and 10. [Zhou et al. \(2016\)](#) developed a semi-analytical friction factor model by using the Forchheimer formula that includes viscosity resistance and inertia resistance, by accounting for fracture roughness (asperity). As well, it could be used in turbulent flow, not only laminar flow. However, this model excluded the matrix effect by only considering impermeable fracture surfaces. [Chen et al. \(2017\)](#) modelled experimentally and numerically by ANSYS CFD Fluent FVM horizontal fractures, for different conceptualized patterns of roughness with Newtonian single-phase fluid and turbulent flow. Fracture surfaces were impermeable (no matrix/fracture flow). In this study, a new correlation of fracture friction factor was introduced, which accounted for a concept of "equivalent diameter", that equals fracture average apertures minus twice the average asperity height of the fracture's rough surfaces. [Su et al. \(2019\)](#) experimentally developed a rough fracture friction factor from fractures that were obtained from cores, and considered non-permeable fracture surfaces with the matrix. The proposed model accounted for non-linear flow effects and relative roughness of fracture surfaces. All friction factor models were classified and illustrated in [Table 2.1](#) below.

Table 2.1 Summarizes the developed models of fracture friction factors

Model	Model Formula	Matrix Effect	Fracture Roughness	(Re) Limit	Method
Parallel Plate	$f = \frac{96}{Re}$	--	--	--	Conceptual analytical model
Masciopinto (1999)	$f = \frac{96}{Re} + 1.48 + \frac{10.08}{\sqrt{Re}} - \frac{28.88}{e^{Re}}$	--	--	--	Porous media data interpretation
Nazridoust, et al. (2006)	$f = \frac{123}{Re_{\bar{H}}} (1 + 0.12 Re_{\bar{H}}^{0.687})$	--	Yes	$Re_{\bar{H}} \leq 10$	Numerical CFD
Crandall, et al. (2010)	$f = \frac{123}{Re_{\bar{H}}} \frac{(1 + 0.12 Re_{\bar{H}}^{0.687})}{1 + 61.5 (1 + \theta) (1 + 0.12 Re_{\bar{H}}^{0.687}) \left(\frac{Kh_m}{H^3}\right)}$	Yes	Yes	$Re_{\bar{H}} \leq 10$	Analytical
Qian et al. (2011)	$f_w = \frac{g e \Delta h}{L V^2}$, $e = \frac{Vol_f}{\frac{1}{2}(h_1 + h_2)L}$	--	Yes	$Re > 10$	Experimental
Zhang and Nemcik (2013)	$f = \frac{96}{Re} \left[1 + 9.57115 \times 10^{-4} \left(\frac{a}{eh}\right)^{1.1172} \right]$	--	Yes	$Re < 10$	Experimental
Zhou et al. (2016)	$f = \frac{96}{Re} + 4a \cdot \left(\frac{\delta}{2eh}\right)^b$	--	Yes	--	Semi-analytical
Chen et al. (2017)	$f = \frac{96}{Re} \left(1 - \frac{2\Delta}{b} \exp\left(-\frac{A}{0.058 Re}\right)\right)^{-3}$	--	Yes	--	Experimental
Su et al. (2019)	$f = \frac{96}{Re} \left(1 + a_2 \left(\frac{2 m_{out}}{\mu w (1-c)}\right)^{b_2}\right) \cdot \left(1 + c_2 \left(1 - \left(\frac{12 \mu L^3 w^2 (1-c)^2}{A V_v^3}\right)^{\frac{1}{2}}\right)^{d_2}\right)$ $A = \frac{12 \mu}{w e_h^3}$	--	Yes	--	Experimental

Where: f = fracture friction factor, Re = Reynolds number; for [Crandall, et al. \(2010\)'s model](#) (h_m = domain height, K = matrix permeability, θ = tortuosity, \bar{H} = effective fracture aperture height); for [Qian et al. \(2011\)'s model](#) (e = average aperture, Vol_f = volume of water content in fracture (m^3), (h_1, h_2)= water levels, V = average velocity in fracture, L = length, g = acceleration); for [Zhang and Nemcik \(2013\)'s model](#) (e_h = hydraulic diameter, a = height of maximum asperity); for [Zhou et al. \(2016\)'s model](#) ($2 e_h$ or D_h = hydraulic diameter, δ = height of peak asperity, a and b = coefficient values 0.022 and $2/3$ respectively); [Chen et al. \(2017\)'s model](#) ($A = (L_a/\Delta)$ roughness distribution, L_a = the distance between two elements (zones) of rough surfaces, Δ = roughness height, b = average aperture height); for [Su et al. \(2019\)'s model](#) (V_v =void ratio (m^3), c = contact ratio, w = fracture width perpendicular on flow direction (m), L = fracture length, (a_2, b_2, c_2, d_2) = fitting parameters, μ = viscosity, m = mass flow rate (kg/s), A = linear coefficient, e_h = equivalent perpendicular gap of smooth parallel plate fracture (m)).

2.7 Summary of the literature review

In this chapter, fractured formations' characteristics and parameters were reviewed, such as: permeability, porosity, single fracture flow (parallel plates and rough fractures), fracture network flow, imbibition and percolation, and fracture friction factor. The review started with theories, then considered other development works to examine both understanding and the developments within. To the best findings and analysis of the literature materials in this work, it has been found that fractured media are one of most complex challenges to solve and to understand the interior flow. This is due to many reasons, such as: complex geometry of fractures with heterogeneous cross sections along the flow; fracture surface variations (varied roughness); fracture types, whether individual fractures in a matrix or connected with a network of fractures; and the anisotropic properties of the surrounding matrix (permeability, porosity). All these factors have increased the difficulties in understanding and calculating flow inside fractured media, due to the difficulty of accounting for all these variables in one solution to understand the flow phenomena. Therefore, the majority of previous studies relied on simplification assumptions, that can help one to understand the flow, and at the same time have, as much as possible, realistic models which can visualize and

approximate flow as in real fractured media such as subsurface layers of the earth's crust.

Fractured media were investigated experimentally by samples represented in many methods, such as core samples from reservoir formations and fractured representative materials such as rough sheets of fibres or glass with different roughness's degrees. As well, these were investigated numerically, by using many kinds of Computational Fluid Dynamics simulators (CFD), such as: FVM, FEM, Lattice Boltzmann method (LBM), and multiple in-house software which were developed based on the desired investigation. In these numerical simulations, fracture geometries were drawn and represented in a range of ways: as single parallel plates fractures with single apertures; as rough fractures obtained from cores, where X-rays were used to transfer surface geometries' data coordinates into software; and by using representative methods such as Discrete Fracture Network (DFN) which generate fracture geometries as network groups, where each fracture is a parallel plates fracture with single aperture height. Many of the studies used assumptions in their models, such as: smooth fractures with single apertures; rough fractures without matrix effects; fracture networks which consist of smooth fractures with single apertures without matrix effects; rough network fractures but with isotropic matrix properties or without inclusion of matrix; and fractures considered as sole fluid conductor, while the matrix is purely a fluid storage provider. Thus, there are many gaps in understanding and modelling fracture media flow. Models are required that have more options to mimic fractured media conditions, in order to obtain the best and most accurate results and avoid errors in flow calculations, and these are covered in the following chapters.

3 CFD Methodology

3.1 Overview

The summary of the literature review (section 2.8) highlighted the complexity of fractured media and the assumptions that were considered in the literature's models. Therefore, to account for all these challenges of flow modelling in fractured media, it is mandatory to have a tool that is capable of accounting for as many variables as possible, and able to solve them. This makes it possible to get an approximate image of flow in fractured media, and to have improved and optimised flow calculations, minimising errors. With the current development of numerical modelling software, particularly in the last two decades, researchers have extensively used CFD to investigate flow in fractured media by using ANSYS CFD Fluent FVM. This has enabled the inclusion of many variables in one model to optimise the calculation results. ANSYS CFD Fluent FVM was used by many researchers of fractured media to validate their work experimentally and theoretically, such as: [Suri et al. \(2020\)](#); [Karimzade et al. \(2019\)](#); [Chen et al. \(2017\)](#); [Liu, Li and Jiang \(2016\)](#); [Rasouli and Rasouli \(2012\)](#); [Hosseinian \(2011\)](#); [Rasouli and Hosseinian \(2011\)](#); [Sarkar, Toksöz and Burns \(2011\)](#); [Crandall, Ahmadi and Smith \(2010\)](#); [Crandall, Bromhal and Karpyn \(2010\)](#); [Crandall, Bromhal and Smith \(2009\)](#); [Koyama et al. \(2009\)](#); [Petchsingto and Karpyn \(2009\)](#); [Kulatilake et al. \(2008\)](#); [Petchsingto 2008](#); [Nazridoust et al. \(2006\)](#); [Sarkar \(2002\)](#); and [Zimmerman and Yeo \(2000\)](#). These pieces of research have confirmed that Ansys-FLUENT (FVM) is one of most efficient and powerful tools available to be used in fractured media calculations, due to many factors, such as: the ability to investigate and include complex variables; the ability to visualise flow and quantify velocity and pressure in fractures and the surrounding matrix; and that the Navier-Stokes equation gives a reasonable representation of laminar, Newtonian fluids, and complex passages of fracture models which are modelled as a series of narrow pipes or channels. Thus, in this research ANSYS CFD Fluent FVM was used as a tool to investigate fractured media models. This chapter highlights the ANSYS CFD Fluent FVM equations and parameters. As well, it delineates the previous models of fractured media with ANSYS CFD Fluent FVM and the limitations

in their work, then clarifies this study's approach by combining ANSYS CFD Fluent FVM as a tool with the new models.

3.2 Fracture Flow Modelling

After reviewing previous works of fractured media in the literature, it has been observed that their works (experimental, numerical and analytical) have valuable outcomes for understanding flow in fractured media. However, these works have used assumptions in their modelling, as follows:

1. [Su et al. \(2019\)](#); [Chen et al. \(2017\)](#); [Zhou et al. \(2016\)](#); [Briggs, Karney and Sleep \(2014\)](#); [Zhang and Nemcik \(2013\)](#); [Qian et al. \(2011\)](#); [Petchsingto and Karpyn \(2009\)](#); [Petchsingto \(2008\)](#); [Piri and Karpyn \(2007\)](#); [Nazridoust, Ahmadi and Smith \(2006\)](#); and [Yamatomi et al. \(2001\)](#) considered single rough fracture geometry, but assumed impermeable fracture surfaces (matrix flow from the media was excluded and no fluid transfer between matrix and fracture was assumed).
2. [Rasouli and Rasouli \(2012\)](#); and [Crandall, Ahmadi and Smith \(2010\)](#) considered rough fractures with matrix flow effect (permeable fracture surfaces); however, only isotropic matrix properties were considered.
3. [Luo et al. \(2018\)](#); [Sarkar, Toksöz and Burns \(2011\)](#); and [Popov et al. \(2009\)](#) considered parallel plates fractures with single aperture geometry without matrix flow effect (impermeable fracture surfaces). [Luo et al. \(2018\)](#) and [Popov et al. \(2009\)](#) considered matrix effect (permeable fracture surfaces); however, only isotropic matrix properties were considered.
4. [Hyman et al. \(2015\)](#); and [Sarkar, Toksöz and Burns \(2004\)](#) considered fracture network geometry with smooth parallel plates fractures with impermeable fracture surfaces. While [Luo, Tang and Zhou \(2019\)](#); [Ahmadi et al. \(2018\)](#); [Lu et al. \(2017\)](#); and [Popov et al. \(2009\)](#) considered similar types of geometry, but with isotropic properties of matrix effect (permeable fracture surfaces).
5. [Zou, Jing and Cvetkovic \(2017\)](#); and [Liu, Li and Jiang \(2016\)](#) considered fracture network geometry with rough fractures and impermeable fracture surfaces. While [Yi and Xing \(2018\)](#) considered rough fracture networks with matrix flow effect (permeable fracture surfaces) with isotropic matrix properties.

To understand the behaviour of flow in rough fractures (also known as real fractures) in subsurface layers of earth crust, it's mandatory to compare these models' set-up with the real flow conditions of subsurface layers. This makes it possible to get a conclusion of these models' limitations, and highlight the required developments which were needed in order to build a model which increased flow understanding in these media. Thus, the main limitations that these studies had are:

- Assumed impermeable fracture walls (no fluid transfer between matrix and fracture). However, [Rasouli and Rasouli \(2012\)](#); and [Crandall, Ahmadi and Smith \(2010\)](#) stressed that matrix flow has a big impact on fracture flow.
- Assumed permeable fracture surfaces with isotropic permeability of surrounding matrix along the flow. However, fractured formations are highly anisotropic, and properties such as permeability and porosity vary from point to point in these formations ([Sahimi 2011](#); [Tiab and Donaldson 2004](#); [Nelson 2001](#); [Golf-Racht 1982](#); [Saidi 1987](#)).
- Assumed single smooth parallel plates fractures with single apertures. However, fractures are constructed from rough stone surfaces with varied apertures ([Sahimi 2011](#); [Tiab and Donaldson 2004](#); [Nelson 2001](#); [Saidi 1987](#); [Golf-Racht 1982](#)). As well, many researchers such as [Rasouli and Rasouli \(2012\)](#); [Petchsingto and Karpyn \(2009\)](#); [Petchsingto \(2008\)](#); [Piri and Karpyn \(2007\)](#); and [Nazridoust, Ahmadi and Smith \(2006\)](#) stressed that rough fractures have a key effect on pressure drop and flow in comparison with smooth parallel plates fractures with single apertures.
- Assumed single horizontal fracture in fractured domain. However, fractures are highly heterogeneous and are distributed randomly in fractured formations, with varied types of connection degrees and angles among them ([Nelson 2001](#); [Golf-Racht 1982](#); [Ruhland 1973](#)). Moreover, many researchers such as [Luo, Tang and Zhou \(2019\)](#); [Ahmadi et al. \(2018\)](#); [Yi and Xing \(2018\)](#); [Lu et al. \(2017\)](#); [Zou, Jing and Cvetkovic \(2017\)](#); [Liu, Li and Jiang \(2016\)](#); and [Popov et al. \(2009\)](#) stressed the effect of fracture network on flow distribution in a fractured domain, in comparison with a single fracture effect.

Therefore, based on these limitations of previous works in the literature, the outcomes of these pieces of research therefore don't reflect many of the real

conditions of fractured media fluid flow. There are many gaps which needed to be covered in a model, in order to have a better calculation, understanding and accuracy, to optimise flow calculations in fractured media due to the highly anisotropic properties of fractured subsurface layers ([Sahimi 2011](#); [Tiab and Donaldson 2004](#); [Nelson 2001](#); [Saidi 1987](#); [Golf-Racht 1982](#)). Thus, the following points outline this work's plan to cover a deeper vision of fluid flow in fractured media, such as:

- a) A parallel plates fracture was created with the surrounding matrix, considering fracture surfaces permeable with the matrix and impermeable, where the matrix permeability is considered isotropic and anisotropic. This kind of fracture geometry is a simplified geometry of fractures in subsurface layers, and is widely used due to the simplicity of modelling, enabling the summarizing of all fracture apertures in one single aperture to present the average of entire fracture apertures.
- b) A two-dimensional ANSYS CFD Fluent FVM rough fracture model was developed, based on models from literature, to validate the outcome of these study models. This work was achieved by re-modelling [Nazridoust, Ahmadi and Smith \(2006\)](#); and [Crandall, Ahmadi and Smith \(2010\)](#)'s models, then extending the investigation of the models to get a better understanding and vision of flow in fractured media, by considering a permeable fracture interface with anisotropic matrix properties surrounding the fracture along the flow.
- c) A two-dimensional ANSYS CFD Fluent FVM rough fractures network was developed. This work was achieved by re-modelling [Nazridoust, Ahmadi and Smith \(2006\)](#)'s single rough fracture and creating different fracture positions of network patterns from [Yi and Xing \(2018\)](#)'s model, for widening the expectations of fractures' positions in the subsurface layer of fractured media. ANSYS CFD Fluent FVM was then used to observe the pressure, velocity and flow in the fractured media. This part is described in more detail in chapter six due to the importance of this effect.

Based on this outline, ANSYS CFD Fluent FVM was employed in this work as the main tool to create these models, as it has the ability to solve the instantaneous equations that govern flow in fractured media, and the outcomes were observed.

3.3 Computational Fluid Dynamics - ANSYS CFD Fluent FVM Overview

Computational fluid dynamics ANSYS CFD Fluent FVM is a numerical system (computer-based simulation) that involves solving problems that are associated with fluid motion. It is able to analyse complex fluid phenomena, such as heat transfer, fluid flow, and related phenomena. This technique is very powerful and has been applied and used by a wide range of industries due to many reasons, such as: cheap in cost in comparison with expensive experimental facilities to achieve accurate results; the results of simulations have been validated with experiments, proving the accuracy of ANSYS CFD Fluent FVM results; an essential reduction in time to get results in comparison with experiments; an ability to study new designs and areas that experimentally is so difficult to achieve, and likewise, the ability to study areas which are hazardous to investigate; and the ability to get wide ranges of results by changing the designs of the targeted goals (ANSYS, 2013; Versteeg and Malalasekera 2007 p. 1). As stated in the previous section, ANSYS CFD Fluent FVM has been used in many studies and researches of fluid flow in fractured media and validated with experiments and theoreticals, and its validity and capability of visualising accurate calculations of fluid flow, velocity and pressure have been proven. Sarkar, Toksöz and Burns (2004) p. 16 stated that investigating fractured media flow by Computational Fluid Dynamics flow simulations is a most reliable method, and stressed further: in most cases, perhaps it's the only reliable method to estimate hydraulic parameters of fractured media. Crandall, Ahmadi and Smith (2010); and Nazridoust, Ahmadi and Smith (2006) confirmed the importance of ANSYS CFD Fluent FVM in investigating fluid flow in fractured media, due to its efficiency and the reliability of observed results. Hosseinian (2011) stated that modelling a 2D fracture is very effective in demonstrating fracture properties' effects on fluid flow in rough fractures. However, the difference with 2D models is that when fracture apertures are zero, then, fluids will stop flowing, whereas a 3D model will provide another path for fluids to flow. Rasouli and Hosseinian (2011) modelled rough fracture geometry (non-permeable fracture surfaces with matrix), in order to investigate (JRC) effects of synthesized rough fracture on flow. They used 2D- ANSYS CFD Fluent FVM models, and stressed that the main difference between 2D and 3D models is that 2D models are important and give sufficient flow representations, but fluid flow in

narrow fractures should not be with zero value, as it will lead to no fluid flow with zero velocity if a fracture is closed. While, in 3D, fluid will take different paths in case apertures have zero value along the flow. Therefore, an assumption was considered that the minimum fracture apertures for a 2D model is not zero value at any point along the flow. Similar 2D models were considered in other studies, such as: [Rasouli and Rasouli \(2012\)](#); [Sarkar, Toksöz and Burns \(2011\)](#); [Crandall, Ahmadi and Smith \(2010\)](#); [Koyama et al. \(2009\)](#); [Petchsingto and Karpyn \(2009\)](#); [Kulatilake et al. \(2008\)](#); [Petchsingto \(2008\)](#); [Nazridoust, Ahmadi and Smith \(2006\)](#); [Sarkar \(2002\)](#); and [Zimmerman and Yeo \(2000\)](#), which each confirmed a similar approach in modeling 2D geometries of fractures.

[Karimzade et al. \(2019\)](#) stated that Finite-Volume Method FVM was introduced in the previous decade as a powerful tool in CFD. It has good features that make it popular in CFD, such as high flexibility in the discretization method implementation, which will carry a physical domain directly without transformation between physical and computational coordinates systems. In other words, CFD FVM has the ability to model complex geometries without any necessity to transfer the coordinate system, and the discretization of conservation equations in finite volume (as some terms defined as fluxes), and the shared adjacent faces, will be conserved. This feature is the main reason which attracts engineers and researchers to use CFD FVM in modeling rough and complex fractures. However, there are some works which used Finite Element Method FEM, and had two main issues in complex flow. Firstly, it doesn't guarantee conservation firmly, while physical laws of fluid flow rely on conservation laws. Secondly, there was a difficulty in coordinate transformations between physical and computational systems, due to the geometry complexity. In this research, the desired investigation was fluid flow in open fractures, with no flow obstruction at any point or any apertures with zero value aperture height. Thus, a 2D model in ANSYS CFD Fluent FVM was considered in all the models of this research. [Figure 3.1](#) below illustrates the iterative loop of calculation procedure in ANSYS CFD Fluent FVM.

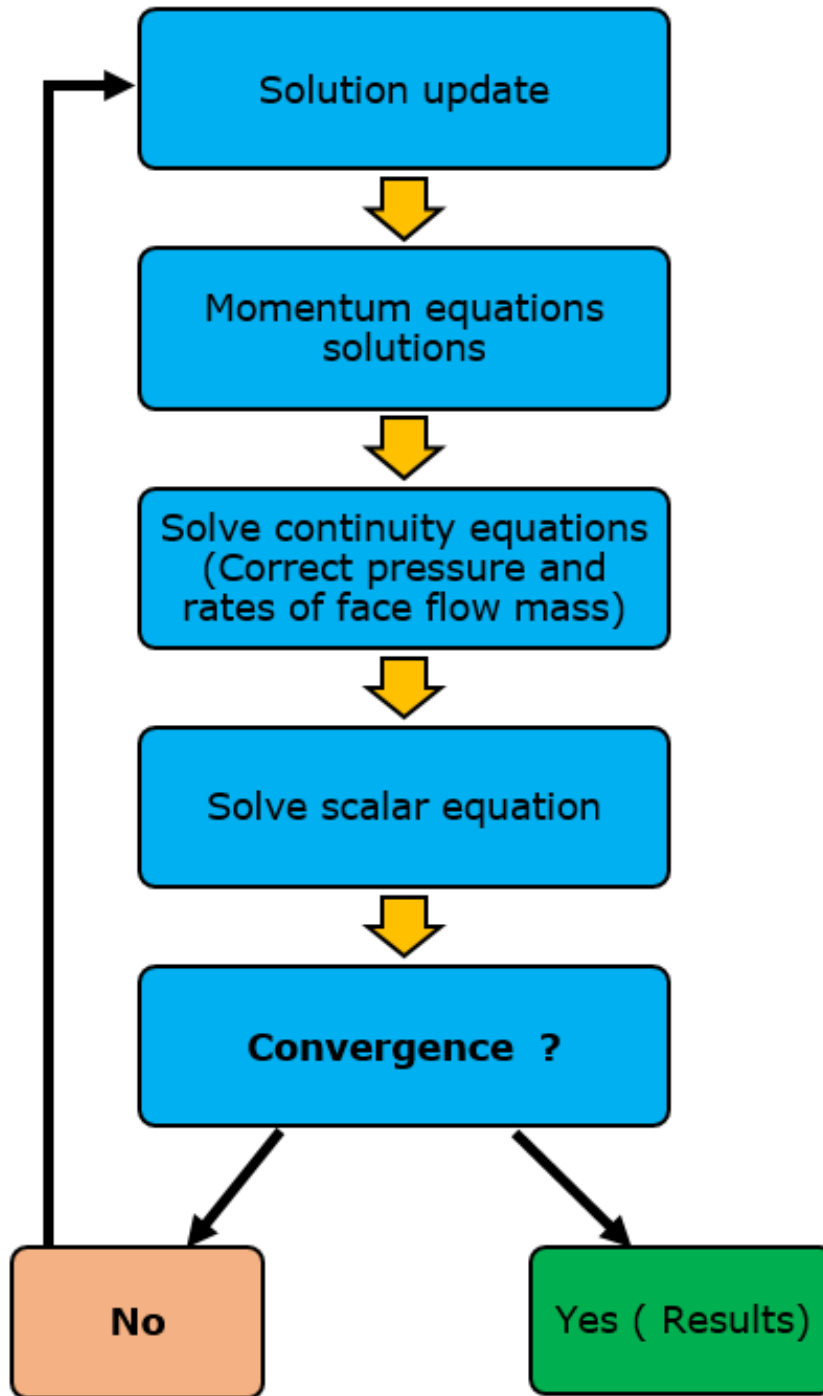


Figure 3.1 Iterative loop of calculations in ANSYS CFD Fluent FVM
(adapted from Zabaleta 2007)

3.3.1 Governing equations

All ANSYS CFD Fluent FVM packages, with all kinds and forms, are based on the fundamentals of governing equations, such as continuity and momentum. These represent the mathematical statements of physical principles that all fluid dynamics rely on, which are: Conservation of mass (fluid mass is conserved), and, Momentum conservation (second law of Newton “ ΣF (forces)=m (mass) x a (object acceleration)” - the rate of change of momentum equals forces summation of fluid particles). Flow of fractured porous media in this study’s conditions was assumed to be isothermal system, steady-state, and incompressible single-phase fluid (ANSYS 2013; Sarkar, Toksöz and Burns 2011 p. 3; Crandall, Ahmadi and Smith 2010 p. 501; Versteeg and Malalasekera 2007 p. 2). Thus, the governing equations: first, mass conservation (continuity equation); with the assumptions of flow in this study, the continuity equation is as equation 3.1, transit terms effect is neglected. And second, the momentum of porous media was solved by using Navier-Stokes equation as equation 3.2, transit terms effect (unsteady acceleration) is neglected.

$$\nabla \vec{u} = 0 \quad (3.1)$$

$$\rho [\nabla \cdot (\vec{u}\vec{u})] = -\nabla p + \mu \nabla^2 \vec{u} + F \quad (3.2)$$

Where: \vec{u} = velocity, ∇p = pressure gradient, ρ = density, F = a source term of momentum related to surfaces (external) body force added to the momentum equation, which account for flow in porous media, and is represented by re-arranged Darcy law as equation 3.3 below (ANSYS 2013; Sarkar, Toksöz and Burns 2011 p. 3; Crandall, Ahmadi and Smith 2010 p. 501; Versteeg and Malalasekera 2007 p. 2).

$$F = \nabla p = \frac{\mu}{K} u \quad (3.3)$$

Where: k = permeability

Ansyz (2011) p. 229-231 stated that specifying porous zones in ANSYS CFD Fluent FVM geometry models will empirically incorporate flow resistance determination, which builds in models of porous media that add momentum sink into governing

momentum equations. These models do have limitations and assumptions; for example, FLUENT by default uses superficial velocity in porous media zones, based on volumetric rate, to ensure continuity and velocity vectors across the entire domain. In general, this gives good representations of bulk pressure loss through a porous zone. Likewise, porosity is assumed isotropic; and ANSYS CFD Fluent FVM models' thermal equilibrium between solids and fluids of porous zones and others, which are not covered in the scope of this research. Moreover, porous media can be modelled with ANSYS CFD Fluent FVM by adding a source term of momentum to the standard equations of fluid flow, as [equation 3.4](#) below. This source term consists of two parts. The first part is Darcy's loss term of viscosity (first part of the right-hand side in the [equation 3.4](#)), and the second part a term of inertia loss (second part of right-hand [equation 3.4](#)). The contribution of this momentum sink, for porous zone pressure gradient, creates a pressure drop which is proportional to the velocity of fluid.

$$S_i = - \left[\sum_{j=1}^3 D_{ij} \mu V_j + \sum_{j=1}^3 C_{ij} \frac{1}{2} \rho |V| V_j \right] \quad (3.4)$$

Where: S_i = momentum equations source term for i^{th} (x,y,z) Cartesian directions, $|V|$ = velocity magnitude, (D and C)= proscribed matrices, μ = viscosity, ρ = fluid density

For isotropic porous media, the source term is as [equation 3.5](#).

$$S_i = - \left(\frac{\mu}{k} V_j + C_2 \frac{1}{2} \rho |V| V_j \right) \quad (3.5)$$

Where: k = porous media permeability, C_2 = a factor of inertial resistance (1/k)

When flow is laminar in porous media, the pressure drop is proportional to velocity; in this case, C_2 will be considered zero, and the porous media model will be reduced to Darcy's law as [equation 3.6](#) below. In FLUENT, the pressure drop was computed in (x,y) Cartesian axis directions, then Darcy's law is as [equations 3.7](#) and [3.8](#).

$$\nabla p = - \left(\frac{\mu}{k} \vec{V} \right) \quad (3.6)$$

$$\Delta p_x = \sum_{j=1}^3 \frac{\mu}{k_{xj}} V_j \Delta n_x \quad (3.7)$$

$$\Delta p_y = \sum_{j=1}^3 \frac{\mu}{k_{yj}} V_j \Delta n_y \quad (3.8)$$

Where: $\Delta n_x, \Delta n_y$ = porous medium thicknesses in (x,y,z) Cartesian axis

3.4 Boundary Conditions In ANSYS CFD Fluent FVM

In any numerical model, boundaries can be defined as a domain bordered with surfaces which are closed, and possibly, with segments at infinity. These surfaces represent arbitrary mathematical surfaces. Fluid flow models are governed with partial differential balance equations, which describe extensive transport of quantities. These equations require information regarding a models' materials (solids and fluids), flow rates in and out, velocities, pressures and etc. When this information is put together, a set of equations is solved for a range of required variables, which provides information of future fluid behaviour in any particular interest in a model. These equations of models have an infinite solution number; therefore, in order to study any particular case, it's mandatory to provide adequate information for these models, such as: geometry data of where fluid flow takes place; a good description of the initial state of a model (initial conditions); and domain interaction description, with external surrounding environments and internal, known as "boundary conditions". Boundary conditions reflect real conditions that are available for a problem, and it is vital that they are stated accurately, because different conditions lead to different results. Usually, these conditions are observed from the known external side of a model, which in general is available and in some cases is assumed, based on the approximated surrounding environment (Bear and Buchlin 1991 p. 78-79). Ansys (2011) p. 261; and Versteeg and Malalasekera (2007) p. 267 stated that all ANSYS CFD Fluent FVM models are defined based on terms of initial boundary conditions; therefore, it's very important to specify these conditions correctly and understand their effect on a numerical model's algorithm. In Finite Volume method FVM of ANSYS CFD Fluent, the most common boundary conditions are: inlet; outlet; wall; symmetry; interior; and other boundaries, which are out of this research interest. The boundaries of this research interest are highlighted briefly in the following sections, as well, these boundaries will be assigned and locations clarified in the models of this research in this chapter, under each model's section.

3.4.1 Pressure inlet boundary conditions

Boundary conditions of a pressure inlet are used to define fluid flow pressures at inlet boundaries of a model with other flow properties, which are suitable for compressible and incompressible fluids. Moreover, these conditions can be used when only inlet pressure is known, and other variables such as inlet velocity or inlet flow rate are not known (Ansys 2011 pp. 267, 270; Versteeg and Malalasekera 2007 p. 68). At the pressure inlet dialog box, much information is required to be logged-in, such as whether static or total pressure, fluid phases, flow direction and etc.

3.4.2 Pressure outlet boundary conditions

The boundary conditions of pressure outlet are used in conjunction with inlet boundaries; if the outlet location is selected far away from the inlet, and the distance between them allows fully developed flow with no flow direction changing, then that surface can be chosen as outlet and all variables can be stated. Generally, outlet surfaces are predicted based on flow direction, and are perpendicular on flow (Ansys 2013 p. 487; Ansys 2011 p. 294; Versteeg and Malalasekera 2007 pp. 271-273).

3.4.3 Wall boundary conditions

The wall boundary is the most common boundary which is usually encountered in confined domains' fluid flow problems. Considered solid walls and parallel to flow, then, at these walls there are two velocities, which are: component of u-velocity (parallel to walls) and component of v-velocity (perpendicular on walls). For solid wall boundaries with no slip conditions, it's appropriate to consider velocity components with ($u=v=0$), which means cells adjacent to walls are set with zero velocities in both directions of velocity components. In ANSYS CFD Fluent FVM, walls conditions were used to bound regions of solids and fluids and viscous flows, which by default enforces no-slip walls. As well, other variables can be specified, such as tangential velocity, slip walls by specifying shear and etc. As well, there

are many inputs which can be specified, based on walls conditions and the desired outcome of a model (Ansys 2013 pp. 45, 67, 90; Ansys 2011 pp. 313-316).

3.4.4 Symmetry boundary conditions

When the geometry of a physical model has patterns of expected flow solutions which are mirrored symmetry, then, applying this model into ANSYS CFD Fluent FVM offers an option of using symmetry boundary conditions. Using this boundary reduces the extension of the ANSYS CFD Fluent FVM model to a subsection of symmetric boundaries of an overall physical system. The benefit of this reduced mirrored model extension is to have a smaller geometry model which can provide the same desired results, whilst saving cost: first, through less simulation time by having a lower mesh cells number; and second, less cost by using a lower specification of computer. One of the most critical points of using symmetry boundary is to determine the location correctly which matches with the reality of a physical model's setups and conditions; similar to other boundaries, this is required to be defined correctly and with roles understood. By enabling the symmetry boundary, there is no need to define any other inputs. By default, this boundary considers: first, flow will not cross it; second, scalar flux will not cross it; third, at the symmetry boundary, normal velocities will be set to zero; and fourth, all other properties' values outside the (domain) symmetry boundary will be equal to the nearest nodes' values, that are adjacent to the symmetry boundary but from the domain side (inside domain). Thus, based on these conditions, the symmetry boundary of FLUENT assumes zero flux quantity, no diffusion of flux, and all normal gradients of flow variables are set with zero at the plane of symmetry. (Ansys 2013 p. 167; Ansys 2011 pp. 334-336; Versteeg and Malalasekera 2007 p. 280).

3.4.5 Interior (face) boundary conditions

An interior face is a double-sided face which can be used to separate two zones or regions with different properties and conditions, with shared internal boundaries, where all cells are contained in a single model. By separating the cells into two distinct zones, it provides more options to mimic real physical models into ANSYS CFD Fluent FVM, as [figure 3.2](#) below. By assigning interior face boundary for any

internal surfaces in the geometry model, the properties of the interior face are applied by default, and do not need any inputs to be added. An interior face boundary lies on the partition line, and has two neighbouring adjacent cells of mesh. Therefore, it does not have any finite thickness and can be applied only in internal boundary zones. Moreover, interior face conditions allow: first, fluid particle movement among internal domain zones in a model; second, the effects of pressure and velocity of fluids on adjacent zones; and third, when fluids are entirely inside any particular zone, then, the fluid will be affected by the assigned conditions of that zone. Therefore, it's much appreciated in modelling physical cases such as porous zones and radiators. The mechanism of interior face in ANSYS CFD Fluent FVM functions by macro vectors that connect between the centres of cells and entire cells' vectors. These macros will return information that will be used in first, evaluating face value scalars, and second, diffusive fluxes of scalars across boundaries of cells. These macros can be clarified in [equations 3.9 and 3.10](#) and [figures 3.2 and 3.2](#) below. In [equation 3.10](#), the first right hand term represents primary gradient which will be directed along the vector, while the second right hand term represents the cross diffusion. To avoid confusion, it's good to note the difference between interior zones and interior faces. An interior zone is a zone of entire FLUENT internal domain after being exported into FLUENT-solution stage. However, if there are many zones, based on the domain type of a model, then the entire internal zones of a model will be considered as an internal zone ([Ansys 2013 p. 160](#); [Ansys UDF Manual, 2013 p. 232, 233, 234, 418, 433](#); [Ansys 2011 pp. 94, 191, 211-212, 214, 640, 1126-1127, 1966, 1977, 2351, 2358](#)).

$$\phi_f = \phi_0 + \nabla_{\phi} \cdot \vec{dr} \quad (3.9)$$

$$D_f = \Gamma_f \frac{(\phi_1 - \phi_0)}{ds} \frac{\vec{A} \cdot \vec{A}}{\vec{A} \cdot \vec{e}_s} + \Gamma_f \left[\bar{\nabla}_{\phi} \cdot \vec{A} - \bar{\nabla}_{\phi} \cdot \vec{e}_s \frac{\vec{A} \cdot \vec{A}}{\vec{A} \cdot \vec{e}_s} \right] \quad (3.10)$$

[\(Ansys UDF Manual, 2013 p.233\)](#)

Where: ϕ_f = gradient scalar of cell face, ϕ_0 = gradient scalar of cell centroid, \vec{dr} = vector connects between centroid and face of a cell, D_f = diffusive flux across face (f), Γ_f = diffusion coefficient at cell face, \vec{A} = face's area of normal vector between adjacent cells, ds = distance between cells centroids, \vec{e}_s = unit normal vector between cells' centroids, $\bar{\nabla}_{\phi}$ = average gradient of two adjacent cells.

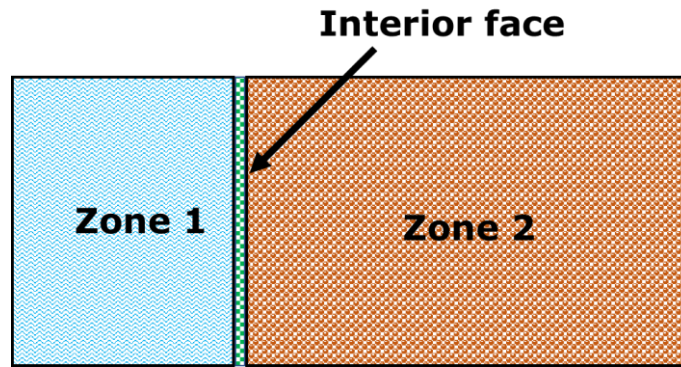


Figure 3.2 Two separated zones with an interior double-sided face (green colour) - interior face was thickened in drawing for clarification
 (adapted from Ansys 2011 p. 191)

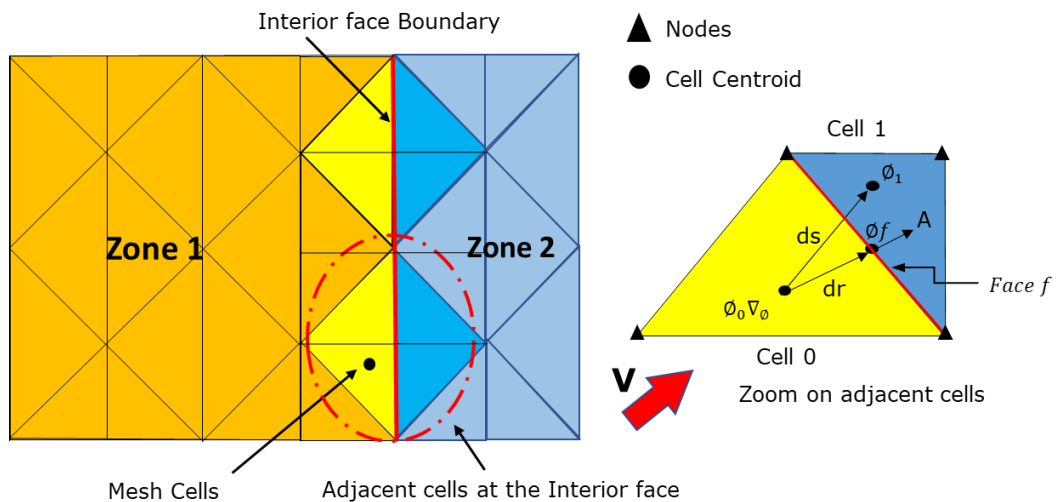


Figure 3.3 Clarifies adjacent cells at the Interior face boundary in ANSYS CFD Fluent FVM, and zoom on cell's gradient scalar with vectors of cell centroid and cell face
 (adapted from Ansys UDF Manual, 2013 p.234, 418)

3.5 Modelling Fractured Media Using ANSYS CFD Fluent FVM

The ultimate goal of the numerical model is to have a better vision of fluid flow inside fractured media. aids a pragmatic approach that will help with understanding flow behaviour and the properties of fluid transportation in naturally fractured media. Thus, as was highlighted in section 3.2, the gaps and the required steps to investigate these gaps were studied. First, parallel plates fractures were studied; secondly, rough fracture (parallel plates fractures with varied apertures

from rough fracture lab core coordinates); thirdly, comparisons between the two case scenarios were made (presented in chapter four); fourthly, fracture friction factor was investigated from these models (presented in chapter five); and lastly fracture network model details were considered (presented in chapter six). It's good to note that ANSYS CFD Fluent FVM models of rough and parallel plates fractures are clarified in the following sections, and then the following chapters present the results and discussions of these numerical models.

3.5.1 Parallel plates fracture

A parallel plates fracture model with a single fracture height has been used widely in describing fractures of fractured media, and has been reported in many studies in literature (Dietrich et al. 2005; Tiab and Donaldson 2004; Warren and Root 1963); the reason it has been used widely is due to the simplicity of flow calculations and descriptions in fractured media. This method is based on the evaluation of fracture cross-sections that change along the flow path, by taking the average height of fracture cross-sections, and using the average value of fracture heights as a single fracture height with two parallel plates. The total fracture connectivity will be a parallel plates fracture with only one height; figures 3.4 and 3.5 demonstrate this model. Thus, to prove the validity and applicability of this kind of geometry that conceptualizes fractures of fractured media, a parallel plates model was needed to investigate the flow and interaction with the surrounding matrix. This was a model that could be compared with other models that were more complex, which made it possible to: first, understand this method's applicability as a simplified model; and second, clarify the effect of more complex geometries that have closer similarities to fractured media in real subsurface layers.

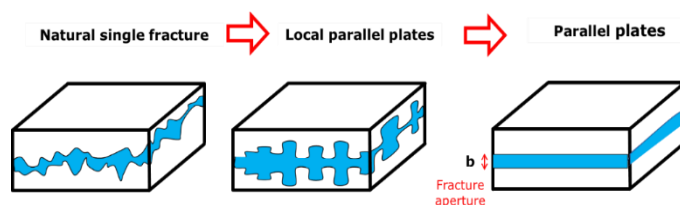


Figure 3.4 Concept of going from rough fracture in nature to parallel plates fracture with single aperture

(adapted from Dietrich et al. 2005)

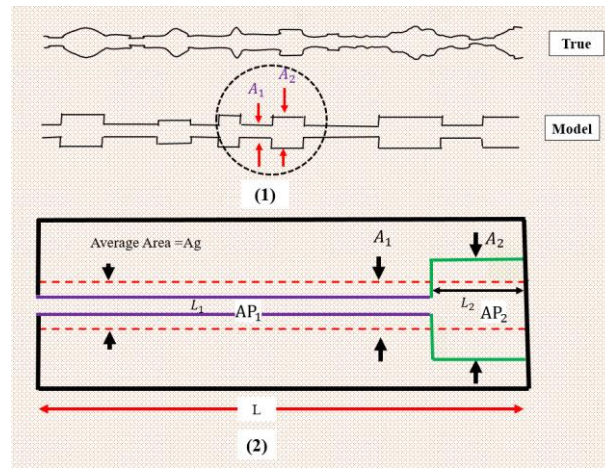


Figure 3.5 Fracture cross-section variations

1. True and rough conceptualized fracture models. 2. Zoom on rough conceptualized fracture part, which clarify the average Area of fracture cross-sections with rough fracture (parallel plate geometry with varied apertures)

(Adapted from Tiab and Donaldson 2004)

3.5.1.1 Parallel plates fracture geometry

ANSYS CFD Fluent FVM DesignModeler was used to draw the geometry. The task was to create the fracture geometry (2D) in the middle of the matrix domain with a square shape (10.15x10.15) cm. To achieve this task by FLUENT DesignModeler, first, the matrix domain was drawn with (10.15x10.15) cm. Then, a parallel plates fracture was created with a single height (H_f), which was similar to the average value of fracture apertures of Nazridoust, Ahmadi and Smith (2006)'s fracture (D), which was (581) micometre. The reason for considering this fracture aperture average value was because the same fracture has been considered in the following sections of this chapter, and it represented the rough fracture, or fracture with varied apertures along with the flow of fracture. Figure 3.5A below clarifies the parallel plates geometry.

3.5.1.2 Meshing the geometry

Two main operations of pre-processing were accomplished: first, the geometry was meshed; and second, the geometry boundary conditions were named. The meshing process can be defined as the discretisation of the geometry with suitable grids or cells, so that the ANSYS CFD Fluent FVM equations can be read among other surrounding cells in order to interpret the phenomena in that particular section. These cells, or grids of mesh, were constructed from a matrix of elements, which were constructed from a series of connecting flat surfaces with varied

shapes, such as: squares, rectangles, triangles, tetrahedrons, hexahedrons and polyhedrons. These shapes could be constructed based on geometry shapes, whether regular or irregular shapes_ (ANSYS 2013). As the geometry was a regular geometry with straight lines, therefore the mesh that was used in the ANSYS DesignModeler (pre-processing) was an automatic mesh with element size type, and quadrilateral based. The geometry was divided into three zones: fracture; matrix around fracture (more than 10 times the fracture aperture height in each direction - above and below the fracture - to capture the interaction between fracture and matrix); and the rest of matrix media. Each zone was assigned with different cell numbers based on the priorities, and, as stated that (due to the large discrepancy between the properties of the matrix and the fracture) large gradients occur in the vicinity of the fracture-matrix interface (Dietrich et al. 2005 p. 42), to get a numerical accuracy, the model's mesh needed a high degree of refinement in these areas (Rasouli and Rasouli 2012 p. 4; Dietrich et al. 2005). In this model, the fracture and the matrix surrounding the fracture had the highest priority and were assigned with finer mesh than the rest of matrix, in order to get the best results possible of interaction between fracture and matrix. Thus, the size of each cell in different zones were: Zone (A), the far matrix zone, was assigned with (120) micrometre size; while, Zone (C) the fracture zone and Zone (B) the matrix surrounding fracture, both had the highest priorities and were assigned with (12) micrometre size per mesh cell: Figure 3.6C clarifies the domain zones. The total number of mesh cells for the entire domain was more than one million and six hundred and fifty-six thousand (1656468) cells. Figure 3.6D and Table 3.1 clarify mesh cells' quality and cells number. In addition, grid sensitivity analysis was carried out in the following chapter in section 4.2.1, which clarifies the reason behind selecting this cells number for the mesh.

After the meshing was completed, the boundary conditions were named and assigned for the domain, as follows. The inlet was set to be "pressure inlet" instead of velocity inlet; this was to mimic the real conditions in subsurface layers in the earth's crust, and to represent pressure as the main drive mechanism of fluids in fractured porous media; the flow was in X-direction, parallel to the fracture domain. The domain outlet was set to be "pressure outlet" and kept with zero value, to allow pressure to build inside the domain between the inlet and the outlet. The upper and lower boundaries of the matrix edges were set to be symmetrical boundary, to mimic the conditions of a matrix continuously outstretching in Y-direction beyond matrix edges; this was because, generally in ANSYS CFD Fluent

FVM, the main effect of the fracture on the surrounding matrix is approximately 10 times that of the fracture aperture, and more matrix area in the model is not required to be added to the model to observe further matrix effects (Hussain 2016; ANSYS 2013; ANSYS 2011). The matrix and the fracture were set up as interior zones domains. The fracture surfaces were set up as “Walls boundary”, when the aim was to investigate a fracture that was not interacting with matrix (as in some cases), and as “Interior face boundary” when the effect of fracture interaction with matrix was investigated (in most of the cases). This was because the “Interiors face” set-up allowed the interaction between the fracture domain and the matrix domain, so fluid particles could pass between these two domains; Figure 3.6B below clarifies the domain boundaries and interior zone names. At this stage, the mesh was completed and the domain was ready to be transferred into post-processing stage ANSYS CFD Fluent FVM.

Table 3.1 Mesh cells statistics

Cells	Faces	Nodes	Partitions
1656468	3315740	1659273	4

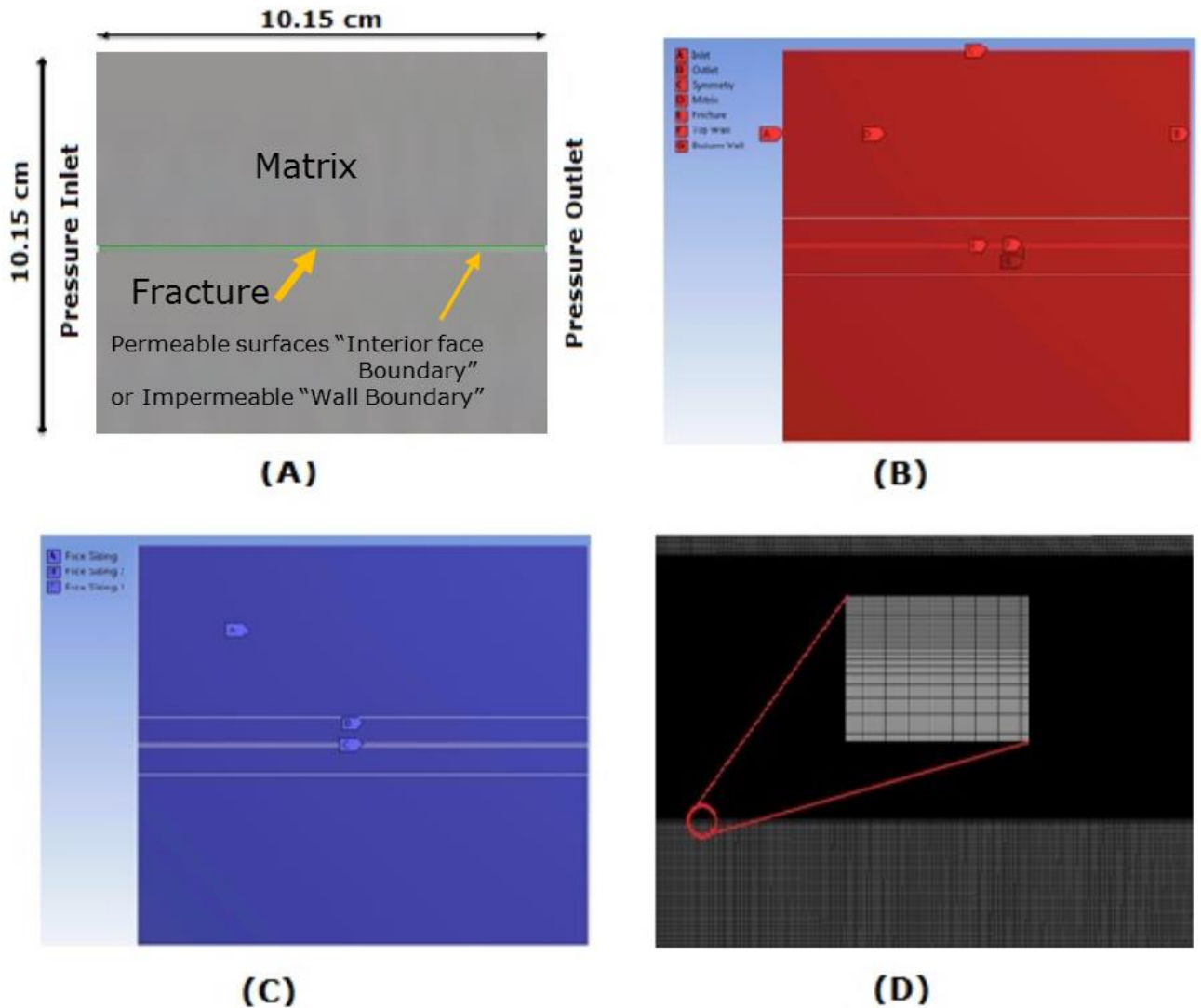


Figure 3.6 parallel plates fracture with single aperture by ANSYS CFD Fluent FVM DesignModeler

A. geometry of parallel plates fracture with surrounding matrix (the matrix is grey, the fracture is green), B. domain boundary conditions, C. zones for the meshing process, and D. section of the fracture mesh, clarifying the three zones of mesh cells' density

3.5.1.3 Simulation set up of parallel plates fracture

At this stage, many processes needed to be completed, which were: the physics set-up of the model was assigned; the fluid type was chosen; the values and types of the boundary conditions were assigned; the simulation iterations residuals were selected; and the simulations were started. The model conditions that were considered were a viscous, laminar, single-phase fluid model, because the targeted goals of this research were to focus on laminar flow in fractured porous media. This is due to the low Reynolds number of flows in fractured media that were reported in the literature. In addition, this enabled a comparison with previous studies' results. Water was considered as the fluid flow in the fracture and the matrix. The properties of the water were: density 998.2 kg/m^3 , viscosity 0.001003

kg/m.s, and chemical formula H_2O . The model was divided into two main geometry zones (fracture and matrix) and each zone had different conditions: the fracture zone was considered as an open channel and doesn't need further specific details, while the matrix zone was considered a porous zone surrounding the open fracture. The fluid in both zones was considered as water. A porous zone is a permeable medium, and many properties had to be assigned here. Matrix permeability: different permeabilities were considered (as clarified in chapter four of each model), this can be different for each flow direction X and Y in the case of (Anisotropic permeability), or the same for X and Y directions in the case of (Isotropic permeability). Matrix porosity: this was considered 20 % in these models. Different pressure inlet values were considered for both zones, fracture and matrix, such as (5, 100, 1000, 2000) Pa, and zero pressure value at the outlet for both zones too; this will result the flow in X-direction and is parallel to the fracture domain. Just to clarify here, these conditions were created to be similar to the conditions of the [Crandall, Ahmadi and Smith \(2010\)](#) model, which enabled the comparison of this model's results with their results. The momentum equation in this solution used "Simple scheme" second-order upwind, and for pressure "second-order" ([Ansys 2013 p. 160](#); [Ansys UDF Manual 2013 p.234, 418](#); [Ansys 2011 pp. 94, 191, 211-212, 214, 640, 1126-1127, 1966, 1977, 2351, 2358](#)). All the results and discussions of this model are clarified in Chapter Four of this research.

3.5.2 Rough Fracture - parallel plates fractures with varied aperture heights (regeneration [Crandall, Ahmadi and Smith \(2010\)](#)'s model)

Rough fracture geometry, most of the time, is simplified with a parallel plates fracture, due to the difficulties of flow calculations, and of creating a geometry which has accurate details of fracture geometry that can be used in the numerical simulations. However, the simplification of the parallel plates fracture with one fracture aperture height does not represent the reality of flow conditions in fractured subsurface layers of earth crust. Therefore, as highlighted in Chapter Two (literature), some researchers and industry experts have used rough fractures that have varied fracture heights along the flow, to approximate or mimic real flow conditions, to optimise the outcome results of flow calculations in fractured media. These kinds of fractures are called different names within the literature, such as:

parallel plates with varied fracture aperture height; real fracture conditions; fracture with local paralleled plates; or rough fractures. It's good to note here that this kind of fracture still doesn't represent the full vision of flow in a rough fracture, but it does approximate flow conditions in varied fracture apertures. This enables better accuracy of flow calculations because of the following: first, flow suffers from changing pressure and velocity along fracture's flow, so this flow calculation will reflect better understating of interaction between fracture and surrounding matrix; and secondly, vortices are initiated inside a fracture due to the changing of fracture apertures, which reduce fracture flow contributions, as a percentage of flow will not contribute to main bulk fracture's flow (as well, vortices affect the mechanism of imbibition between the fracture and the matrix and vice versa). Thus, to create a model of a rough fracture, it was essential to consider one of the models that had been created in the previous literature, so that this research could validate the new models. Therefore, in this work, the rough fracture geometry that was generated was a parallel plate with varied fracture apertures height. This fracture was generated from a rough fracture by using an x-ray method, and transferred into parallel plates fractures with high-resolution CT scan imaging with voxel 240 microns by [Piri and Karpyn \(2007\)](#). As well, [Nazridoust, Ahmadi and Smith \(2006\)](#); and [Crandall, Ahmadi and Smith \(2010\)](#) used the geometry of the same fracture for their models. Thus, in this work, one of the fractures that was considered in [Nazridoust, Ahmadi and Smith \(2006\)](#); and [Crandall, Ahmadi and Smith \(2010\)](#)'s papers was used, and the methods explained below. This model was a core scale model, which reflects flow in a sample of fracture media. [Glover and Hayashi \(1997\)](#) clarified that modeling a fracture with a centimeter scale can be applied to a field scale flow calculation with 100m scale.

3.5.2.1 Geometry of rough fracture

The rough fracture geometry that was created in the modelling of this research was based on one of the fracture images chosen from the [Nazridoust, Ahmadi and Smith \(2006\)](#)'s paper, which is the same as in [Crandall, Ahmadi and Smith \(2010\)](#)'s paper. This fracture is fracture (d) in [Nazridoust, Ahmadi and Smith \(2006\)](#)'s paper, (figure 2 p 318); [Figure 3.7](#) below clarifies it. All the steps of recreating this fracture and validations are clarified in [Appendix 1](#). After completing the statistical features of fracture apertures of this fracture, and being assured that the fracture had the same fracture properties of [Nazridoust, Ahmadi and Smith \(2006\)](#)'s fractures, ANSYS CFD Fluent FVM DesignModeler was next used to draw the

geometry. The goal was to draw the fracture geometry in the middle of the matrix domain, with a square shape sized (10.15x10.15) cm, which was similar to Nazridoust, Ahmadi and Smith (2006)'s fracture profile and Crandall, Ahmadi and Smith (2010) fracture's domain with surrounding matrix, and to achieve this task by FLUENT DesignModeler. First, the matrix domain was drawn with a size of (10.15x10.15) cm, then, the fracture coordinates were imported into the design module of FLUENT and fracture surfaces were drawn, as clarified in Appendix 1. Figure 3.8 below clarifies the final geometry shape.



Figure 3.7 Rough fracture, fracture (d) from Nazridoust, Ahmadi and Smith (2006)'s paper, figure 2 p. 318

(permission for academic reuse from Elsevier Number: 4755041107899)

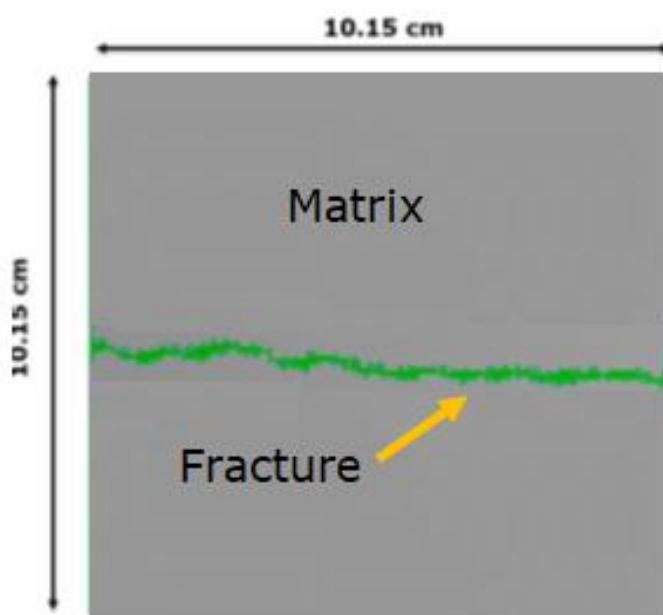


Figure 3.8 The final geometry of the rough fracture inside the matrix domain (the matrix is grey, the fracture is green)

3.5.2.2 Meshing rough fractured media geometry

Meshing was a very important stage and special care was mandatory; this was particularly true when the geometry had irregular shapes, as if the mesh was not good, then this would affect the accuracy of the simulation's results (ANSYS 2013; Sarkar, Toksöz and Burns 2011 p. 3; Versteeg and Malalasekera 2007 p. 3; Zabaleta 2007). In this stage, two main operations of pre-processing were achieved: first, the geometry was meshed; and second, the geometry boundary conditions were assigned and named. Similarly, as the section 3.5.1.2, the

geometry of this model was divided into three sections: the fracture, the matrix around the fracture and the rest of the matrix media. Each section was assigned with different sizes of cells based on the priorities; the fracture and the matrix surrounding the fracture were assigned with finer mesh than the rest of matrix, in order to have the best results possible of interaction between fracture and matrix, [Figure 3.9C](#) clarifies it. As well, efficient and limited numbers of cells of the domain were used in order to reduce the time consumptions of the simulation. Thus, Zone A, the far matrix zone, was assigned with 72 micrometre size of each cell. Zone B, the fracture zone, which had the highest priority, was assigned with 12 micrometre size, and Zone C, the matrix near the fracture (2nd highest priority after the fracture) was assigned with 24 micrometre size. The total mesh cells number of the entire domain was more than four million and ten thousand cells. [Sarkar, Toksöz and Burns \(2011\) p. 13](#) stressed that automatic mesh shapes consider different shapes in different locations during meshing irregular geometry shapes models, such as quadrilateral and triangular mesh elements; the reason for that is to keep the mesh's skewness at minimum level, and it does not lead to adverse effects on fluid flow simulation convergence. Chapter four-section 4.3.1 presents the grid sensitivity analysis, and clarifies the reason why we have chosen this number of cells. [Figure 3.9D](#) and [Table 3.2](#) below clarify the final mesh of the domain. After the meshing was completed, the boundary conditions of the domain were named, similarly, as the section 3.5.1.2, which were: inlet; outlet; interior fracture; interior matrix with three sections; top and bottom fracture surfaces domain; and symmetry edges of the matrix. [Figures 3.9A and 3.9B](#) below present rough fracture geometry and the domain names. At this stage, the mesh was completed and the domain was ready to be transferred into post-processing stage in FLUENT solver, version 18.1.

Table 3.2 Mesh cells statistics

Cells No.	Faces	Nodes	Partitions
4011566	7288318	3276753	4

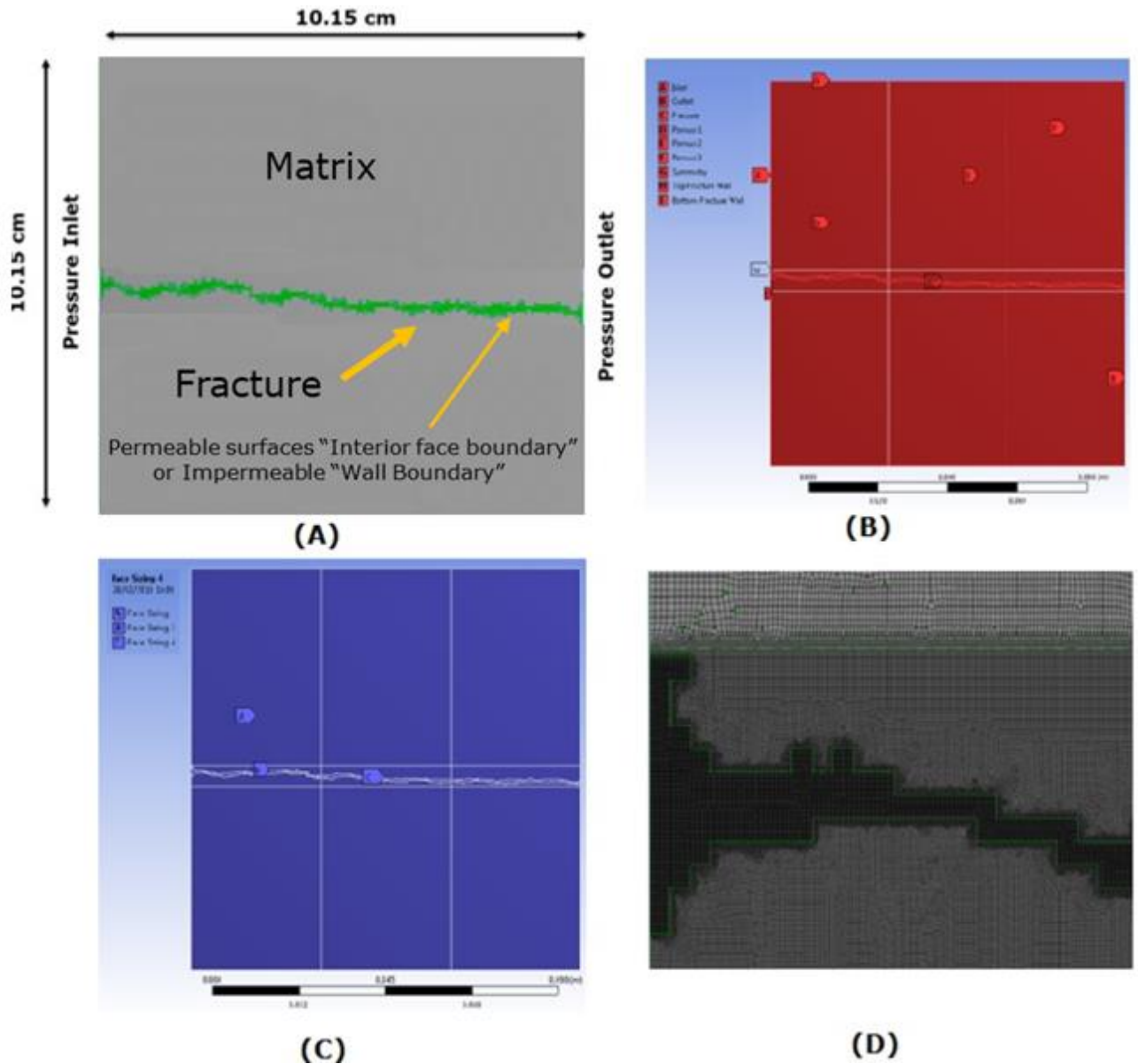


Figure 3.9 Rough fracture model by ANSYS CFD Fluent FVM DesignModeler
 A. geometry of rough with surrounding matrix (the matrix is grey, the fracture is green), B. domain boundary conditions, C. zones for the meshing process, and D. section of the fracture mesh, clarifying the three zones of mesh cells' density

3.5.2.3 Simulations set up of rough fracture

Similar set-ups were considered as the parallel plates fracture with single aperture in section (3.5.1.3). All the results and discussions of this model are clarified in Chapter Four of this research.

4 Solution Procedure, Validation And Results Of Parallel Plates And Rough Fractures

4.1 Overview

In this chapter, the simulations results by using ANSYS CFD Fluent FVM of two types of fractures: parallel plates fracture with single aperture; and rough fracture (also known as real fracture) are presented with validations. As well, comparisons among different boundary conditions of the same fracture type and with another type were conducted. Grid sensitivity analysis (mesh independence study) of the two fracture types were performed and are presented here. [Figure 4.1](#) below clarifies the structure of this chapter. The details of ANSYS CFD Fluent FVM models of these two fractures types are described in Chapter 3.

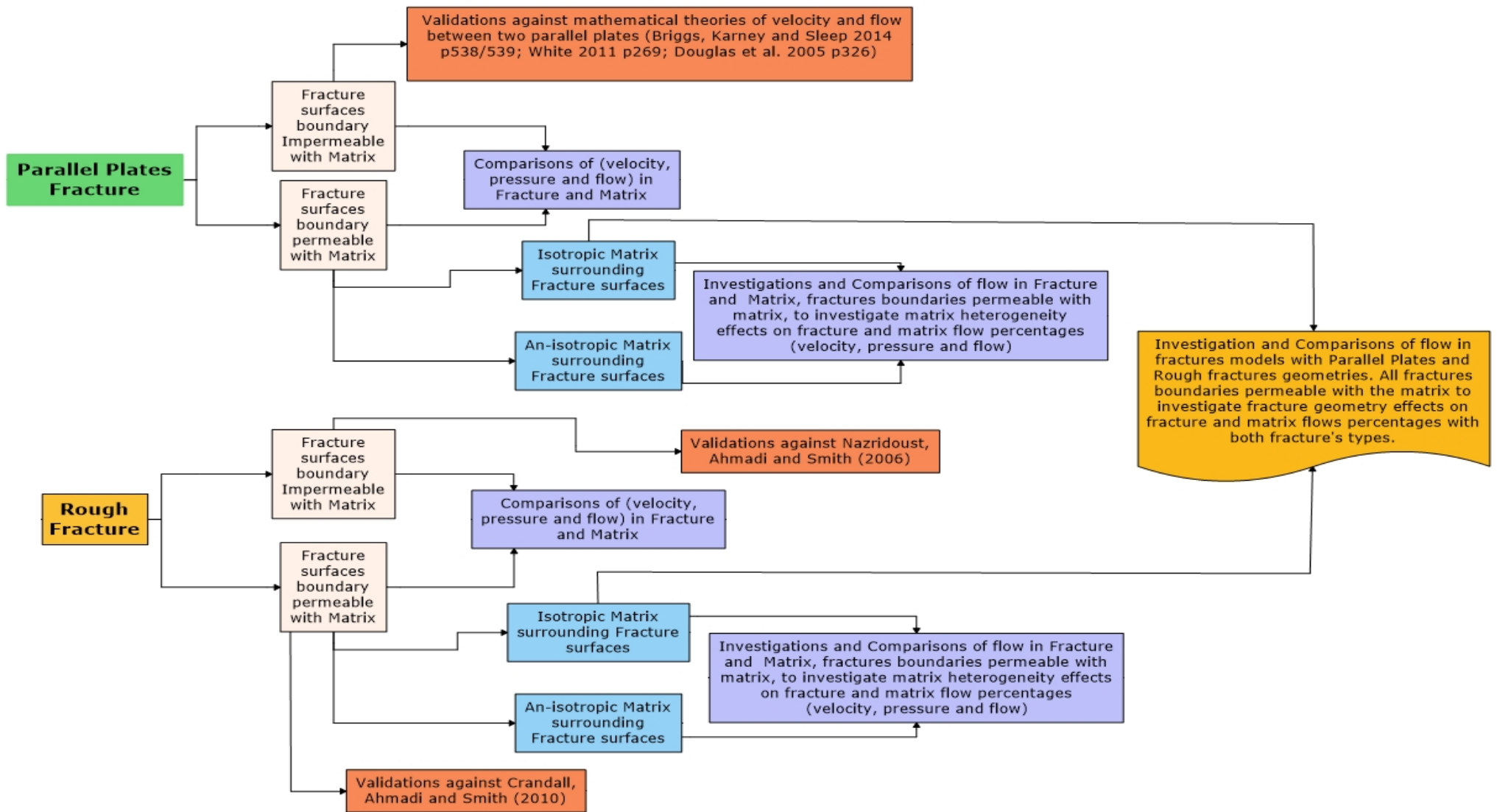


Figure 4.1 Diagram clarifying the structure of the models' results, validations, and comparisons among models in this chapter

4.2 Parallel Plates Fracture Simulations, Results extraction method and validations

Chapter 3, Section 3.51 clarified the details of the parallel plates fracture model in ANSYS CFD Fluent FVM. One of the main changings among these models was the boundary conditions of fracture surfaces. The fracture surfaces were set as “Walls boundary” when the investigation required the fracture to not be permeable with the matrix, and “Interior face boundary” when the investigation required the fracture to be permeable and interact with the matrix. In each simulation, result calculations were observed, such as: pressure drop vs. flow rate inside fracture; fracture flow; % fracture flow vs. matrix flow; and friction factor vs. Reynolds number (this topic will be covered in Chapter 5). For the case where the fracture surfaces were set as “Interior face boundary”, calculations were observed, and considered isotropic and anisotropic permeability of the matrix domain. The same calculations were observed and compared between isotropic and anisotropic, to investigate the effects of the anisotropic permeability on fracture flow.

To extract the results from the ANSYS CFD Fluent FVM model simulations, two separate lines were created at the same location, which were near the exit of the domain just before the outlet, to find the velocity profiles: first, inside the fracture only of 581 micrometre at (X, Y) Cartesian coordinates (0.1, 0.05043) (0.1, 0.05107) m; and second, inside the matrix only at coordinates outside the fracture in the above and below the fracture. [Figures 4.2 and 4.5](#) below illustrate the locations of these lines, and [figures 4.3 and 4.5](#) give examples of the extracted velocity profiles on these lines. At each line, X-velocity values were observed at each point, and each point reflected a reading value of a mesh cell on that line. Then, the average velocity value of the entire points of each line was taken, separately for fracture and matrix. In this model, for fracture reading line only there were 54 points, and for matrix reading line only there were 1910 points. As well, it’s good to clarify that the point numbers were based on the mesh density of the model, and could be changed if the model had a higher or lower number of mesh cells. From these average velocities, the flow rates were calculated inside the fracture and the matrix. The details of the fracture flow rate were as [equation 4.1](#); similarly, the matrix flow rate as [equation 4.2](#) below. The flows summation of a fracture and matrix domain will result in the total flow of the entire fractured domain, as [equation 4.3](#).

$$Q_{\text{Fracture}} = A_{\text{Fracture}} \times V_{\text{Fracture}} \quad (4.1)$$

$$Q_{\text{Matrix}} = A_{\text{Matrix}} \times V_{\text{Matrix}} \quad (4.2)$$

$$Q_{\text{Total}} = Q_{\text{Matrix}} + Q_{\text{Fracture}} \quad (4.3)$$

Where: A_{Fracture} = fracture aperture height as one dimension instead of two dimensions section; the reason is due to very long depth in Z-Cartesian coordinates of fractured media domain in comparison with fracture aperture height, most of the calculation considering it as a one direction (Dietrich et al. 2005; Tiab and Donaldson 2004; Golf-Racht 1982 p. 38).

V_{Fracture} = average value of velocity profile in that particular fracture's section only.

Q_{Fracture} = fracture's flow rate (usually in fractured media can be described m^2/s or mm^2/s , instead of m^3/s or mm^3/s , due to fracture section area considered as one-unit length of fracture aperture). A_{Matrix} = Matrix section length as one dimension, V_{Matrix} = average value of velocity profile in that particular matrix's section, and Q_{Matrix} = Matrix's flow rate and can be described as m^2/s or mm^2/s similar as fracture. Q_{Total} = Total flow of the entire fractured domain flow.

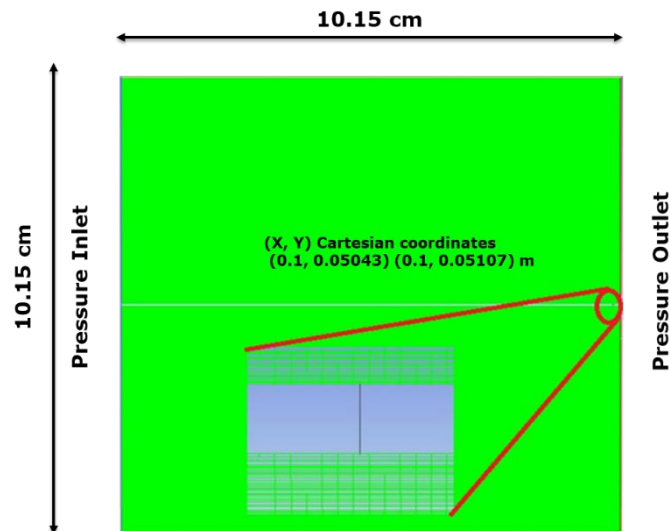


Figure 4.2 Surface line inside the fracture only, to read X-velocity values (green colour is matrix, and blue colour fracture)

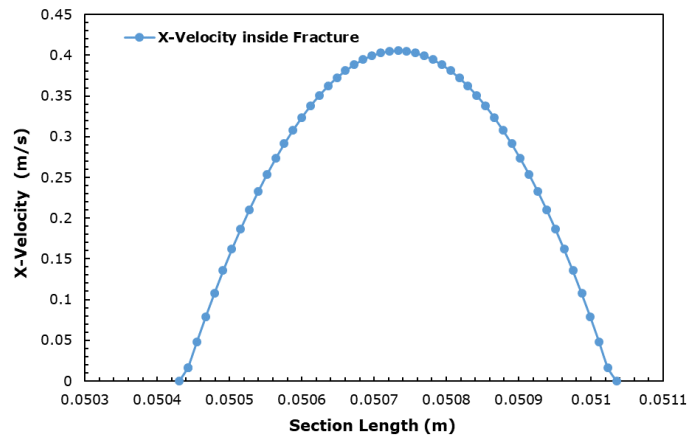


Figure 4.3 X-velocity values, inside fracture only, on the fracture reading line for pressure 1000 Pa, fracture surfaces interacting with matrix (interior face boundary) with isotropic matrix ($K_x=K_y= 2000$ mD)

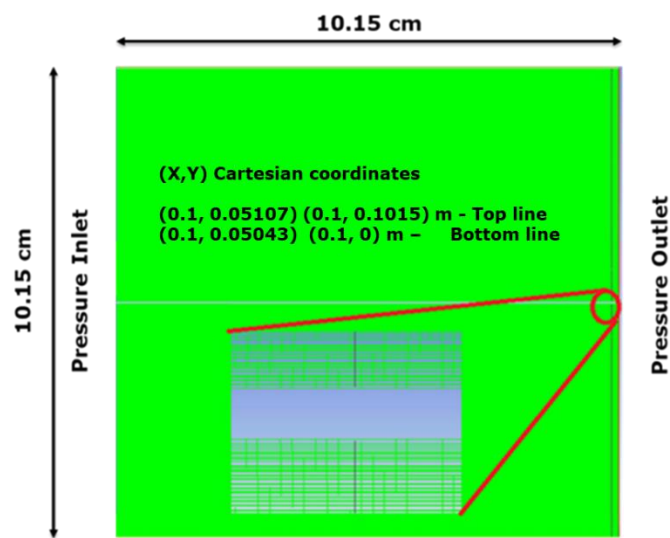


Figure 4.4 Surface line inside the matrix only, to read X-velocity values (green colour is matrix, and blue colour fracture)

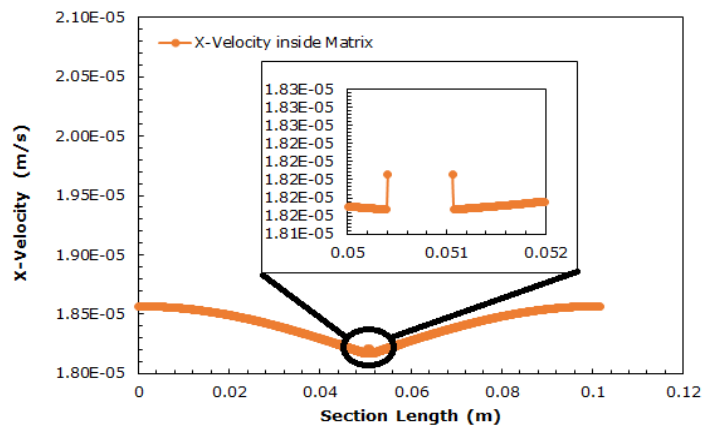


Figure 4.5 X-velocity values inside matrix only, on the matrix reading lines for pressure 1000 Pa, fracture surfaces interacting with matrix (interior face boundary), with isotropic matrix ($K_x=K_y= 2000$ mD)

4.2.1 Grid sensitivity analysis

As mentioned in meshing the geometry (Chapter 3 Section 3.5.1.2), which clarified the mesh quality and the cells number of the domain (more than 1.65 million cells), it was vital to investigate the cells number effect of the domain on the simulations' results (ANSYS 2013; Sarkar, Toksöz and Burns 2011 p. 3; Versteeg and Malalasekera 2007 p. 3; Zabaleta 2007). This was done by comparing the average velocity values for the same section inside the fracture with different cells numbers to be sure that the ANSYS CFD Fluent FVM model had accurate values with the optimised value of mesh cells number. Thus, the same geometry was meshed with three meshes: first, above 1.65 million cells; second, above 1.86 million cells; and third, above 2.175 million cells. All these models were simulated with the same boundary conditions, ie.: 1000 pa pressure inlet, isotropic matrix permeability ($K_x=K_y=2000$ mD) with 20% porosity, and fracture surfaces boundary considered permeable interior faces; this means they were permeable with the matrix and the flow could move between the fracture and the matrix and vice versa. The average velocity values were calculated from converged solutions. Then, the same surface line located inside the fracture was created, with fracture aperture 581 micrometre just before the fracture outlet at X, Y coordinates of the reading line (0.1,0.05043) (0.1,0.05107) in all models, to read X-Velocity values, as Figure 4.2 above. Table 4.1 clarifies the meshes' details with the average velocity values inside the fracture of each model, and Figure 4.6 clarifies the velocity profiles of the models with three different meshes.

As can be seen in the simulations' results in table 4.1, the velocity profiles among these three meshes remained the same, and the average velocity values had less than 1.5% deviation between first and third meshes. The increase in the mesh did not reflect any significant increase or decrease in the average velocity of the fracture. Therefore, the first mesh was selected to be used in the ANSYS CFD Fluent FVM simulations of this model. The reasons for this were: first, increasing the mesh number had no significant change in simulation readings, with less than 1.5% deviation; and secondly, using a higher cell number would have required more time to compute simulations (approximately twice the time) without any significant effect on the results' accuracy, and accordingly, would have led to more delay in obtaining the results.

Table 4.1 ANSYS CFD Fluent FVM model's mesh details with the average velocity values of the sections inside the parallel plates fracture models

CFD models Meshes	Cells No.	Faces	Nodes	Partitions	Average Velocity of the section (m/s)
First Mesh	1656468	3315740	1659273	4	0.286
Second Mesh	1864584	3732218	1867635	4	0.289
Third Mesh	2175066	4353549	2178484	4	0.290

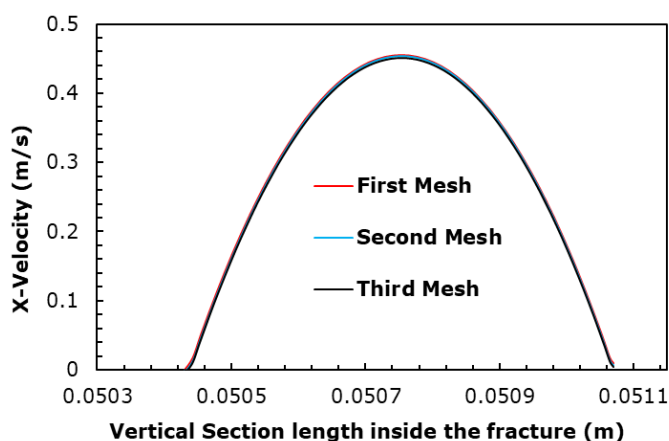


Figure 4.6 X-velocity profiles inside fracture 581-micrometre 1000 Pa with three meshes

4.2.2 Validation of parallel plates fracture model

To validate the parallel plates fracture ANSYS CFD Fluent FVM models of this thesis, with one fracture aperture height, mathematical theories of velocity and flow between two parallel plates were used as clarified in Chapter 2 [Section 2.5.1](#); particularly, for the velocity profile and flow as [equations 2.21](#) and [2.22](#) respectively. However, fracture surfaces were considered as impermeable “wall boundary” and matrix permeability K_x and $K_y=0.2$ mD, but with no effect of matrix permeability on fracture flow as the fracture surfaces boundary was impermeable (no fracture/matrix interaction). This meant no flow between the fracture and the matrix, so that the ANSYS CFD Fluent FVM results could be compared with the equation results ([Briggs, Karney and Sleep 2014 pp. 538-539](#); [White 2011 p. 269](#); [Douglas et al. 2005 p. 326](#); [Eskinazi 1968 pp. 378, 382](#)). To be able to use [equations 2.21](#) and [2.22](#), it was essential to check that the vertical reading line section, was in a region with fully developed flow, which was located inside the fracture in (X, Y) coordinates (0.1, 0.05043) (0.1, 0.05107), Therefore, a reading line in the centre of the fracture along the flow was created to check X-Velocity values along the fracture's centre; [Figure 4.7](#) clarifies the location of the reading line in the centre fracture longitudinally. The ANSYS CFD Fluent FVM model was simulated under two pressures inlets: first, 100 Pascal; and second, 2000 Pascal,

to investigate how far from the inlet the flow would be fully developed along the fracture length, by observing the X-Velocity values along the fracture's centre. The outcome was that at 100 pa pressure inlet, the flow was developed near the inlet at approximately (0.0025) m, while with 2000 pa pressure inlet the flow was developed slightly further from the inlet at (0.01) m, which was still relatively near to the inlet as well. Thus, the vertical reading line section that was inside the fracture in (X, Y) coordinates (0.1, 0.05043) (0.1, 0.05107) was clearly located in a fully developed flow region within the fracture, and was suitable for comparing the X-velocity values with the values of the equations. [Figure 4.8](#) below illustrates the X-velocity values at fracture's centre with the two pressure inlets.

To validate the parallel plates fracture ANSYS CFD Fluent FVM model of this research, comparisons were made between ANSYS CFD Fluent FVM values of the velocity profile, the flow values and the theory [equations 2.21](#) of velocity and [2.22](#) of flow with four pressure drops, which were (5, 100, 1000, 2000) Pa, using the same boundary conditions, ie. impermeable wall boundary and fully developed flow. The average difference value (ADV) of each model was calculated for four pressure drops between the ANSYS CFD Fluent FVM models and theory equations, as [equation 4.4](#).

The outcome of the comparison between the velocity profile of [equation 2.21](#) and the ANSYS CFD Fluent FVM parallel plates fracture model was that ADV was only 3%; [Figure 4.9A](#) below clarifies this. As well, the comparison of flow values of the ANSYS CFD Fluent FVM model were in good agreement with the flow equation values, with ADV value of 4% only; [Figure 4.9B](#) below illustrates this comparison. From both comparisons of the two theory equations and the ANSYS CFD Fluent FVM values of parallel plate fracture, it was proved that this model was in good agreement with these mathematical theories of velocity profiles and flow. Therefore, this ANSYS CFD Fluent FVM model was in a good validation stage, and was ready for the next investigation of flow in fractured media.

$$ADV = \left(\frac{X_i - Y_i}{\frac{X_i + Y_i}{2}} \right) * 100 \quad (4.4)$$

Where: ADV= average difference value, X_i , Y_i = comparison values

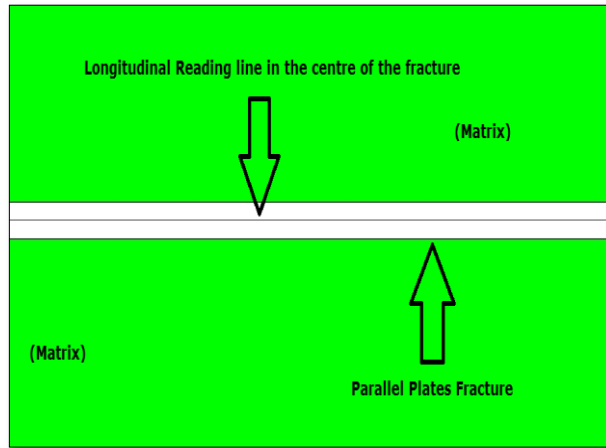


Figure 4.7 The longitudinal reading line in the centre of the parallel plates fracture (matrix is green, fracture is white)

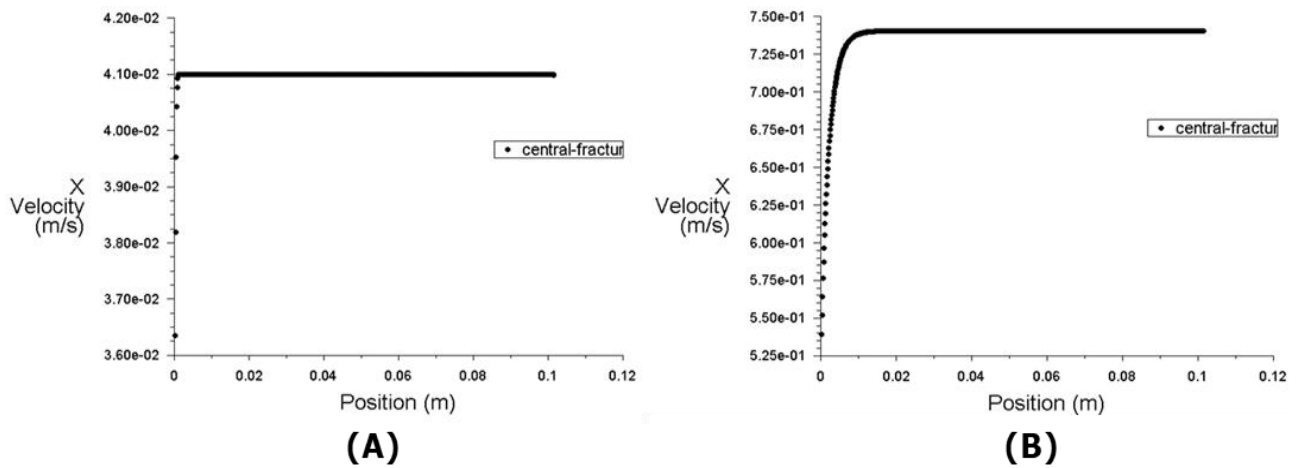


Figure 4.8 X-velocity value along the parallel plates in the centre of the fracture, with inlet pressure A: 100 pa and B: 2000 Pa, fracture surfaces set as impermeable wall boundary, and matrix permeability K_x and $K_y=0.2$ mD (no flow interaction between fracture and matrix)

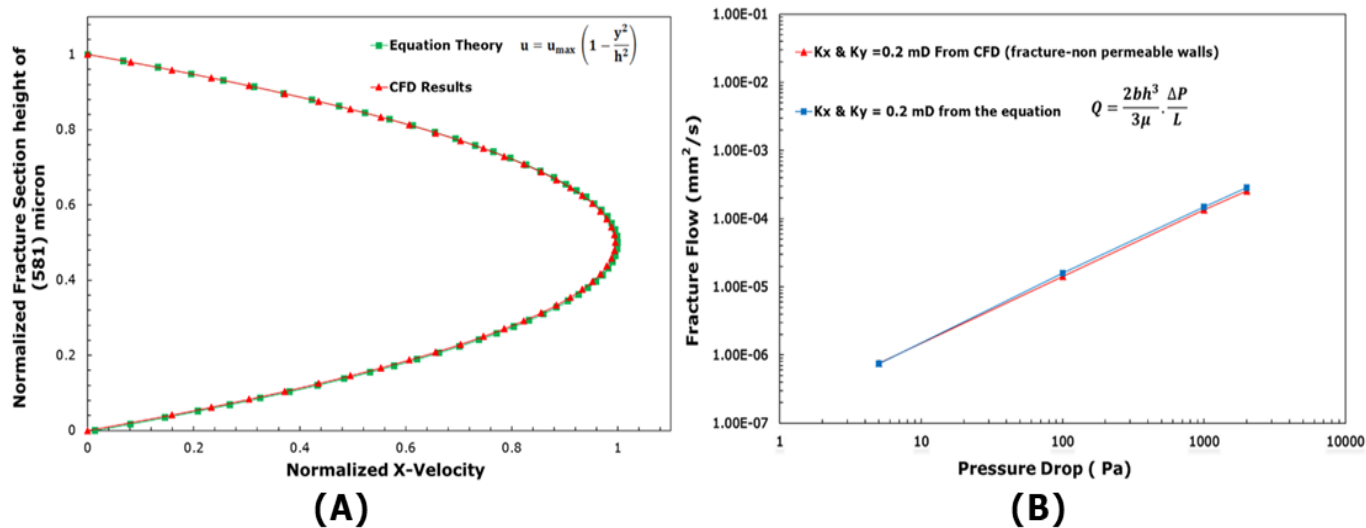


Figure 4.9 Validation of X-velocity and fracture flow rate between parallel plates fracture ANSYS CFD Fluent FVM model and theory equations. A: X-velocity at the vertical section in 581-micron aperture with pressure 5 pa, and B: pressure drop against fracture flow rate. In all models fracture had impermeable surfaces with wall boundary (no flow interaction between fracture and matrix), and isotropic matrix K_x and $K_y=0.2$ mD

4.2.3 Parallel plates fracture ANSYS CFD Fluent FVM models with surface boundaries as “impermeable Walls” and “Permeable Interior face”, with isotropic matrix permeability

This model was created with a fracture as a single parallel plates fracture with 581 micrometre aperture height and surrounding matrix media. The fracture surfaces were in two boundary conditions: first, set as “Wall boundary”, which means non-porous walls of the fracture with non-permeable surfaces that would not allow fluid to interact or move between the fracture and the matrix; and second, “Interior face boundary”, which means porous walls and fracture surfaces that were permeable to fluid and interact with the surrounding matrix. The matrix properties that surrounded the fracture were set as isotropic matrix permeability ($K_x=K_y=2000$ mD), with four pressure inlets values (5, 100, 1000, 2000) Pa and zero pressure at the outlet, and the other boundaries were the same as stated in [chapter 3 section 3.5.1.2](#). The goal of these ANSYS CFD Fluent FVM models was to compare the effect of the fracture when the fracture surfaces are permeable

and impermeable with the surrounding matrix. In all the simulations, the velocity profiles inside the fracture with 581 micometre were observed at the end of the fracture and also within the matrix but outside the fracture in the same point at X-direction Cartesian, just before the outlet. Then, fracture, matrix and total flows of the fractured domains were calculated, as clarified in [section 4.2](#).

The outcome of these simulations showed that with these two conditions of fracture surfaces (permeable and impermeable), ADV of total flow rate increased in the fracture model with permeable surfaces by approximately 7.8%. This increase was reflected in the increase of ADV fracture flow around 8%; however, the matrix flow decreased 3% ADV of the permeable fracture surfaces model. [Figures 4.11 and 4.12](#) present these comparisons. This comparison proved that the flow inside the fracture slightly increased when the fracture surfaces were permeable to the fluid with the matrix. This proved that the interaction between the fracture and surrounding matrix was quite low with parallel plates fracture geometry and, as can be seen in pressure and velocity contours [Figures 4.10A and 4.10B](#), the pressure distribution between the matrix and fracture was minorly affected with permeable fracture surfaces (interior face boundary), and showed no sign of interaction, as well reflected linear pressures drop along the flow, which confirmed the findings of [Rasouli and Rasouli \(2012\)](#); [Crandall, Bromhal and Karpyn \(2010\)](#) and [Crandall, Bromhal and Smith \(2009\)](#). This case was further investigated by observing the velocity streamlines of both models by ANSYS CFD Fluent FVM -Post [Figure 4.10A and 4.10B](#); the finding was that the flow inside the matrix or inside the fracture was interacting very slightly when the fracture surfaces were set as permeable. However, as expected, there was no interaction at all when the fracture surfaces were set as impermeable "Walls boundary", which proves that the model set-up conditions were accurate.

This comparison between models with permeable and impermeable fracture surface conditions reflected that considering impermeable fracture surfaces with wall boundaries will underpredict flow in fractured media. This has confirmed the findings of [Rasouli and Rasouli \(2012\)](#), that considering the matrix effect on fracture's flow increases fractured formation connectivity and accordingly flow. Likewise, it has confirmed that, as stated by [Popov et al. \(2009\)](#), the interface permeable layer between the fracture and matrix is affected by the components of tangential velocities, which will affect various fluid jump (movements) conditions between matrix and fracture. Accordingly, this will affect fluid stresses in both

media. Moreover, these comparison results confirmed the statement by [Luo et al. \(2020\) p. 3](#) that matrix flow contribution in fractured formations cannot be neglected, especially, despite the fact that previous studies of fractured formations assumed impermeable matrices and that flow occurred in fractures only. [Figure 4.13](#) presents the percentages of fracture flow with two conditions of fracture surfaces, and % fracture flow increased with permeable fracture surfaces boundary.

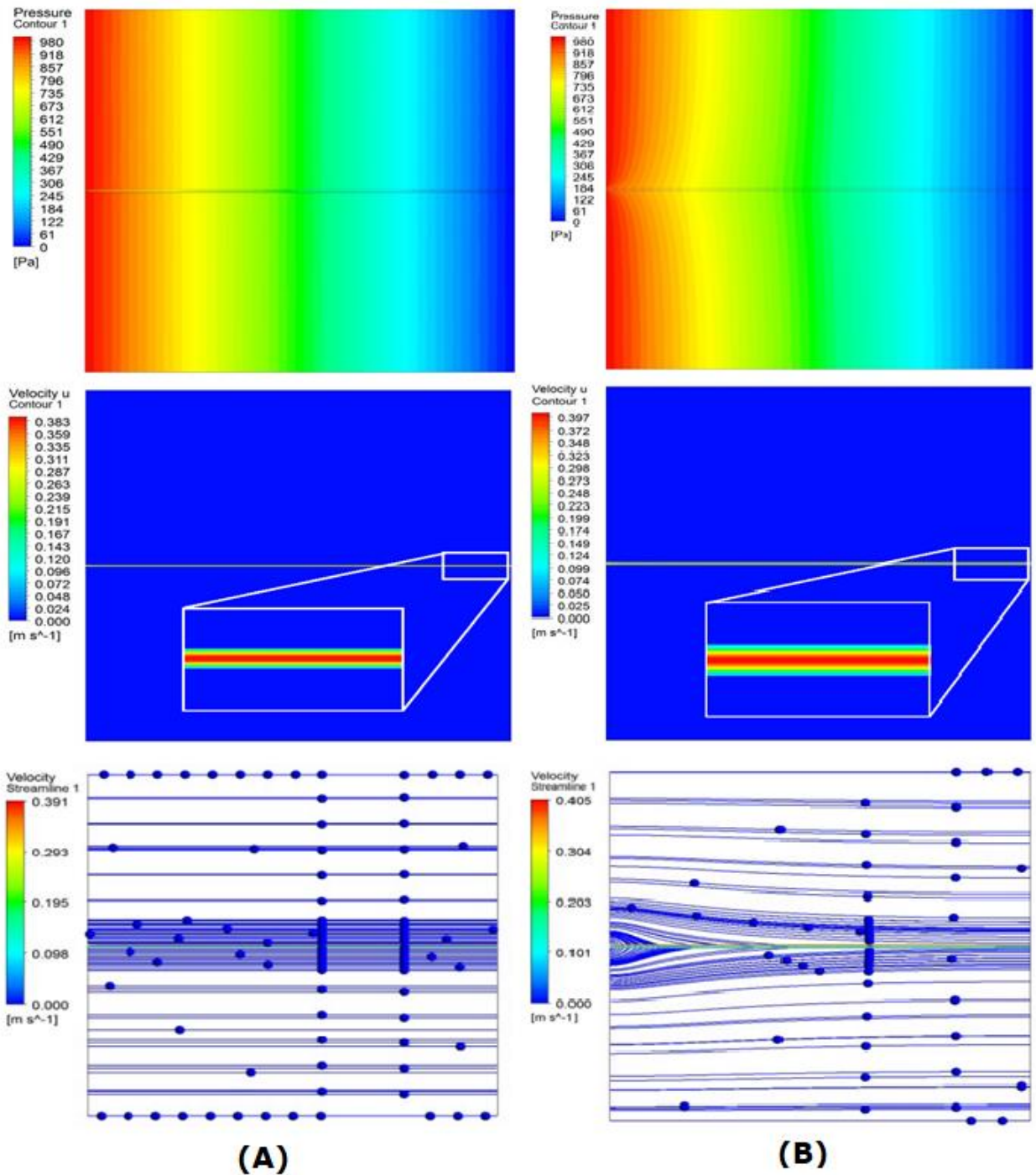


Figure 4.10 Total pressure contours, X-velocity contours and Velocity streamline respectively (top to bottom) of parallel plates fracture models, matrix permeability K_x and $K_y = 2000$ mD, $P = 1000$ Pa, with two fracture surface boundaries set ups: A. impermeable with surrounding matrix "walls boundary", and B. permeable with surrounding matrix "interior face boundary"

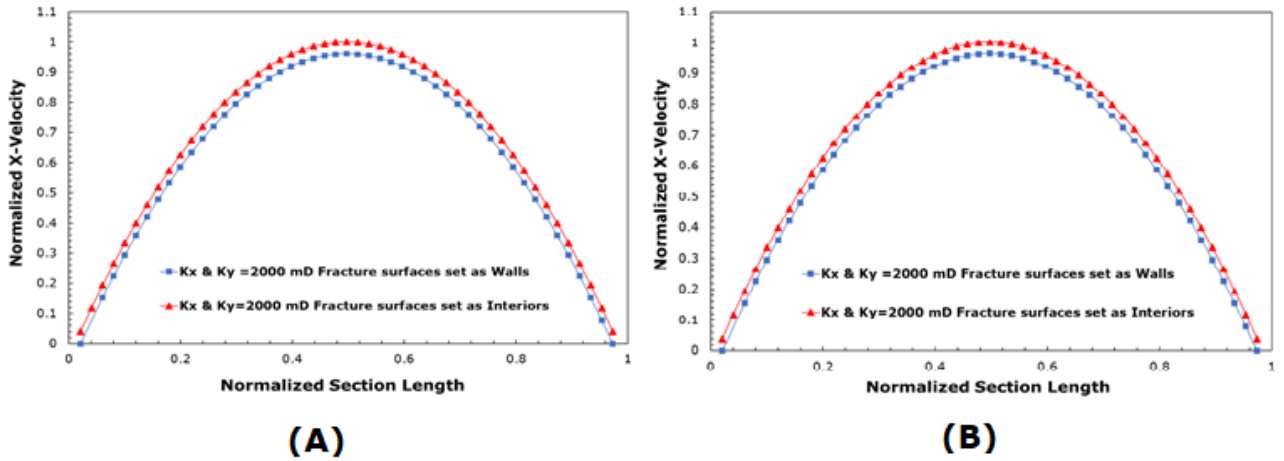


Figure 4.11 Velocity profiles of parallel plates fracture of 581-micrometre fracture apertures height, at the end just before fracture outlet, isotropic matrix permeability K_x and $K_y = 2000$ mD. Comparing models with permeable “interior face boundary” and impermeable “walls boundary” fracture surface boundaries with two pressures: A. 5 Pa, and B. 1000 Pa

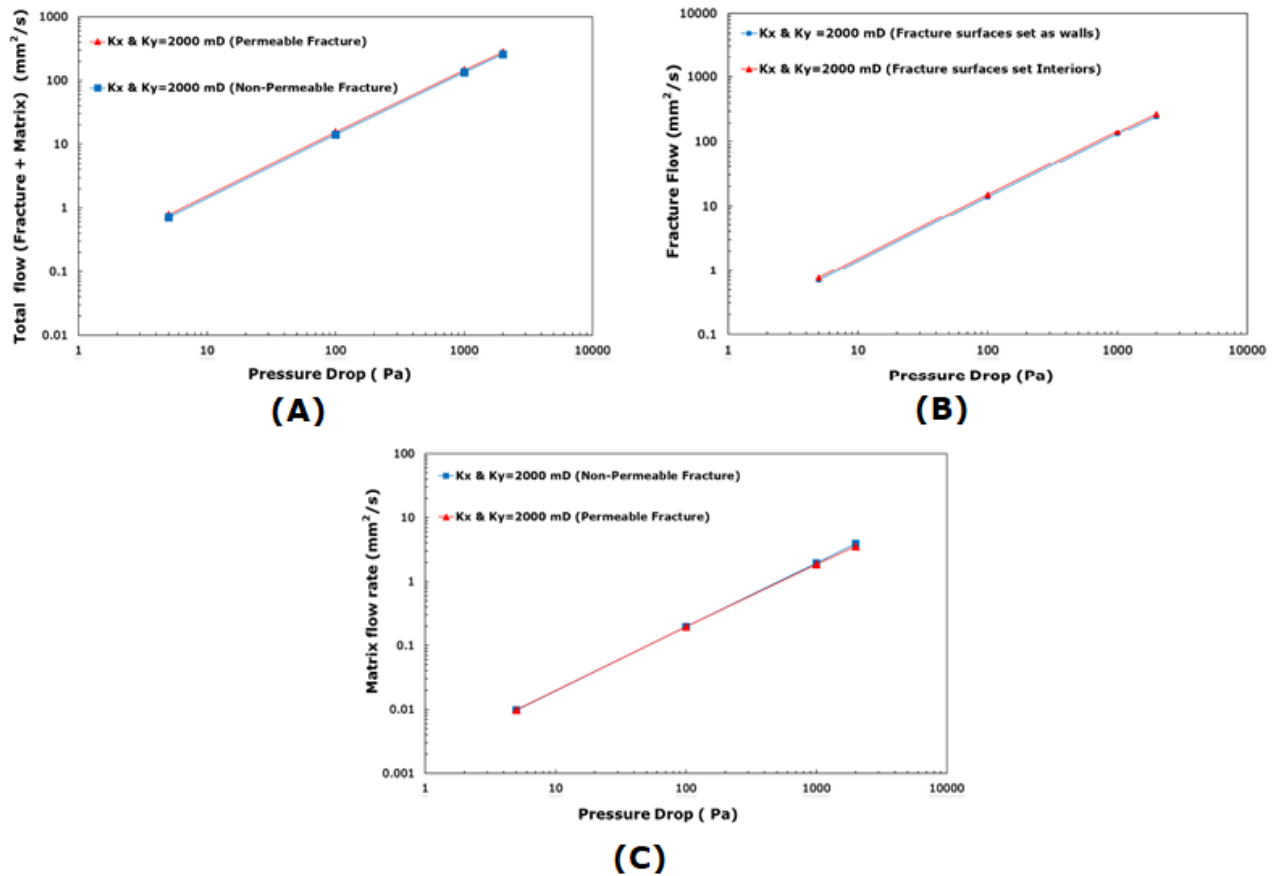


Figure 4.12 Parallel plates fracture comparisons of: A. total flow rate (fracture + matrix), B. fracture flow rate and C. matrix flow rate (mm^2/s), between impermeable “walls boundary” and permeable “Interior face boundary” of fracture surface with (K_x & $K_y = 2000$ mD)

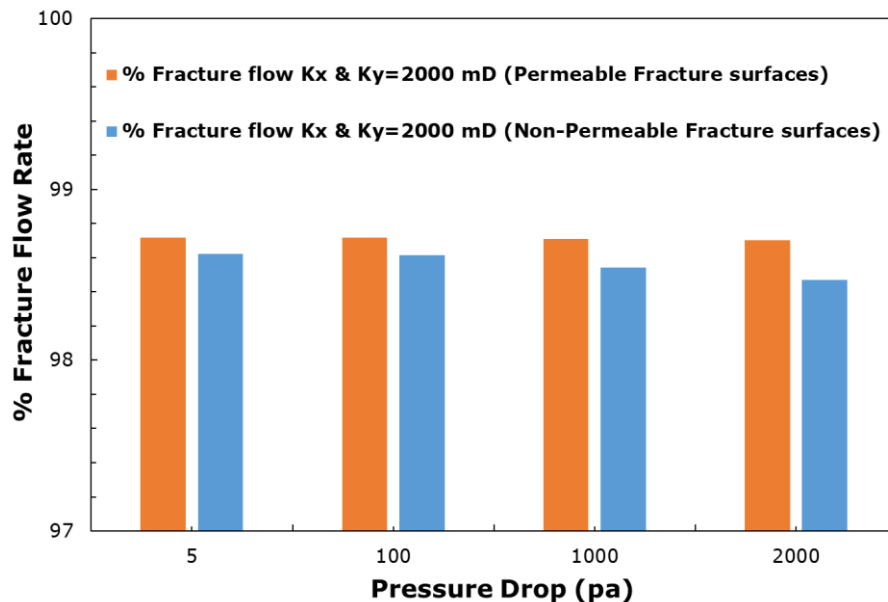


Figure 4.13 Comparison of (% fracture flow rate) of parallel plates fracture between permeable and impermeable fracture surfaces boundaries with the matrix, isotropic matrix permeability K_x and $K_y = 2000$ mD

4.2.4 Parallel plates fracture ANSYS CFD Fluent FVM models with permeable surface “Interior faces boundary” with anisotropic matrix permeability: results

This model was created with a fracture as a single parallel plates fracture with 581 micrometre aperture height and surrounding matrix media, similar to the previous model. The fracture surface boundary was considered as permeable, and the interior face boundary was applied, which meant porous fracture surfaces, and that there were permeable surfaces with the surrounding matrix and interaction on each other. All other boundaries of the fractured domain were the same as [chapter 3 section 3.5.1.2](#), except the matrix permeability which is stated below. In all the simulations, the velocity profiles inside the fracture with 581 micrometre were observed at the end of the fracture, and within the matrix outside of the fracture in the same point at X-Cartesian coordinate, just before the outlet. The matrix properties that surrounded the fracture were set as anisotropic matrix permeability. Different permeabilities were considered for in-plane (x) and through plane (y) directions of Cartesian coordinates ($K_x \neq K_y$), while matrix porosity was considered a fixed value in all the models 20%, due to the following reasons:

1. Permeability is one of the most important properties in reservoir rock, as it highly affects fluid flow in these formations ([Al-Yousef 2005](#)).

2. Permeability of fractured media varies locally due to the key effect of a fracture's geological structure (Yang et al. 2019).
3. Permeability is affected by the overburden stresses on fracture and matrix, and will change based on a formation's layer's depth and pore pressure; this change will influence matrix permeability in-plane (x) and through plane (y) directions of Cartesian coordinates (Su et al. 2019; Tiab and Donaldson 2004).
4. Permeability in fractured formations is a critical property as matrix permeability has a key effect on fractured formations' connectivity; as well, permeability is partially in the matrix and partly in the fracture, and when overburden stresses are high and fracture apertures reduce significantly, then the majority of fluid will be immigrated through the matrix (Rasouli and Rasouli 2012).
5. Permeability and fluid transport in porous media are in close relation with detailed geometries of matrix pores, such as pore scale, tortuosity, connectivity, and shape; as well, pore structure plays an important role in adsorption of fluids in formations. This relation will not be easy to obtain from macroscopic parameters such as porosity (Yin et al. 2017; He et al. 2014; Ingham and Pop 2005 p. 367).
6. Porosity represents void spaces among grains of matrix due to varied sizes and shapes of grains, while permeability represents rocks' ability to transmit fluids, and it depends on the effective porosity of the rock (connectivity among void spaces of matrix). This is affected by many factors, such as: grain shape, grain size, grain distribution, grain packing, cementation among grains, sedimentary environment and the existence of fractures. Therefore, some subsurface formations exist with high porosity, but permeability remains low due to poor connections among void spaces of the matrix (He et al. 2014; Tiab and Donaldson 2004 p. 100; Nelson 2001 p. 83; Golf-Racht 1982 p. 147; Dake 1978). Thus, matrix permeability is a highly significant property in fractured formation. For this reason, this research used ANSYS CFD Fluent FVM fracture models to consider the anisotropic permeability effect.

To achieve these scenarios of different matrix permeability, field and reasonable data was applied to reflect an optimised effect of anisotropic matrix permeability on fracture/matrix flow. Lang, Paluszny and Zimmerman (2014) and Tiab and

Donaldson (2004) p. 158 presented a formula as equation 2.14 (Section 2.4.2), that calculates the anisotropy ratio of permeability in anisotropic formations when K_x is not equal to K_y in X and Y Cartesian directions. As well, a field data table was provided by Tiab and Donaldson (2004) (table 3.6 p. 160) as an example of this type of anisotropic permeability formation. Thus, different values of K_x and K_y scenarios of each simulation in this model were observed by applying equation 2.14. Three random values of the anisotropic ratio (I_A) were chosen from the given table data, (1.45, 3.87, 5.27), and K_x was considered 2000 mD to give us a comparison case with the previous model of isotropic permeability ($K_x=K_y=2000$ mD). The outcome was three values of K_y . Table 4.2 below clarifies K_x and K_y in each scenario. In Table 4.2 for the first set permeability of K_x was fixed 2000 mD and K_y was varied based on chosen anisotropy ratio of permeability values. Then, in the second set of permeability, it was assumed that the values of K_x and K_y were the reversed value of the first set of permeability, which meant fixing the K_y value to be 2000 mD and changing K_x . There were six anisotropic permeability scenarios in total which were considered in ANSYS CFD Fluent FVM simulations, and each anisotropic scenario was considered in one model of the matrix permeability in both directions K_x and K_y . It's good to clarify that ANSYS CFD Fluent FVM gives a chance to log-in permeability of each Cartesian direction in a model, instead of effective permeability of anisotropic permeability as one value in both directions when K_x not equal to K_y . This makes it possible to investigate the effect of difference between K_x and K_y on a model with the same flow direction, on the flow of fracture and matrix, and this effect will be explained in the following sections. Fracture surfaces were set permeable "Interior face boundary" in all the simulations that allowed flow and interaction between fracture and the matrix and vice versa, and all other boundaries and the fractured domain model set-ups were the same as stated in Chapter 3 section 3.5.1.2. Different pressure inlet values were considered (5, 100, 1000, 2000) Pa in each anisotropic model, and the pressure outlet was fixed zero pressure in all models.

Table 4.2 Six scenarios of anisotropic matrix permeability of the simulations set-up

Anisotropic ratio ($I_A = \frac{K_x}{K_y}$)	Kx (mD) (Considered)	Ky (mD) (From I_A formula)	First Set Permeability scenarios	Second set Permeability scenarios	% Difference between Kx and Ky in each scenario
1.45	2000	1389	(First Scenario) Kx=2000 Ky=1389	(Second Scenario) Kx=1389 Ky=2000	30 %
3.87	2000	517	(Third Scenario) Kx=2000 Ky=517	(Fourth Scenario) Kx=517 Ky=2000	74%
5.27	2000	380	(Fifth Scenario) Kx=2000 Ky=380	(Sixth Scenario) Kx=380 Ky=2000	81 %

4.2.4.1 Simulation results

In each ANSYS CFD Fluent FVM model, an anisotropic matrix permeability scenario was assigned for in-plane (Kx) and through plane (Ky) directions ($K_x \neq K_y$), as the six scenarios in Table 4.2. These models were simulated, then, fracture, matrix and total flows of the fractured domains were calculated, as clarified in section 4.2. The first scenario (Kx=2000, Ky=1389) was compared with the second scenario (Kx=1389, Ky=2000), and the outcome was ADV of total flow rate was decreased in the second scenario 0.45%. This decrease reflected reductions of ADV in fracture flow of around 0.052%, and matrix flow of 36.15%. This comparison showed that in the second scenario, the flow decreased in the matrix and the fracture; however, the percentage of fracture flow was higher in the second scenario domain with an average value of 0.4%. A similar comparison occurred between the third (Kx=2000, Ky=517) mD and fourth (Kx=517, Ky=2000) mD scenarios; ADV total flow rate was decreased in the fourth scenario 1.01%. This decrease reflected the reduction of ADV fracture flow of around 0.124% and matrix flow 118.5%. This comparison shows that in the fourth scenario, the flow was decreased in the matrix and the fracture, but the percentage of fracture flow was higher in the fourth

scenario with an average value of 1%. Lastly, in comparison between the fifth ($K_x=2000$, $K_y=380$) mD and sixth ($K_x=380$, $K_y=2000$) mD scenarios, the outcome was, ADV of total flow rate was decreased in the sixth scenario 1.2%. This decrease was reflected in the reduction of ADV fracture flow around 0.134% and matrix flow 137%. This comparison shows that in the sixth scenario, the flow was decreased in the matrix and the fracture, but the percentage of fracture flow was higher in the sixth scenario, with an average value of 1.055%. [Table 4.3](#) below present all these results, and [Figures 4.14, 4.15, and 4.16](#) clarify these comparisons. These comparisons have reflected results such as: for the total and fracture flows, there was very minor change in flows among these models; and for the matrix flow, there were moderate changes in flow among these models with permeability changes of K_x and K_y due to low interaction between fracture and matrix. However, in comparisons among these models with anisotropic permeability, the highest change occurred in lowest K_y value of anisotropic scenario in the flow percentages of fracture and matrix. As well, the percentage of matrix flow was low in the fractured domain; [figure 4.17](#) presents it.

As can be seen, the sixth scenario had the highest rate of flow reduction in ADV total flow rate. Therefore, further comparisons were conducted with the isotropic scenario model when (K_x and $K_y = 2000$ mD), and the outcome was that ADV of total flow rate was decreased in the sixth scenario 1.2%. This decrease was reflected in the reduction of ADV fracture flow around 0.145% and matrix flow 136.4%. As well, velocity profiles inside fractures of models with scenarios 5, 6 and isotropic were compared with two pressure drops, and the finding was that the highest velocity profile was in the isotropic permeability model with $K_x=K_y=2000$ mD, and the lowest velocity in the anisotropic model with permeability $K_x=380$ $K_y=2000$ mD, while anisotropic $K_x=2000$ $K_y=380$ mD was in the middle. [Figures 4.18A and 4.18B](#) present these comparisons. This shows the effect of in-plane K_x and through plane K_y permeabilities on fracture flow.

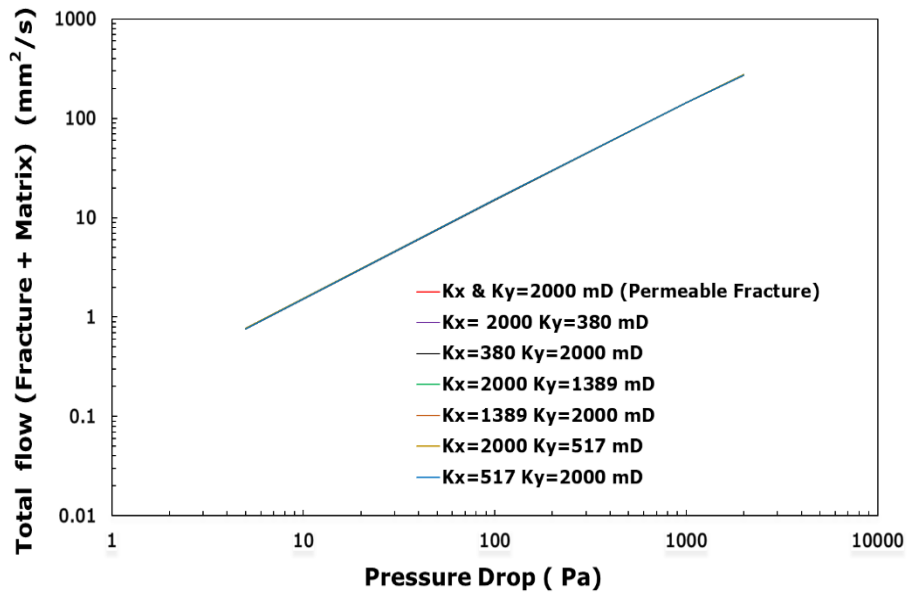


Figure 4.14 Comparisons of total flow rate (mm^2/s) of parallel plates ANSYS CFD Fluent FVM model fractures, with isotropic and all anisotropic matrix permeability scenarios, with permeable fracture surface boundaries

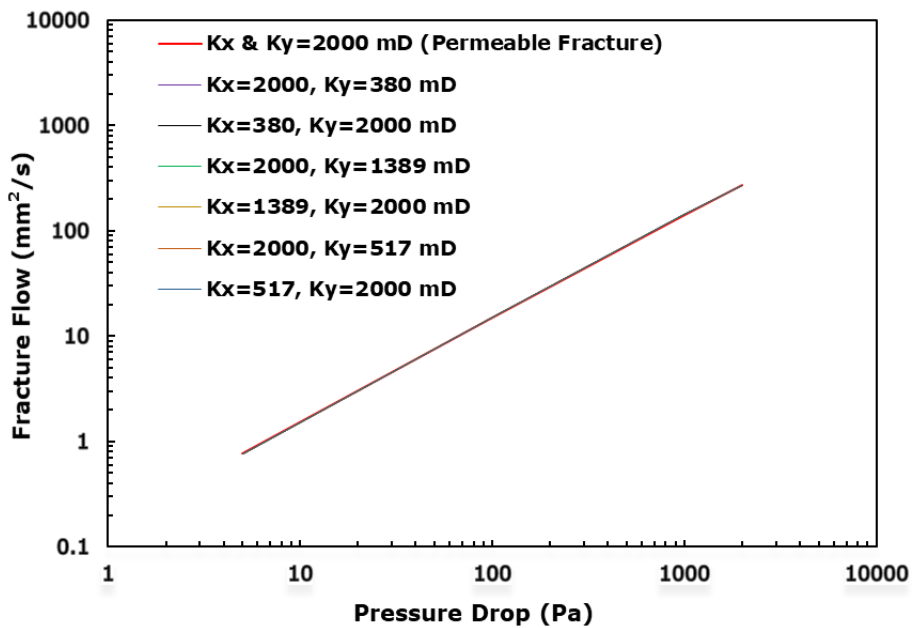


Figure 4.15 Comparisons of fracture flow rate (mm^2/s) of parallel plates ANSYS CFD Fluent FVM model fractures, with isotropic and all anisotropic matrix permeability scenarios, with permeable fracture surface boundaries

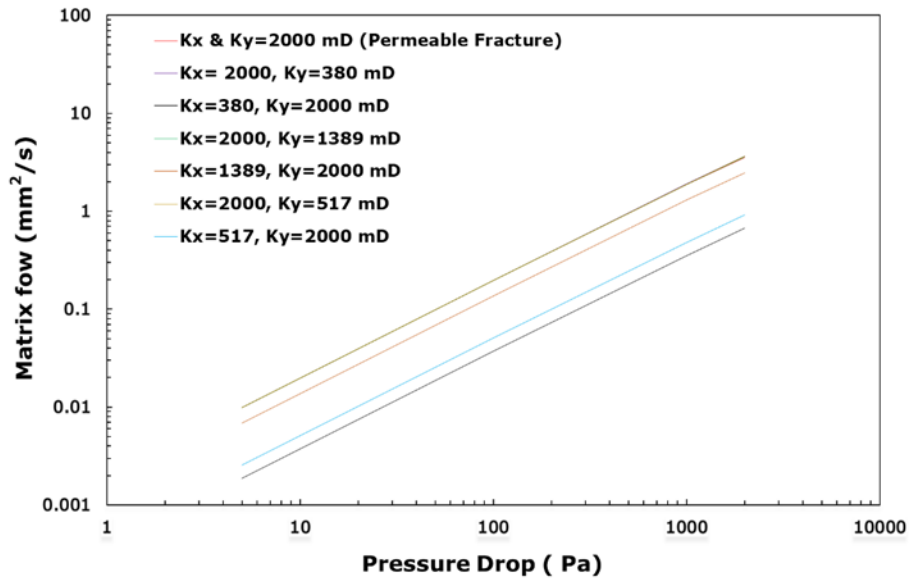
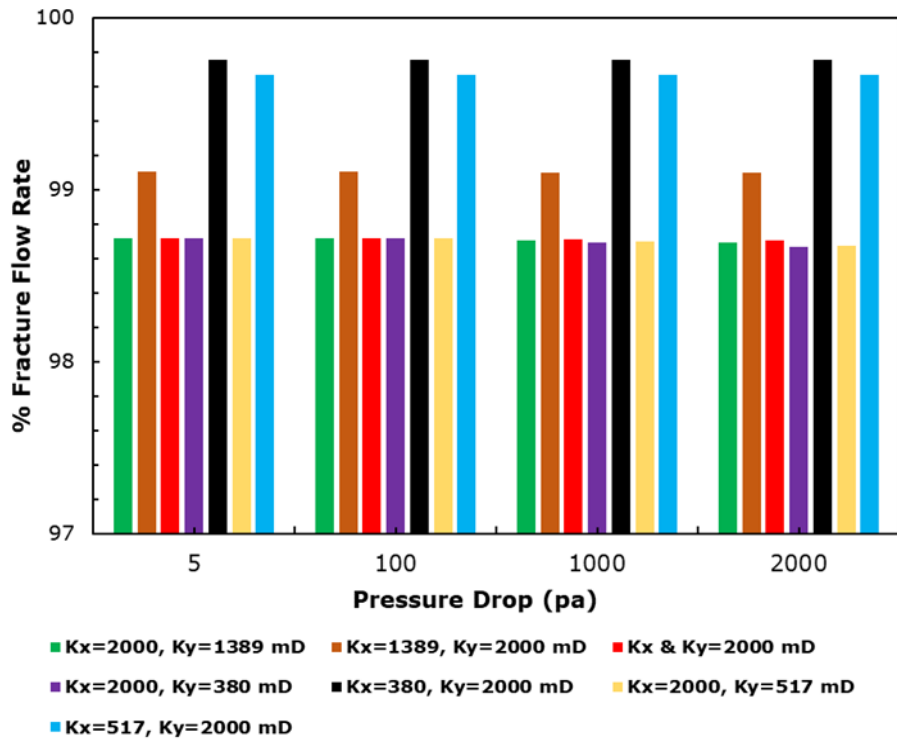
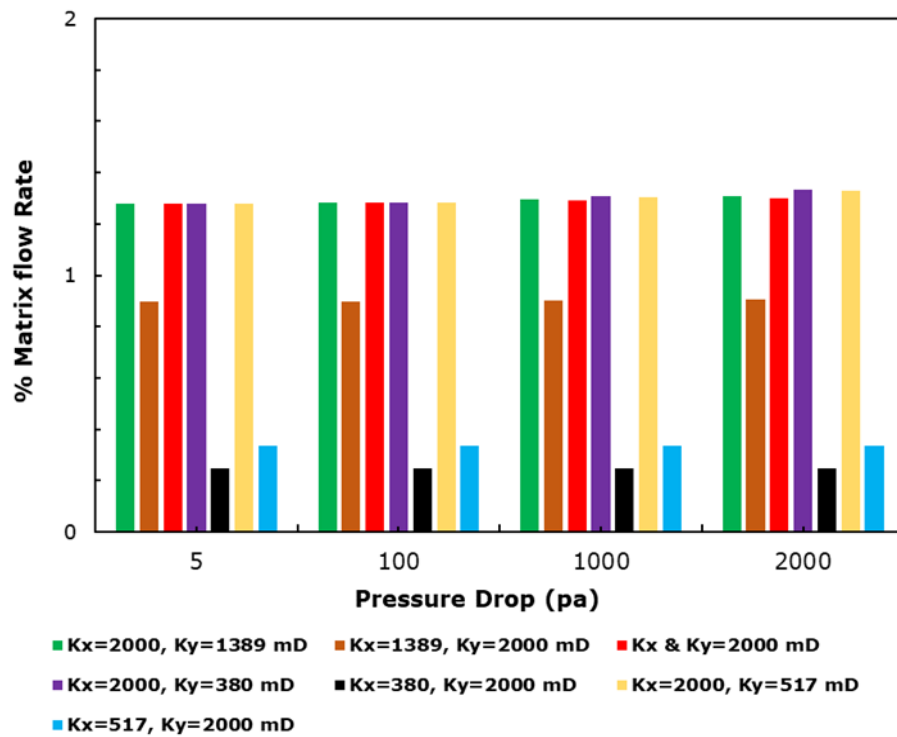


Figure 4.16 Comparisons of matrix flow rate (mm^2/s) of parallel plates ANSYS CFD Fluent FVM model fractures, with isotropic and all anisotropic matrix permeability scenarios, with permeable fracture surface boundaries

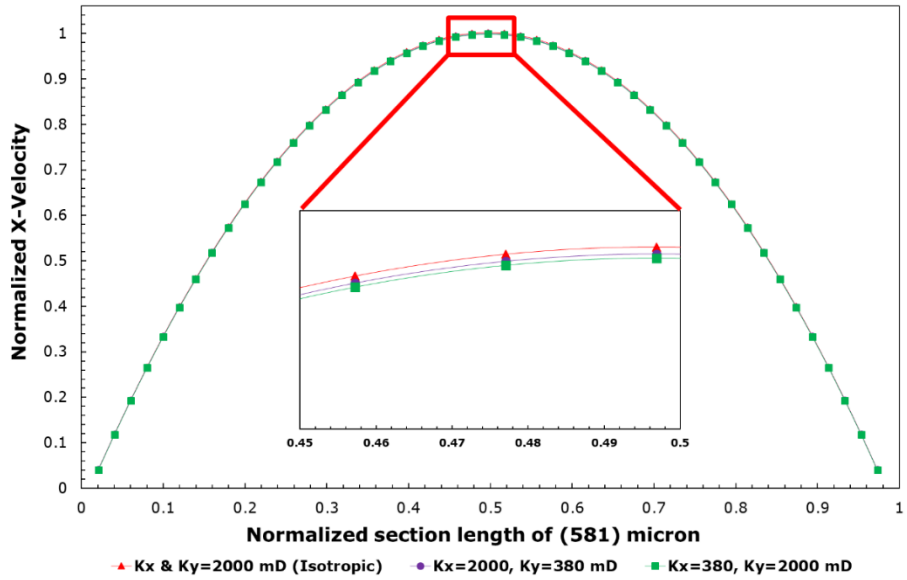


(A)

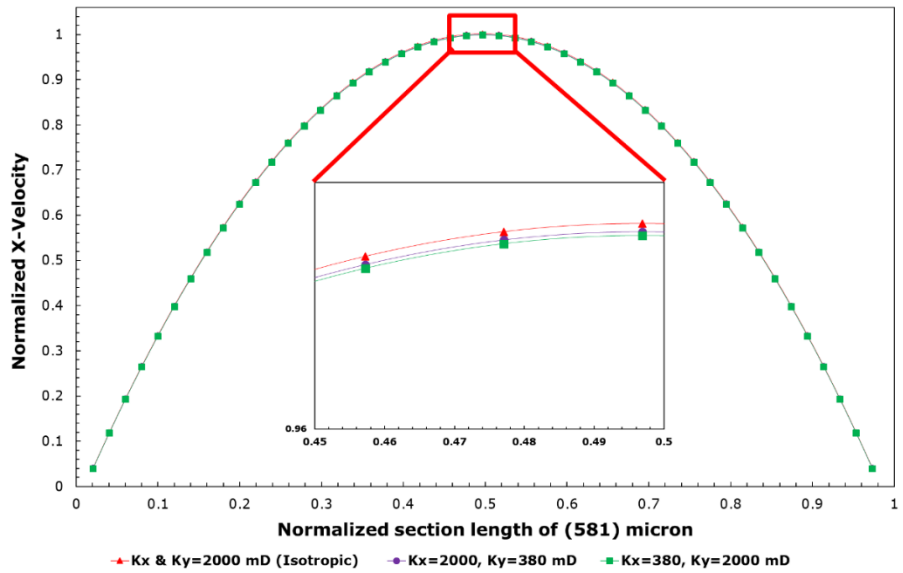


(B)

Figure 4.17 Comparisons of parallel plates ANSYS CFD Fluent FVM model fractures: A. % fracture flow rate and B. % matrix flow rate, with isotropic and all anisotropic matrix permeability models, and permeable fracture surface boundaries



(A)



(B)

Figure 4.18 normalized velocity profiles of parallel plates fracture at 581 Micron section: A. (5) Pa and B. 1000 Pa, between models with isotropic ($K_x=K_y=2000$ mD) and anisotropic matrix permeabilities ($K_x=380$ $K_y=2000$ mD) and ($K_x=2000$ $K_y=380$ mD)

Table 4.3 Summarising flow results of ANSYS CFD Fluent FVM models with anisotropic permeability of parallel plates fractures - average values of four pressure drops (5, 100, 1000, 2000) Pa

CFD models with different Matrix permeability scenarios	Total Flow (mm ² /s)	Fracture Flow (mm ² /s)	Matrix Flow (mm ² /s)	Compared models	Affected Scenario	(ADV) Total flow (decrease of the effected scenario)	(ADV) Fracture flow (decrease of the effected scenario)	(ADV) Matrix flow (decrease of the effected scenario)	% fracture flow (Increase of the effected scenario)
1	108.740	107.323	1.4151	1 & 2	2	0.45	0.052	36.15	0.4
2	108.246	107.269	0.9773	-	-	-	-	-	-
3	108.743	107.310	1.4336	3 & 4	4	1.01	0.124	118.5	1
4	107.544	107.183	0.3612	-	-	-	-	-	-
5	108.745	107.306	1.4388	5 & 6	6	1.2	0.134	137	1.056
6	107.435	107.170	0.2650	-	-	-	-	-	-
Isotropic (Kx=Ky= 2000 mD)	108.735	107.327	1.4085	6 & Isotropic	6	1.2	0.145	136.4	1.046

4.2.4.2 Summary of anisotropic permeability simulations of parallel plates fractures

The simulations of parallel plates fractures with single fracture aperture height and with anisotropic matrix permeability have clarified the importance and necessity of considering anisotropic matrix permeability in fractured reservoirs, as this has been shown to have an effect on the flow of the fracture and the matrix (Tiab and Donaldson 2004 p. 103). This is especially important as the majority of subsurface earth crust and hydrocarbon reservoirs have highly anisotropic permeabilities in-plane (K_x) and through plane (K_y) directions of Cartesian axis, due to the overburden stresses, layers sedimentation and etc (Di Fratta et al. 2016; Lang, Paluszny and Zimmerman 2014; Tiab and Donaldson 2004 p. 162; Golf-Racht 1982 p. 52; Hutchinson, Dodge and Polasek 1961).

These comparisons of the six permeability scenarios of ANSYS CFD Fluent FVM models have reflected interesting findings as below:

1. Changing in-plane (x) permeability in Cartesian axis has led to decrease the total flow rate, and the higher decrease of flow was observed with the highest percentage of permeability reduction, starting from 30%, 74% and 81% respectively. This has confirmed the findings of Hidayati, Chen and Teufel (2000); Saidi (1987) p. 82; Parsons (1966); and Scheidegger (1963) that average permeability of anisotropic permeability formations is effected significantly by in-plane (K_x) permeability in Cartesian coordinates (ie, the permeability that is parallel with flow direction). Also, that when average permeability has been calculated from pressure buildup or any similar tests, it usually reflects close values to horizontal permeability. As well, these results have confirmed the findings of Lei et al. (2015); and Rasouli and Rasouli (2012), that matrix permeability which is parallel to a fracture (K_x) has greater effect than the perpendicular direction (K_y); particularly, when the permeability is aligned with flow direction, as perpendicular direction (K_y) will be decreased due to overburden stresses increasing with production time as pore pressure decrease. Moreover, the reduction of permeability aligned with flow direction in fractured media causes higher pressure drop in formations for the same fracture apertures size, and accordingly, on flow, which has confirmed the findings that were stated by Rasouli and Rasouli (2012).

2. Despite total flow reduction due to the in-plane (K_x) permeability reduction, increasing through plane (K_y) permeability led to increase the fracture flow percentage in the domain; [Table 4.3](#) below clarifies this result. This is due to the effect of pressure drop increasing in-plane (x) direction, while flow through plane (y) in perpendicular contact with fracture permeable surfaces, faced less resistance. As well, the fracture/matrix interface layer is affected by the components of tangential velocities, which affect various fluid jump (movement) conditions for matrix and fracture ([Lei et al. 2015](#); [Rasouli and Rasouli 2012](#); [Popov et al. 2009](#)), and fluid flow movements always occur due to the response of the fracture-matrix interface layer ([Lang, Paluszny and Zimmerman 2014](#)).
3. Comparisons were made of average flow of four pressure values (5, 100, 1000, 2000) Pa for the fracture and the matrix, among the first set of anisotropic permeabilities' ANSYS CFD Fluent FVM models with scenarios 1, 3 and 5 from [table 4.2](#), where K_x was fixed with 2000 mD and K_y was varied with values 380, 517, 1389 mD, and among the second set of anisotropic permeabilities' ANSYS CFD Fluent FVM models with scenarios 2, 4 and 6 in [table 4.2](#), where K_y was fixed with 2000 mD and K_x was varied with 380, 517, 1389 mD. The comparison results of the first set reflected an increase in fracture flow, but matrix flow dropped, which proved that despite in-plane (K_x) permeability being a fixed value, the increase of through plane (K_y) permeability reduced matrix flow and directed flow toward the fracture through fracture/matrix interface layer and increased fracture flow, [Figure 4.19](#) below illustrates the results of these comparisons. This is consolidation of the finding which proves the effects of fracture permeable surfaces through fracture/matrix interface layer (which in this research is considered Interior face boundary in ANSYS CFD Fluent FVM models), due to less flow resistance in through plane (K_y) axis, and fluid jump through fracture/matrix interface layer, due to the effects of the components of tangential velocities inside fracture surfaces. As well, this proves the importance of through plane (K_y) permeability in the matrix, as it does assist fluid paths towards a fracture, in case in-plane (K_x) permeability is low ([Lei et al. 2015](#); [Lang, Paluszny and Zimmerman 2014](#); [Rasouli and Rasouli 2012](#); [Popov et al. 2009](#)). Comparison of the second set of permeabilities reflected an increase in fracture and matrix flow with increasing__in-plane (K_x) permeability whilst through plane (K_y) permeability remained fixed, which proves the effects of permeability

aligned with flow direction on fractured domain flow, as reported by [Lei et al. \(2015\)](#); [Rasouli and Rasouli \(2012\)](#); [Hidayati, Chen and Teufel \(2000\)](#); and [Saidi \(1987\)](#) p.82. These comparisons have provided evidence that K_y permeability is important in fractured formations, as it provides another flow path from matrix toward fracture. To consolidate this finding, the average total flow of the two sets were compared, and the outcome was that the first set with K_y permeability changing had higher average total flow with 0.5% than the first set with K_x permeability changing. This finding is against the findings of [Lei et al. \(2015\)](#); and [Rasouli and Rasouli \(2012\)](#) that matrix permeability aligned with flow direction K_x has greater effect on fractured media flow than that aligned with K_y , and in this research's point of view, the main reasons which led them to this conclusion are: first, they didn't quantify flow percentages in fracture and matrix separately with consideration of anisotropic permeability in-plane (K_x) permeability and through plane (K_y) permeability; and second, as the fracture carries biggest flow percentage, through plane (K_y) permeability has led to increase in fracture flow, which will lead to a higher total flow percentage of a fractured domain.

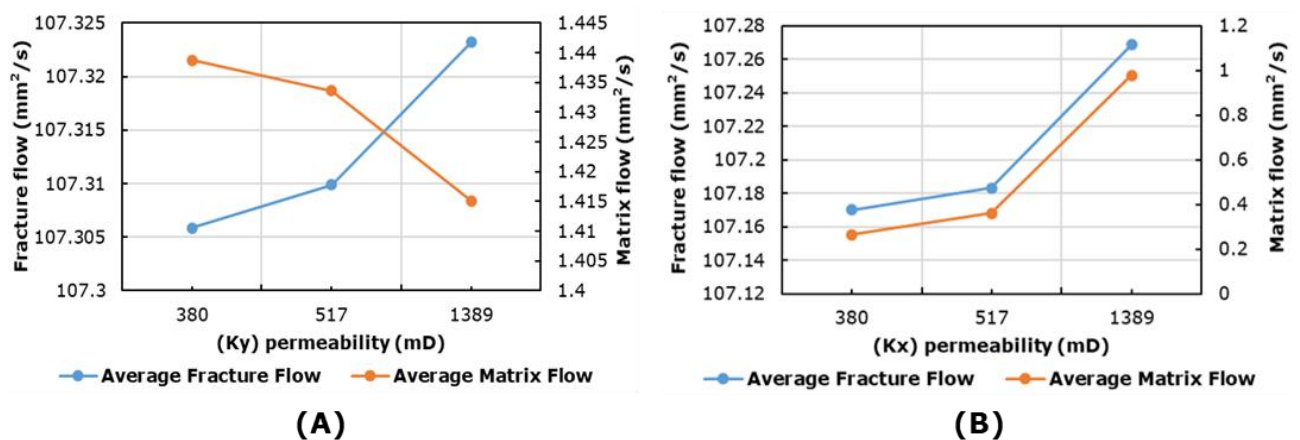


Figure 4.19 Average flow of four pressure values (5, 100, 1000, 2000) Pa for the fracture and the matrix in ANSYS CFD Fluent FVM parallel plates fracture models A. first set permeability scenarios ($K_x=2000$ mD fixed, $K_y= 380, 517, 1389$ mD); B. second set permeability scenarios ($K_y=2000$ mD fixed, $K_x= 380, 517, 1389$ mD)

- These ANSYS CFD Fluent FVM simulations of parallel plates fractures with one fracture height showed that flow inside a fracture will have a slight change when the fracture surfaces are permeable to the fluid with the matrix ([Lang, Paluszny and Zimmerman 2014](#)). This proves that the interaction between the fractures and surrounding matrix is quite low in the

conditions of parallel plates fracture geometry with one aperture height along the flow, which will lead to the wrong prediction of flow, because real fracture geometry is rough and interaction is high and critical for flow analysis (Popov et al. 2009). The main reason for this low interaction is fracture shape, as a single aperture fracture will not suffer from abrupt changing in velocity/pressure along flow, as pressure gradients will be linear in single aperture fracture, and accordingly, will affect fluid movements negatively. A rough fracture, on the other hand, will suffer from higher pressure drop, the effects of fluid recirculation “eddies or vortexes”, and abrupt changes in pressure/velocity along the fracture flow, which increase fluid jump movements between matrix and fracture (Karimzade et al. 2019; Briggs, Karney and Sleep 2014; Popov et al. 2009; Karpyn, Grader and Halleck 2007; Yamatomi et al. 2001). Therefore, assuming a parallel plates fracture with single aperture height will not reflect an actual fracture’s geometry and rough surface, and will lead to wrong prediction/calculations as it excludes real pressure drop in formations and fracture/matrix interaction, which is critical for flow analysis as reported by Lang, Paluszny and Zimmerman (2014); Crandall, Ahmadi and Smith (2010); Popov et al. (2009); and Moreno et al. (1988).

5. Thus, to conclude the points and findings in these analyses, if both K_x and K_y are changing at the same time (as point 1 and 2) then K_x has the highest effect on fractured domain flow. However, if only one of K_x or K_y is changing, then K_y has the highest effect on fractured domain flow (as point 3). Therefore, for a better estimation of flow in fractured media, it is necessary to consider real conditions of subsurface layers rather than simplified conditions, and to consider anisotropic values of permeability, as this has an effect on fractured domain (fracture+matrix) flow.

4.3 Rough Fracture Simulations Results and Validations

In Chapter 3 Section 3.5.2 clarified the details of rough fracture models in ANSYS CFD Fluent FVM. One of the main changings among these models was the boundary conditions of fracture surfaces. The fracture surface boundaries were set as “Walls boundary” when the investigation results required the fracture to not be permeable with the matrix, and these simulations were validated against Nazridoust, Ahmadi and Smith (2006)’s work. The fracture surface boundaries

were set as “Interior faces boundary” when the investigation results required for the fracture to be permeable and interact with the matrix, and these simulations were validated against [Crandall, Ahmadi and Smith \(2010\)](#)’s work. This was because both papers used the same fracture, but with different fracture surface boundary conditions (permeable and non-permeable fracture surfaces). In each simulation, many calculations were observed, such as: pressure drop versus flow rate inside fracture, % fracture flow versus matrix flow, and friction factor versus Reynolds number (clarified in Chapter 5). For the case where the fracture surface boundaries were set as permeable “Interior face boundary”, calculations were observed for the validations of simulations first, and considered isotropic matrix permeability only in order to be able to validate the simulations results against [Crandall, Ahmadi and Smith \(2010\)](#)’s paper. This is because only isotropic permeability of the matrix was considered in that paper’s simulations. Then, secondly, anisotropic permeability of the matrix was set for different scenarios as [Table 4.2](#). The same calculations as in Parallel plates fracture above were observed and compared with the isotropic permeability ANSYS CFD Fluent FVM models, to investigate the effects of anisotropic permeability on fracture flow.

To extract the results from the ANSYS CFD Fluent FVM model simulations, two surface lines were created inside the Fluent models to read the velocity profiles: one inside the fracture in the smallest fracture aperture, 240 micron at (X, Y) coordinates (0.1, 0.0472) (0.1, 0.04754) m; and the other inside the matrix, separately, but in the above and below matrix until the end of the domain (the matrix surface reading lines which were outside the fracture surfaces). These lines were located at the same section, at the end of the domain just before the outlet, to enable this research to investigate the flow changes in the domain for changing pressures and other properties such as matrix permeability (K). The total flow, and flow inside the matrix and fracture was calculated as mentioned in the previous model of parallel plates fracture above, [section 4.2](#). [Figure 4.20](#) below illustrates the lines’ locations.

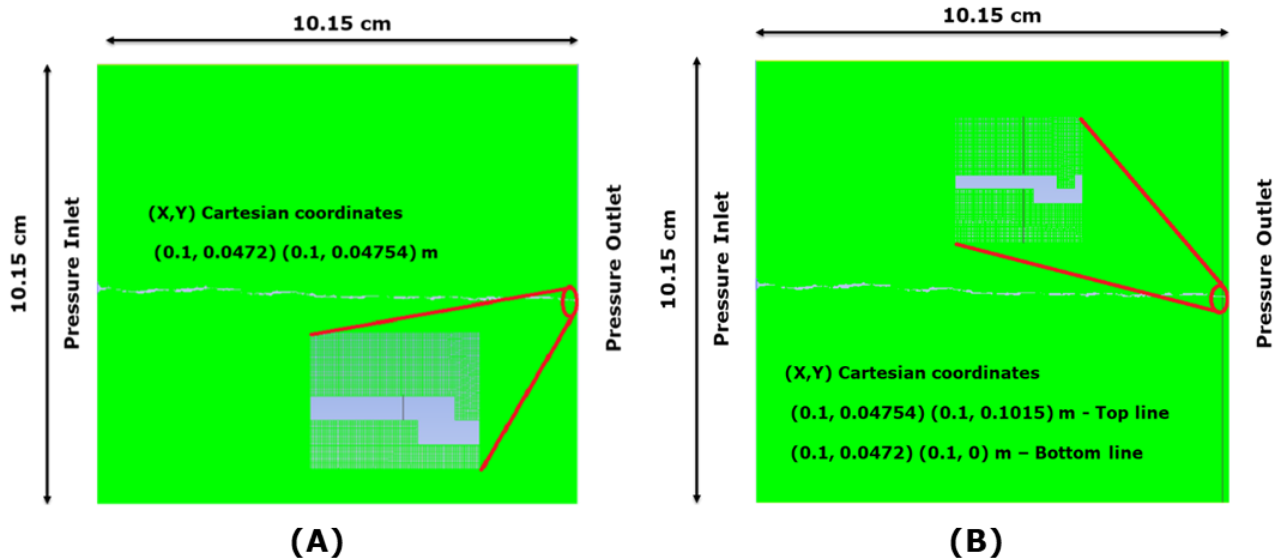


Figure 4.20 Surface lines to read X-velocity profiles: A; inside the fracture only, and B; inside the matrix only (matrix is green, and fracture is blue)

4.3.1 Grid sensitivity analysis

As mentioned in [section 4.2.1](#) of the Grid sensitivity analysis procedure of the previous model (parallel plates fracture), it was vital to investigate the cells number effect of the domain on the simulations' results, by comparing the average velocity values for the same section inside a fracture with different cells numbers. This was in order to be sure that the ANSYS CFD Fluent FVM model had accurate results with an optimised value of mesh cells number.

Thus, the same geometry was meshed with four meshes: first above 1 million cells; second, above 3.6 million cells; third, above 4 million cells; and fourth, above 4.56 million cells. All these models were simulated with the same boundary conditions which were 1000 pa pressure inlet, zero pressure outlet, isotropic matrix permeability ($K_x=K_y=2000$ mD) with 20% porosity, and the fracture surfaces were considered permeable with interior face boundaries; this means they were permeable with the matrix, and the flow could move between the fracture and the matrix and vice versa, and all other set ups of the model as stated in [Chapter 3 Section 3.5.2](#). These models were simulated and all of them were converged, then, the same surface line was located inside the fracture with the smallest fracture aperture (240) micron just before the fracture outlet at coordinates (0.1, 0.0472) m (0.1, 0.04754) m. This was created in all models to read X-Velocity values as [Figure 4.20 A](#), and calculated the average values of these profiles as [Section 4.2](#). [Table 4.4](#) below clarifies the meshes' details and the average velocity values inside

the fracture of each model, [Figure 4.21](#) clarifies velocity profiles inside fracture 240-micron aperture, 1000 Pa with four fracture meshes.

Table 4.4 ANSYS CFD Fluent FVM models mesh details with the average velocity values of the sections inside the rough fracture models

CFD models Meshes	Cells No.	Faces	Nodes	Partitions	Average Velocity of the section (m/s)
First Mesh	1003791	1937685	933895	4	0.122
Second Mesh	3637851	6956154	3318304	4	0.117
Third Mesh	4011566	7288318	3276753	4	0.120
Fourth Mesh	4567263	8099580	3532312	4	0.121

As can be seen in these simulations' results, the difference of the average velocity of the reading line inside the fracture among these four meshes was very small, and the increase in the mesh did not reflect any significant increase or decrease. Comparisons among these four meshes show that less than 1.5% deviation in average value was observed among first, second, third and fourth. Therefore, the third mesh was selected to be used in the ANSYS CFD Fluent FVM simulations of this model. The reasons for this were: first, increasing the mesh number had no significant change in simulation readings, with less than 1% deviation between the third and fourth meshes; second, using a higher cells number would require more time to compute simulations (approximately 2.5 the time) without any significant effect on results' accuracy as deviation is less than 1%, and accordingly, would lead to more delays to obtain the results; and third, despite the fact that the results had no significant change/deviation between the first and fourth meshes, the third mesh was selected just to be sure that all the details of irregular fracture shapes (rough fracture) were captured. As stressed by [Rasouli and Rasouli \(2012\) p. 4;](#) and [Dietrich et al. \(2005\) p. 42,](#) due to the large differences between the properties of the matrix and the fracture, the model's mesh should have a high degree of refinement in these borderline areas.

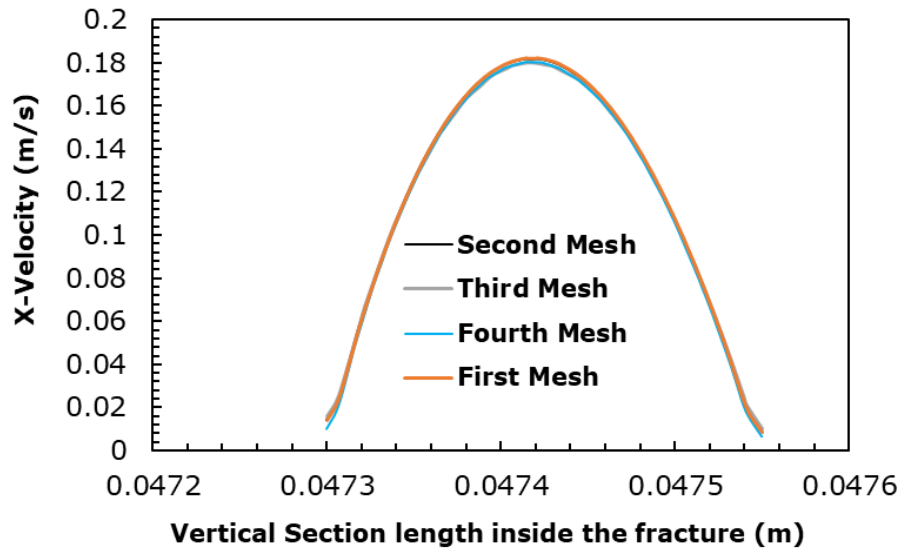


Figure 4.21 X-velocity inside fracture 240- micrometre aperture, 1000 Pa with four fracture meshes

4.3.2 Rough Fracture surfaces set up as “Impermeable Walls boundary conditions” with Validation

This model was created with a fracture having the same fractal properties clarified in Chapter 3 and Appendix 1, and the surrounding matrix media. However, the fracture surface boundaries were set as “Walls boundary”, which means non-porous walls of the fracture, with non-permeable surfaces that did not allow fluid to interact or move between fracture and the matrix. In all the simulations, the velocity profiles inside the fracture with 240 microns were observed at the end part of the fracture, just before the outlet. Two sets of isotropic permeabilities ($K_x=K_y$) were considered of the matrix, 0.2 mD and 2000mD, with four pressure values (5, 100, 1000, 2000) Pa and zero pressure outlet in all of them, and all other set ups of the model as stated in [Chapter 3 Section 3.5.2](#), then comparisons were made among velocity profiles inside the fracture. These were with same pressure drop but different matrix permeability, in order to see the effect of the matrix permeability on fracture flow when fractures’ surfaces were considered as non-porous wall boundaries. This approach was not considered in [Nazridoust, Ahmadi and Smith \(2006\)’s](#) model, and the outcome of these comparisons was that flow inside the fracture was not changed while the fracture surfaces were set as “impermeable wall boundaries”. As well, pressure contours’ distribution reflected no interaction between fracture and matrix due to the impermeable wall boundary, which proved that there was no interaction between the fracture and surrounding matrix, and proof of walls boundary efficiency in ANSYS CFD Fluent

FVM's model that do not allow fluid movement or interaction between fracture and matrix. Velocity contours clarified the highest velocity occurred in the smallest fracture apertures as [Figures 4.22](#). X-velocity profiles inside the fracture did not change with permeability changes of matrix with the same pressure, due to no interaction between fracture and matrix with impermeable fracture surface boundaries; [Figure 4.23](#) below presents the comparison of the velocity profiles inside fracture.

ANSYS CFD Fluent FVM models are required to be validated and compared with other ANSYS CFD Fluent FVM models; if this is not possible, they can be validated with other models from the literature, such as analytical equations or experiment results ([Briggs, Karney and Sleep 2014 p. 539](#)). Therefore, in these ANSYS CFD Fluent FVM models the values of pressure drop-versus fracture flow rate that were calculated from the simulations of four pressure values (5, 100, 1000, 2000) Pa and zero outlet pressure, with two sets of isotropic permeabilities considered of the matrix 0.2 mD and 2000 mD, were validated against the values of [Nazridoust, Ahmadi and Smith \(2006\)'s](#) paper, because in their model, only fracture flow was considered without matrix, and this model with impermeable wall boundary of fracture surfaces has accounted for only fracture flow and excluded matrix effect. The fracture flow of this research's models were a good match with [Nazridoust, Ahmadi and Smith \(2006\)'s](#) model, with a small deviation of around 5.5% for both models with different matrix permeabilities because matrix effects were excluded; even this deviation was accrued due to observing/transferring the data from the image digitizing from [Nazridoust, Ahmadi and Smith \(2006\)'s](#) paper log-log graph. [Figure 4.24](#) below presents these validations. This case shows the validity and reliability of this model for further investigations.

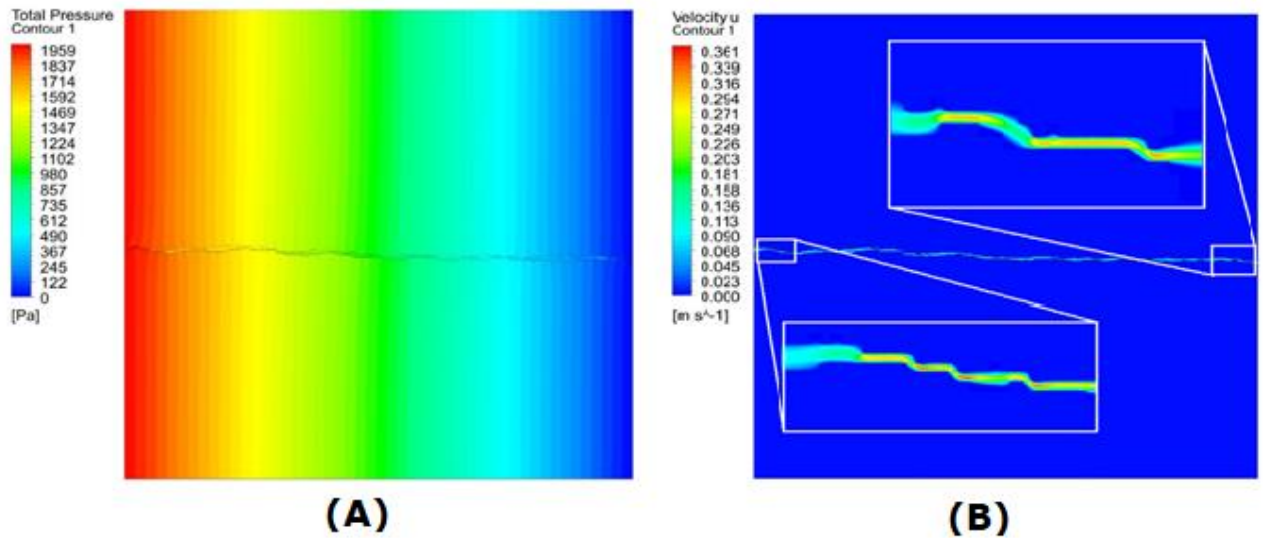


Figure 4.22 Rough fracture simulations total pressure and velocity contours with isotropic matrix permeability (K_x & $K_y=2000$ mD) and $P=2000$ Pa with zero outlet pressures, fracture surface boundaries set as impermeable “Walls boundary”. A. Total pressure, B. velocity contours

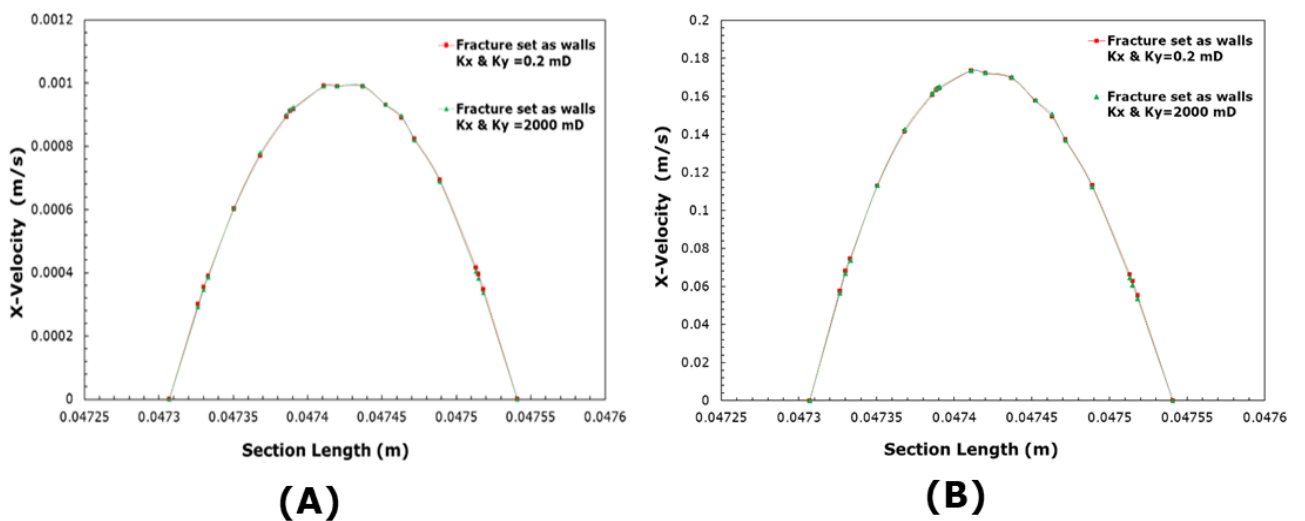


Figure 4.23 Comparisons of X-velocity profiles of rough fracture models at the 240 micrometre vertical section at the end of fracture, with isotropic matrix permeabilities K_x & $K_y=2000$ mD, and K_x & $K_y=0.2$ mD, fracture surfaces set as impermeable boundaries “Walls”, with two pressures: A. 5 Pa, and B. 1000 Pa

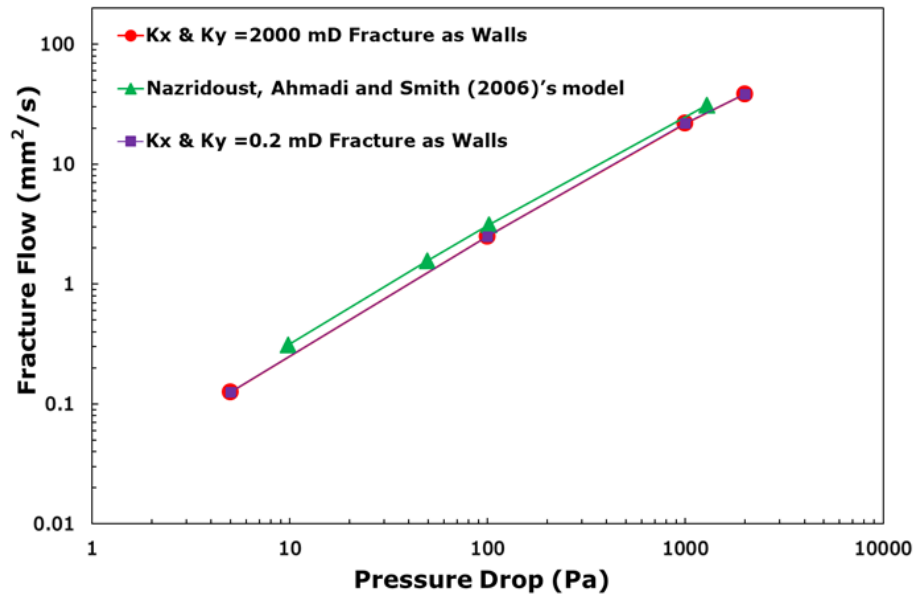


Figure 4.24 Validation of pressure drop with a fracture flow rate between this research's ANSYS CFD Fluent FVM models and Nazridoust, Ahmadi and Smith (2006)'s model, fracture surfaces set with impermeable boundaries "Walls", with two sets of isotropic matrix permeabilities: K_x & $K_y=2000$ mD, and K_x and $K_y=0.2$ mD.

4.3.3 Rough fracture surfaces set-up "Interior faces" permeable boundary conditions with validation

This model was created with a similar fracture to the fractal specification clarified in previous sections above, but the surrounding matrix media and the fracture surfaces were set as "Interior face boundary" permeable boundary conditions, meaning the fracture surfaces were porous and permeable, allowing fluid to interact or move between the fracture and matrix and vice versa. In all the simulations, isotropic permeabilities were considered of the matrix $K_x=K_y=2000$ mD with four pressure drop values (5, 100, 1000, 2000) and zero pressure outlet, and all other set ups of the model as stated in Chapter 3 Section 3.5.2, then, the velocity profiles inside the fracture with 240 micrometres were observed at the end part of the fracture, just before the outlet, and flow calculated as Section 4.2. The values of pressure drop versus fracture flow rate were calculated from these simulations and validated against the values of Crandall, Ahmadi and Smith (2010)'s paper, because in their work the matrix effect on the fracture domain flow was considered. The fracture flow of this research's model was highly matched with Crandall, Ahmadi and Smith (2010)'s model, with a small deviation of around

1.9%. In this model's simulations, pressure contour distribution reflected interaction between fracture and matrix due to the permeable fracture surfaces; particularly, variation was observed around interface layer of fracture/matrix and adjacent matrix, and velocity contours clarified the highest velocity occurred in smallest fracture apertures. Figures 4.25 and 4.26 below present the results of simulations and the velocity profiles inside fracture, and Figure 4.27 clarifies the validation. This showed the validity and reliability of this model for further investigations, which are clarified in the following sections.

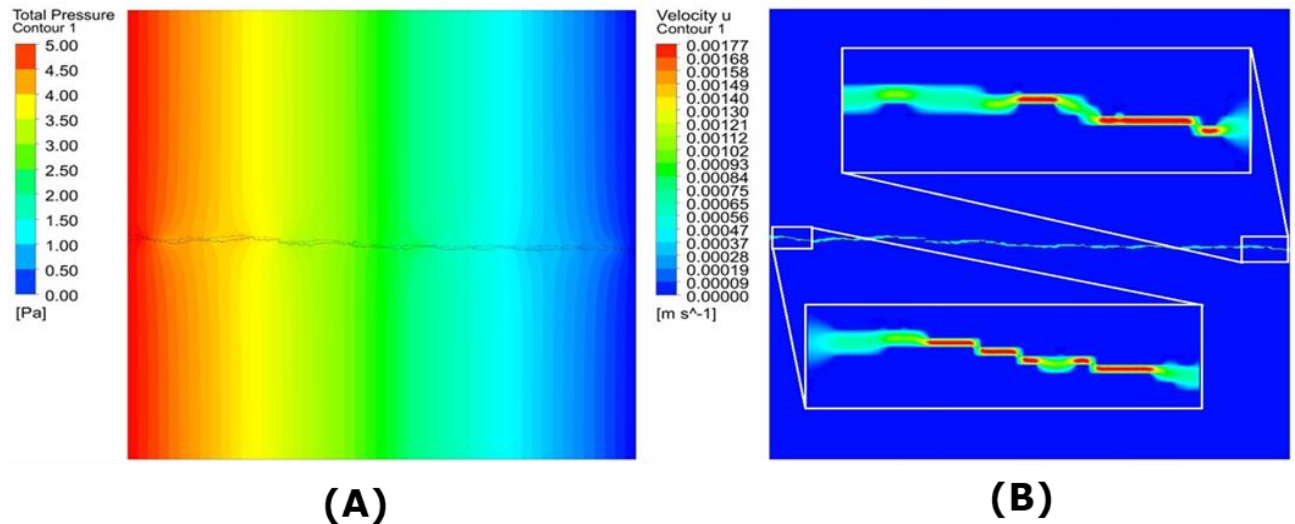


Figure 4.25 Rough fracture simulations' total pressure and velocity contours with isotropic matrix permeability (K_x & $K_y=1000$ mD) and $P=5$ Pa, fracture surface boundaries set as permeable "Interior faces": A. Total pressure, B. velocity contours

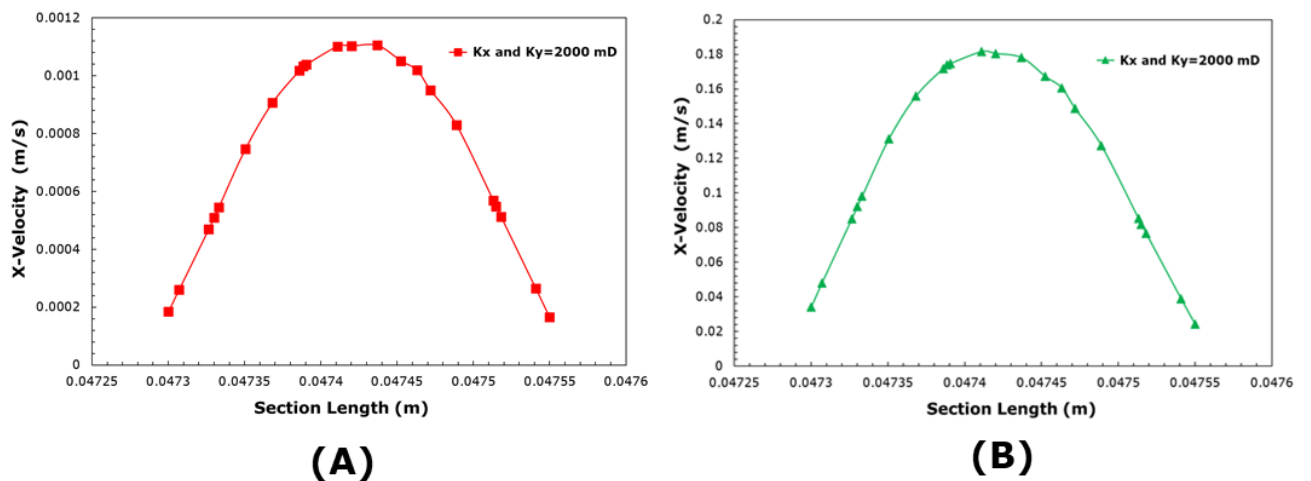


Figure 4.26 Comparisons of X-velocity profiles of rough fracture models at the 240 micrometre vertical section at the end of fracture (with isotropic matrix permeability K_x & $K_y=2000$ mD, fracture surfaces set with permeable boundaries "Interior faces", with two pressures: A. 5 Pa, and B. 1000 Pa)

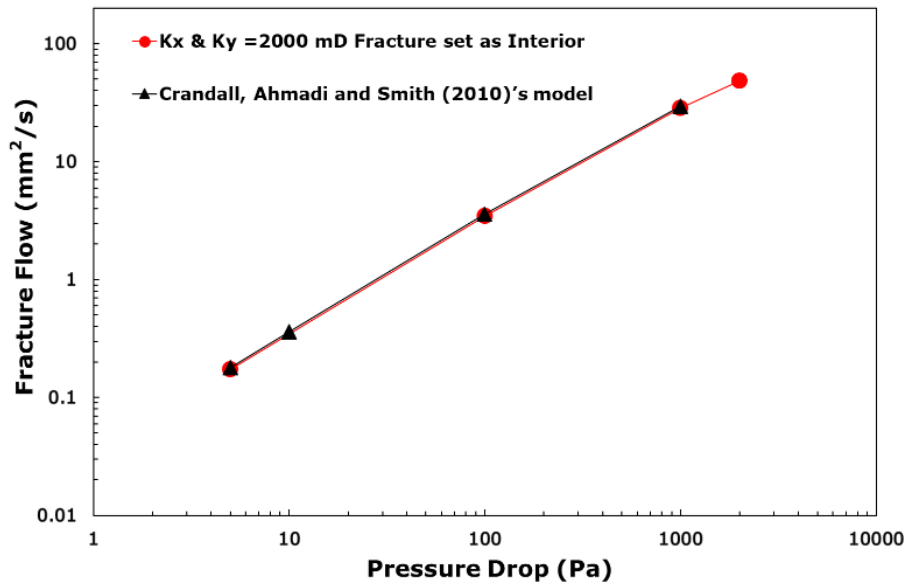


Figure 4.27 Validation of pressure drop with a fracture flow rate between ANSYS CFD Fluent FVM rough fracture and [Crandall, Ahmadi and Smith \(2010\)](#)'s models with isotropic matrix permeability K_x & $K_y=2000$ mD, fracture surfaces set with permeable boundaries "Interior faces"

4.3.4 Rough fracture ANSYS CFD Fluent FVM models with surface boundaries as "Walls" and "Interior faces", with isotropic matrix permeability

This comparison was to check the effect and differences of fracture surface set-ups, whether as permeable "Interior faces boundary" or impermeable "Walls" boundaries, and how changing fracture surfaces from porous to non-porous with the matrix could change the flow percentage in the fracture and matrix. The two models were simulated with the same conditions: isotropic matrix permeability ($K_x=K_y=2000$ mD); 20% matrix porosity; and different pressure drops (5, 100, 1000, 2000) Pa and zero pressure outlet, and all other set ups of the model as stated in [Chapter 3 Section 3.5.2](#). The only condition that was different between these two models was the fractures' surface boundaries: one was set with permeable "Interior faces", which allowed fluid flow between the matrix and the fracture and vice versa; and the second model was set with impermeable "Walls boundary", which meant no flow or any interaction took place between the matrix and the fracture, then the total, fracture and matrix flows were calculated as [Section 4.2](#). The outcome of comparisons of these two cases is summarised below:

1. The outcome of these simulations showed that with these two conditions of fracture surfaces (permeable and impermeable), ADV of total flow rate increased in the fracture model with permeable surfaces by approximately 38.6%. This increase was reflected in the increase ADV of fracture flow around 28.16%; and matrix flow around 106.152%. [Figures 4.28A, 4.28B](#) and [4.28D](#) present these comparisons. As well, the velocity profiles of the section 240 micrometre for both fracture surface boundary conditions, "walls" and "interior" were compared, and permeable fracture surfaces showed an increase, [Figure 4.29](#) clarifies it.

This comparison proved that flow inside the fracture increased by more than 25% when the fracture surfaces were permeable to the fluid with the matrix. However, the results showed that the increase in fracture flow was much higher with permeable fracture surfaces than reported in the previous study, conducted by [Crandall, Ahmadi and Smith \(2010\)](#). That study stated that flow inside fractures had increased by only 10% in comparison with impermeable fracture's walls. This proved that interaction between the fracture and surrounding matrix was quite high, particularly with rough fracture geometry. As can be seen in pressure contour [Figure 4.25A](#), for pressure distribution between the matrix and fracture, particularly, the pressure disturbance in matrix pressure surrounding the fracture permeable interface layer was very high, showing clear signs of interaction. As well, this was reflected by non-linear pressure gradient drop inside the fracture, which confirmed the findings of pressure drop in rough fractures as reported by [Rasouli and Rasouli \(2012\)](#); [Crandall, Bromhal and Karpyn \(2010\)](#); [Crandall, Bromhal and Smith \(2009\)](#); [Petchsingto \(2008\)](#); [Piri and Karpyn \(2007\)](#); [Nazridoust, Ahmadi and Smith \(2006\)](#); [Zimmerman and Bodvarsson \(1996\)](#); and [Moreno et al. \(1988\)](#). This case was further investigated by observing the velocity streamlines of both these models by ANSYS CFD Fluent FVM -Post, and the finding was that flow inside the matrix or fracture interacted highly when the fracture surfaces were set as "Interior faces". However, as expected, there was no interaction at all when the fracture surfaces were set as impermeable "walls", therefore, no pressure/velocity effects between two domains, which proved the model set-up conditions were accurate; [Figures 4.31](#) and [4.32](#) clarify this. This finding has disqualified the vision of neglecting matrix effect in

fractured media, as was believed that that fractures' conductivity differences were expected to be minimal when these are embedded in permeable or impermeable host rock, as reported by [Berkowitz \(2002\) p. 867](#).

Moreover, it was observed that the effects of eddies and vortices in rough fractures, and their sizes and locations, were higher with higher pressure gradients/velocity applied, when there were abrupt changes of fracture apertures along the flow, as reported by [Karimzade et al. \(2019\)](#); and [Tsang, Y. W. \(1984\)](#). To expand on this, [Briggs, Karney and Sleep \(2017\)](#); [Dippenaar and Van Rooy \(2016\) p. 4](#); and [Briggs, Karney and Sleep \(2014\)](#) stated that eddies do not contribute to bulk flow in a fracture as these are isolated zones; however, the streamline analysis of this research has reflected a different vision, that zones of eddies in fractures' narrow corners increased the interaction between fracture and matrix, through changing pressure and velocity as these zones were in unsettled pressure and velocity status, and helped fluid movement (jump) between the two media (fracture and matrix). This has confirmed the findings of [Crandall, Ahmadi and Smith \(2010\)](#); and [Popov et al. \(2009\)](#), that in the surrounding porous media where the velocity is at lowest value and high pressure, fluid moves through the interface layer to the fracture's open space and vice versa, and that the interface permeable layer between fracture and matrix is affected by components of tangential velocities inside a fracture, which affect various fluid jump (movements). Thus, considering permeable fracture surfaces in rough fracture geometry has led to increased total flow in the fracture and surrounding matrix; in addition, the effects of eddies and vortices increased bulk flow in the rough fracture. This has disqualified the negative impact as reported by [Briggs, Karney and Sleep \(2017\)](#); [Chen et al. \(2017\)](#); [Dippenaar and Van Rooy \(2016\) p. 4](#); [Briggs, Karney and Sleep \(2014\)](#); and [Karpyn, Grader and Halleck \(2007\)](#), as these studies considered fracture surface roughness and eddies' effects on flow inside the fracture space only, neglecting the effect of fracture aperture changes and eddies on flow interaction with the matrix. Particularly, that rough fractures have more proportion of contact area with the matrix ([Zimmerman and Bodvarsson 1996](#)), which consolidates the finding that considering impermeable fracture surfaces, and neglecting matrix flow contribution, will lead to an underestimation of flow in fractured media.

This confirmed the findings of [Rasouli and Rasouli \(2012\)](#); and [Crandall, Ahmadi and Smith \(2010\)](#) that considering the matrix effect increases fractured formation connectivity, and the matrix effect's importance as reported by [Luo et al. \(2020\)](#) p. 3.

Thus, the ANSYS CFD Fluent FVM analysis of this study has reflected the findings that in fractured media, two key parameters must be considered in order to mimic real fracture flow conditions: rough fracture surfaces and permeable fracture interface layer with matrix. This is in order to include the matrix effect with flow contribution of fracture and matrix, and interaction variation along fracture flow.

2. A validation procedure of matrix flow in rough fractured media was conducted between the ANSYS CFD Fluent FVM model results and the Darcy equation of flow in porous media: [Equation 2.3 Chapter 2](#). The ANSYS CFD Fluent FVM model with fracture surfaces as impermeable boundary "Walls" was compared with the Darcy equation of flow in the matrix. The result of this comparison was that the ANSYS CFD Fluent FVM model matched highly with the Darcy flow equation, with less than 1.5% deviation. This high match result added further credit and validated the ANSYS CFD Fluent FVM model results. [Figure 4.28C](#) below illustrates these results.

Further comparison was made between matrix flow of ANSYS CFD Fluent FVM models with impermeable fracture surfaces "Walls boundary" and permeable fracture surfaces "interior face boundary" boundaries. This investigation gave a clear vision of flow in the matrix when the fracture surfaces were considered permeable with the matrix. The outcome of this comparison was that the matrix flow with surrounding permeable fracture surfaces increased 106.152%; [Figure 4.28D](#) presents this comparison. This comparison is proof that matrix flow in fractured media be non-linear flow, which is further proof that the findings regarding fracture/matrix interaction are highly significant, as reported by [Luo et al. \(2020\)](#); [Dippenaar and Van Rooy \(2016\)](#); [Rasouli and Rasouli \(2012\)](#); [Crandall, Ahmadi and Smith \(2010\)](#) and [Popov et al. \(2009\)](#). This case was further investigated by comparing the percentage of fracture flow of the fracture domain in comparison with the total flow. The outcome of this comparison showed that the average percentage of fracture flow

with the permeable surface boundaries model was 82%, while the average percentage for the impermeable fracture surfaces model was around 92%. As well, % fracture flow decreased with increasing pressures due to the effect of pressure to increase flow in matrix and more fluid movement from fracture to matrix, and % matrix flow increased with increasing pressure due to the effect of pressure to increase flow in matrix and more fluid movement from fracture to matrix, flow resistance overcome with higher pressure values. [Figures 4.30A and 4.30B](#) clarify this result. In other words, despite the fact that the total flow (fracture flow and matrix flow) of the fracture domain models with permeable fracture surfaces increased, the percentage of fracture flow in these models was less than the impermeable fracture surfaces models. This means that flow inside the matrix was more efficient due to the interaction between matrix and fracture. This is clarified in the velocity streamline in [Figure 4.32](#), as All streamline locations presented high flow interactions or movements between fractures and matrix through interface layer with permeable fracture surface boundaries setup. As well, abrupt changes in fracture apertures with fractures' sharp/ narrow corners generated eddies and vortices, representing gateways or clusters of fluid movement between fractures and matrix, due to the pressure/velocity changing and fluid momentum between the two domains. These fluid movements along the fracture led to increase % matrix flow as more fluid moved from fracture towards matrix; this has clarified the importance of matrix flow contribution in fractured domains. This change in the average percentage of fracture flow rate clarifies the increase in the matrix flow rate, as flow leaves from fracture into matrix in some zones, and in other zones vice versa.

It's good to stress here as the matrix flow in fractured ANSYS CFD Fluent FVM models reflected non-linear increase, that only Darcy law was considered for the comparison, not Forchheimer formula. This was because of the inertial coefficients β of the Forchheimer formula (a non-linear term). This has many ambiguities and controversies, and there is no general agreement on its value; therefore, in most practical application, β value is observed from best fit lines of numerical and experimental data on formations ([Arthur 2018](#); [Dippenaar and Van Rooy 2016](#); [Sobieski and Trykozko 2014 p. 321](#); [Jambhekar 2011 p. 15](#);

Sobieski and Trykozko 2011 p. 156; Takhanov 2011; Evans and Civan 1994). Therefore, as the aim of this research was to have a solid understanding of flow in fractured media, thus, Forchheimer formula was excluded from the comparisons.

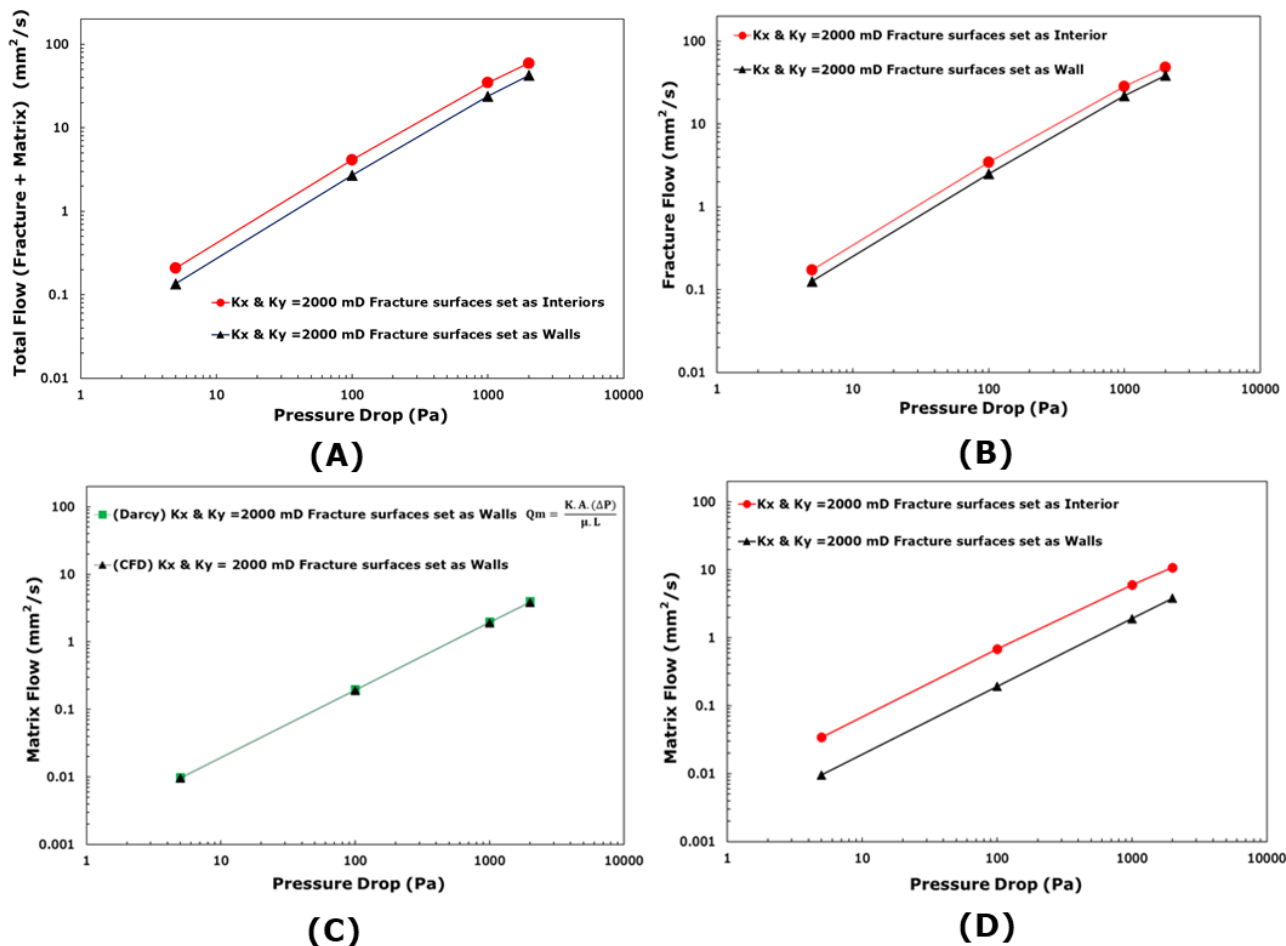
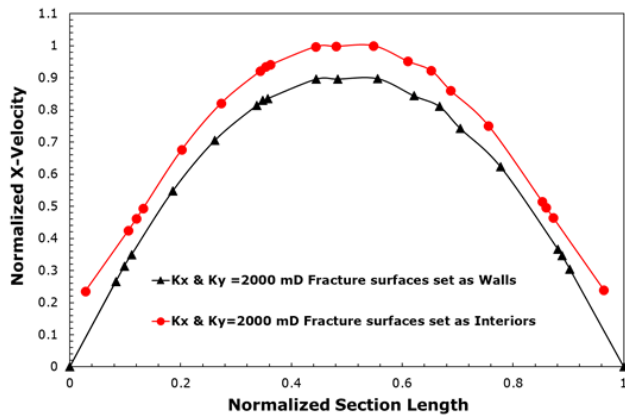
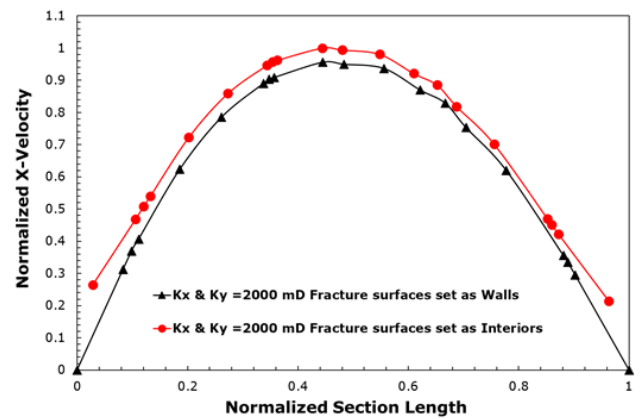


Figure 4.28 Rough fracture ANSYS CFD Fluent FVM models' flow comparisons between impermeable "Walls boundary" and permeable "Interior faces boundary" of fracture surface boundaries with (Kx & Ky=2000 mD) A. total flow rate; B. fracture flow rate; C. validation of ANSYS CFD Fluent FVM models' matrix flow rate with impermeable fracture surface boundaries with Darcy formula of flow in matrix; and D. comparison between matrix flow rate with two set-ups of fracture surface boundaries, permeable "Interior" and impermeable "Walls"

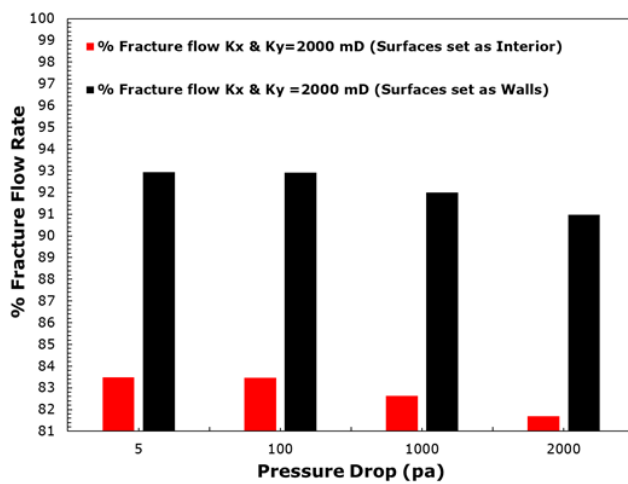


(A)

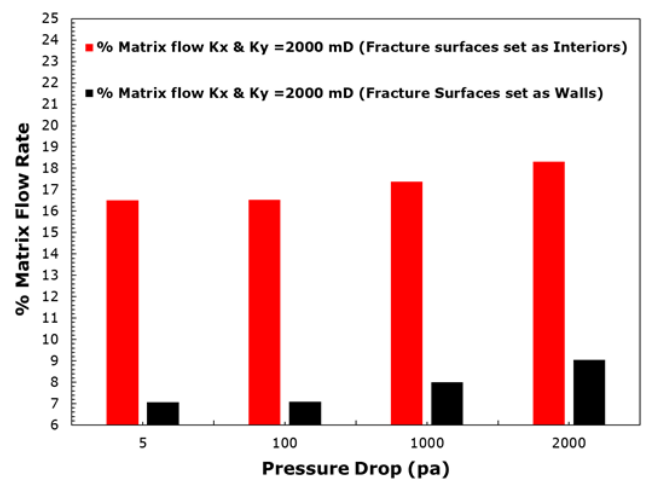


(B)

Figure 4.29 Normalized Velocity profiles of rough fracture ANSYS CFD Fluent FVM models of 240 micrometer fracture aperture height, at the end just before fracture outlet, isotropic matrix permeability K_x and $K_y = 2000$ mD- comparing models with permeable "Interior faces" and impermeable "Walls" fracture surface boundaries with two pressures: A. 5 Pa, and B. 1000 Pa



(A)



(B)

Figure 4.30 Comparison of rough fracture ANSYS CFD Fluent FVM models' flow percentages between permeable and impermeable fracture surface boundaries with the matrix, isotropic matrix permeability K_x and $K_y = 2000$ mD. A. % fracture flow; and B. % matrix flow

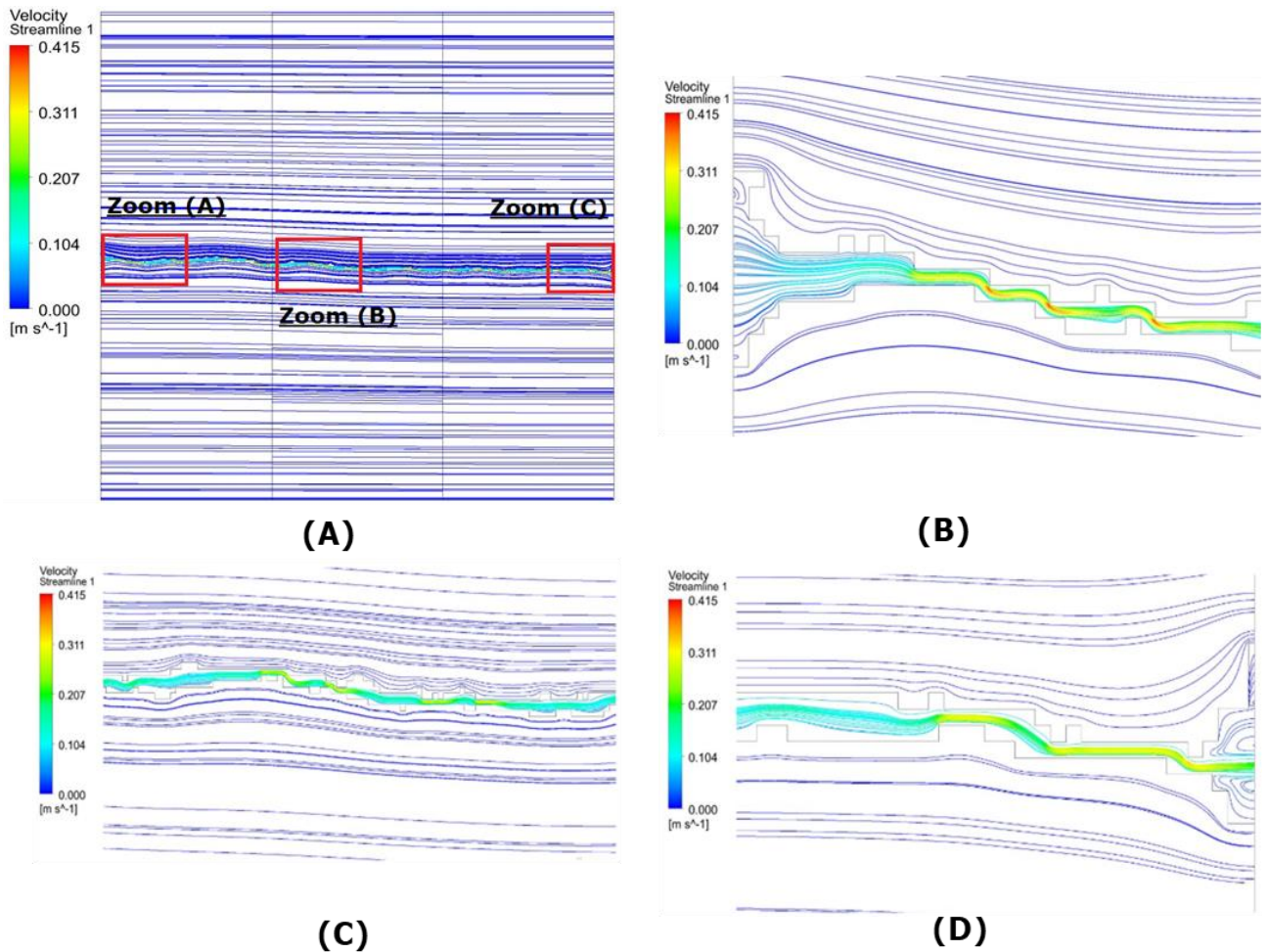


Figure 4.31 Velocity streamlines of rough fracture $P=2000$ Pa, isotropic matrix permeability (K_x & $K_y= 2000$ mD), with fracture surface boundaries set as impermeable “Walls”

A. zooms on three random locations between fracture and matrix; B. velocity streamlines on location (A); C. velocity streamlines on location (B); and D. velocity streamlines on location (C).

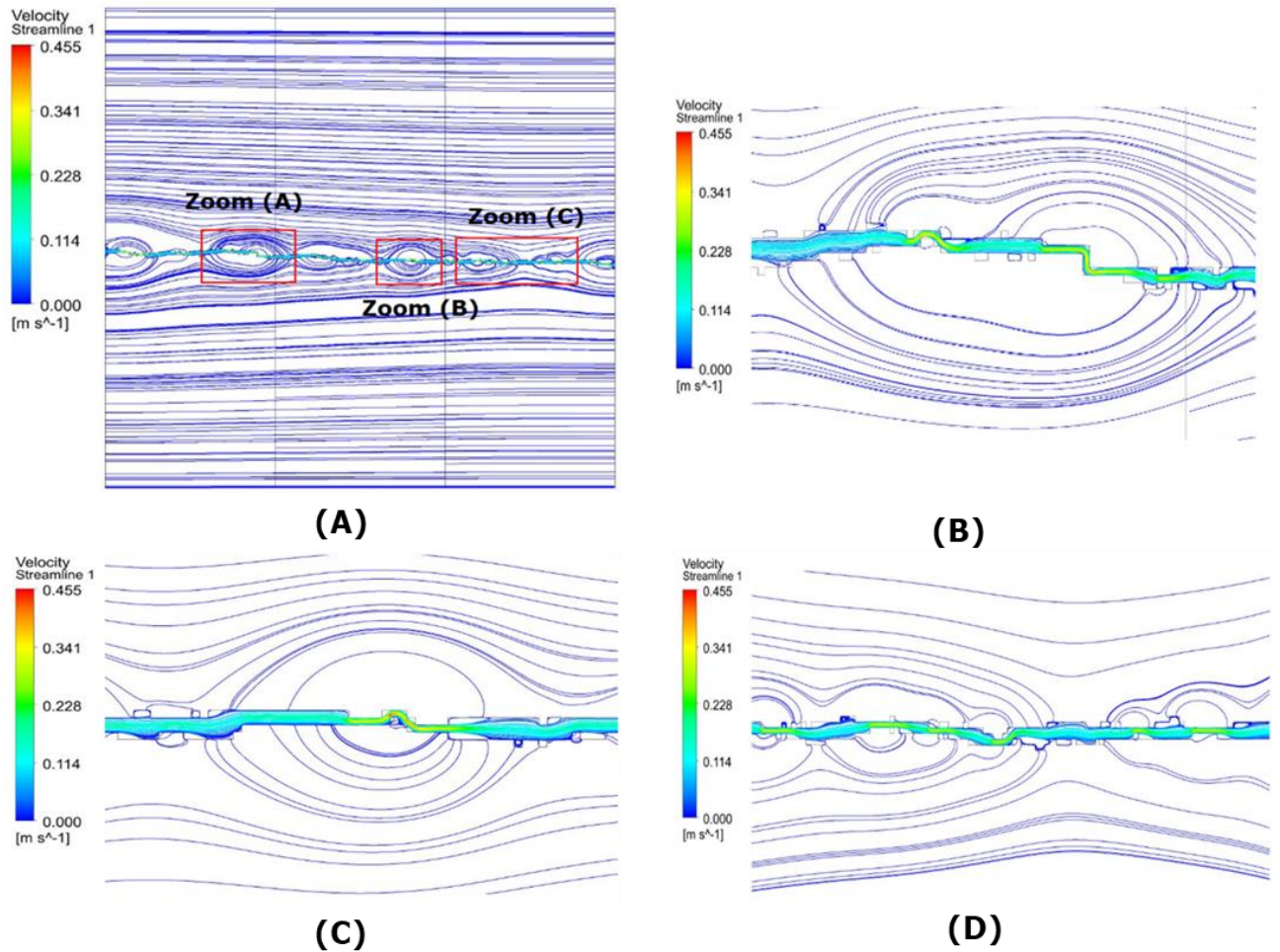


Figure 4.32 Velocity streamlines of rough fracture $P=2000$ Pa, isotropic matrix permeability (K_x & $K_y= 2000$ mD), with fracture surface boundaries set as permeable "Interior faces"

A. zooms on three random locations between fracture and matrix; B. velocity streamlines on location (A); C. velocity streamlines on location (B); and D. velocity streamlines on location (C).

4.3.5 Rough fracture ANSYS CFD Fluent FVM models with permeable surface boundary “Interior faces” with anisotropic matrix permeability results

This section illustrates the ANSYS CFD Fluent FVM models' results of flow in rough fractures, but with matrix anisotropic permeability in fractured media. As stated by Li et al. (2021); Zhu et al. (2020); Suri et al. (2020); Ju et al. (2019); Karimzade et al. (2019); Luo et al. (2018); Chen et al. (2017); Zou, Jing and Cvetkovic (2017); Liu, Li and Jiang (2016); Briggs, Karney and Sleep (2014); Zhang and Nemcik (2013); Rasouli and Rasouli (2012); Hosseinian (2011); Rasouli and Hosseinian (2011); Sahimi (2011); Sarkar, Toksöz and Burns (2011); Crandall, Ahmadi and Smith (2010); Crandall, Bromhal and Karpyn (2010); Crandall, Bromhal and Smith (2009); Koyama et al. (2009); Petchsingto and Karpyn (2009); Popov et al. (2009); Kulatilake et al. (2008); Petchsingto (2008); Nazridoust et al. (2006); Tiab and Donaldson (2004); Nelson (2001); Zimmerman and Yeo (2000); Golf-Racht (1982) and Ruhland (1973), that fractured formations in subsurface layers of earth crust, or in reservoirs, have decidedly anisotropic properties, and in some cases among points to points with small distance. Therefore, this model created a close image or condition of anisotropic matrix properties of fractured media, particularly, anisotropic permeability of the matrix that surrounded fracture permeable surfaces. This was due to reasons as clarified in Section 4.2.4, that one of the key matrix properties is permeability and this has a fundamental effect on flow in the matrix. This model aided understanding and visualisation of fracture/matrix flow effects with a matrix's anisotropic permeability. As proved in the previous sections, allowing for flow movement between fracture and matrix, and vice versa, has a significant effect on flow percentage in fracture and matrix in the fractured domain.

To achieve this goal, the same rough fracture domain was considered as in the previous section: the same rough fracture properties; the same matrix length; and fracture surfaces were considered permeable “Interior faces boundary” to allow fluid movement between matrix and fracture and vice versa. However, the difference was that matrix permeability was considered anisotropic in in-plane (x) and through plane (y) of Cartesian directions with different scenarios. By using the same model, this enabled the quantification and calculation of differences when comparisons were necessary with an isotropic permeability model. The matrix

anisotropic permeability scenarios were the same scenarios that were adapted in [Section 4.2.4: Table 4.2](#). Fracture surfaces were set as permeable surface boundaries “Interior faces” in all the simulations. Different pressure inlet values were considered: (5, 100, 1000, 2000) Pa and zero pressure outlet, and all other set ups of the model as stated in [Chapter 3 Section 3.5.2](#), then the total, fracture and matrix flows were calculated as [Section 4.2](#).

4.3.5.1 Simulation results

Matrix permeability was changed in in-plane (K_x) and through plane (K_y) directions of Cartesian coordinates ($K_x \neq K_y$), as the six scenarios in [Table 4.2](#) showed. The first scenario ($K_x=2000$ $K_y=1389$) was compared with the second scenario ($K_x=1389$, $K_y=2000$), with ADV of total flow rate was decreased in the second scenario by more than 4.07%. This decrease was reflected in the reduction ADV of fracture flow by around 0.81% and matrix flow by 22%. In spite of this, the comparison shows that in the second scenario, flow decreased in the matrix and the fracture, but that the percentage of fracture flow was higher in the second scenario with an average value of 2.76%. A similar comparison occurred between the third ($K_x=2000$ $K_y=517$) mD and fourth ($K_x=517$ $K_y=2000$) mD scenarios; ADV of total flow rate was decreased in the fourth scenario by 4.6%. This decrease was reflected in the reduction of ADV fracture flow by around 0.131% and matrix flow by 30%. Despite this, the comparison shows that in the fourth scenario, the flow was decreased in the matrix and the fracture, but the percentage of fracture flow was higher in the fourth scenario with an average value of 3.77%. Lastly, comparisons were made between the fifth ($K_x=2000$, $K_y=380$) mD and sixth ($K_x=380$, $K_y=2000$) mD scenarios, and the outcome was that, ADV of total flow rate was decreased in the sixth scenario by more than 5%. This decrease was reflected in the reduction of ADV fracture flow by around 0.138% and matrix flow by 32.6%. However, this comparison showed that in the sixth scenario, the flow had decreased in the matrix and the fracture, but the percentage of fracture flow was higher in the sixth scenario with an average value of 4.14%. As can be seen, the sixth scenario had the highest rate of flow reduction in the ADV in total flow rate. Therefore, further comparisons were conducted with the isotropic scenario model (when K_x and $K_y = 2000$ mD). The outcome was that ADV of total flow rate was decreased in the sixth scenario by more than 5.34%. This decrease was reflected in the reduction of ADV fracture flow by around 0.18% and matrix flow by 34.4%. Thus, the highest increase in % fracture flow occurred in lowest K_x value of anisotropic scenario ($K_x=380$, $K_y=2000$) mD, and lowest % matrix flow

occurred in same scenario. Table 4.5 and Figures 4.33, 4.34, 4.35 and 4.36 present these comparisons.

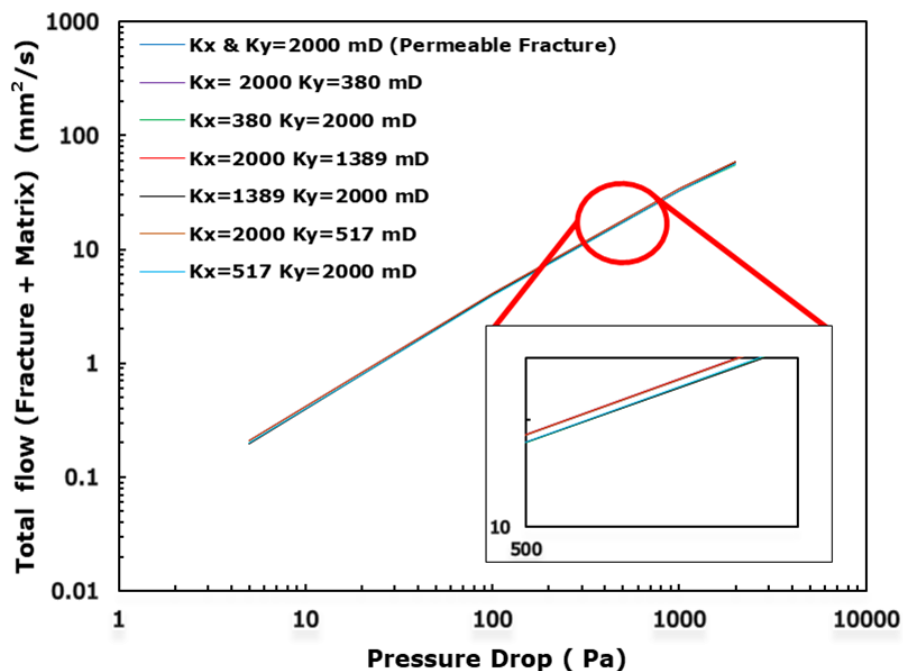


Figure 4.33 Comparisons of total flow rate (mm^2/s) of Rough ANSYS CFD Fluent FVM fracture models, with isotropic and all anisotropic matrix permeability scenarios, with permeable fracture surface boundaries

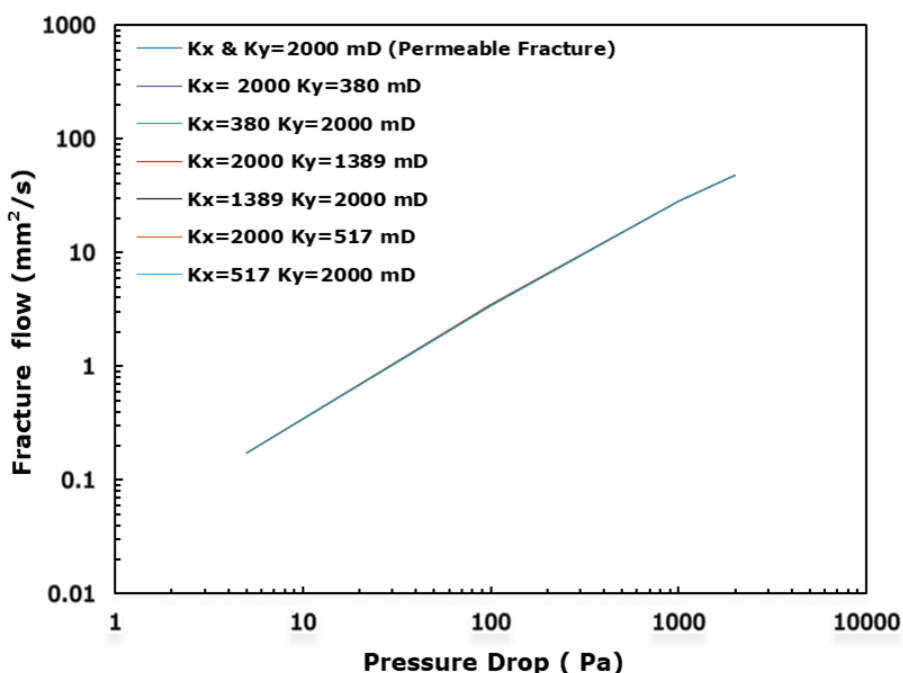


Figure 4.34 Comparisons of fracture flow rate (mm^2/s) of rough ANSYS CFD Fluent FVM fracture models, with isotropic and all anisotropic matrix permeability scenarios, with permeable fracture surface boundaries

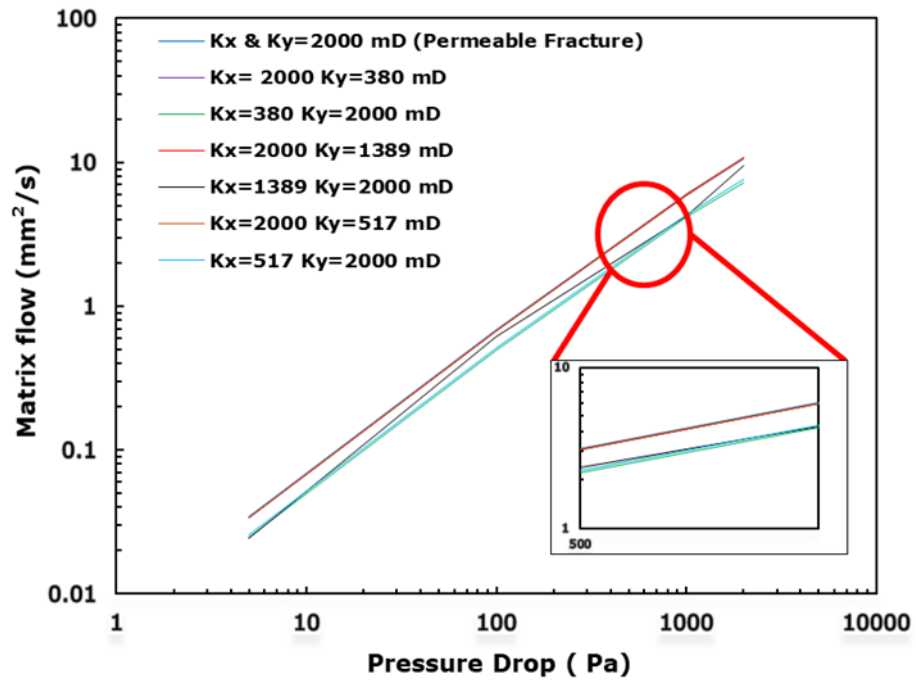
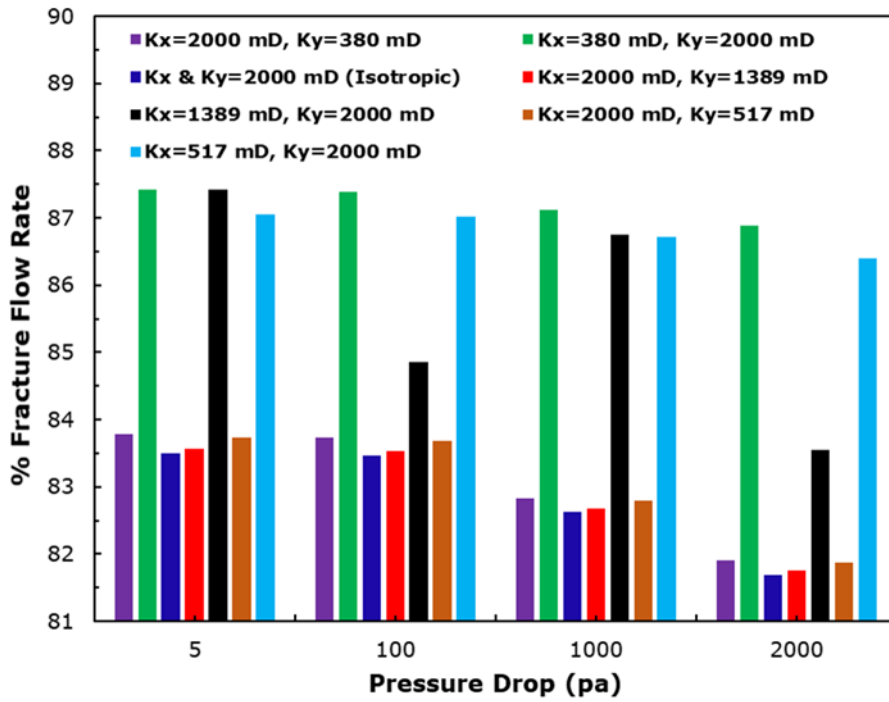
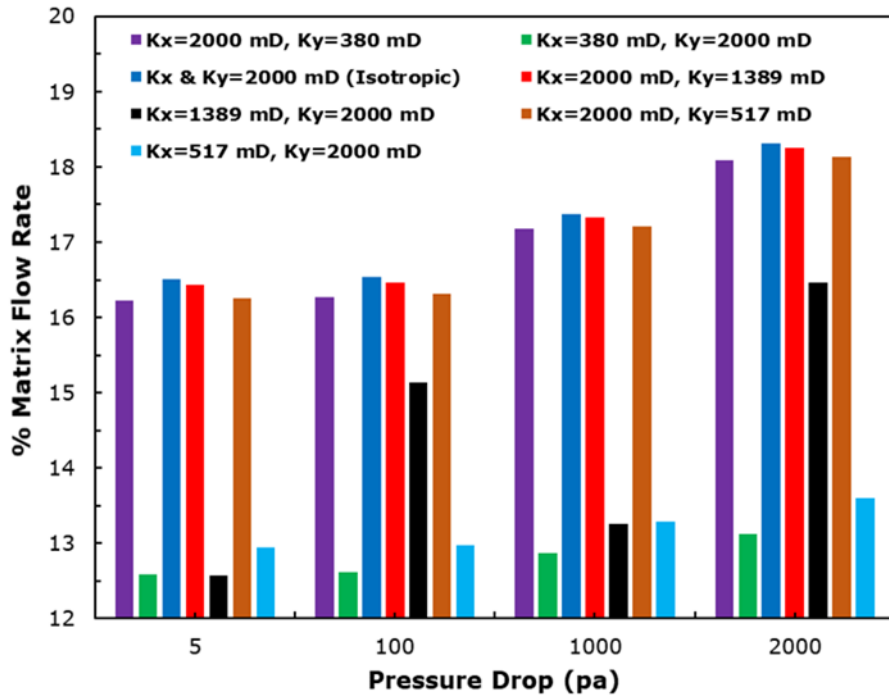


Figure 4.35 Comparisons of matrix flow rate (mm²/s) of ANSYS CFD Fluent FVM rough fracture models, with isotropic and all anisotropic matrix permeability scenarios, with permeable fracture surface boundaries



(A)



(B)

Figure 4.36 Comparisons of rough ANSYS CFD Fluent FVM model fractures: A. % fracture flow rate and B. % matrix flow rate. Isotropic and all anisotropic matrix permeability scenarios included, with permeable fracture surface boundaries

Table 4.5 Summarising flow results of ANSYS CFD Fluent FVM models with anisotropic permeability of rough fractures - average values of four pressure drops (5, 100, 1000, 2000) Pa

CFD models with different Matrix permeability scenarios	Total Flow (mm ² /s)	Fracture Flow (mm ² /s)	Matrix Flow (mm ² /s)	Compared models	Affected Scenario	(ADV) Total flow (decrease of the effected scenario)	(ADV) Fracture flow (decrease of the effected scenario)	(ADV) Matrix flow (decrease of the effected scenario)	% fracture flow (Increase of the effected scenario)
1	24.524	20.148	4.3759	1 & 2	2	4.07	0.81	22	2.76
2	23.643	20.027	3.6160	-	-	-	-	-	-
3	24.462	20.127	4.3350	3 & 4	4	4.6	0.131	30	3.77
4	23.225	20.099	3.1262	-	-	-	-	-	-
5	24.445	20.120	4.3241	5 & 6	6	5	0.138	32.6	4.14
6	23.097	20.0920	3.0056	-	-	-	-	-	-
Isotropic (Kx=Ky=2000 mD)	24.549	20.154	4.395	6 & Isotropic	6	5.34	0.18	34.4	1.056

4.3.5.2 Summary of anisotropic permeability simulations of rough fractures models

These simulations of a rough fracture with anisotropic matrix permeability clarified the importance and necessity of considering anisotropic matrix permeability in fractured reservoirs, particularly with rough fracture geometry to mimic fractured formations flow conditions, as this has an effect on the flow of the fracture and matrix (Tiab and Donaldson 2004 p. 103). As clarified in Sections 4.3.5 and 4.2.4.2, the majority of subsurface earth crust and hydrocarbon reservoirs have highly anisotropic permeabilities in in-plane (K_x) and through plane (K_y) of Cartesian directions (Di Fratta et al. 2016; Lang, Paluszny and Zimmerman 2014; Tiab and Donaldson 2004 p. 162; Golf-Racht 1982 p. 52; Hutchinson, Dodge and Polasek 1961). The comparisons of these six permeability scenarios of ANSYS CFD Fluent FVM models reflected interesting findings; some of these were similar to Section 4.2.4.2 but with different values, and other different, as below:

1. Changing in-plane (K_x) permeability in Cartesian axis led to a decrease in total flow rate, and the highest decrease of flow was observed with highest permeability reduction between K_x and K_y in each scenario, starting from 30%, 74% and 81% respectively; Table 4.5 summarises the simulation results. This has confirmed the findings of Hidayati, Chen and Teufel (2000); Saidi (1987) p. 82, Parsons (1966); and Scheidegger (1963) that average permeability of anisotropic permeability formations is affected significantly by in-plane (K_x) permeability in Cartesian coordinates (ie, the permeability that is parallel with flow direction). Also, average permeability that is calculated from pressure buildup or any similar tests usually reflects close values to horizontal in-plane (K_x) permeability. As well, these results confirmed the findings of Lei et al. (2015); and Rasouli and Rasouli (2012) which were that matrix permeability that is parallel to fractures (K_x) has greater effect than the perpendicular direction (K_y); particularly, the permeability aligned with flow direction, as perpendicular direction (K_y), is decreased due to overburden stresses increasing with production time as pore pressure decreases. Moreover, the reduction of permeability aligned with flow direction in fractured media will cause higher pressure drop in formations for the same fracture aperture size, and accordingly, on flow, which has confirmed the findings that were stated by Rasouli and Rasouli (2012).

2. Despite total flow reduction due to the in-plane (K_x) permeability reduction, increasing through plane (K_y) permeability led to an increase of fracture flow percentage in the domain; [Table 4.5](#) above clarifies this result. This was due to the effect of pressure drop increase in in-plane (K_x) direction, whilst flow through plane (K_y) in perpendicular contact with fracture permeable surfaces, faced less resistance. As well, the fracture/matrix interface layer was affected by the components of tangential velocities, which affect various fluid jump (movements) conditions for matrix and fracture ([Lei et al. 2015](#); [Rasouli and Rasouli 2012](#); [Popov et al. 2009](#)), and the fluid flow movements which always occur due to the response of the fracture-matrix interface layer ([Lang, Paluszny and Zimmerman 2014](#)). It's good to note, despite the fact that the change in flow percentages had similar patterns of increase/decrease in the fracture and matrix of fractured domain, the percentages of these values were much bigger than for the results of parallel plates fracture with single aperture as stated in [Section 4.2.4.2](#). This has proved the findings of [Yang et al. \(2019\)](#); [Rasouli and Rasouli \(2012\)](#); [Popov et al. \(2009\)](#); [Lespinasse \(2000\)](#) and [Zimmerman and Bodvarsson \(1996\) pp. 44-45](#) that rough fractures have bigger areas of contact with the surrounding matrix, and that surface roughness and abrupt fracture aperture changes along a fracture have effects on flow. This is because narrow corners with sharp edges create clusters of fluid movement between fracture and matrix, due to velocity/pressure variation, which lead fluid to use different paths as stated by [Li et al. \(2021\)](#); [Wu et al. \(2019\)](#) and [Sahimi \(2011\) p. 45](#). Moreover, matrix pore structure heterogeneity in rough surfaces of fractures is increased, which affects adsorption of fluids in formations ([Yin et al. 2017](#); [Sahimi 2011 pp. 15, 18, 244](#)), and spatial pressure gradients inside a fracture will have substantial effects on fluid movement ([Andersen and Zhou 2020](#)). This is particularly true with velocity variations in the fracture and surrounding matrix, which change the mechanisms of adhesion (the attraction force between fluid and mineral surfaces), cohesion (the attraction force between fluid minerals), and pore imbibition which have significant effect on fluid percolation ([Dippenaar and Van Rooy 2016](#); [Ingham and Pop 2005 p. 367](#)). As well, flow channeling in a fractured domain increases matrix effects, as reported by [Zou, Jing and Cvetkovic \(2017\)](#); and [Ishibashi et al. \(2012\)](#), and instability momentum in these zones, due to the vortices and flow recirculation inside the fracture, which create more fluid movement

between matrix and fracture as reported by [Karimzade et al. \(2019\)](#); and [Chen et al. \(2017\)](#). This has disqualified the findings that fluids are trapped in these zones and have no contribution, as reported by [Suri et al. \(2020\)](#); [Briggs, Karney and Sleep \(2017\)](#); [Dippenaar and Van Rooy \(2016\)](#); and [Briggs, Karney and Sleep \(2014\)](#). This is due to these literatures having neglected the fracture/matrix interface layer, and momentum exchange between fracture and matrix due to velocity/pressure variations. In fact, the models in this research have shown that these areas are the gateway of fluid movement between fracture and matrix. [Figure 4.32](#) shows streamlines of velocity between fracture and matrix, and fracture vortices zones to bulk flow, which have proved the findings of [Karimzade et al. \(2019\)](#) and [Chen et al. \(2017\)](#), and proved the impact of matrix effects in fractured media, as stated by [Spence et al. \(2014\)](#) and [Narr, Schechter and Thompson \(2006\)](#). The effects of matrix permeability in these heterogeneous media is higher ([Di Fratta et al. 2016](#); [Al-Yousef 2005](#); [Tiab and Donaldson 2004 p. 162](#); [Golf-Racht 1982 p. 52](#)); especially, matrix flow importance increases with decreasing fracture apertures during production, due to overburden stress effects with fracture pore pressure ([Rasouli and Rasouli 2012](#)). This disqualifies a concept of neglecting matrix effect, as reported in some literature such as [Zou, Jing and Cvetkovic \(2017\)](#); [Hyman et al. \(2015\)](#); [Sarkar, Toksöz and Burns \(2011\)](#); [Piri and Karpyn \(2007\)](#); [Nazridoust et al. \(2006\)](#); and [Berkowitz \(2002\) p. 867](#).

3. An analysis was made of comparisons of average flow of four pressure values (5, 100, 1000, 2000) Pa for fracture and matrix. This was conducted firstly among the set of anisotropic permeability ANSYS CFD Fluent FVM models with scenarios 1, 3, and 5 of [Table 4.2](#), where K_x was fixed with 2000 mD and K_y was varied with values 380, 517, 1389 mD, and, secondly among the set of anisotropic permeability ANSYS CFD Fluent FVM models with scenarios 2, 4 and 6 of [Table 4.2](#), where K_y was fixed with 2000 mD and K_x was varied with 380, 517, 1389 mD. The comparison results of the first set of models reflected a slight increase in fracture flow, but larger increase in matrix flow, which has proved that despite in-plane (K_x) permeability was a fixed value, the increase of through plane (K_y) permeability has increased matrix flow and directed flow toward the matrix through the fracture/matrix interface layer. This is more consolidation of

the finding which proved the effects of permeable surfaces of rough fractures through the fracture/matrix interface layer, due to the reduced flow resistance in through plane (y) axis. Likewise, it has provided evidence of fluid jump through fracture/matrix interface layer, due to the effects of the components of tangential velocities inside the fracture surfaces, fractures' sharp corners with rough surfaces, and abrupt changes of fracture apertures, which have created gateway clusters of fluid movement and increased matrix flow contribution in the domain (Li et al. 2021; Andersen and Zhou 2020; Wu et al. 2019; Yang et al. 2019; Yin et al. 2017; Dippenaar and Van Rooy 2016; Lei et al. 2015; Lang, Paluszny and Zimmerman 2014; Rasouli and Rasouli 2012; Sahimi 2011 pp. 15, 18, 45, 244; Popov et al. 2009; Ingham and Pop 2005 p. 367; Lespinasse 2000; and Zimmerman and Bodvarsson 1996 pp. 44-45). The comparison of the second set of models reflected an increase in fracture flow, but with matrix flow decreasing. With increasing in-plane (K_x) permeability and fixed through plane (K_y) permeability, pressure drop was decreased, and with pressure/velocity changing along the rough fracture flow, fluid movements were higher through fracture/matrix interface layer. This led to increased fracture flow through gateway clusters as reported by Li et al. (2021); Wu et al. (2019); and Sahimi (2011) p. 45. This case represents a scenario were adapted in some studies in literature which consider fracture only as main fluid conductor and matrix as main fluid supply (Luo et al. 2020; Nelson 2001; Sahimi 2011; and Golf-Racht 1982).

This comparison has provided evidence that K_y permeability is important in fractured formations, as it provides another flow path from matrix toward fractures. To consolidate this finding, the average total flow of the two sets was compared. The outcome was that the first set, with K_y permeability changing, had higher average total flow with 2.42% than the second set with K_x permeability changing. This finding has contradicted the literature of Lei et al. (2015); Rasouli and Rasouli (2012); Hidayati, Chen and Teufel (2000); and Saidi (1987) p. 82 that permeability aligned with flow direction K_x has greater effect on fractured media flow than K_y . This is because rough fracture surfaces' interaction with the matrix has significant impact on flow contribution of fracture and matrix in a fractured domain. Figure 4.37 illustrates these results.

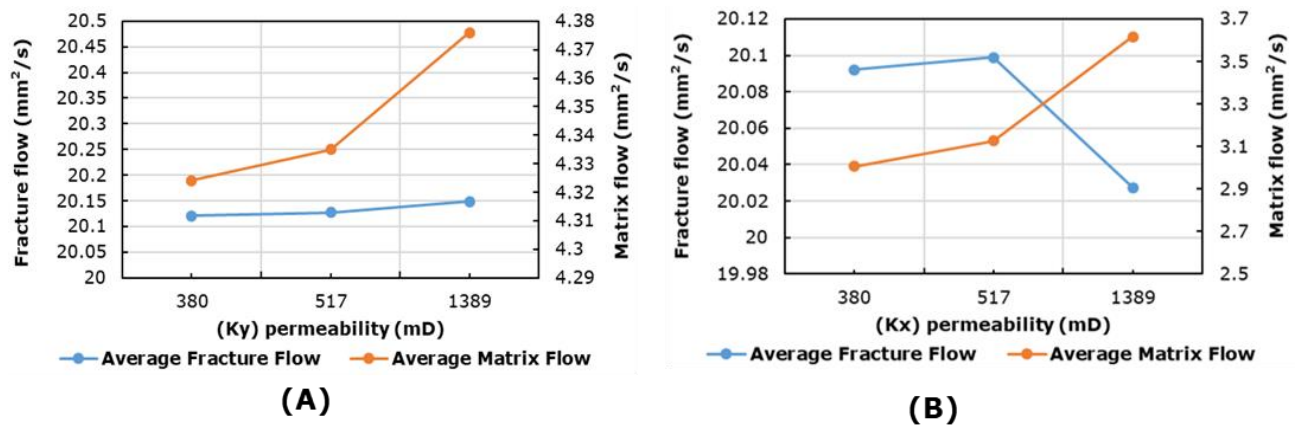


Figure 4.37 Average flow comparisons of fracture and matrix in ANSYS CFD Fluent FVM rough fracture models of four pressure values (5, 100, 1000, 2000) Pa

A. first set permeability scenarios ($K_x = 2000$ mD fixed, $K_y = 380, 517, 1389$ mD);
 B. second set permeability scenarios ($K_y = 2000$ mD fixed, $K_x = 380, 517, 1389$ mD)

- The ANSYS CFD Fluent FVM simulations of a rough fracture with permeable fracture surfaces and anisotropic matrix permeability proved that the flow inside the fracture will have a significant change when the fracture surfaces are permeable to the fluid with the matrix (Lang, Paluszny and Zimmerman 2014). This has proved that the interaction between the fractures and surrounding matrix is active, and neglecting of this will lead to the wrong prediction of flow, because rough fracture geometry has rough surfaces and interaction is high, and critical for flow analysis (Popov et al. 2009). The main reasons are that rough fractures will suffer higher pressure drop, the effects of fluid recirculation "eddies or vortices", and abrupt changes in pressure/velocity along the fracture flow, which will increase fluid jump movements between matrix and fracture (Karimzade et al. 2019; Briggs, Karney and Sleep 2014; Popov et al. 2009; Karpyn, Grader and Halleck 2007; Yamatomi et al. 2001). Therefore, the geometry of rough surfaces, will reflect accurate pressure drop, particularly, with inclusion of fracture/matrix interaction, which is vital for flow analysis as reported by Lang, Paluszny and Zimmerman (2014); Crandall, Ahmadi and Smith (2010); Popov et al. (2009); and Moreno et al. (1988).
- Thus, the findings of models in this research have confirmed that considering impermeable fracture surfaces, neglecting matrix flow contribution and not using rough fracture geometry in modelling will mislead flow calculations in fractured media. This has confirmed the findings of Rasouli and Rasouli (2012); and Crandall, Ahmadi and Smith

(2010), that considering matrix effect will increase fractured formation connectivity, and the importance of matrix effect as reported by Luo et al. (2020) p. 3. As well, to conclude the points in these analyses, when both K_x and K_y were changing at the same time (as point 1 and 2) then K_x had the highest effect on fractured domain flow; however, if one of K_x or K_y was changing and the other was fixed, then K_y had highest effect on fractured domain flow, as it led to increased flow percentages in the fracture and surrounding matrix. Therefore, for a better estimation of flow in fractured media, it is necessary to consider real conditions of subsurface layers rather than simplified conditions: to consider anisotropic values of permeability, as these values have an effect on fractured domain flow (fracture+matrix).

4.4 Comparisons Between Parallel Plates And Rough Fractures

It was mandatory to make a comparison between parallel and rough fracture geometries, in order to investigate the effect of fracture geometry shape/type on fractured domain flow. As can be seen in the previous sections of this chapter, both types of fractures were simulated in ANSYS FVM Fluent with the same conditions, to check the effect on pressure, velocity and flow inside the fracture and the matrix. Different conditions were considered, such as: pressure drop, isotropic and anisotropic matrix permeability, and different boundaries of fracture surfaces: permeable "Interior face boundary" and impermeable "Walls boundary". The outcome of these comparisons was that considering permeable fracture surfaces with a rough fracture had a significant effect on the total flow of the domain (fracture and matrix).

In order to clarify fracture geometry further, a comparison was conducted between a parallel plates fracture, with one fracture aperture height, and a rough fracture, with varied fracture apertures along the flow, with permeable fracture surfaces only "interior faces boundary" in order to clarify and quantify the interaction effect between the matrix and the fracture in the domain; both types of fractures shared the same average fracture aperture height, 581 micrometre. The simulations were compared with four pressure drops (5, 100, 200, 1000) pa with Isotropic matrix permeability ($K_x=K_y=2000$ mD), and zero pressure outlet, and all other set ups

of the model as stated in [Chapter 3](#), then, different values were calculated, such as: total flow rate, fracture flow rate, matrix flow rate as [section 4.2](#), and the percentage of the fracture/matrix flow in the domain. The outcome of this comparison was that the total flow rate for the rough fracture was $24.55\text{mm}^2/\text{s}$, the average value of fracture flow rate was 83%, and the matrix flow was 17%. In comparison, for the parallel plates fracture, the total flow rate was $109\text{mm}^2/\text{s}$, the average value of fracture flow rate was 98%, and the matrix flow was 2%.

The total flow rate had decreased in the rough fracture domain by more than four times in comparison with the parallel plates fracture. This decrease was reflected in the reduction in fracture flow of more than 5 times. This has confirmed similar findings of flow reduction, but with different flow percentages, which were reported in other studies such as [Crandall, Bromhal and Karpyn \(2010\)](#); [Crandall, Bromhal and Smith \(2009\)](#); [Karpyn, Petchsingto \(2008\)](#); [Grader and Halleck \(2007\)](#); and [Lespinasse \(2000\)](#). However, the matrix flow had increased more than 3 times. [Figures 4.38 and 4.39](#) present these comparisons. This comparison has clarified that considering a parallel fracture with a single aperture height will overestimate the total flow of the fracture domain and the fracture flow; in addition, it will underestimate the matrix flow continuation in a fractured domain. This case was investigated further by observing the fluid velocities and pressures on the fracture surfaces (the interface layer between the fracture and the matrix) for the Rough fractures and Parallel plates fractures, to check what the effect of fracture geometry on the velocity and the pressure inside the fracture and inside the surrounding matrix was. [Figure 4.40](#) clarifies the observation of velocity. As can be seen, the fracture surface velocity continued changing along the flow of the rough fracture, while for the parallel plates fracture the velocity had a steady decline along the flow with smooth declination. Also, the pressure of the fracture surfaces for the rough fracture kept fluctuating along the flow with sharp decrease/increase, whilst for the parallel plates fracture, the pressure was steady and smooth whilst declining along the flow. Moreover, a reading line inside the matrix was drawn for both types of fractured domains on coordinates (0, 0.052) (0.1015, 0.052) m, to observe the fluid X-velocity inside the matrix. The finding was that both trends had different behaviour of fracture surface X-Velocity: smooth decline for the parallel plates fracture and fluctuation for the rough fracture. This proved the effects of fracture surface geometry on the matrix velocity, and respectively on the domain flow. As can be seen, the velocity change along the flow of the rough fracture was reflected in the pressure inside the fracture and the surrounding matrix, which was changing along with the flow, while for the parallel

plates fracture, it had smooth declining behaviour along with the flow, and slight effect between the matrix and the fracture.

The velocity change along with the flow in each point inside the rough fracture was due to the fracture aperture changing, which changed the pressure also. [Dietrich et al. \(2005\)](#) and [Sen \(1995\)](#) studied the interface layer between the matrix and the fracture, and [Sen \(1995\)](#) clarified the [equation 2.41 \(Section 2.5.5\)](#) which describes fluid movement between the fracture and the matrix along the interface layer, as clarified in summaries of results analysis sections 4.3.3, 4.3.4 and 4.3.5.2 which showed the effects of rough fractures and of considering permeable fracture surfaces (interface layer between matrix and fracture). This means that the flow between the matrix and the fracture changes too, due to the pressure differences between the matrix and the fracture. This changing of velocity /pressure has been reflected in the fluid movements between the matrix and the fracture (imbibition mechanism), which leads to active transfer of fluid between the matrix and the fracture and vice versa. Accordingly, this has been reflected on the fracture/matrix fluid flow percentage of the rough fracture, whilst for the parallel plates fracture, the results have indicated that there is very low interaction between the matrix and the fracture. [Figure 4.41](#) clarifies the schematic movements between the fracture and the matrix.

4.4.1 Summary of the comparisons between parallel plates fractures and rough fractures

Thus, to conclude, the outcome of this comparison is as below:

1. Considering a parallel plates fracture with one fracture aperture height does not reflect the reality of flow inside a fracture, and it will overestimate (% fracture flow), whether the conditions of fractures surfaces are permeable or impermeable, and underestimate matrix flow in the case that fracture surfaces are permeable with the matrix. This is because it will not account for the effect of changing fluid velocity/pressure along the flow in the fractured domain. Despite this, this type of fracture has been used widely as a single fracture or network fractures in fractured domains modelling, as reported by [Luo et al. \(2020\)](#); [Luo, Tang and Zhou \(2019\)](#); [Luo et al. \(2018\)](#); [Lu et al. \(2017\)](#); [Rasouli and Rasouli \(2012\)](#); [Sahimi \(2011\)](#); [Popov](#)

- et al. (2009); Tiab and Donaldson (2004); Sen (1995); and Golf-Racht (1982).
2. As well, assuming impermeable fracture surfaces will mislead flow estimation of fractures; therefore, permeable fracture surfaces should be considered as this gives a more accurate flow estimation in fracture and matrix, because it considers the effect of how the fracture/matrix interact upon each other in the same domain (Lei et al. 2015; Lang, Paluszny and Zimmerman 2014; Rasouli and Rasouli 2012; Crandall, Ahmadi and Smith 2010; Popov et al. 2009; Moreno et al. 1988). This finding is against the wide neglect of matrix effect on flow in fractured media, as reported in Briggs, Karney and Sleep (2017); Chen et al. (2017); Liu, Li and Jiang (2016); Briggs, Karney and Sleep (2014); Sarkar, Toksöz and Burns (2011); Nazridoust et al. (2006); Berkowitz (2002) p. 868 and Yamatomi et al. (2001).
 3. Thus, this research has shown that combining two main characteristics in fractured media modelling: rough fracture geometry with varied aperture along the flow; and permeable fracture surfaces, will reflect a more accurate estimation of flow in fractured media, in the subsurface layers of earth crust and reservoirs.

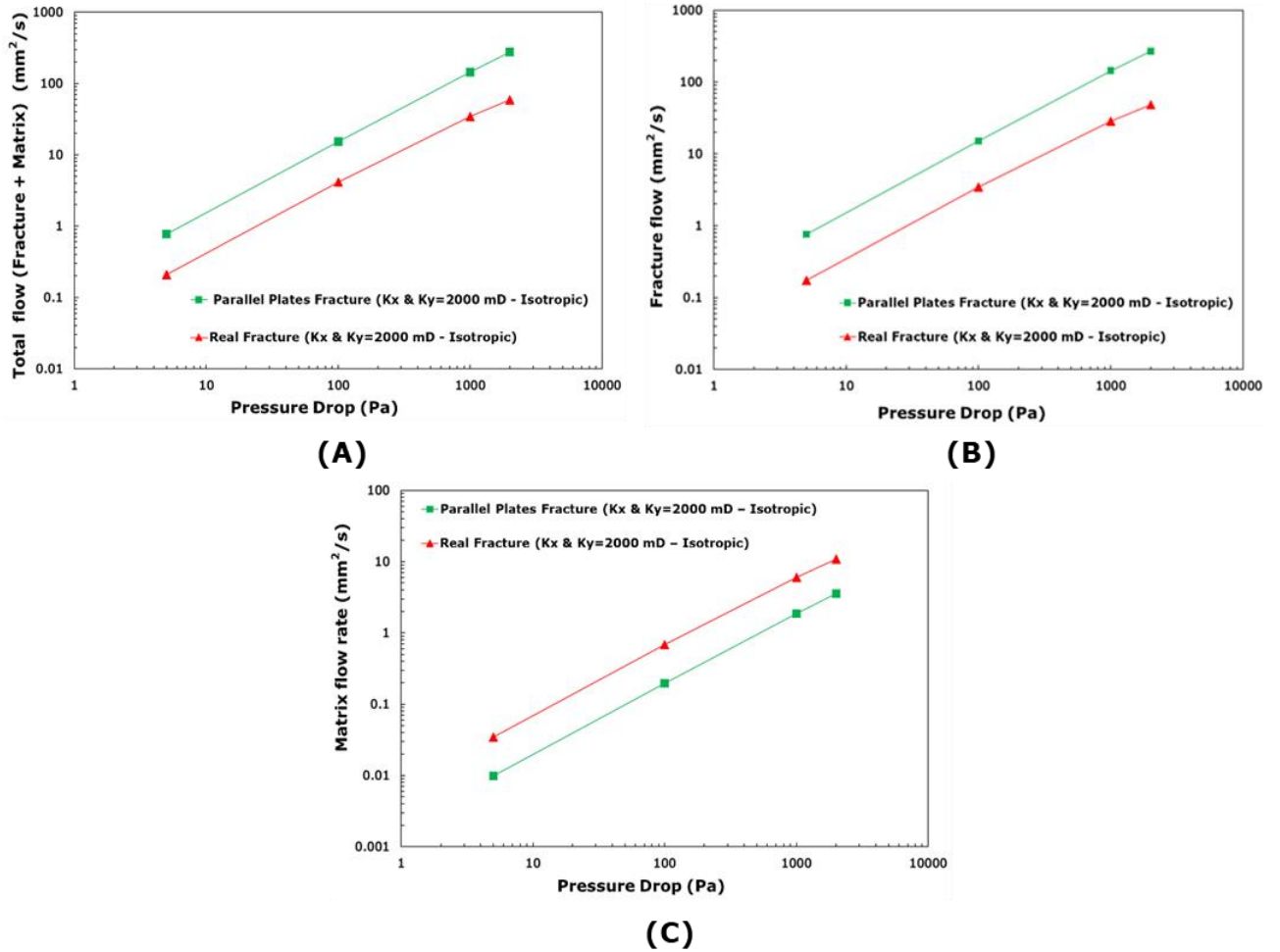


Figure 4.38 Flow comparisons (mm^2/s) between ANSYS CFD Fluent FVM models of rough fracture and parallel plates fracture with permeable surfaces ($K_x=K_y=2000$ mD), with pressure drops (5, 100, 1000, 2000) Pa, permeable fracture surface boundaries "Interior faces" A. total flow rate, B. fracture flow rate, and C. matrix flow rate.

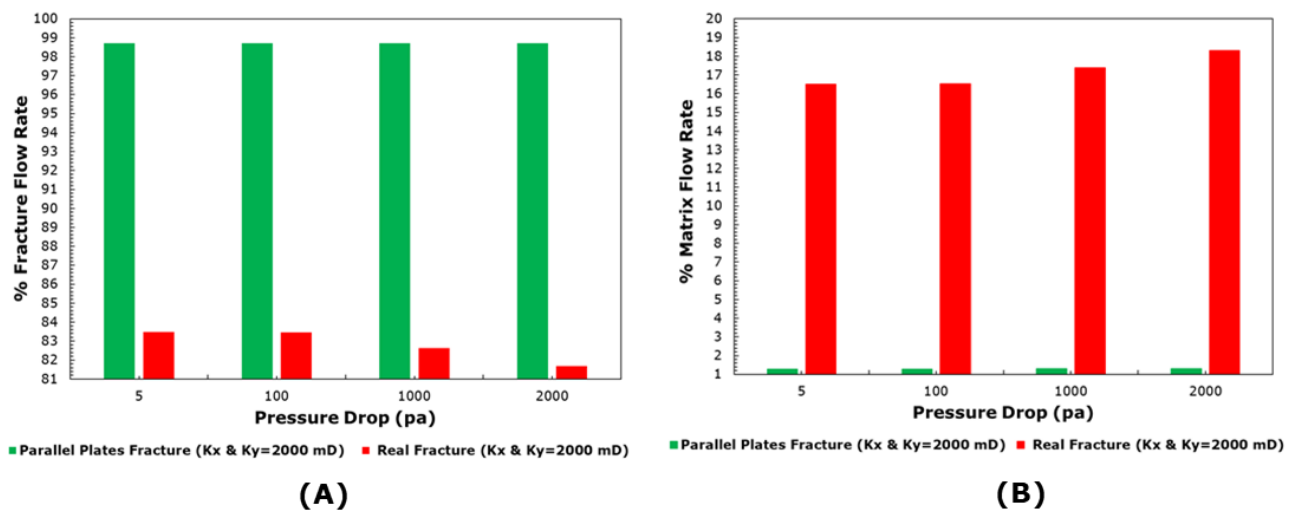


Figure 4.39 % Flow comparisons between ANSYS CFD Fluent FVM models of rough fracture and parallel plates fracture with permeable surfaces ($K_x=K_y=2000$ mD), with pressure drops (5, 100, 1000, 2000) Pa A. % fracture flow, and B. % matrix flow.

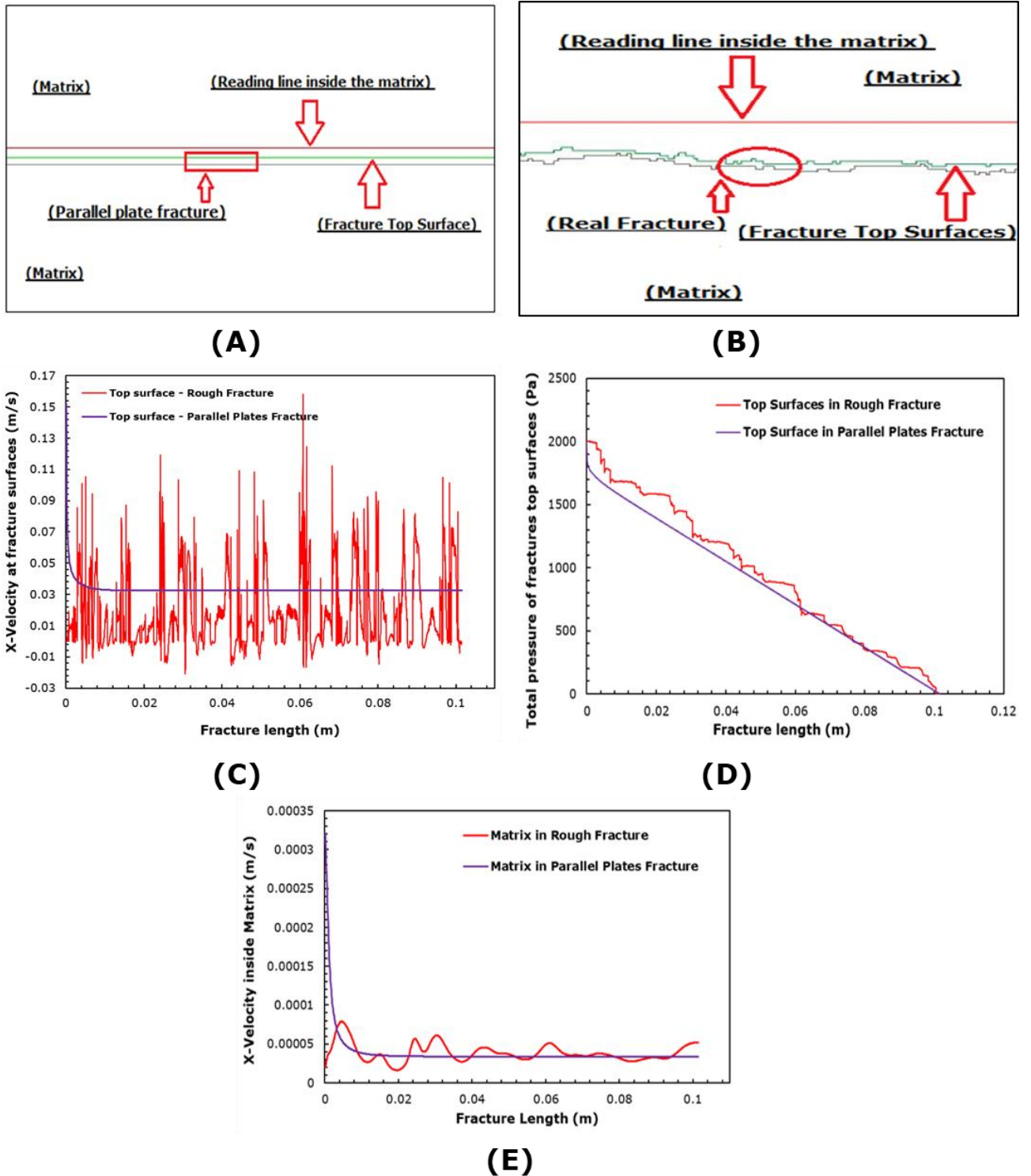


Figure 4.40 Comparisons of X-velocity and total pressure, at fracture's top surfaces and inside matrix, between rough fracture and parallel plate fracture ANSYS CFD Fluent FVM models, with isotropic permeability ($K_x=K_y=2000$ mD) and $P=2000$ Pa with zero pressure outlets, and permeable fracture surface boundaries

A and B: Schematic sections of parallel plate and rough fracture, respectively, with matrix domains, highlighting the fractures' top surfaces and the reading lines inside the matrix (both lines had same coordinates); C: X-velocity at fractures' top surfaces D: Total pressure at fractures' top surfaces; and E: X-velocity inside the matrix reading lines

matrix is quite low in a parallel plates fracture; it will overestimate (% fracture flow), whether the conditions of fracture surfaces are permeable or not, and underestimate (matrix flow %), because it will not account for the effect of changing fluid velocity/pressure along the flow in the fractured domain.

2. Considering rough fracture geometry with varied apertures along the flow will reflect a more accurate estimation of flow in fractured media in subsurface layers of earth crust and reservoirs. As it mimics real conditions of flow as in fractured formations (rough fracture flow resistance, matrix/fracture interaction, etc.) the outcome will reflect optimised results with higher accuracy.
3. Matrix interaction with fracture is very important; therefore, it's vital to include this in fractured media flow calculations, especially with rough fracture geometry, as the interaction between matrix and fracture is high. It has been proven and validated that matrix flow has good contribution to flow in fractured media with rough fracture geometry. Thus, considering impermeable fracture surfaces and excluding the matrix will lead to highly underestimating or overestimating flow, based on fractures' orientations and fractal properties of fractures' geometry (roughness, tortuosity, standard deviations of fracture apertures).
4. One of the very interesting findings is that the well-known Darcy formula of fluid flow in matrix was under predicting value, and may not be accurate for complicated scenarios in fractured media's matrix, when fractures' interaction with matrix are considered, as the matrix flow reflected a nonlinear increase.
5. Anisotropic permeability effects of in-plane (K_x) permeability and through plane (K_y) permeability were investigated in both types of fractured media: parallel plates fracture with single aperture and rough fracture. K_x and K_y reflected two visions in these two types of fractures, with either similar or different effects based on different percentages of fracture and matrix flow. As it has been clarified that parallel plates fractures have misled flow calculations, therefore, here rough fractures only will be highlighted. For the rough fracture, if both in-plane K_x and through plane K_y permeabilities were changing at the same time, then, K_x had the highest effect on fractured domain flow. However, if one of the permeabilities (K_x or K_y) was changing, then through plane K_y had the highest effect on fractured domain flow, as it showed proven increase in fracture flow and, significantly, in matrix flow

too. This finding is very significant, as it gives evidence that through plane (Ky) permeability is important in fractured formations, not only in-plane (Kx) permeability as reported in the literature by [Lei et al. \(2015\)](#); [Rasouli and Rasouli \(2012\)](#); [Hidayati, Chen and Teufel \(2000\)](#); [Saidi \(1987\) p. 82](#); [Parsons \(1966\)](#); and [Scheidegger \(1963\)](#).

5 Friction Factor In Fractured Media

5.1 Introduction

As clarified in [Chapter 2 section 2.6](#), in fluid dynamics the friction factor will be called “Darcy Friction Factor”, or “Darcy–Weisbach friction factor”; this is an empirical equation that relates loss of pressure along the flow due to surface friction with average velocity of incompressible fluid, and is a dimensionless value ([Winterton 2014 chap. 6](#); [White 2011](#); [Simmons 2008](#); [White 2003](#); [Swanson 1970](#); [Eskinazi 1968](#)). Friction factor in naturally fractured reservoirs represents pressure loss due to fluid contact with fracture surfaces along a fracture’s length. The friction value relies on many factors, such as: fluid velocity, fluid type, the shape of fracture geometry, and the roughness value of fracture surfaces. Friction behaviour in fractured media has been extensively examined in the 20th century, due to high effects on pressure loss, and many studies have been performed to mimic its different conditions ([Tiab and Donaldson 2004 p. 459](#); [Saidi 1987 pp. 169, 306](#); [Golf-Racht 1982 p. 306, 310](#)). However, until now, many challenges remain to estimating the accurate value of friction factor, due to the complication of calculations, and the difficulty of including all ambient conditions of fractured media of subsurface earth crust reality in the calculation. This attracts researchers to include more variables for developing better fracture friction factor prediction, as reported by [Su et al. \(2019\)](#); [Chen et al. \(2017\)](#); [Zhou et al. \(2016\)](#); [Singh, Singh and Pathegama \(2014\)](#); [Zhang and Nemcik \(2013\)](#) ; [Qian et al. \(2011\)](#); [Crandall, Ahmadi and Smith \(2010\)](#); [Nazridoust, Ahmadi and Smith \(2006\)](#); [Dietrich et al. \(2005\)](#); [Tiab and Donaldson \(2004\)](#); [Masciopinto \(1999\)](#); and [Golf-Racht \(1982\)](#), yet further variables still remain to be included to develop better accuracy. Therefore, more investigation was required to include more realistic conditions, in order to optimize a better predication of friction factor value in fractured media.

Thus, in the chapter, the friction factor value was investigated by the same ANSYS CFD Fluent FVM fracture models as clarified in Chapters 3 and 4, but only considered rough fracture models. The reason for this was that, as proven in

Chapter 4, parallel plates fractures with single aperture would mislead flow calculations, and flow estimations would be wrong with no major deviation observed from simulations for including permeable fracture surfaces with matrix or changing matrix permeabilities from isotropic to anisotropic, and investigating friction factor in this manner would not give accurate results. Therefore, rough fractures only were considered in this chapter, with both boundary conditions of fracture surfaces: permeable with the matrix “Interior faces boundary” and impermeable with the matrix “walls boundary”. As well, the investigation was expanded further with anisotropic matrix permeability with permeable fracture surfaces boundary.

The goals of these investigations were as follows. Firstly, to clarify the prediction of friction factor in fractured media with rough fractures with impermeable and permeable fracture surfaces with matrix; to consider the effects of isotropic and anisotropic matrix permeability; and to optimise mimicked conditions of the fractured media, by including the extra factor of subsurface anisotropic matrix’s effect on friction factor prediction. Secondly, to develop analytical and numerical models of friction factor in fractured media that have the most optimised conditions of fractured media, in order to mimic real flow in fractured media of the earth crust, which will give a better prediction of a fracture’s friction factor.

5.2 Extraction Of Friction Factor Value From ANSYS CFD Fluent FVM Models

The ANSYS CFD Fluent FVM models of this chapter are the same models as Chapter 4’s fracture models, which were used to extract the friction factor values. Because these models have already been validated against existing papers from the literature, therefore, the details of the ANSYS CFD Fluent FVM rough fracture models are the same as stated in [Chapter 3 Section 3.5.2](#), except the details that are related to fracture/matrix properties and friction factor values will be clarified in each section.

In this study, ANSYS CFD Fluent FVM simulation models were used to extract the average velocities profiles and pressure drop inside the fractures as stated in [Chapter 4 Section 4.2](#), then these values were used in the friction factor [equation](#)

5.1. However, in order to get an accurate value of the friction factor from the equation, there were some values which needed to be applied from the fracture's fractal properties, which are clarified in the equation details below:

$$F = \frac{2 D \Delta P}{L \cdot \rho \cdot V^2} \quad (5.1)$$

(White 2003)

Where: F= friction factor, D= fracture apertures (average value of entire fracture apertures for the rough fracture geometry), ΔP = pressure drop along fracture flow, L= fracture length or domain length (in rough fractures: this will not consider equivalent length of both top and bottom fracture surface lengths to include the tortuosity effect, because the extracted average velocity/pressure drop values of ANSYS CFD Fluent FVM models have already faced this effect, and will be reflected on its values), ρ = fluid density, V= fracture's average velocity (the average velocity value of the entire fracture "not the average velocity profile", which will be explained below)

The application of [equation 5.1](#) in rough fracture models is clarified in detail in the following sections. As well, it's good to note as clarified in [equation 5.1](#) that the relation between the friction factor and the velocity is a reverse value; this means that as the velocity value increases, friction factor value will be decreased. This is reflected in the friction factor when a fracture's flow increases; this will lead to increased velocity as [equation 5.2](#). Thus, in general, friction factor values will be drawn in graphs with Reynolds number values similar to Moody diagram style. This is because the Reynolds number is a measure of velocity and based on its value; flow can be classified as either laminar, turbulent or, transition between the two flow behaviours ([White 2011 p. 356](#); [Simmons 2008 p. 1028](#); [Swanson 1970](#); [Eskinazi 1968](#)). [Equation 5.3](#) below clarifies the details of calculating the Reynolds number value in fractures.

$$Q_{\text{Fracture}} = A_{\text{Fracture}} \times V_{\text{Fracture}} \quad (5.2)$$

Where: A_{Fracture} = fracture area or fracture aperture height, as one dimension instead of a two-dimensional section; the reason for this is due to a very long depth in Z-Cartesian coordinates of fractured media domain, in comparison with fracture aperture height, most of the calculation considering it as a one direction ([Dietrich et al. 2005](#); [Tiab and Donaldson 2004](#); [Golf-Racht 1982-38](#)), $V_{\text{Fracture}} =$

average value of velocity profile in that particular fracture's section, Q_{Fracture} = fracture's flow rate (usually in fractured media this can be described in m^2/s or mm^2/s , instead of m^3/s or mm^3/s , due to one dimensional representation of fracture area).

$$\text{Re} = \frac{\rho}{\mu} V.D \quad (5.3)$$

(White 2011; Eskinazi 1968 p. 90)

Where: ρ = fluid density, μ = dynamic viscosity, D = fracture aperture (average value of entire fracture apertures for rough fracture geometry), V = average fracture velocity (the average velocity value of the entire fracture); this can be observed by applying equation 5.2 twice, first to extract the average velocity profile inside the section of the fracture, then observe fracture flow. And second, as the fracture flow is now known, then apply equation 5.2, but change the A fracture as an average section height 581 micrometre of the entire fracture instead of section height at the velocity profile. Then, the results will be average velocity value of the entire fracture.

5.3 Friction Factor In A Rough Fracture (Re-generating Crandall, Ahmadi and Smith (2010)'s Paper)

Rough fracture geometry that was created to investigate flow and velocity by ANSYS CFD Fluent FVM in Chapter 4 was also used here, and the friction factor in this kind of fracture was investigated by using friction factor [equation 5.1](#). a rough fracture with varied apertures with average sections height (581) micrometre in the middle of the matrix was created by ANSYS CFD Fluent FVM; the total domain (fracture + matrix) size was (10.15 x 10.15) cm, and all the details of the model are in [Chapter 3 Section 3.5.2](#). The fracture that was used in this investigation was used by [Nazridoust, Ahmadi and Smith \(2006\)](#) and [Crandall, Ahmadi and Smith \(2010\)](#), but each one used it with different set-up, such as fracture surfaces as impermeable "Walls boundary" and permeable "Interior faces boundary" respectively.

The X-velocity profiles inside the fracture were calculated by creating a surface line inside the fracture in the smallest fracture aperture 240 micron, just before the fracture outlet at (X, Y) Cartesian coordinates (0.1, 0.0472) (0.1, 0.04754) m,

Figure 4.20A in Chapter 4 clarifies this line. Then, the average value of the X-velocity was extracted at the section inside fracture as stated in Chapter 4 Section 4.2, then, the average value of the entire fracture as clarified in each model set up below. This model was simulated with: four values of pressure drop (5, 100, 1000, 2000) Pa and zero pressure outlets; two fracture surface conditions considered, impermeable "Walls boundary" and permeable "Interior faces boundary" to include matrix effect and interactions with fracture; and matrix porosity 20%. Two kinds of matrix permeability, isotropic and anisotropic, as Table 4.2 in Chapter 4 were considered. The outcome of each setup is clarified below.

5.3.1 Friction factor in rough fracture with fracture's surface boundaries set as impermeable "Walls boundary" with Validation

These ANSYS CFD Fluent FVM fracture models were set as isotropic matrix permeability ($K_x=K_y$) with two values $K=0.2$ mD and $K=2000$ mD, fracture surface boundaries were set as impermeable "Walls boundary", which meant no fluid flow between the matrix and the fracture and vice versa, other set up as stated above in Section 5.3. The average value of the X-velocity values was observed inside the fracture, then, friction factor equation 5.1 was used. The setup of this ANSYS CFD Fluent FVM model was similar to the setup of that of Nazridoust, Ahmadi and Smith (2006). Therefore, the comparison outcomes of this model were used: first, to validate this model's friction factor values with Nazridoust, Ahmadi and Smith (2006)'s results; and second, to compare the results of impermeable fracture surface models with different values of permeable isotropic matrix permeability, to investigate whether there is any effect on friction factor values when matrix permeability changes and there is no interaction surface or fluid movement, with fracture "Walls boundary".

The friction factor and Reynolds number inside the fractures of both models with two values of isotropic permeability $K=0.2$ mD and $K=2000$ mD were calculated and compared, and the outcomes were: ADV of Reynolds number versus pressure drop and fracture friction value versus Reynolds number were almost matched between the two models results at all pressure drops. Figures 5.1A and 5.1B below illustrate these comparisons. This outcome proved that when the boundary conditions of the fracture surfaces were set with impermeable "Walls boundary" there was no interaction (pressure/velocity) between the fracture and the matrix.

Thus, the flow inside the fracture was not affected when the matrix permeability changed, and accordingly, fracture friction factor was not changed due to the permeability change (no fluid movement existed between the two coexisting domains). However, matrix flow was changed when the permeability changed, but this didn't affect the fracture flow due to the impermeable fracture surfaces "Walls boundary" as clarified in [chapter 4 section 4.3.2](#).

As well, a validation of friction factor between the ANSYS CFD Fluent FVM model of rough fracture results and [Nazridoust, Ahmadi and Smith \(2006\)'s model](#) of friction factor ([Section 2.6.3, table 2.1](#)) was conducted, by applying Reynolds number values that were extracted from ANSYS CFD Fluent FVM into [Nazridoust, Ahmadi and Smith \(2006\)'s equation](#). The result of this comparison was that the ANSYS CFD Fluent FVM model was a good match with the values of friction factor as reported by [Nazridoust, Ahmadi and Smith \(2006\)'s model](#), with deviation less than 9%. As well, it's good to note that this deviation of friction factor in fact was much less when Re was less than 10, around 3%, as can be seen in [Figure 5.2](#). However, as the comparison was conducted of full trends values, even after Re 10, the friction factor after Re 10 continued to increase; the reason for this difference in increase between two trends is as stated in [Nazridoust, Ahmadi and Smith \(2006\)'s model](#), that the model is suitable to be used when ($Re \leq 10$) only. Thus, this model was a good match with [Nazridoust, Ahmadi and Smith \(2006\)'s model](#), and was in a good state of validation.

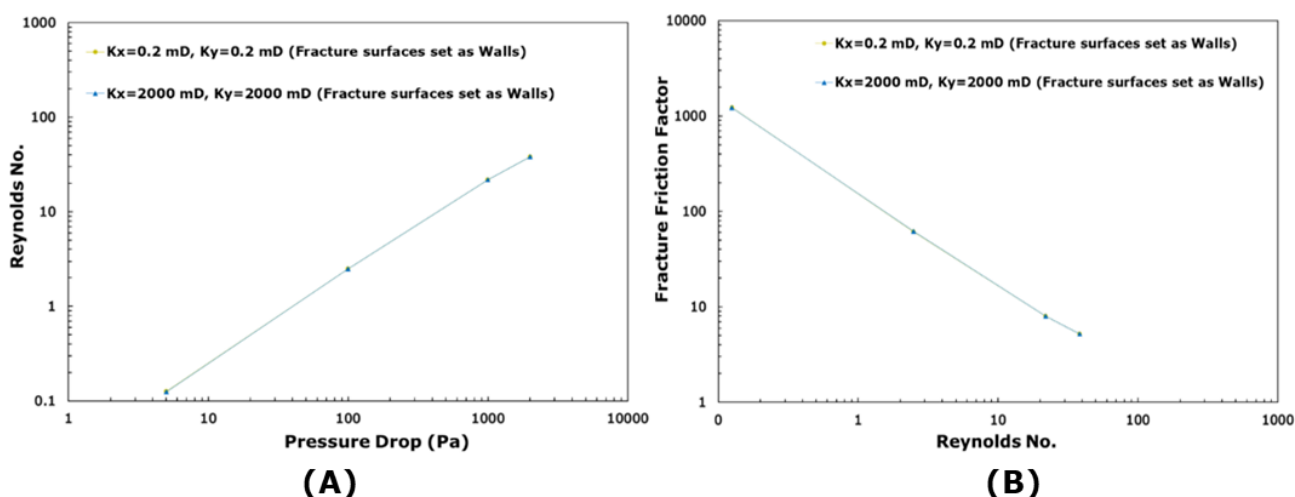


Figure 5.1 Comparison of rough fracture ANSYS CFD Fluent FVM models with fracture surfaces set as impermeable "Walls boundary", between different isotropic permeabilities ($K_x = K_y = 0.2 \text{ mD}$) and ($K_x = K_y = 2000 \text{ mD}$). A. Reynolds number, and B. Friction factor

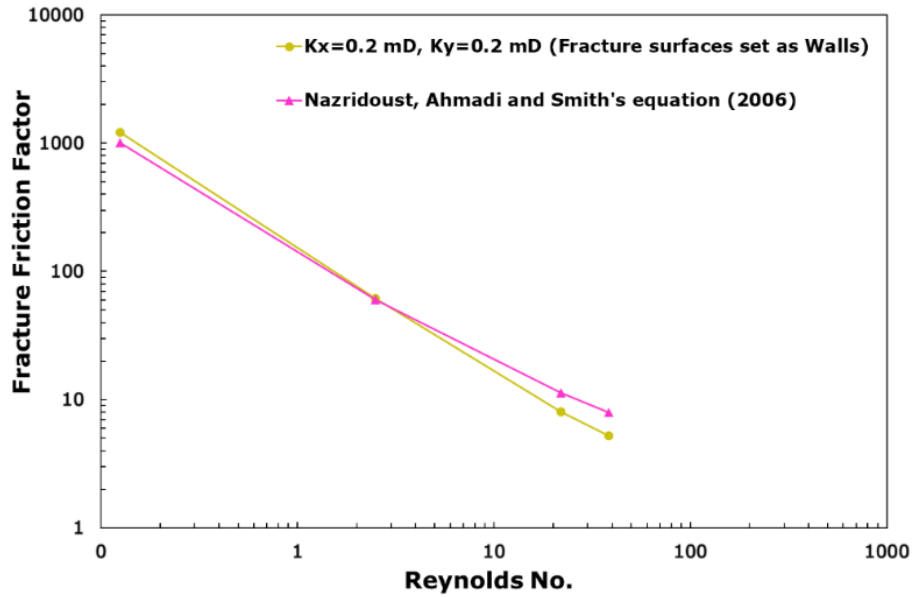


Figure 5.2 Friction factor validation and comparison between rough fracture of ANSYS CFD Fluent FVM model with isotropic permeability ($K_x=K_y=0.2$ mD), fracture surfaces were set as impermeable boundary “Walls boundary”, and Nazridoust, Ahmadi and Smith (2006)’s model of friction factor

5.3.2 Friction factor in rough fracture with two boundary conditions of fracture surfaces set up as impermeable “Walls boundary” and permeable “Interior faces boundary” with Validation

To check the effects of the interaction between matrix and fracture on friction factor in the rough fracture, ANSYS CFD Fluent FVM models of a rough fracture were simulated with the boundary conditions as in Section 5.3.1, but changing the fracture surface boundary conditions from impermeable “Wall boundary” to permeable “Interior faces boundary”. This allowed fluid movement between the fracture and matrix and vice versa, and considered isotropic matrix permeability with ($K_x=K_y=2000$ mD). The setup of this ANSYS CFD Fluent FVM model was similar to the setup of Crandall, Ahmadi and Smith (2010)’s paper as stated above in Section 5.3. Then, a similar procedure was followed to calculate the friction factor, as clarified in section 5.2. Therefore, the comparison outcomes of this

model were used to: first, validate this model's friction factor values with [Crandall, Ahmadi and Smith \(2010\)](#)'s model's results; and second, compare the results of permeable fracture surface models "Interior faces boundary" with isotropic matrix permeability, with impermeable fracture surfaces "Walls boundary". This enabled an investigation of friction factor when the matrix was interacting with the fracture and fluid movement between them was allowed.

The friction factor and the Reynolds number inside the rough fracture with permeable fracture surfaces "Interior faces" were calculated, then compared with the rough fracture with non-permeable fracture surfaces "Walls conditions", with isotropic permeability ($K_x=K_y=2000$ mD) in both models. The outcomes of these comparisons were: ADV of Reynolds number increased 28.15% in the rough fracture with permeable fracture surfaces; and ADV of the fracture friction decreased in the fracture model with $K_x=K_y=2000$ mD around 55.2%. [Figures 5.3A and 5.3B](#) illustrate these comparisons.

As well, a validation comparison of the friction factor between ANSYS CFD Fluent FVM model of rough fracture results with boundary surfaces set up as permeable "interior faces" and [Crandall, Ahmadi and Smith \(2010\)](#)'s model ([Section 2.6.3, table 2.1](#)) was conducted. The result of this comparison was that the ANSYS CFD Fluent FVM model was very well matched with the values of friction factor of [Crandall, Ahmadi and Smith \(2010\)](#) with 2.6% deviation. [Figure 5.4](#) clarifies this comparison. This comparison proved that this model was in a good stage of validation and was ready for further investigation.

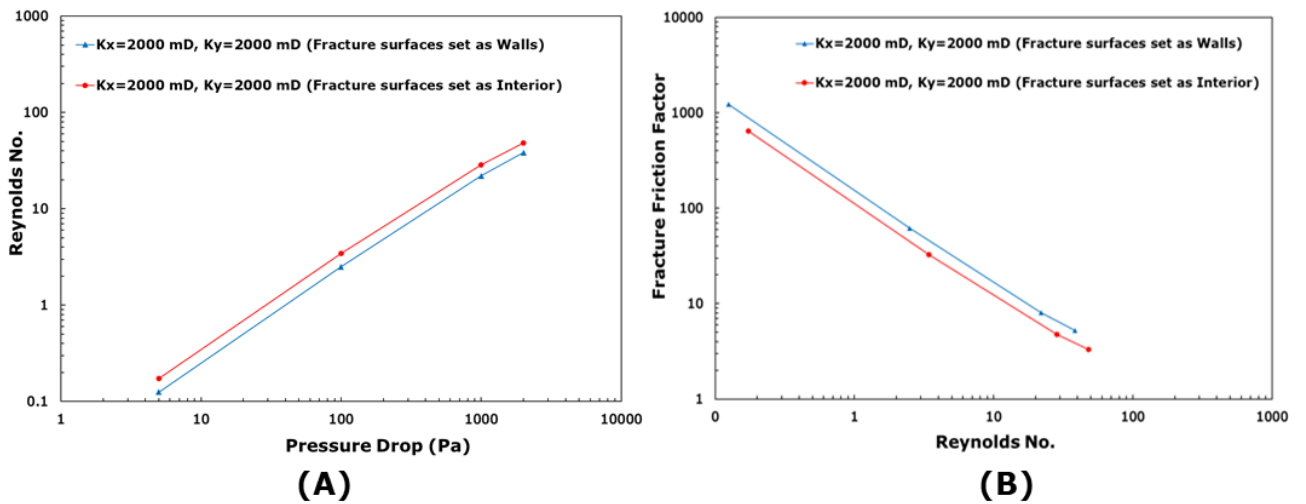


Figure 5.3 Comparison of rough fracture ANSYS CFD Fluent FVM models with fracture surface boundaries set as impermeable “Walls boundary” and permeable “Interior faces boundary”, with isotropic permeability ($K_x = K_y = 2000$ mD) A. Reynolds number; and B. Friction factor

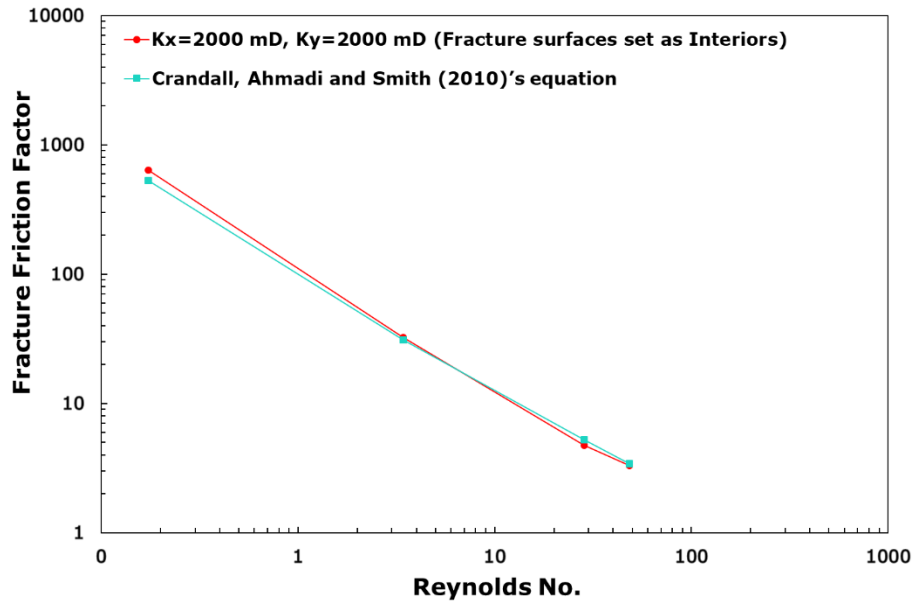


Figure 5.4 Friction factor validation and comparison between rough fracture ANSYS CFD Fluent FVM model with isotropic permeability ($K_x = K_y = 2000$ mD), fracture surfaces set as permeable “Interior faces boundary”, and [Crandall, Ahmadi and Smith \(2010\)'s](#) model

5.3.3 Friction factor in rough fracture with anisotropic matrix permeability and fracture surface boundaries set up as permeable “Interior faces boundary”

The previous section [5.3.2](#) showed the effects when fluids were allowed to move between the matrix and fracture, and how this interaction affected the friction factor and Reynolds number values. Therefore, in this section, more investigation was conducted, focusing on the effects of anisotropic matrix on the friction factor and Reynolds number inside the fracture. Thus, these ANSYS CFD Fluent FVM fracture models were set with permeable fracture surface boundaries “Interior faces boundary”, to allow fluid movement between fracture and matrix, and other set ups as stated above in [Section 5.3](#). the matrix permeability was considered anisotropic permeability, as the data in [Table 4.2](#) with six anisotropic scenarios in Chapter 4. similar procedure was followed to calculate the friction factor and Reynolds number, as clarified in [section 5.2](#), then, were compared for these models.

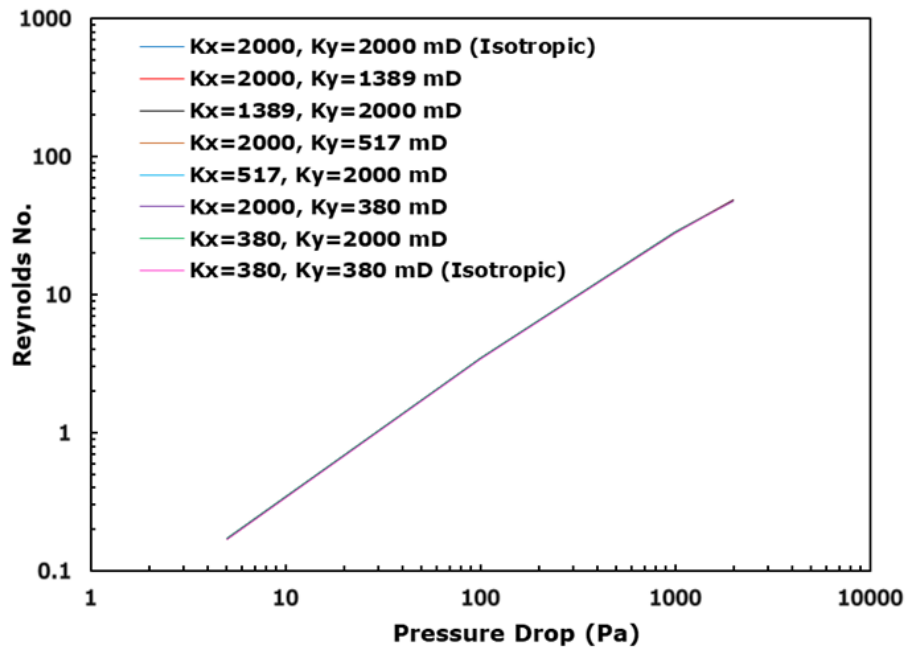
The first scenario model ($K_x=2000$, $K_y=1389$), compared with the second scenario model ($K_x=1389$, $K_y=2000$), ADV of Reynolds number decreased in the rough fracture with the second scenario matrix permeability 0.81%, and ADV of the fracture friction value increased 1.621%. Similar comparisons occurred between the third scenario model ($K_x=2000$, $K_y=517$) mD and fourth scenario model ($K_x=517$, $K_y=2000$) mD; ADV of Reynolds number decreased in in the fourth scenario 0.131%, and ADV of the fracture friction value increased 0.261%. Lastly, the fifth scenario model ($K_x=2000$, $K_y=380$) mD and sixth scenario model ($K_x=380$, $K_y=2000$) mD were compared, ADV of Reynolds number decreased in the sixth scenario 0.138%, and ADV of the fracture friction value increased 0.277%. As can be seen, the second scenario had the highest value of ADV friction factor. Therefore, further investigation was conducted by comparing its value with a isotropic matrix permeability model with ($K_x=K_y=2000$ mD); ADV of Reynolds number decreased in the second scenario 0.81%, and ADV of the fracture friction value increased 1.63%.

Moreover, this case was investigated further by two ANSYS CFD Fluent FVM models were compared, both with isotropic matrix permeability, first ($K_x=K_y=2000$ mD) and second ($K_x=K_y=380$ mD), with similar set ups as stated above in [Section 5.3](#).

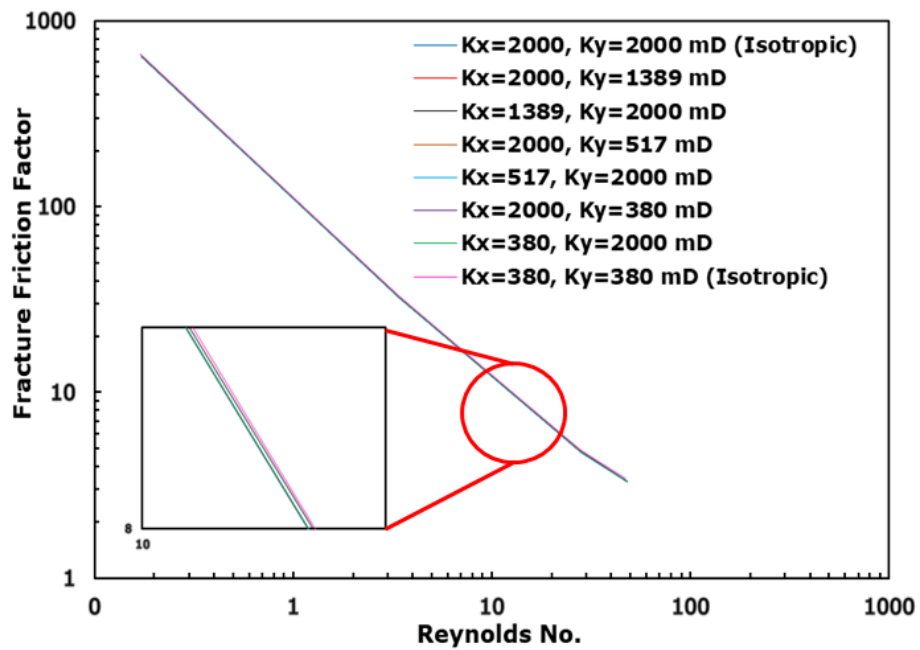
The outcome of these comparisons was that ADV of Reynolds number decreased in the low matrix permeability models 1.663%, and ADV of the fracture friction value increased 3.33%. [Figures 5.5A and 5.5B](#) below clarify these comparisons and [Table 5.1](#) summarises the results.

Table 5.1 Summarising Reynolds and friction factors ADV of ANSYS CFD Fluent FVM models' simulation results, for isotropic and anisotropic permeability of rough fractures

CFD models with different Matrix permeability scenarios	Compared models	Affected Scenario	(ADV) Reynolds number (Decrease of the effected scenario)	(ADV) Fracture friction factor (Increase of the effected scenario)
1 	1 & 2	2	0.81	1.621
2 	-	-	-	-
Isotropic (2000 mD) 	2 & Isotropic (2000 mD)	2	0.81	1.63
Isotropic (380 mD) 	Isotropics (2000 mD) & (380 mD)	Isotropic 380 mD	1.663	3.33
3 	-	-	-	-
4 	3 & 4	4	0.131	0.261
5 	-	-	-	-
6 	5 & 6	6	0.138	0.277



(A)



(B)

Figure 5.5 Comparisons of rough fracture ANSYS CFD Fluent FVM models between isotropic and all anisotropic matrix permeability scenarios A. Reynolds numbers, and B. friction factor, and fracture surfaces were set as permeable boundaries in all models

5.3.4 Summary of friction factor for rough fracture models with surface boundaries set up as impermeable “Walls boundary” and permeable “Interior faces boundary” with isotropic and anisotropic matrix permeability

The investigation of friction factor in rough fractures with fracture surfaces set up as impermeable “Walls boundary” and permeable “Interior faces boundary”, with isotropic and anisotropic matrix permeability, has reflected interesting findings, which are summarised below:

1. Considering fracture/matrix interaction, and fluid movement between fracture and matrix in rough fracture models, is essential in accurate calculation of fracture friction factor. As the comparisons of rough fracture ANSYS CFD Fluent FVM models between impermeable and permeable fracture surfaces with the same isotropic matrix permeability ($K_x=K_y=2000$ mD) showed, the rough fracture with permeable surfaces reflected a significant decrease in fracture friction factor by 55.2%. This result confirmed the findings in Chapter 4 [sections 4.3.4 and 4.3.5.2](#) that fracture flow proportions increased in the rough fracture, due to fluid movement between matrix and fracture. However, rough fractures with impermeable walls are not able to detect this effect, which would lead to misleading fracture friction factor calculation in fractured media. This comparison proved the findings that were reported by [Crandall, Ahmadi and Smith \(2010\)’s model](#), that permeable fracture surfaces have a significant effect on rough fracture friction factor calculations.
2. As the effects of fracture/matrix interaction were proven in point 1, this research added a further mimicked condition of subsurface layers, which was anisotropic matrix permeability effects on fracture friction factor instead of isotropic permeability. Therefore, comparisons of fracture friction factor were made of the six scenarios of ANSYS CFD Fluent FVM models with anisotropic matrix permeability, as [Table 4.2](#), that changed with percentages (30%, 74% and 81%) of K_x and K_y . The outcome of these comparisons was that if both in-plane permeability K_x and through plane permeability K_y were changing at the same time, then K_x had the highest

effect on fracture friction factor and would lead to increasing it, due to flow reduction in the rough fracture, as clarified in Chapter 4 [section 4.3.5.2](#).

3. Further mimicked scenarios were then considered to investigate the effects of in-plane K_x permeability and through plane K_y permeability, when both at the same time were reduced. Therefore, the comparison was conducted of ANSYS CFD Fluent FVM rough fracture models with isotropic matrix permeabilities ($K_x=K_y=2000$ mD) and ($K_x=K_y=380$ mD). The results showed an increase in friction factor with lowest isotropic permeability models ($K_x=K_y=380$ mD) with increase of 3.33%, as clarified in [Table 5.1](#). This proved that when both directions of the matrix permeability K_x and K_y were reduced, flow was decreased in the fracture, which will affects the friction factor, and increases its value.
4. Comparisons were made of average fracture friction factor values of four pressure values (5, 100, 1000, 2000) Pa, among the first set of anisotropic permeability ANSYS CFD Fluent FVM models, with scenarios 1,3, 5 in [Table 4.2](#), where K_x was fixed with 2000 mD and K_y was varied with values 380, 517, 1389 mD. Separately, comparisons were made among the second set of anisotropic permeability ANSYS CFD Fluent FVM models with scenarios 2, 4, 6 in [Table 4.2](#), where, K_y was fixed with 2000 mD and K_x was varied with 380, 517, 1389 mD. The results of the first comparison reflected a slight increase in friction factor, which proved that although in-plane (K_x) permeability was a fixed value, the increase of through plane (K_y) permeability had increased friction factor value. While comparison of the second set reflected an increase in fracture friction factor, with increasing in-plane (K_x) permeability with fixed through plane (K_y) permeability, [Figure 5.6](#) below clarifies this comparison. This was consolidation of the finding which proved the effects of permeable surfaces of rough fractures through fracture/matrix interface layer on fracture flow proportion in a fractured domain, as clarified in Chapter 4 [section 4.3.5.2](#). This is because the flow proportion in the fracture void changes with changing surrounding matrix properties.

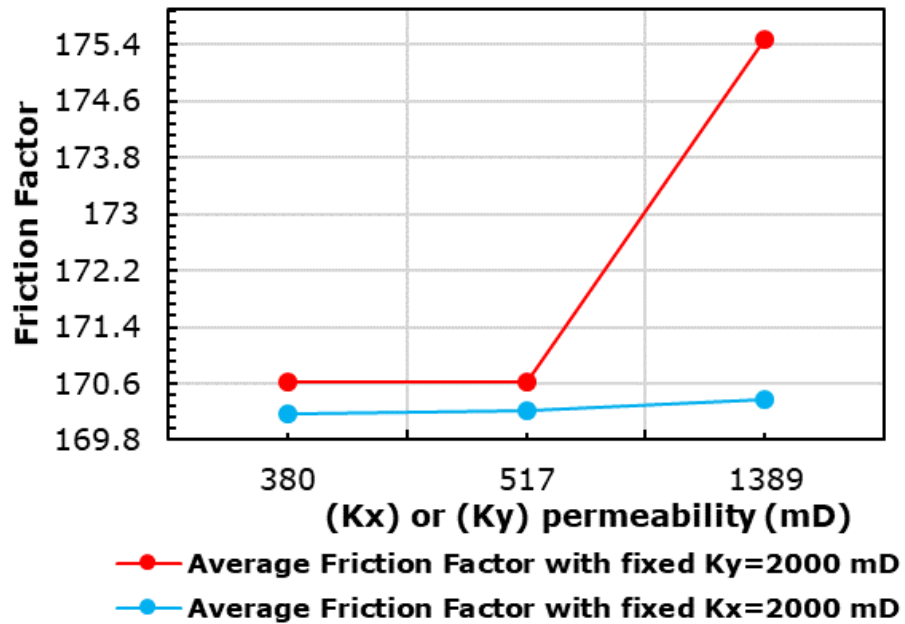


Figure 5.6 Average fracture friction factor at four pressure values (5, 100, 1000, 2000) Pa, zero outlet pressure, in ANSYS CFD Fluent FVM rough fracture models of two anisotropic permeability sets (first set permeability scenarios ($K_x=2000$ mD fixed, $K_y= 380, 517, 1389$ mD); and second set permeability scenarios ($K_y=2000$ mD fixed, $K_x= 380, 517, 1389$ mD))

- To conclude the findings in these analyses, fracture surface interaction with matrix is an essential consideration, as it has massive effect on fracture friction factor. If both K_x and K_y were changing at the same time, then K_x had highest effect on fractured domain flow, and accordingly on fracture friction factor. However, if one of either K_x or K_y was changing and the other was fixed, then K_x had highest effect, as it led to decreasing flow proportion in fracture and, accordingly, increased fracture friction factor. The comparison of these scenarios has reflected that matrix permeability effects with fractured models that account matrix/fracture flow interaction have an effect on fracture friction factor values. This demonstrates that it is essential to consider real conditions of subsurface layers rather than simplified conditions, and to consider anisotropic values of permeability, as this has an effect on fractured domain (fracture+matrix) flow. This is especially true for fractured formations in subsurface layers of earth crust or in reservoirs, which have very anisotropic permeability and are varied from point to point, with rough fracture geometries and surfaces as reported by [Li et al. \(2021\)](#); [Suri et al. \(2020\)](#); [Zhu et al. \(2020\)](#); [Ju et al. \(2019\)](#); [Karimzade et al. \(2019\)](#); [Luo et al. \(2018\)](#); [Liu, Li and Jiang \(2016\)](#); [Tiab and Donaldson \(2004\)](#); [Nelson \(2001\)](#); [Golf-Racht \(1982\)](#);

and [Ruhland \(1973\)](#). Thus, these findings have provided clear evidence that the previous models of fracture friction factor, with assumption of impermeable fracture surfaces with the surrounding matrix and no fluid interaction between fracture and matrix, as reported by [Su et al. \(2019\)](#); [Chen et al. \(2017\)](#); [Zhou et al. \(2016\)](#); [Zhang and Nemcik \(2013\)](#); [Qian et al. \(2011\)](#); [Nazridoust, Ahmadi and Smith \(2006\)](#); [White \(2003\)](#); [Masciopinto \(1999\)](#) and [Saidi \(1987\) p. 169](#), will mislead fracture friction factor calculations and give erroneous results. More details cover this in the following sections in this chapter.

5.4 New Proposed Analytical Model Of Fracture Friction Factor

As clarified in Chapter 2 [section 2.7.3](#), former equations of friction factor have been based on simplified assumptions, either to exclude matrix flow effect or to consider a matrix with isotropic matrix permeability. However, these assumptions do not reflect common reality, and in fact occur seldom, because these formations are stratified and consist of layers of rocks with isotropic properties. These stratifications and heterogeneity result in variations of dimension, deposition, composition and varied texture of every layer before the deposition of another layer. This process of building layers over an extensive period of time has led to subsurface layers of anisotropic formation properties. Thus, most classic subsurface formations/reservoirs have varied permeability in both flow directions, lateral and perpendicular, as well as varied types of fracture geometries, fracture surface roughness, fractured apertures, and etc. ([Li et al. 2021](#); [Wang et al. 2020](#); [Dippenaar and Van Rooy 2016](#); [Singh, Singh and Pathegama 2014](#); [Spence et al. 2014](#); [Rasouli and Hosseinian 2011](#); [Sahimi 2011](#); [Crandall, Bromhal and Smith 2009](#); [Ingham and Pop 2005 p. 367](#); [Tiab and Donaldson 2004 p. 469](#); [Berkowitz 2002](#); [Nelson 2001](#); [Golf-Racht 1982](#); [Zimmerman and Bodvarsson 1996](#); [Saidi 1987](#); and [Ruhland 1973](#)).

In order to connect these anisotropic properties of fractured subsurface formations/reservoirs with the calculations and developments of this study, the outcomes were first compared between the parallel plates fracture with single aperture and the rough fracture in Chapter 4. This clarified the effect of fracture

geometry and the surrounding anisotropic matrix permeability on velocity and flow inside the fracture and matrix. As well, the effect on the friction factor inside the rough fracture was discussed in Chapter 5. The conclusion was that the parallel plates fracture with a single height could not accurately represent fracture calculations in comparison with the rough conditions of fractured media, due to many reasons as stressed in this chapter. Therefore, a rough fracture was the best opportunity to get optimised calculations of flow, velocity and friction factor. Whilst rough fractures were used in the friction factor calculations of the previous studies, this was with limitations of the fractures' boundary conditions, which left many missing gaps to calculate accurate values or make better predictions of the friction factor. To the best knowledge and efforts of this study, the gaps of the previous studies in their fracture friction models are highlighted as follows:

- a. [Saidi \(1987\) p. 169](#) and [Golf-Racht \(1982\) pp. 306, 310](#) presented a general empirical fracture friction factor formula in parallel plates fracture with single aperture geometry, with a rectangular cross section area and smooth surfaces, and considered impermeable fracture surfaces (excluded matrix/fracture interaction and flow movement), as [equation 2.107](#) ($f=96/Re$) in Chapter 2 ([Section 2.6.3](#)).
- b. [Su et al. \(2019\)](#); [Chen et al. \(2017\)](#); [Zhou et al. \(2016\)](#); [Zhang and Nemcik \(2013\)](#); [Qian et al. \(2011\)](#); [Nazridoust, Ahmadi and Smith \(2006\)](#); [White \(2003\)](#); [Masciopinto \(1999\)](#); and [Saidi \(1987\) p. 169](#) presented a developed friction factor model for fractures, based on either experimental, numerical or empirical calculations, and considered rough fracture geometries. However, these models assumed solid impermeable fracture surfaces; no matrix surrounding the fracture was considered, and matrix/fracture interaction and fluid movement were neglected.
- c. [Crandall, Ahmadi and Smith \(2010\)](#) extended the work of [Nazridoust, Ahmadi and Smith \(2006\)](#) and used the same rough fracture geometry with permeable fracture surfaces (the matrix surrounding the fracture was considered, with matrix/fracture interaction and fluid movement). However, only isotropic matrix permeability was considered.
- d. [Singh, Singh and Pathegama \(2014\)](#); [Qian et al. \(2011\)](#); [Zimmerman and Yeo \(2000\)](#); [Oron and Berkowitz \(1998\)](#); [Schrauf and Evans \(1986\)](#) and [Louis \(1969\)](#) stressed that Reynolds number (Re) in fractures was affected by many factors, such as fracture apertures, fracture surface roughness and fluid flow velocity. As well, it was stated that the critical value of Re is 10,

as flow in fractures can be turbulent with Re greater than 10, and flow will reflect a non-linear behaviour. [Singh, Singh and Pathegama \(2014\)](#) stated that, based on fracture's surface roughness, fracture flow could be turbulent with Re values between 4 or 10.

- e. It is good to stress that all the above models also assumed a single-phase fluid type inside the fracture.

Thus, the previous models' developments of friction factor in fractures used these assumptions, as clarified, to consider the challenges of determining the correct values of pressure drop ($\frac{\Delta P}{L}$), velocity, flow and friction factor inside fractures. However, these models had many limitations. It was found in this research that there were many gaps that needed to be addressed in order to get an accurate or optimised model to estimate friction factor values, that mimicked the real conditions of flow inside fractures unlike the previous models. Thus, the gaps this research considered in the modelling were:

1. Considered rough fracture geometry (various heights of fracture apertures along fracture flow)
2. Considered permeable fracture surfaces (fracture/matrix fluid interactions and fluid movement occurrence along the fracture flow)
3. Considered anisotropic permeability of the matrix that surrounded fracture surfaces.

To address the gaps mentioned above, the models of this research used optimum conditions of a real fractured formation, to gain an outcome of better estimates of flow inside fractured media. This led to a better prediction of friction factor and pressure head loss ($\frac{\Delta P}{L}$) in fractured rock reservoirs, by considering the effects of these gaps; this is clarified in the below sections. Thus, there was a necessity to have a better prediction relationship of friction factor, which is a measure of pressure loss and velocity along the fracture to account for these variables, explained as following:

The total flow in fractured formations can be expressed as [equation 5.4](#) below; flow in the matrix was assumed linear and following Darcy's law.

$$Q_t = Q_m + Q_f \tag{5.4}$$

[\(Dietrich et al. 2005; Tiab and Donaldson 2004; Golf-Racht 1982\)](#)

Where:

Q_t = total flow domain of fracture media (matrix+ fracture), Q_m = matrix flow, Q_f = fracture flow.

$$Q_m = \frac{K h_m}{\mu} \frac{\Delta P}{L} \quad (5.5)$$

(Tiab and Donaldson 2004; Dake 1998; Golf-Racht 1982)

Where:

K = matrix permeability (isotropic), h_m = formation height, L = formation length, μ = fluid viscosity, ΔP = pressure drop.

Li et al. (2021); Wang et al. (2020); Dippenaar and Van Rooy (2016); Singh, Singh and Pathegama (2014); Spence et al. (2014); Rasouli and Hosseinian (2011); Sahimi (2011); Crandall, Bromhal and Smith (2009); Ingham and Pop (2005) p. 367; Tiab and Donaldson (2004) p. 469; Berkowitz (2002); Nelson (2001); Golf-Racht (1982); Zimmerman and Bodvarsson (1996); Saidi (1987) and Ruhland (1973) stressed that isotropic properties in subsurface layers or reservoirs are rare; in most formations/reservoirs matrix permeability is varied in both horizontal and vertical directions of Cartesian coordinates along flow in the formation. However, the former equations of steady state flow required a single value of permeability. Flow in subsurface formations is directional, and is affected by flow direction with formations' permeability directions. Therefore, it's essential to have an average value of permeability, due to the anisotropy of matrix permeability. Matrix permeability in layered formations is divided into many types, based on the properties of layered formations, such as: cross flow layers, layers without cross flow, and composite formations (Tiab and Donaldson 2004; Nelson 2001 pp. 215, 279; Dake 1998 pp. 157, 397, 415). However, in this study, composite formations were considered in the model to adopt the scenario of a fracture passing through anisotropic matrix layers. As well, Lei et al. (2015); Rasouli and Rasouli (2012); Tiab and Donaldson (2004) p. 474; Hidayati, Chen and Teufel (2000); Saidi (1987) p. 82; Parsons (1966); and Scheidegger (1963) confirmed that the horizontal direction of matrix permeability was very important due to the significant effect on subsurface flow and reservoir productivity. Thus, to have a better permeability value of composite formations, the details of permeability are clarified in the Figure 5.7A and Equations 5.6, 5.7, 5.8, 5.9 and 5.10 below, to clarify the derivatives of average permeability in each layer.

This model consisted of many segments (layers) with varied matrix permeability. However, permeability of each segment was isotropic, thus:

$$\Delta p_t = P_1 - P_n = \Delta p_1 + \Delta p_2 + \Delta p_3 + \dots + \Delta p_n \quad (5.6)$$

Flow was assumed as incompressible fluids, then pressure drop for each segment is:

$$\Delta p_i = \left(\frac{q \cdot \mu}{A} \right) \frac{L_i}{K_i} \quad (5.7)$$

While total pressure drop can be expressed as equation

$$\Delta p_t = \left(\frac{q \cdot \mu}{A} \right) \frac{L_t}{K} \quad (5.8)$$

Substitute [Equations 5.7, 5.8 in 5.6](#), then cancel identical terms of q , μ and A then:

$$\frac{L_t}{K} = \frac{L_1}{K_1} + \frac{L_2}{K_2} + \dots + \frac{L_n}{K_n} \quad (5.9)$$

Thus, the average matrix permeability of (n) segments in formation is:

$$\bar{K} = \frac{\sum_{i=1}^n L_i}{\sum_{i=1}^n \left(\frac{L_i}{K_i} \right)} \quad (5.10)$$

[\(Tiab and Donaldson 2004; Nelson 2001 pp. 215, 279; Dake 1998 p. 397\)](#)

Where:

\bar{K} = average permeability of matrix domain, L_i = segment length of formation layer, K_i = matrix permeability of layer (i).

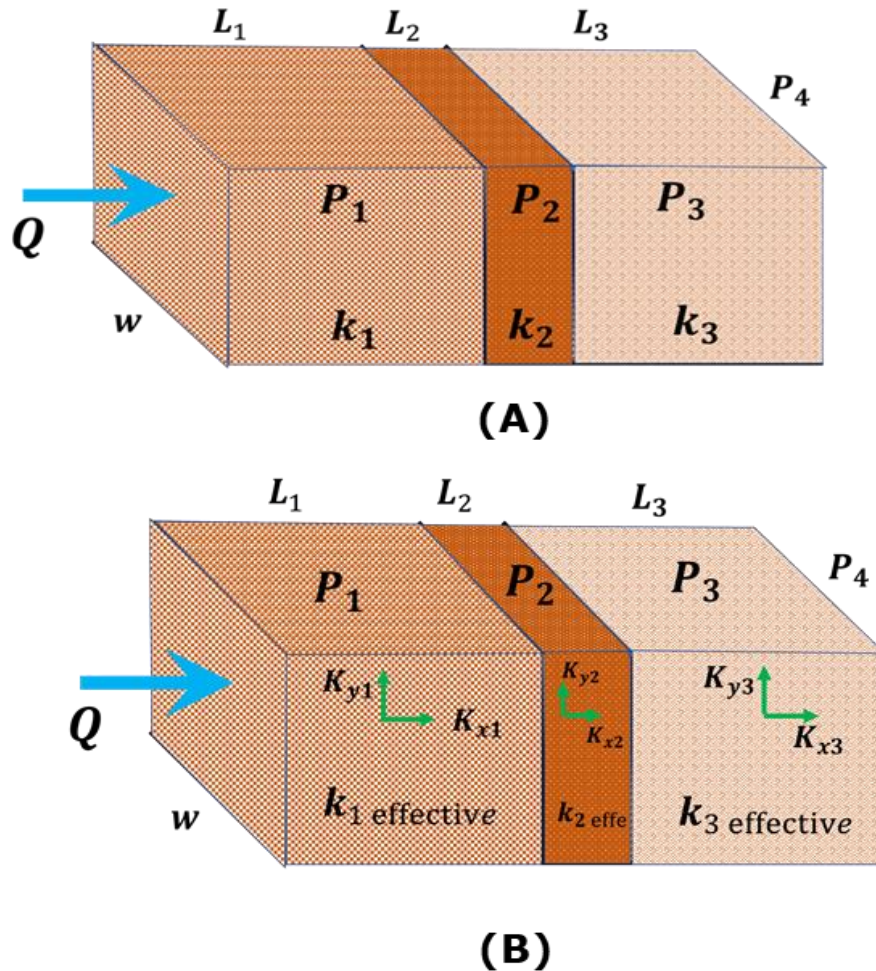


Figure 5.7 Composite formations with varied permeability

A. Composite formation with varied permeability in each layer along the flow (adapted from Tiab and Donaldson 2004); B. Composite formation with varied permeability in each layer along the flow, as well as in each layer in both directions (in-plane (K_x) parallel and through plane (K_y) vertical on flow)

Di Fratta et al. (2016) developed experimentally an equation of effective anisotropic matrix permeability of each layer, for both directions in-plane (K_x) parallel and through plane (K_y) vertical on flow, as Equation 5.11. The angle Θ was considered to be the most critical scenario of unidirectional permeability, which is 45° ; a similar angle effect on flow in formations was stressed by Zhu et al. (2020). The benefit of this equation was that when K_x and K_y were equal it was reduced to be isotropic; as well, the effective matrix permeability equation could reflect the difference between K_x and K_y value directions. In other words, when reversing the same values of permeability and putting K_x into K_y and K_y into K_x , the equation gave a different value. This was an extra benefit, which matched with the important of parallel permeability K_x in comparison with vertical permeability K_y in flow directions.

$$K_{\text{Effective}} = \left(\frac{K_{xi} \cdot K_{yi}}{K_{xi} \cdot \sin^2 \theta + K_{yi} \cdot \cos^2 \theta} \right) \quad (5.11)$$

Substitute [equation 5.11](#) in [equation 5.10](#) to get equivalent matrix permeability of entire matrix domain with varied permeability in each layer along the flow: as well, in each layer both directions in-plane (Kx) parallel and through plane (Ky) vertical on flow, as [figure 5.7B](#). Thus:

$$K_{\text{Equivalent}} = \frac{\sum_{i=1}^n L_i}{\sum_{i=1}^n \left[\frac{L_i}{\left(\frac{K_{xi} \cdot K_{yi}}{K_{xi} \cdot \sin^2 \theta + K_{yi} \cdot \cos^2 \theta} \right)} \right]} \quad (5.12)$$

Substitute [equation 5.12](#) in [equation 5.5](#), thus:

$$Q_m = \frac{\left[\frac{\sum_{i=1}^n L_i}{\sum_{i=1}^n \left[\frac{L_i}{\left(\frac{K_{xi} \cdot K_{yi}}{K_{xi} \cdot \sin^2 \theta + K_{yi} \cdot \cos^2 \theta} \right)} \right]} \right] \cdot h_m}{\mu L} \cdot \Delta P \quad (5.13)$$

[Equation 5.13](#) represents matrix flow rate in anisotropic matrix permeability with many different segments; as well, varied permeability in-plane Kx and through plane Ky permeability directions of each segment.

$$Re = \frac{\rho \cdot V \cdot D}{\mu} \quad (5.14)$$

[Nazridoust, Ahmadi and Smith \(2006\)](#) and [Crandall, Ahmadi and Smith \(2010\)](#) suggested that (D) can be replaced with (\bar{H}) to include a fracture's roughness effect on the fracture's flow. Where: ($\bar{H} = h_{\text{avg}} - \sigma$), h_{avg} = average aperture heights of fracture; σ = standard deviation. Thus, Re can be rewritten as:

$$Re = \frac{\rho \cdot V \cdot \bar{H}}{\mu} \quad (5.15)$$

($V \cdot \bar{H}$) will be equivalent to (Q_f), then (Re) will be:

$$Re = \frac{\rho \cdot Q_f}{\mu} \quad (5.16)$$

Rearrange [equation 5.16](#) for (Q_f), then

$$\text{Then, } Q_f = \frac{Re_{\bar{H}} \cdot \mu}{\rho} \quad (5.17)$$

Nazridoust, Ahmadi and Smith (2006) and Crandall, Ahmadi and Smith (2010) considered the tortuosity effect on fracture length to the friction factor equation. Thus:

$$F = \frac{2 D \Delta P}{L \cdot \rho \cdot V^2} \quad (5.18)$$

(White 2003)

$$F = \frac{2 \cdot \Delta P \cdot \bar{H}}{L \cdot \rho \cdot V^2} \quad (5.19)$$

Consider ($Q_f = V \cdot \bar{H}$) and substitute it in equation 5.18, then:

$$F = \frac{2 \cdot \Delta P \cdot \bar{H}^3}{L (1+\theta) \cdot \rho \cdot Q_f^2} \quad (5.20)$$

Nazridoust, Ahmadi and Smith (2006) developed a fracture friction factor equation numerically, with best fit regression line when the fracture surfaces were considered non-permeable walls, as:

$$F = \frac{123}{Re_{\bar{H}}} (1 + 0.12 \cdot Re_{\bar{H}}^{0.687}), \quad Re_{\bar{H}} \leq 10 \quad (5.21)$$

Substitute equation 5.21 and 5.15 into 5.20 and solve for Q_f ,

$$\frac{123}{Re_{\bar{H}}} (1 + 0.12 \cdot Re_{\bar{H}}^{0.687}) = \frac{2 \cdot \Delta P \cdot \bar{H}^3}{L (1+\theta) \cdot \rho \cdot Q_f^2} \quad (5.22)$$

$$Q_f = \frac{2 \cdot \Delta P \cdot \bar{H}^3}{123 \cdot \mu \cdot L \cdot (1+\theta) (1+0.12 \cdot Re_{\bar{H}}^{0.687})} \quad (5.23)$$

Substitute equations 5.13 and 5.23 into 5.4 Then:

$$Q_t = \frac{\left[\frac{\sum_{i=1}^n L_i}{\left[\frac{L_i}{K_{xi} \cdot K_{yi}} \right] \left[\frac{K_{xi} \cdot \sin^2 \theta + K_{yi} \cdot \cos^2 \theta}{\mu \cdot L} \right]} \right] \cdot h_m}{\mu \cdot L} \cdot \Delta P + \frac{2 \cdot \Delta P \cdot \bar{H}^3}{123 \cdot \mu \cdot L \cdot (1+\theta) (1+0.12 \cdot Re_{\bar{H}}^{0.687})} \quad (5.24)$$

solve for ΔP , then:

$$\Delta P = \frac{Q_t \mu L \cdot [61.5 (1+\theta)(1+0.12 \cdot \text{Re}_{\bar{H}}^{0.687})]}{\left[\frac{\sum_{i=1}^n L_i}{\left(\frac{L_i}{K_{xi} \cdot K_{yi}} \right)} \right]} \cdot h_m [61.5 (1+\theta)(1+0.12 \cdot \text{Re}_{\bar{H}}^{0.687}) + \bar{H}^3] \quad (5.25)$$

consider ($Q_t = Q_f = V \cdot \bar{H}$) , then:

$$\Delta P = \frac{(Q_f) \mu L \cdot [61.5 (1+\theta)(1+0.12 \cdot \text{Re}_{\bar{H}}^{0.687})]}{\left[\frac{\sum_{i=1}^n L_i}{\left(\frac{L_i}{K_{xi} \cdot K_{yi}} \right)} \right]} \cdot h_m [61.5 (1+\theta)(1+0.12 \cdot \text{Re}_{\bar{H}}^{0.687}) + \bar{H}^3] \quad (5.26)$$

Substitute [equation 5.26](#) in [5.19](#)

F

$$F = \frac{2 \cdot \bar{H} \cdot \left[\frac{Q_f \mu L \cdot [61.5 (1 + \theta)(1 + 0.12 \cdot \text{Re}_{\bar{H}}^{0.687})]}{\left[\frac{\sum_{i=1}^n L_i}{\left(\frac{L_i}{K_{xi} \cdot K_{yi}} \right)} \right]} \cdot h_m [61.5 (1 + \theta)(1 + 0.12 \cdot \text{Re}_{\bar{H}}^{0.687}) + \bar{H}^3] \right]}{L \cdot \rho \cdot V^2} \quad (5.27)$$

Solve the [equation 5.27](#) and consider the length of the fluid path to be the equivalent length ($L=Le$). As well, consider ($Q_t = Q_f = V \cdot \bar{H}$) , as highest fluids proportion pass through the fracture domain in comparisons with matrix, and will be as:

$$F = \frac{123}{\text{Re}} \frac{[(1+0.12 \cdot \text{Re}_{\bar{H}}^{0.687})]}{1 + 61.5 (1+\theta)(1+0.12 \cdot \text{Re}_{\bar{H}}^{0.687}) \cdot \left[\frac{\sum_{i=1}^n L_i}{\left(\frac{K_{xi} \cdot K_{yi}}{K_{xi} \cdot \sin^2 \theta + K_{yi} \cdot \cos^2 \theta} \right)} \right]} \cdot \text{hm} \quad (5.28)$$

This developed model of fracture friction factor had many benefits. First, it had the ability to consider fracture tortuosity effects. Second, it considered matrix/fracture interaction with anisotropic matrix permeability along layers of formations along fracture length, and, in two directions of flow X and Y (consider Kx and Ky anisotropic effect on lateral and perpendicular flow of each layer). Third, it considered fracture roughness by considering ($\bar{H} = h_{\text{avg}} - \sigma$). Fourth, this new developed formula had an ability that if formations had isotropic properties of permeability, then it would be reduced and would give the same value as [Crandall, Ahmadi and Smith \(2010\)](#)'s model. This was an extra benefit as it can also be used in subsurface formations with very low permeabilities.

5.4.1 Validation of the new proposed Analytical model of fracture friction factor

As mentioned in [Section 5.4](#), the proposed model [equation 5.28](#) was reduced to give similar values to [Crandall, Ahmadi and Smith \(2010\)](#)'s model when the matrix permeability values in Kx and Ky directions were similar. Therefore, similar values of Reynolds number and friction factors were extracted from [Crandall, Ahmadi and Smith \(2010\)](#)'s journal of two images of isotropic matrix permeability ($K_x=K_y$), which are ($k=0.2$ mD, $K=2000$ mD), by image digitizer online software. Then, these values were applied in the new proposed model, and fracture friction factor values were extracted. These were compared with the friction factors of [Crandall, Ahmadi and Smith \(2010\)](#)'s model. [Figure 5.8](#) clarifies the comparison. ADV were calculated of the fracture friction factor between the new proposed model of this research and the [Crandall, Ahmadi and Smith \(2010\)](#) model, and the outcome was that for $k=0.2$ mD it deviated by 1.9% and for $K=2000$ mD it deviated by 2.8%.

Thus, this model had very strong agreement with [Crandall, Ahmadi and Smith \(2010\)](#)'s values when the matrix permeability was considered as isotropic.

The proposed model was therefore validated with the isotropic matrix permeability of [Crandall, Ahmadi and Smith \(2010\)](#)'s values; however, the main goal of this model was to check the sensitivity prediction of rough fracture friction factor with anisotropic matrix permeability. Therefore, friction factors were calculated from ANSYS CFD Fluent FVM as clarified in section 5.3.3 of this chapter, for ANSYS CFD Fluent FVM models of rough fractures with different permeability scenarios. These included isotropic matrix permeability ($K_x=K_y=2000$ mD) and the scenarios with highest change in anisotropic permeability in [Table 4.2](#), which were scenarios 5 and 6, with permeability ($K_x=2000$ mD, $K_y=380$ mD) and ($K_x=380$ mD, $K_y=2000$ mD): 81% permeability change in both directions. The Reynolds number values were extracted from these ANSYS CFD Fluent FVM models and applied in the new proposed model of friction factor, then comparisons were conducted between ANSYS CFD Fluent FVM friction factor and the new proposed analytical model of this study. The outcomes of these comparisons were that the new model of friction factor values had a very good match with ANSYS CFD Fluent FVM friction factor values, with average deviation around 6% in $Re \leq 10$. [Figure 5.9](#) clarifies the comparison.

Thus, the new proposed friction factor model was validated with ANSYS CFD Fluent FVM friction factor and with the literature paper values, and the results showed that the proposed model had better prediction of fracture friction factor in anisotropic matrix permeability along the fracture flow with different matrix layers and varied matrix permeability in X and Y-Cartesian directions in the same layer. However, this model could only measure until Reynolds number valued equal or less (≤ 10), because after this value, the trend started to be non-linear on log-log graph. The explanation of this limitation is that in the development procedure of the new equation, particularly in the fracture flow (Q_f), the friction factor of [Nazridoust, Ahmadi and Smith \(2006\)](#) was used, so this equation has the same limitation, which has been reflected in the proposed model too.

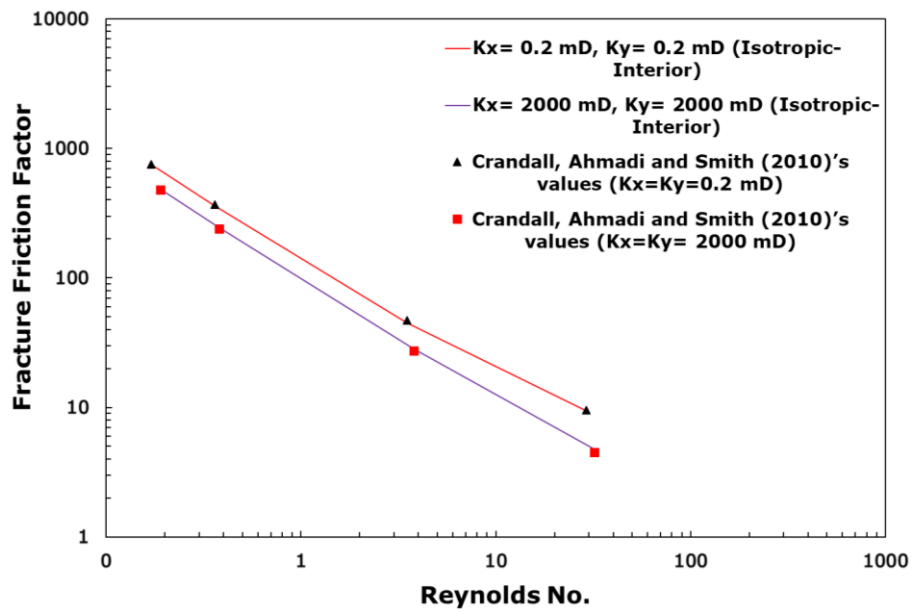


Figure 5.8 Friction factor validation of rough fracture between the proposed model (equation 5.28) and Crandall, Ahmadi and Smith (2010)'s model's data for different isotropic matrix permeability ($K_x=K_y$) 0.2 mD and 2000 mD

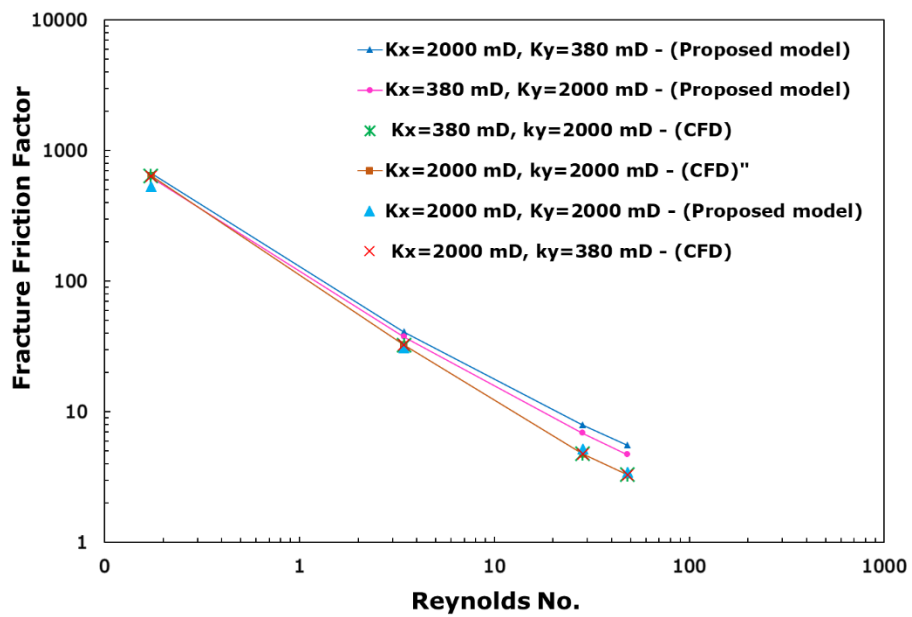


Figure 5.9 Validation of the proposed friction factor model with ANSYS CFD Fluent FVM friction factor with isotropic and anisotropic permeability matrix scenarios

5.5 A New Friction Factor Numerical Model In Rough Fractures With Anisotropic Permeability, Using ANSYS CFD Fluent FVM Fracture Models

The details and the gaps of the available former fracture friction factors have been clarified in the previous sections; as well, that the new proposed analytical model had the limitation until ($Re \leq 10$). Therefore, there was a necessity to get a model to cover these gaps and have less limitations, in order to gain a better prediction of friction fracture in rough fractures. Thus, ANSYS CFD Fluent FVM fracture models were used to conduct a deep investigation, considering all the gaps that this study focused on, which were: permeable fracture surfaces with the surrounding matrix; rough fracture geometry which accounts for fracture apertures and variations in heights; roughness; fluid flow tortuosity inside fractures; anisotropic matrix permeability scenarios, which involved varied data in in-plane K_x and though plane K_y with percentage changes 30%, 74% and 81% between K_x and K_y ; and different pressure inlet values (5, 100, 1000, 2000) Pa with zero pressure outlets, for widening the boundary conditions. The number of the simulations of the rough fracture with these boundary conditions was 32, and these were selected to be used in the analysis of the fracture friction factor numerical model as [Figures 5.10 and 5.11](#) below. From these 32 simulations, a numerical friction factor model by regression best fit line was extracted as [equation 5.29](#), which described the friction factor in the fractures with anisotropic matrix permeability that surrounded the fracture surfaces. The quality of this regression-best fit line was investigated by using the R-squared value or coefficient of the determination, to check the variations between the points in the graph and the regression line. These values were calculated by using the Excel function of the R-squared value on the chart, and was 0.9985. This proved the accuracy of the regression line with friction factor points versus Reynolds number.

$$f = \frac{120}{Re^{0.942}} \quad (5.29)$$

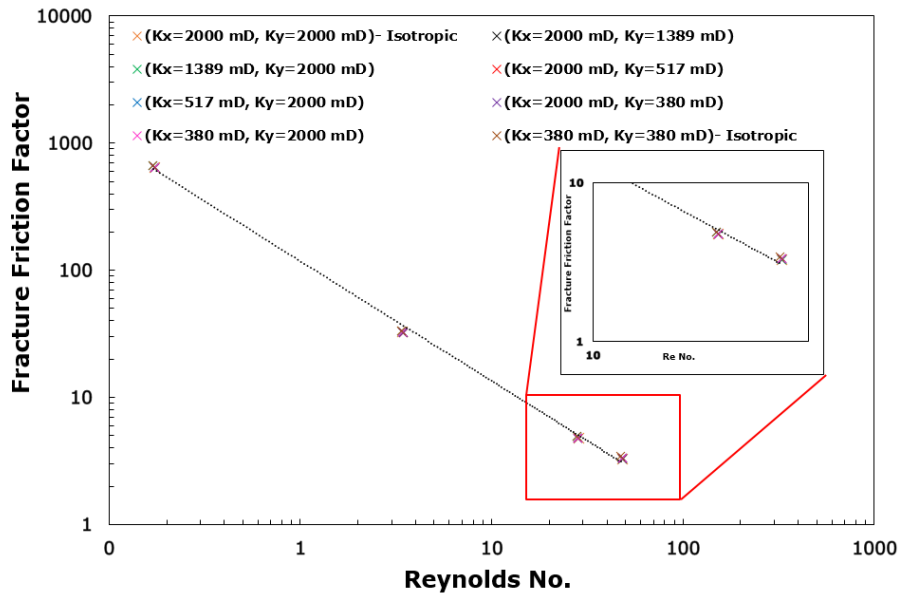


Figure 5.10 Fracture friction factor values by ANSYS CFD Fluent FVM with different scenarios of matrix isotropic and anisotropic permeability, with best fit regression line

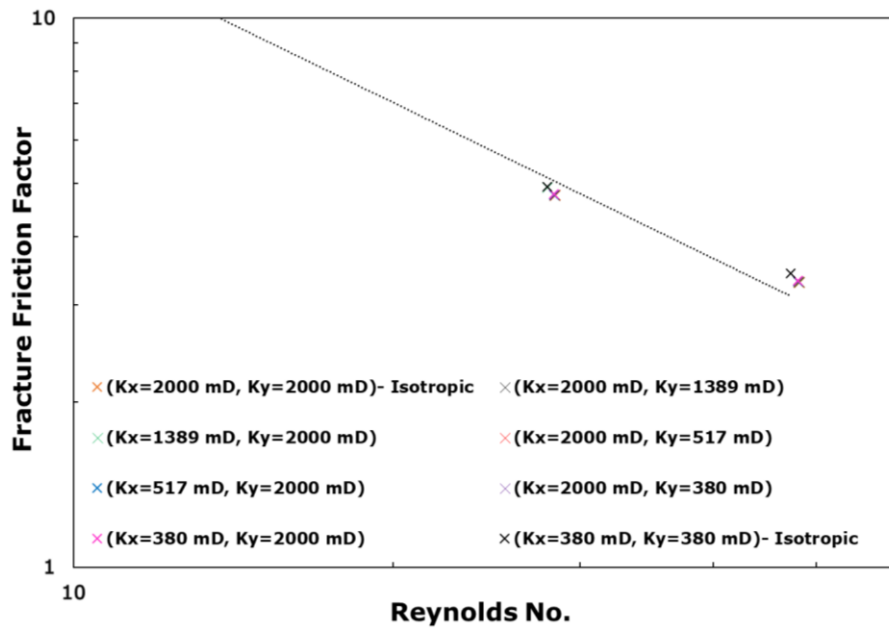


Figure 5.11 Zoom on fracture friction factor values by ANSYS CFD Fluent FVM with different scenarios of matrix isotropic and anisotropic permeability, with best fit regression line

5.5.1 Analysis and validation of the new Numerical friction factor model with the previous models, in rough fractures with anisotropic permeability

The previous fracture friction factor predictor models such as parallel plates model ($f=96/Re$), [Su et al. \(2019\)](#); [Chen et al. \(2017\)](#); [Zhou et al. \(2016\)](#); [Zhang and Nemcik \(2013\)](#); [Qian et al. \(2011\)](#); [Nazridoust, Ahmadi and Smith \(2006\)](#); [White \(2003\)](#); [Masciopinto \(1999\)](#); and [Saidi \(1987\)](#) had considered smooth parallel plates fractures with single aperture or rough fracture geometries; as well, all these models assumed impermeable fracture surfaces with no fluid interaction between fracture and matrix (except [Crandall, Ahmadi and Smith \(2010\)](#)'s model; however, this considered only isotropic matrix permeability). Thus, the new model in this study will be compared only with [Crandall, Ahmadi and Smith \(2010\)](#)'s model, to check the accuracy of this new proposed model, due to the reason that a model should be compared with a model that has similar assumptions and setup, as stated by [Zhou et al. \(2016\)](#) p. 3058. Therefore, a set of data was required to be applied in both the models, to check the trends and behaviours of each. As well, it should be noted here that [Crandall, Ahmadi and Smith \(2010\)](#)'s model considered only isotropic permeability in order to be usable and get results; therefore, isotropic permeability data was considered, and random data of Reynolds number were chosen that were used in both models. Four of these data were selected from the simulation data from each model, and the rest of the data were selected randomly below the lowest value, in between and above Reynolds number with a total of 22 points. The comparison is presented in [Figure 5.12](#) below as a Moody-type diagram on the logarithmic scale.

The behaviour difference of these two models was that [Crandall, Ahmadi and Smith \(2010\)](#)'s model values of the fracture friction factor underestimated the proposed model with 13.5% in ADV between 0.01 Reynolds number value and 25. When Reynold number reached 26 and above, [Crandall, Ahmadi and Smith \(2010\)](#)'s model values overestimated the proposed model, with ADV 16% for the selected data until 300 Reynolds number. As stated in [Crandall, Ahmadi and Smith \(2010\)](#)'s model, it was eligible for maximum Reynolds number 10 because the model did not behave linearly after 10 value of Reynolds number. However, the proposed model continues decreasing with increasing Reynolds number with a linear behaviour. It's good to note here, that although [Crandall, Ahmadi and Smith](#)

(2010)'s model is only valid until 10 Reynolds number, it was still used in this study for more values after 10 Reynolds number, in order to make the comparison with the new proposed model. The comparisons between the two models continued with higher Reynolds number values until 3000 Reynolds number. Crandall, Ahmadi and Smith (2010)'s model continued overestimating friction factor with higher deviations, while the proposed model continued with the linear behaviour. These comparisons show that the proposed model was more valid for the higher Reynolds numbers than the previous models.

More validation was conducted by checking the linearity of the proposed model, and, as stated in the previous sections, the proposed model was compared with Crandall, Ahmadi and Smith (2010)'s model only, because this was the only model that had considered fracture/matrix interaction. However, to clarify this effect, the proposed model was also compared with Nazridoust, Ahmadi and Smith (2006)'s model, because this model had also used the same geometry, but considered fracture surfaces as walls and no flow interaction between the fracture and the matrices. The outcomes of these comparisons were: the proposed model versus Crandall, Ahmadi and Smith (2010)'s showed deviation approximately 3% above the linear line with linear behaviour that is approximately parallel to the linear line, while the proposed model versus Nazridoust, Ahmadi and Smith (2006) deviated approximately more than 26% below the linear line. In addition, the deviation behaviour continued to increase with increasing the friction factor. Therefore, the proposed model showed the lowest deviation behaviour, which proved the applicability and accuracy of the proposed model, in comparison with previous models in the literature that considered no interaction between the fracture and matrix. Figure 5.13 presents these comparisons.

To analyse the effect of the behaviour of the proposed rough friction factor model for higher Reynolds number than the previous model, there are many factors that affect it, as clarified below:

1. Most of the previous models were developed based on the assumption that fracture friction factor occurs due to flow in confined or closed spaces, such as pipes, and friction results from fluid motion moving on solid surfaces, due to viscous fluid layers dragging the rough surfaces. This kind of friction relies on solid surfaces' roughness, cross-sectional area, length, fluid type and fluid flow velocity along the flow (White 2011; Ruina and Pratap 2008; Dullien 1992b;

Meriam and Henderson 1992; Saidi 1987 pp. 169-170; Swanson 1970; Eskinazi 1968). However, in rough fractures with permeable surfaces, flow proportion is changing along flow due to abrupt changes of fracture apertures, which accordingly keep changing pressure and velocity proportions at each point of fracture and friction value (Karimzade et al. 2019; Briggs, Karney and Sleep 2017; Dippenaar and Van Rooy 2016; Qian et al. 2011; Crandall, Ahmadi and Smith 2010; Karpyn, Grader and Halleck 2007; Tiab and Donaldson 2004 p. 459).

2. As matrix / fracture interact, and fluid continues moving between these two media due to pressure/velocity changes in the open fracture and surrounding matrix, both share the same physical space with the interface layer separating them, and effects on each other through this layer (Lu et al. 2017; Popov et al. 2009; Golf-Racht 1982). At this interface layer, which can be called "skin friction layer", shear resistance forces between fracture flow and solid surfaces occur, and generate fluid flow resistance (Winterton 2014 chap. 6; White 2011 p. 317; Saidi 1987 p. 171). This interface layer is affected by fluid movement (fluid jump) conditions between matrix and fracture and vice versa; as well, by the components of tangential velocities inside the fracture, which are aligned with bulk fracture flow, will change direction based on fracture shape and roughness, and will have effects on fluid movement proportions through interface layer (Zou, Jing and Cvetkovic 2017; Sahimi 2011; Nelson 2001; Oron and Berkowitz 1998; Saidi 1987). Both these operations of fluid movement have varied effects and directions, and will have an effect on fluid stresses in both media. Particularly, the seepage of the skin fluid layer that is attached to the fracture's solid surface; then, shear stresses of fracture flow resistance at fracture surface layers will be affected accordingly (Lei et al. 2015; Rasouli and Rasouli 2012; Popov et al. 2009; Lang, Paluszny and Zimmerman 2014; Oron and Berkowitz 1998). The effects of interface layer in rough fractures are higher due to the following facts: rough fractures have bigger areas of contact with surrounding matrix; and also surface roughness and abrupt fracture aperture changes along a fracture have effects on flow, as the narrow corners with sharp edges create clusters of fluid movements between fracture and matrix, due to velocity/pressure variation, leading fluid to use different paths. Moreover, pore structure of the interface layer in a rough fracture has higher heterogeneity structure, which affects adsorption of fluids in formations, and spatial pressure

gradients inside a fracture will have high effects on fluid movement, and accordingly on skin fluid layer of fracture flow, which affects shear resistance of flow (Li et al. 2021; Andersen and Zhou 2020; Wu et al. 2019; Yang et al. 2019; Yin et al. 2017; Dippenaar and Van Rooy 2016; Rasouli and Rasouli 2012; Sahimi 2011 pp. 45, 244; Popov et al. 2009; Ingham and Pop 2005 p. 367; Lespinasse 2000; Zimmerman and Bodvarsson 1996 pp. 44-45; Saidi 1987 p. 178).

3. The proportion of fluid movement between matrix and fracture through interface permeable fracture surfaces changes along the fracture flow due to: fracture apertures abruptly changing, fracture surface roughness; and anisotropic matrix permeability variations in in-plane K_x and through plane K_y . As well, flow in matrix with fracture flow effect is non-linear flow and varied from point to point (Dippenaar and Van Rooy 2016; Lei et al. 2015; Rasouli and Rasouli 2012; Tiab and Donaldson 2004 p. 103; Hidayati, Chen and Teufel 2000; Saidi 1987 p. 82; Parsons 1966; Scheidegger 1963). As rough fractures have a high degree of non-uniform pressure decrease and less flow channelling, therefore, this has reflected the ability to verify pressure variations locally (micro-scale) along the flow (Zou, Jing and Cvetkovic 2017; Ishibashi et al. 2012; Rasouli and Rasouli 2012; Crandall, Bromhal and Karpyn 2010; Crandall, Bromhal and Smith 2009). Therefore, fracture friction factor has to be measured in a certain average length instead of point to point, to observe overall pressure drops (White 2003).
4. Eddies' effects in changing velocities create zones of fluid recirculation, called "eddies or vortices zones" (Briggs, Karney and Sleep 2017; Briggs, Karney and Sleep 2014). It was reported that eddies zones can be considered as zones of fluid momentum exchange between matrix on one side and fracture main bulk flow on the other (Chen et al. 2017), and will increase with increasing fluid flow velocity in a fracture due to the inertial effects of fluid (Karimzade et al. 2019; Briggs, Karney and Sleep 2017; Dippenaar and Van Rooy 2016).

Thus, as clarified in the above points, the proposed model had a better chance of accurately predicting fracture's friction factor, by accounting for more conditions of flow in rough fractured subsurface, such as: fracture tortuosity; roughness; matrix/fracture interaction; and anisotropic permeability of the matrix that surrounds fracture surfaces in both directions in plane K_x and through plane K_y .

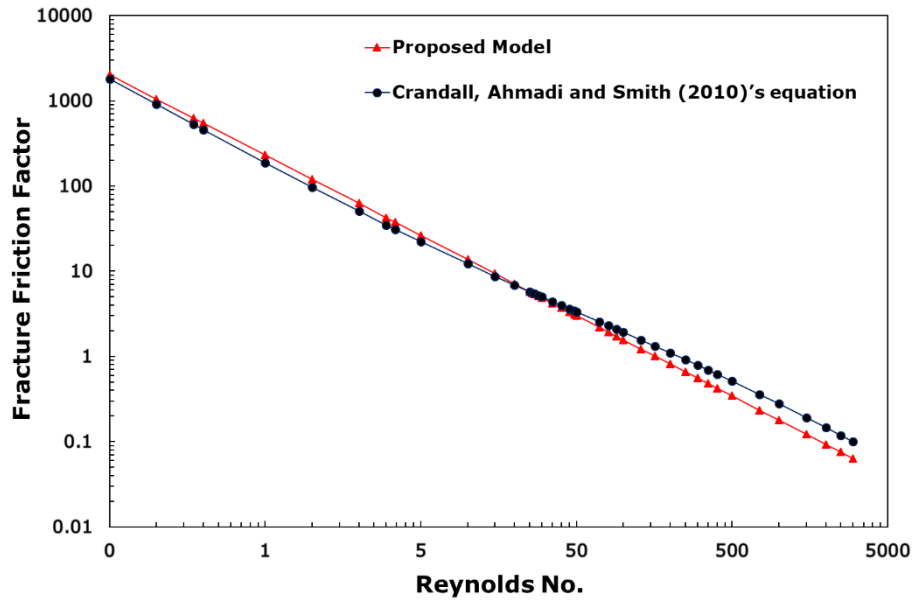


Figure 5.12 Comparison of the friction factor versus Reynolds number between the proposed model (equation 5.29) and Crandall, Ahmadi and Smith (2010)'s equation

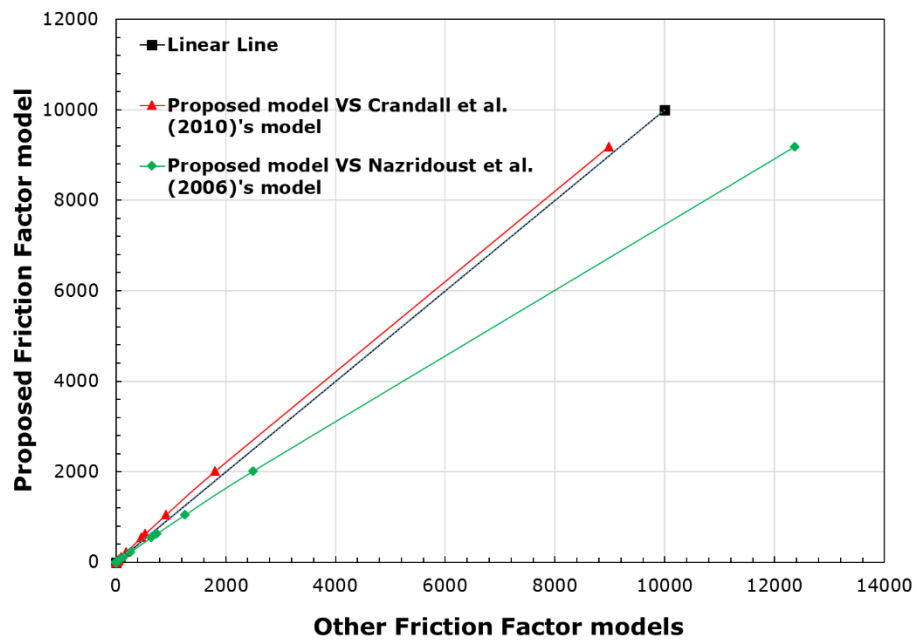


Figure 5.13 linearity of the Proposed friction factor versus other friction factor models

5.6 Conclusion

In this chapter, friction factor values were extracted and investigated in rough fracture geometry by ANSYS CFD Fluent FVM fracture models. As well, many conditions were applied, such as: impermeable and permeable fracture surfaces, to consider fracture/matrix interaction and fluid movement; and isotropic and anisotropic matrix permeability with many different scenarios. The outcomes were:

1. Fracture/matrix interactions with consideration of anisotropic matrix permeability, in both directions in-plane K_x and through plane K_y , had significant effects on rough fracture friction factor values. This led to the conclusion that considering mimicked conditions of subsurface flow in fracture modelling will result in the most optimised results calculations of fracture friction factor.
2. In this chapter, two new proposed rough fracture friction factor models were developed that accounted for anisotropic matrix permeability along the fracture flow with different matrix layers, varied matrix permeability in X and Y Cartesian directions in the same layer, and fracture roughness and tortuosity. The first model, analytical model, was applicable until Reynolds number valued equal or less (≤ 10). This model was validated with ANSYS CFD Fluent FVM [fraction factor values](#) and with the literature paper of [Crandall, Ahmadi and Smith \(2010\)](#)'s model (as clarified in [section 5.4.1](#)), and the results showed that the proposed model had better prediction of fracture friction factor. In the second model, a numerical model from ANSYS CFD Fluent FVM simulations, friction factors were extracted with different isotropic and anisotropic permeability scenarios, with fracture/matrix interactions and fluid movement, by using best-fit regression line, and validated with the previous models of [Crandall, Ahmadi and Smith \(2010\)](#) and [Nazridoust, Ahmadi and Smith \(2006\)](#). This model had a linear behaviour with varied Reynolds number and was suitable to be used until Reynolds number value 3000, while most of the previous models were only valid until Reynolds number valued equal or less (≤ 10). As well, the linearity of the proposed model was compared with the previous models from literature, and the new model showed very low deviation, due to the reasons clarified in [section 5.5.1](#).

6 Fracture Networks

6.1 Overview

As clarified in Chapter Two, fractures in naturally fractured subsurface layers/reservoirs are generated in these rocks by the effects of complex stress/strain distributions which take various irregular shapes, sizes and lengths. Most of these fractures connect together and create fracture networks with different and complex patterns, and these patterns are mostly irregular; as well, other types exist where fractures are located discretely with no connections among them, except matrix media (Li et al. 2021; Luo et al. 2020; Yi and Xing 2018; Lu et al. 2017; Hyman et al. 2015; Rasouli and Hosseinian 2011; Sahimi 2011; Crandall, Bromhal and Smith 2009; Nelson 2001 pp. 12, 217; Golf-Racht 1982). Flow simulations of reservoir/subsurface models, in general, represent geological properties (porosity, permeability, etc.) and interaction with fluid properties (viscosity, fluid type, etc.) to visualise fluid flow, in order to facilitate understanding of fluid flow behaviour in that particular media. Modelling entire fractured media as a big scale is the main goal, but the main challenge is to include all the heterogeneous properties in such a model. One of the main reasons for this challenge is fractures' fractured network orientations, and connection in relation to flow direction, as fractures are located randomly with different angles and locations, which may or may not be ordinated with the flow axis (Sahimi 2011; Tiab and Donaldson 2004; Nelson 2001 p. 32; Sen 1995; Golf-Racht 1982). Therefore, a core scale model of subsurface media that, included as many variables as possible, would be a good representation of subsurface media (Glover and Hayashi 1997). Having reflected these scenarios of fractured media heterogeneous properties, and to the best finding of this study, there were limited studies carried out using ANSYS CFD Fluent FVM to investigate flow in fracture networks, with limitations such as: using parallel plates fractures with single aperture, impermeable fracture surface (flow in fractures only, and excluding fracture/matrix interface layer interaction and fluid movement), and considering isotropic matrix properties, as reported by Suri et al. (2020); Roslin, Pokrajac and Zhou (2019); Liu, Li and Jiang (2016); Rasouli and Hosseinian (2011); and Sarkar, Toksöz and Burns (2004).

As proved and validated in Chapter 4 of this research, by using ANSYS CFD Fluent FVM models, the effects of single fracture geometry (parallel plates and rough fractures), and the inclusion of matrix flow, effect on the entire fracture domain flow with both conditions of isotropic and anisotropic matrix permeability. Therefore, to get an optimised and most accurate visualization of flow in fractured media, it was necessary to mimic flow conditions of fractured networks in an ANSYS CFD Fluent FVM model that had optimised boundary conditions, which had not been considered in previous studies of the literature with ANSYS CFD Fluent FVM models. Therefore, the fracture networks in this research were used to create models by using ANSYS CFD Fluent FVM, and included multiple heterogeneous conditions of fractured networks that were reported in literature by [Li et al. \(2021\)](#); [Luo et al. \(2020\)](#); [Suri et al. \(2020\)](#); [Luo, Tang and Zhou \(2019\)](#); [Roslin, Pokrajac and Zhou \(2019\)](#); [Wu et al. \(2019\)](#); [Yi and Xing \(2018\)](#); [Lu et al. \(2017\)](#); [Zou, Jing and Cvetkovic \(2017\)](#); [Liu, Li and Jiang \(2016\)](#); [Hyman et al. \(2015\)](#); [Rasouli and Hosseinian \(2011\)](#); [Sahimi \(2011\)](#); [Popov et al. \(2009\)](#); [Nelson \(2001\)](#) and [Golf-Racht \(1982\)](#). These were conditions such as: first, rough fracture geometries in networks with different fracture apertures and fractal properties; second, fracture/matrix interaction (including fracture/matrix interface layer interaction and fluid movement between through permeable fracture surfaces); third, isotropic ($K_x=K_y$) and anisotropic ($K_x\neq K_y$) matrix permeability surrounding the fracture network; and fourth, different fracture network patterns with horizontal and inclined orientations with respect to flow in Cartesian coordinates, with worst case scenario effects on fracture network flow at angle 45° ([Zhu et al. 2020](#); [Luo, Tang and Zhou 2019](#); [Di Fratta et al. 2016](#); [Popov et al. 2009](#)), in order to accurately investigate fracture pattern effect on flow in fractured network domains. The details of creating the ANSYS CFD Fluent FVM fracture network models are clarified in the following sections.

6.2 Fracture Network Scenarios

In order to get optimised conditions of studying flow in fractured media, it was mandatory to have scenarios of fracture patterns which were similar or in close orientation to a real fractured media. Therefore, an image of real fractured media, which consisted of the fracture network and surrounding matrix, was used from a referenced journal as reported by [Yi and Xing \(2018\)](#). In the referenced fractured media image, there were many patterns of network scenarios that could be

selected for the investigation. Therefore, the criteria were set to represent several combinations of flow conditions inside each network, to widen the investigatory vision by including many options of fractured media such as: different numbers of inlets and outlets fracture in the network domain; varied network patterns with horizontal and inclined orientations with respect to flow in Cartesian coordinates; a pattern with fractures in the middle of the matrix and connection between inlet and outlet fractures; a network pattern that has inlet fractures but without outlet fracture, except outlet through the matrix; and, that each pattern shall contain at least two fractures in the domain, as [Ruhland \(1973\)](#) stated that a fracture network model should contain at least two fractures inside its fractured domain. Thus, five scenarios were selected from the referenced image of a real fracture network which were suitable with the set criteria of this research. These five patterns of networks represented several different conditions, and enabled a better understanding of flow in fractured networks. As well, this was confined by the available computational resources and simulation times of these models, based on Chapter 4's single rough fracture, (approximately 3.5 million cells, which consumed much time of computers with high spec capabilities to achieve the simulations, around 6-7 hours for each simulation to be converged), and the time prediction was greater in network model simulations due to the higher number of cells needed. Each scenario of these five patterns was clarified in the following sections below. [Figure 6.1](#) clarifies the locations of each of these scenarios.

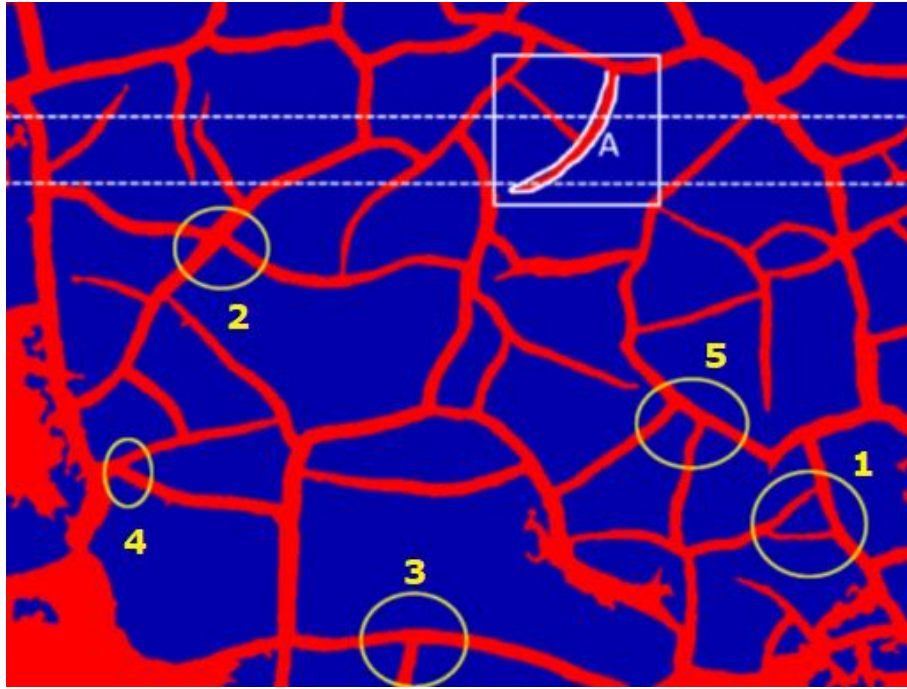


Figure 6.1 Fractured domain image (the selected five scenarios are marked with yellow circles and number 1 to 5) (Yi and Xing 2018)
([permission for academic re-use from Elsevier Number: 4755050991062](#))

6.3 Fracture Networks modelling

6.3.1 Geometry descriptions

After selecting the scenarios, it was important to choose a fracture geometry that would be used to structure these networks. The goal was to create five fracture network geometries in five separate models in the middle of the matrix domain, with a square shape sized (10.15x10.15) cm, by ANSYS CFD Fluent FVM Design Modeler. It was crucial to build fracture networks for which the statistical features and fractures' fractal properties of each network were known, in order to be able to build the fractal data of each fracture network, to help in establishing comparisons among network models and diagnose fracture properties' effects on fractured network flow. As stated in section 6.1, in order to get optimized flow in fractured network media, it was mandatory to use a rough fracture to get the most accurate results. Therefore, the horizontal rough fracture that was built and

modelled in Chapter 3 and 4 was used to construct these fracture networks, because this fracture's properties were calculated and known; as well, it originated from a real fracture geometry. However, each network had a different orientation pattern, different fracture locations inside the domain, and varied inlets and outlets along the domain. Constructing fracture networks from a single horizontal rough fracture in this manner results in different fracture network properties. Thus, the networks of this research consisted of real fracture geometry with real network patterns, which gives more credit to the models of this research as it gives better vision of flow in real fracture networks. The fractal properties of each network are further clarified below in each network description. It's good to note that all the angles in each of these networks were considered 45° , because 45° has the highest negative effect on flow in porous media and fractures, as stressed by [Zhu et al. \(2020\)](#); [Luo, Tang and Zhou \(2019\)](#); [Di Fratta et al. \(2016\)](#) and [Popov et al. \(2009\)](#).

6.3.2 Fracture network geometries

ANSYS CFD Fluent FVM Design Modeler was used to draw the geometry of each network. The task was to create the fracture network of each pattern, in the middle of the matrix domain, with a square shape (10.15x10.15) cm. First, the matrix domain was drawn with (10.15x10.15) cm, then a rough fracture geometry was re-created to match the pattern of each network. The statistical features of fracture aperture of each network are clarified in the following section. The geometry description of these networks is as following:

Fracture Network 1 model had a similar pattern to the first scenario, which mimicked a real case in a fractured domain with one fracture inlet, one fracture outlet and one fracture end at the matrix without outlet. This network consisted of: one full fracture from the top end to the outlet (left to right) with 45° clockwise from X-Cartesian axis; (2/3) of the full fracture from the inlet and connecting to the fracture (left to right) with 45° anti-clockwise from X-Cartesian axis; and the last section was (2/3) of the full fracture, with horizontal orientation, that connected between the two fractures. Fracture Network 2 model had a similar pattern to the second scenario, which mimicked a real case in a fractured domain with one fracture inlet and three fractures ending at the matrix with angles without fracture outlet. As well, it's good to note that this was the only scenario in the

fracture network models that did not have a fracture outlet in the entire fractured domain. This network consisted of: one full fracture and (1/3) of full fracture from the inlet to the matrix (left to right) with 45° clockwise from X-Cartesian axis; and one full fracture and (1/3) of full fracture from bottom matrix to the top matrix (left to right) with 45° anti-clockwise from X-Cartesian axis, These two fractures connected in the centre of the domain. Fracture Network 3 model had a similar pattern to the third scenario, which mimicked a real case in fractured domain with one fracture inlet and two fracture outlets. This network consisted of: one full fracture and (1/3) of full fracture from the inlet to the outlet (left to right) with 45° anti-clockwise from X-Cartesian axis; and (2/3) of the full fracture from the middle of the domain to the outlet with 45° clockwise from X-Cartesian axis, These two fractures connected in the centre of the domain. Fracture Network 4 model had a similar pattern to the fourth scenario, which mimicked a real case in fractured domain with two fracture inlets and one fracture outlet. This network consisted of: one full fracture from the inlet to the outlet (left to right) with horizontal orientation and parallel to the flow direction; and (2/3) of the full fracture from the inlet, connecting with the horizontal fracture outlet (left to right) with 45° anti-clockwise from X-Cartesian axis. And last, Fracture Network 5 model had a similar pattern to the fifth scenario, which mimicked a real case in fractured domain with one fracture inlet, one fracture outlet and two fractures ending at the matrix without outlet. This network consisted of: one full fracture and (1/3) full fracture from the top end to the outlet (left to right) with 45° clockwise from X-Cartesian axis; (2/3) of the full fracture from the inlet, connecting to the longest fracture (left to right) with 45° anti-clockwise from X-Cartesian axis; and the last fracture was (1/3) of full fracture from the bottom end, connecting to the longest fracture (left to right) with 45° anti-clockwise from X-Cartesian axis. [Figure 6.2](#) clarifies fracture networks.

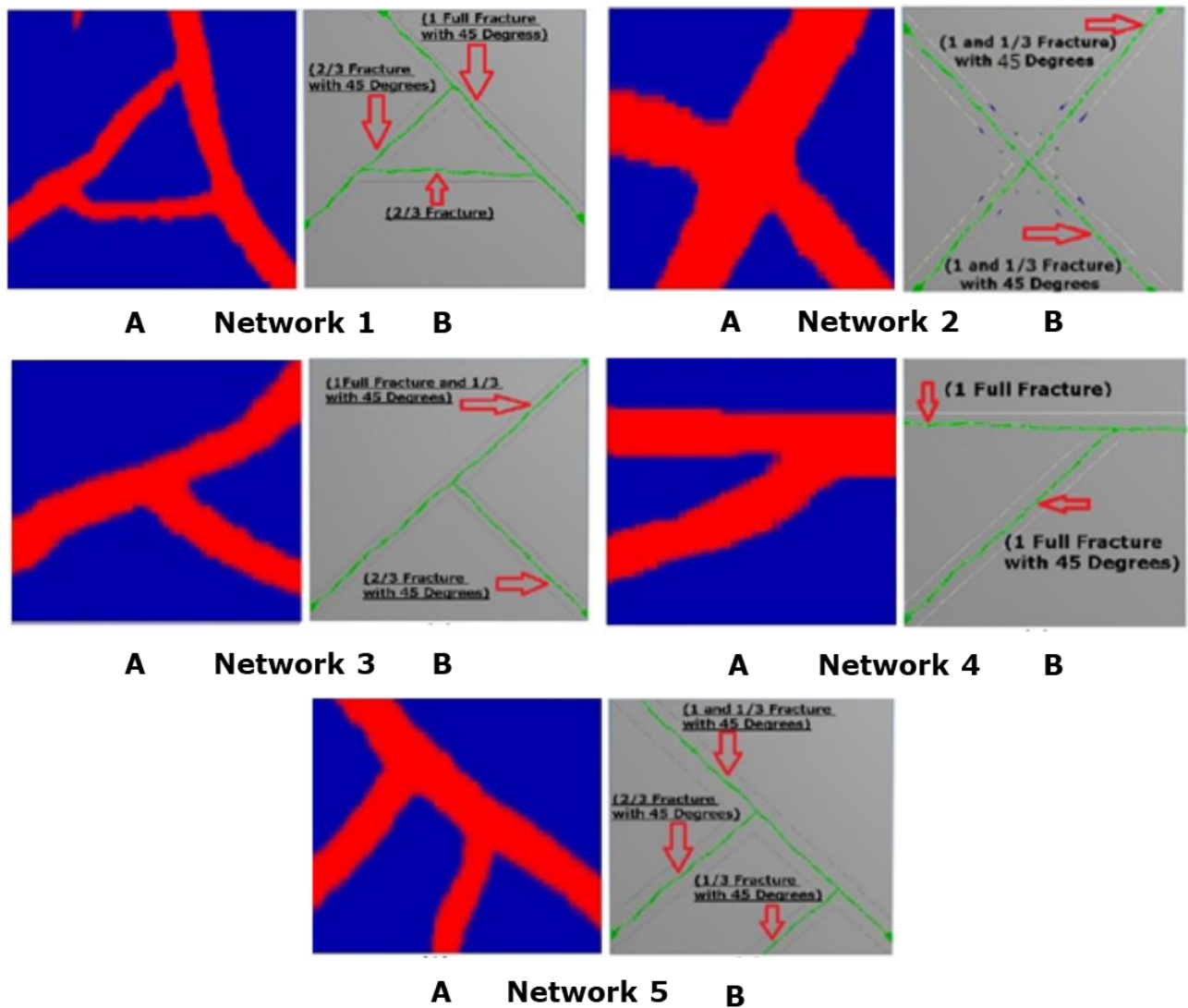


Figure 6.2 Fracture network geometries

A. Pattern scenarios 1 to 5 from [Figure 6.1](#); B. fracture networks geometries ANSYS CFD Fluent FVM Design Modeler with written descriptions (fracture is green, matrix is grey)

6.3.3 Fractal properties of fracture networks

The five scenario models of fracture networks were constructed with the same size domain (10.15 X 10.15) cm and the inlet and the outlet of the flow passed with the same direction (left to right), which was parallel to the x-axis in Cartesian directions with the same pressure drops in the domain of these models. Therefore, to check the effects of fracture network scenarios on the flow of the domain outlet flow (fracture and matrix flow proportions), it was necessary to check the fractures' fractal properties "the statistical features of fracture aperture" of each network, which were: standard deviation, normal distribution, and fracture aperture frequency; in addition, fracture and matrix areas were calculated of each network's mode ([Liu, Li and Jiang 2016](#); [Rasouli and Hosseinian 2011](#); [Crandall, Ahmadi and](#)

Smith 2010; Crandall, Bromhal and Smith 2009; Karpyn, Grader and Halleck 2007; Nazridoust, Ahmadi and Smith 2006; Tiab and Donaldson 2004; Nelson 2001; Sen 1995; Saidi 1987; Golf-Racht 1982). These properties enabled quantitative comparisons to be conducted among these network scenarios, in addition to the patterns, orientations and angles of the fracture networks inside each domain.

In each fracture network model, the fracture apertures' frequency was calculated, the standard deviation formula was applied as equation 6.1 below, and lastly, the normal distribution was calculated to check the apertures' distribution based on the standard deviation of each network. Table 6.1 below clarifies the process of these calculations in network 1, and similar calculations for the other networks were conducted. Table 6.2 clarifies the total statistics of all fracture network models, and Figure 6.3 clarifies the normal distribution which reflects marginal differences in network 1, 2 and 5, due to varied standard deviation values of fractures apertures in these networks.

$$\sigma = \sqrt{\frac{1}{N} \sum_{i=1}^N (X_i - \mu)^2} \quad (6.1)$$

Where; σ = standard deviation, X = fracture aperture, μ = average fracture apertures (Rasouli and Hosseinian 2011; Crandall, Ahmadi and Smith 2010; Nazridoust, Ahmadi and Smith 2006; Nelson 2001)

Table 6.1 Fracture network 1 calculations of apertures' frequency and the standard deviation

Fracture Height (Xi) (micron)	Frequency (N) (Number of Sections)	Sum of Fracture Apertures Heights to get Average Aperture (Xi * N)	Average Aperture (μ) (micron) ($\sum (Xi * N) / \sum N$)	(Xi- μ) ²	[(Xi- μ) ² * Frequency (N)]	The standard deviation
240	83	19920	591.850	123798.505	10275275.91	$\sigma = \sqrt{\frac{1}{N} \sum_{i=1}^N (X_i - \mu)^2}$
480	144	69120	591.850	12510.449	1801504.612	
720	137	98640	591.850	16422.392	2249867.771	
960	58	55680	591.850	135534.336	7860991.504	
1200	2	2400	591.850	369846.280	739692.5602	
1440	0	0	591.850	719358.224	0	
1680	1	1680	591.850	1184070.168	1184070.168	
2640	2	5280	591.850	4194917.943	8389835.886	
	427	252720			32501238.41	275.890
	($\sum N$ =Total Sections)					

Table 6.2 Summary of all fracture networks' calculations, such as: apertures' frequency (total sections), the standard deviation, (%) fracture/matrix area in the domain

Fractures Networks	Number of Sections	Average Aperture (μ) (micron)	The standard deviation (σ)	Fracture area (m^2)	Matrix area (m^2)	(%) Fracture area in models
1	427	592	276	0.00016224	0.010144	1.60
2	473	610	332	0.00017719	0.010129	1.75
3	376	609	322	0.00013533	0.010171	1.33
4	376	609	322	0.00012884	0.010177	1.27
5	424	603	295	0.00015175	0.010155	1.49

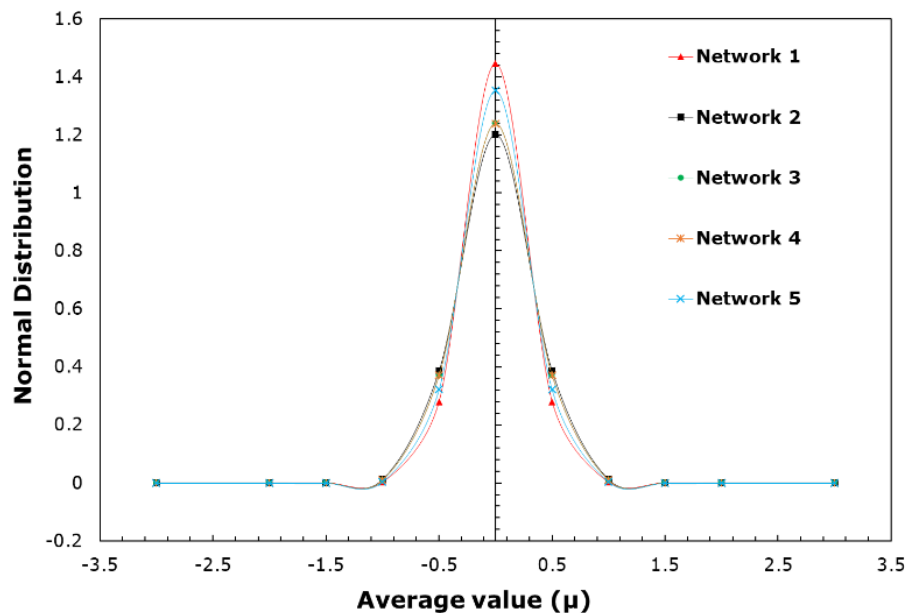


Figure 6.3 Normal distributions of fracture networks

6.3.4 Meshing fracture networks

As clarified in Chapter 3 and 4 sections 3.5.1.2, 3.5.2.3, 4.2.1 and 4.3.1 meshing the geometry was a very important step due to the high effect on the results' accuracy if the mesh is not good quality; as well, it's one of the main steps in the pre-processing of the ANSYS CFD Fluent FVM (ANSYS 2013; Versteeg 1995). In this stage, two main operations of pre-processing were achieved: first, meshing the geometry; and second, the geometry boundary conditions were named. The geometry of each fracture network model was divided into three sections: the fracture; the matrix around the fracture; and the rest of the matrix media. As clarified in Chapter 3, each section of the models was assigned with different sizes

of cells based on the priorities. The fracture and the matrix surrounding the fracture were assigned with finer mesh from the rest of matrix, in order to have the best results possible of interaction between fracture and matrix; as well, efficient and limited numbers of cells of the domain were needed in order to reduce the time consumptions of simulation times.

The mesh was created by the ANSYS DesignModeler (pre-processing) which was an automatic mesh with element size type. The mesh cell shapes were triangles in the fracture network models, due to the irregular shapes of the fractures with angles and the surrounding matrix; it's good to note that there were other cell shapes selected such as quadrilateral based, however, the ANSYS DesignModeler failed to process the meshing of these geometries. As mentioned in [Section 6.3.3](#), the fracture and matrix areas were varied based on each network's pattern, and are clarified in [Table 6.2](#). Therefore, best effort was conducted in this research modelling to choose the most efficient cell numbers, to reduce time consumptions of the simulations. Thus, the cell size of each section of each model was varied among the models. The far matrix zone was assigned with different values as (144, 120, 96) micrometre among the models. The fracture zone, which had the highest priority, was assigned with 12 micrometre in all the models. The matrix near the fracture zones (2nd highest priority after the fracture) was assigned with different values as (72, 48) micrometre among the models. [Figure 6.4](#) below clarifies an example of the zones and meshes of networks. The total mesh cells number of the entire domain was varied for each fracture network model and is clarified in [Table 6.3](#) below.

It's good to note that grid sensitivity analysis of the fracture network models was not conducted, due the reason that the lowest mesh cells number was more than 4 million and 2 hundred thousand cells. The rest of fracture networks used much more than this cells number for analysis of the fracture network, reaching to more than 6 million in one case. As seen that this is more than the grid sensitivity analysis presented in Chapter 4 of rough fracture, therefore this mesh size was sufficient to produce suitable results; in addition, more cells would have added complexity and processing times.

The following step after completing the meshing step was naming the boundary conditions of the domain, which were: inlet; outlet; interior fracture; interior matrix; and symmetry edges of the matrix, similar to the fracture boundaries in the previous chapter as stated in [Chapter 3 Sections 3.5.1 and 3.5.2](#). At this stage,

the mesh was completed and the domain was ready to be transferred into post-processing stage in FLUENT solver, version 18.1; all the details are clarified in [Appendix 2](#).

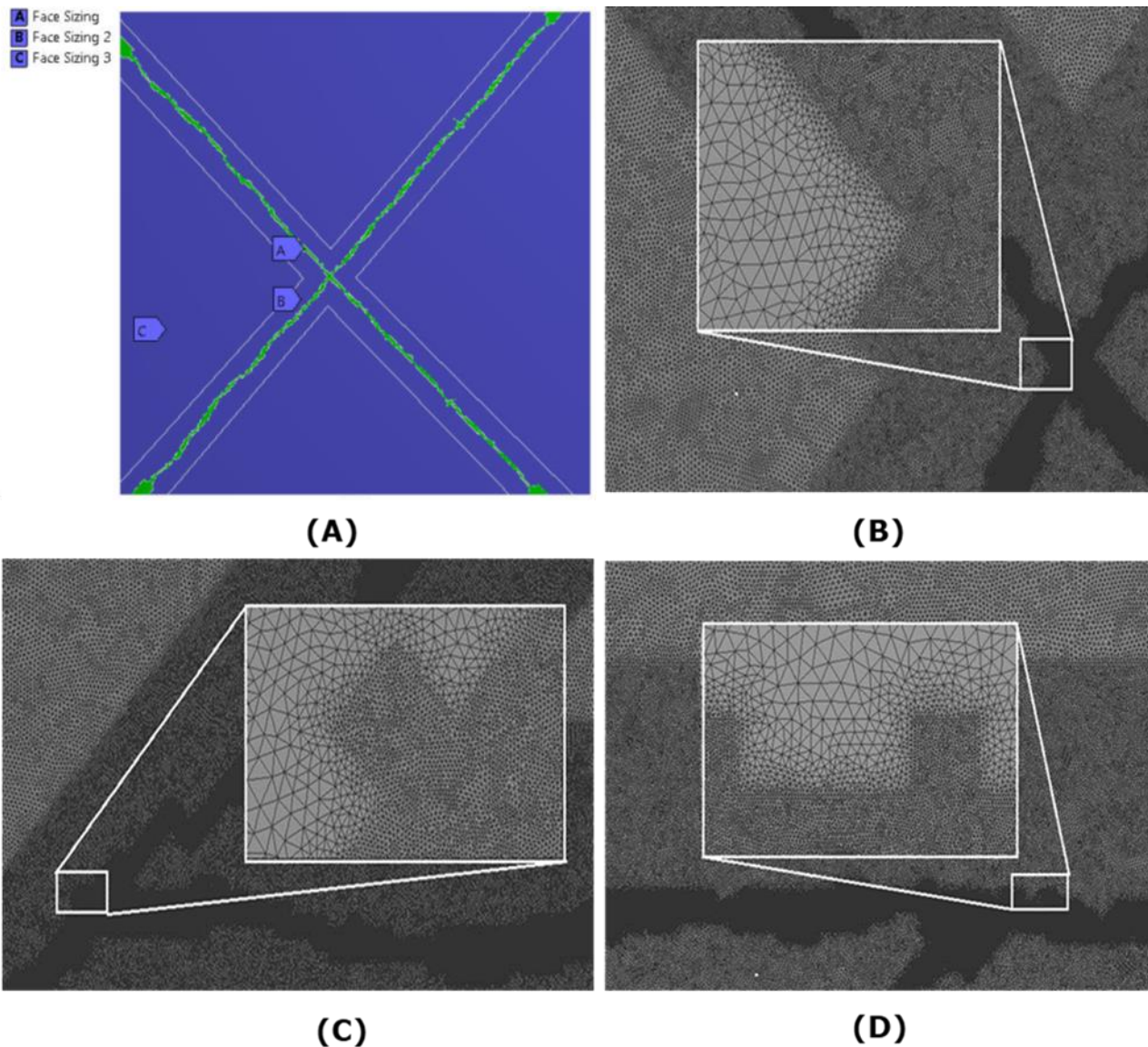


Figure 6.4 Samples of fracture network meshing and face sizing zones by ANSYS DesignModeler

A. Zones of face sizing meshing of network 2 (fractures are green, matrix is dark blue); B. Section in fracture network 2 mesh; C. Section in Fracture network 1 mesh; and D. Section in fracture network 4 mesh

Table 6.3 Mesh statistics of fracture network models

Fractures Networks	Cells number	Faces	Nodes	Partitions
1	6043204	9067373	3024170	6
2	5067791	7603984	2536194	6
3	5360306	8043074	2682769	6
4	4224751	6339247	2114497	6
5	4388247	6584297	2196051	6

6.3.5 Extracting results from surface lines of ANSYS CFD Fluent FVM fracture network simulations

To read the data from the ANSYS CFD Fluent FVM model simulations, separate surface reading lines were created inside the ANSYS CFD Fluent FVM models to read the X-velocity profiles. First, the total reading line, which passed through fracture and matrix to read the X-velocity profile of the total fractured network domain, just before the outlet at (X, Y) coordinates (0.1, 0) (0.1, 0.10152)m; it's good to note that this line was in the same coordinates for all five network models. Second, inside the fractures only at the smallest fracture section, 240 micrometre, which was near to the same location of the total reading line near the outlet to read X-Velocity profile inside fracture only. However, it's good to note that the coordinates of these lines inside fractures were varied with small variations in X and Y-Cartesian coordinates; also, the orientations of these reading lines inside fractures were perpendicular on the fracture section, in case the fracture had an angle orientation above or below 0°. In addition, when some of the networks had two outlet fractures, then two lines inside the fractures were created. [Figures 6.5 and 6.6](#) illustrate samples in some networks of observed velocity profiles from these lines of total domain and inside fractures.

From these X-velocity profiles, the average velocity of each profile was calculated, then, the flow rates were calculated for the total domain and inside the fracture only, similarly as presented in [Chapter 4 Section 4.2](#), but with a little difference for calculating matrix flow rate; first, the total and fracture flow rates were calculated, then, from the total flow rate and fracture flow rate, the matrix flow rate could be observed. The below [equations 6.2, 6.3 and 6.4](#) clarify the case for all the network models' flow calculations.

$$Q_{\text{Total}} = A_{\text{Total}} \times V_{\text{Total}} \quad (6.2)$$

$$Q_{\text{fracture}} = A_{\text{fracture}} \times V_{\text{fracture}} \quad (6.3)$$

$$Q_{\text{Matrix}} = Q_{\text{Total}} - Q_{\text{Fracture}} \quad (6.4)$$

Where: Q_{Total} & Q_{fracture} = total and fracture flow rates (m^2/s or mm^2/s), A_{Total} = total domain height as one dimension, V_{Total} = average value of X-velocity profile of the total reading line, V_{fracture} = average value of X-velocity profile of fractures reading line only, A_{fracture} = fracture aperture height as one dimension, Q_{Matrix} = matrix flow rate (m^2/s or mm^2/s)

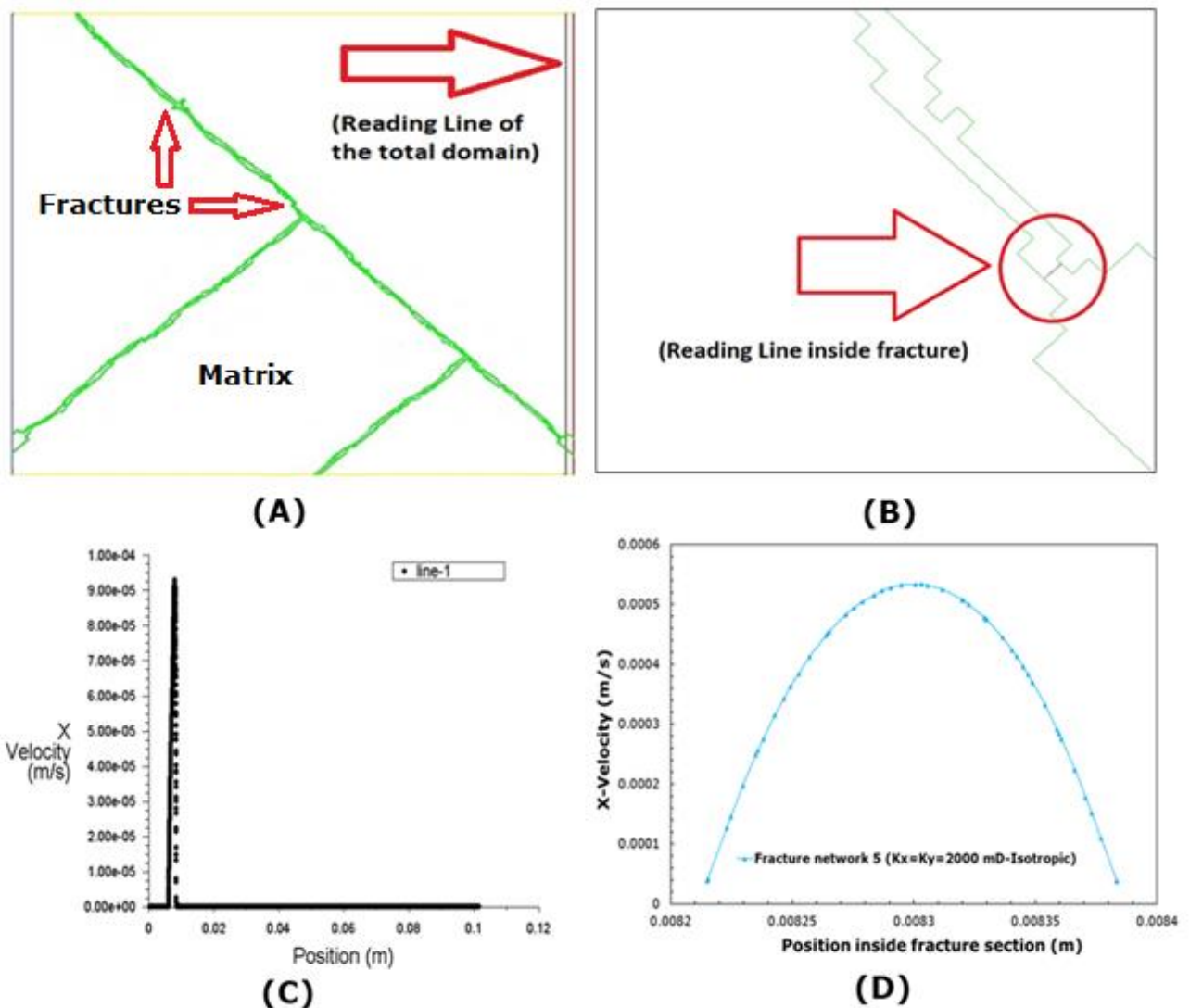


Figure 6.5 Fracture network 5 reading surface lines and X-velocity profiles extracted from ANSYS CFD Fluent FVM fracture models

A. Reading line inside the total domain (fracture is green, matrix is white); B. Reading line inside the fracture only; C. X-velocity profile of total domain (fracture and matrix) with $K_x=K_y=2000$ mD $P=5$ Pa; and D. X-velocity profile inside fracture only, $K_x=K_y=2000$ mD $P=5$ Pa

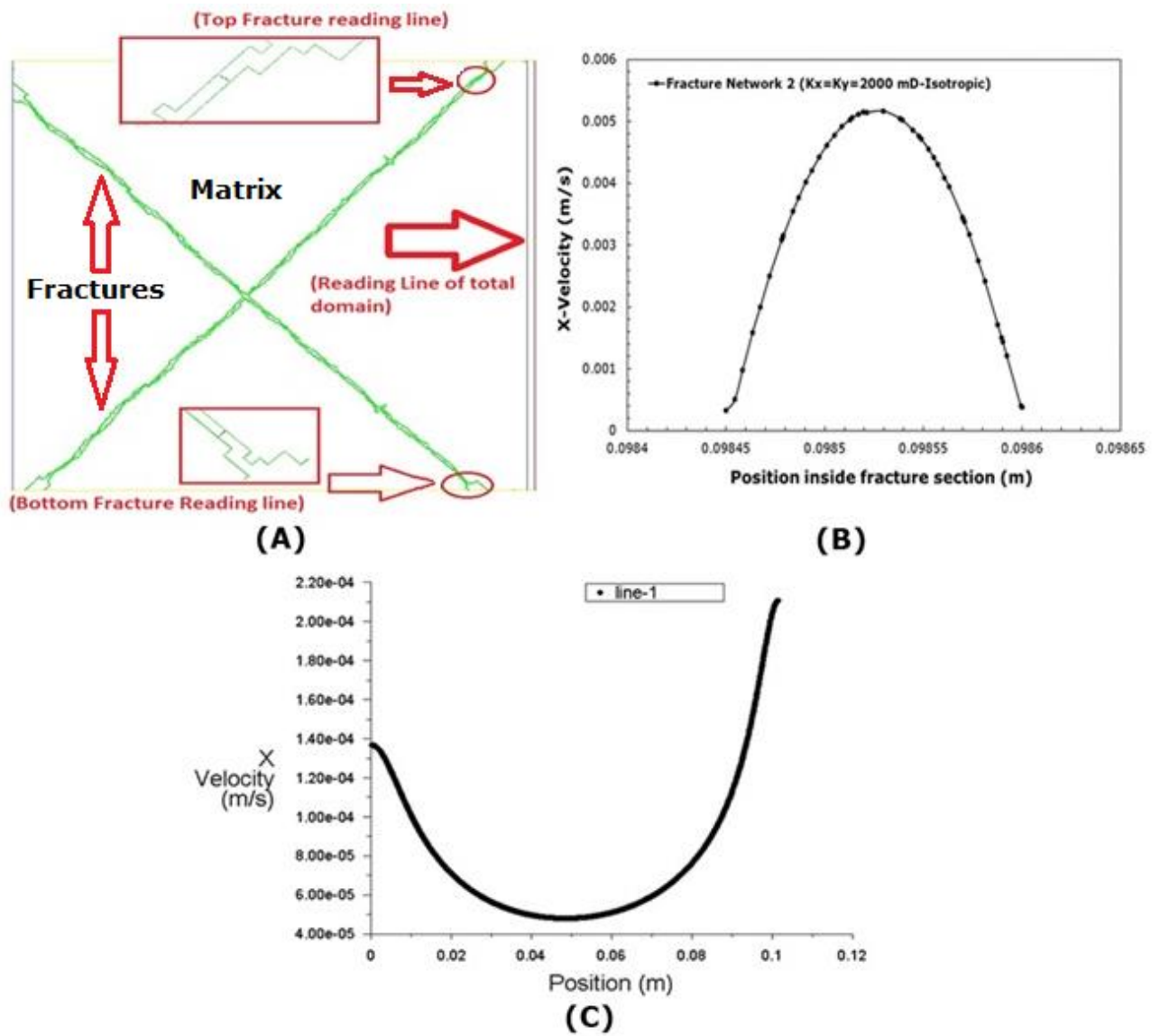


Figure 6.6 Fracture network 2 reading surface lines and X-velocity profiles extracted from ANSYS CFD Fluent FVM fracture models

A. Reading lines inside the total domain (fracture is green and matrix is white); B. X-Velocity profile inside one of the fractures (top fracture) in network 2 with $K_x=K_y=2000$ mD $P=1000$ Pa; and C. x-velocity profile of total domain (matrix only) with $K_x=K_y=2000$ mD $P=1000$ Pa

6.3.6 Fracture network simulations results

Li et al. (2021); Wang et al. (2020); Dippenaar and Van Rooy (2016); Singh, Singh and Pathegama (2014); Spence et al. (2014); Rasouli and Hosseinian (2011); Sahimi (2011); Crandall, Bromhal and Smith (2009); Ingham and Pop (2005) p. 367; Tiab and Donaldson (2004) p. 469; Berkowitz (2002); Nelson (2001); Golf-Racht (1982); Zimmerman and Bodvarsson (1996); Saidi (1987) and Ruhland (1973) stressed that fractured subsurface formations have highly anisotropic properties of fractures and matrices. Therefore, to have the best vision of flow in fractured media, five fracture network patterns were adopted in five ANSYS CFD Fluent FVM models. In all the simulations, the fracture surfaces were set as permeable "Interior faces boundary" to investigate the effects of isotropic and anisotropic matrix permeability on fracture network flow and entire fracture domain; these were isotropic matrix permeability ($K_x=K_y=2000$ mD), and two anisotropic scenarios ($K_x=2000, K_y=380$) mD and ($K_x=380, K_y=2000$) mD, with 81% permeability changing between K_x and K_y as Table 6.4 below, 20% matrix porosity, and different pressure drops (5, 100, 1000, 2000) Pa with zero pressure outlets. The calculations of each fracture network's model were observed for isotropic and anisotropic matrix permeability. Then, total comparisons among the fracture networks were conducted to finalize these fracture patterns' effects on the domain. The below sections clarify these results. These fracture network models included many heterogeneous properties of fractured formations, such as: rough fractures, different network patterns in each network model, and isotropic and anisotropic matrix permeability, as permeability has a high effect on subsurface formations as clarified in Chapter 4. In each simulation, many calculations were observed, such as: fracture flow; matrix flow; total flow (fracture+ matrix); pressure drop versus flow rate inside fracture and matrix; % fracture flow versus matrix flow; and ADV of each network was calculated of 4 pressure drops between the isotropic and anisotropic matrix permeability models.

Table 6.4 Permeability scenarios of the matrix's fracture network models

First Scenario Permeability (mD) (Isotropic)	Second Scenario Permeability (mD) (Anisotropic)	Third Scenario Permeability (mD) (Anisotropic)
Kx=2000 Ky=2000	Kx=2000 Ky=380	Kx=380 Ky=2000

6.3.6.1 Fracture network 1 simulation results

The total flow, fracture flow and matrix flow of the models with isotropic and two anisotropic matrix permeability scenarios were compared. The results were that: the total flow decreased 0.6% and 1.74% respectively for the second and third anisotropic matrix scenarios in ADV, [Figure 6.9C](#) clarifies this. The fracture flow decreased 0.2% and 0.9% respectively for the second and third anisotropic matrix scenarios in ADV. The matrix flow decreased 0.6% and 1.8% respectively for the second and third anisotropic matrix scenarios in ADV. In these models of three scenarios of matrix permeability, the average value of % fracture flow in the domain was around 9%, and the % matrix flow was 91%; [Figures 6.9A and 6.9B](#) clarifies this. Moreover, the matrix flow was compared with Darcy flow as [equation 2.3](#), and for anisotropic permeability scenarios, effective permeability ($K_{effective}$) was calculated as [equation 5.11](#), then applied in Darcy law. The flow increased 196.5%, 199% and 198.3% respectively for the first, second and third matrix of ANSYS CFD Fluent FVM model scenarios in ADV; which shows that Darcy formula underestimates matrix flow in fracture network 1 with approximately 200%, [Figure 6.10](#) clarifies this.

The pressure and velocity contours were presented in [Figures 6.7A and 6.7B](#) respectively, and the pressure contour distribution reflected interaction between fracture and matrix along the network due to the permeable fracture surfaces; particularly, interactions were observed around interface layer of fracture/matrix and adjacent matrix, and around intersection points of networks around the horizontal fractures that connected between the two fractures of inlet and outlet. While, velocity contours clarified the highest velocity occurred in intersection points that connected fractures with horizontal fractures, as a preferential fluid path, while the intersection that connected a fracture with the dead end fracture at the top of domain had lowest velocity. The velocity streamlines were observed as

presented in Figure 6.8, which clarified flow paths in the fractured network domain and showed the following: the higher fluid proportions entered fracture domain; the intersection fractures with dead end fracture, the lowest velocity along the dead end fracture; the intersection fractures between horizontal fracture and outlet fracture, and both had high velocity values. This is as both connected between the preferential fluid path between inlet and outlet; the highest fluid interactions between matrix and fractures occurred along fractures with highest velocity value inside fractures with preferential fluid path; and the abrupt changes in fracture apertures with fractures' sharp/narrow corners generated eddies and vortices; these represented the gateways or clusters of fluid movement between fractures and matrix due to the pressure/velocity changing and fluid momentum between the two domains. The fluid movement along fractures has led to increase % matrix flow as more fluid moved from fracture towards matrix, which explained the highest % of matrix flow in fractured network domain, despite the fact that the fracture had high flow proportion at the inlet. This has clarified the importance of matrix flow contribution in fractured network domains, and that the matrix represents a main provider and conductor of fluids.

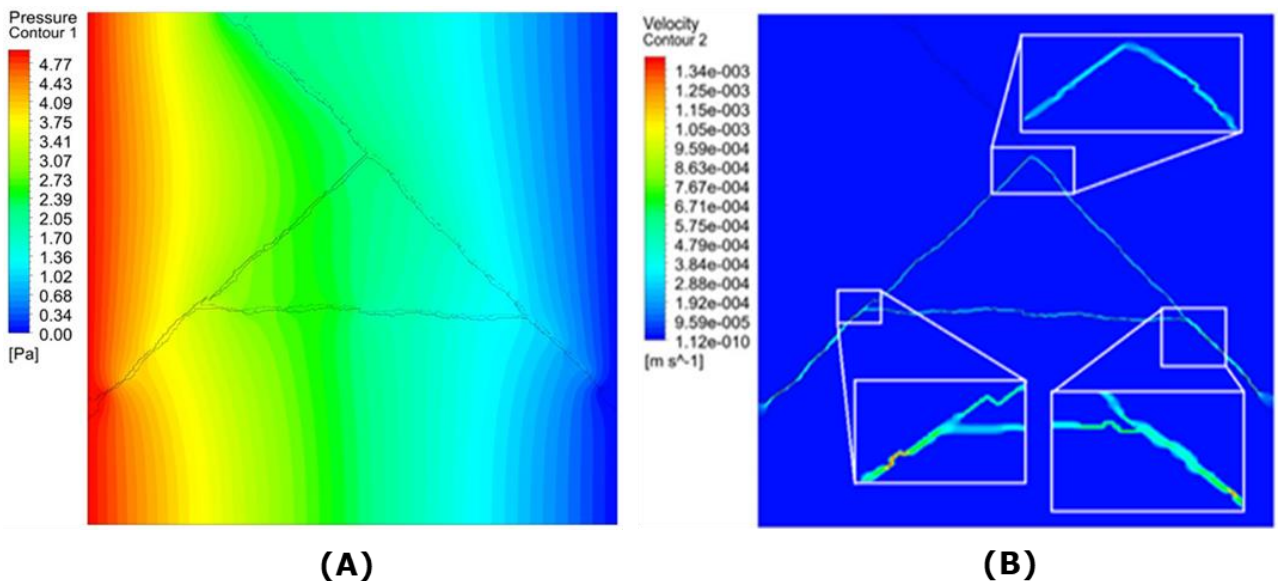


Figure 6.7 Fracture network 1 simulation contours

A. Total pressure at $P=5$ Pa, and B. velocity contours, with isotropic matrix permeability (K_x & $K_y=2000$ mD), and fracture surface boundaries set as permeable "Interior faces".

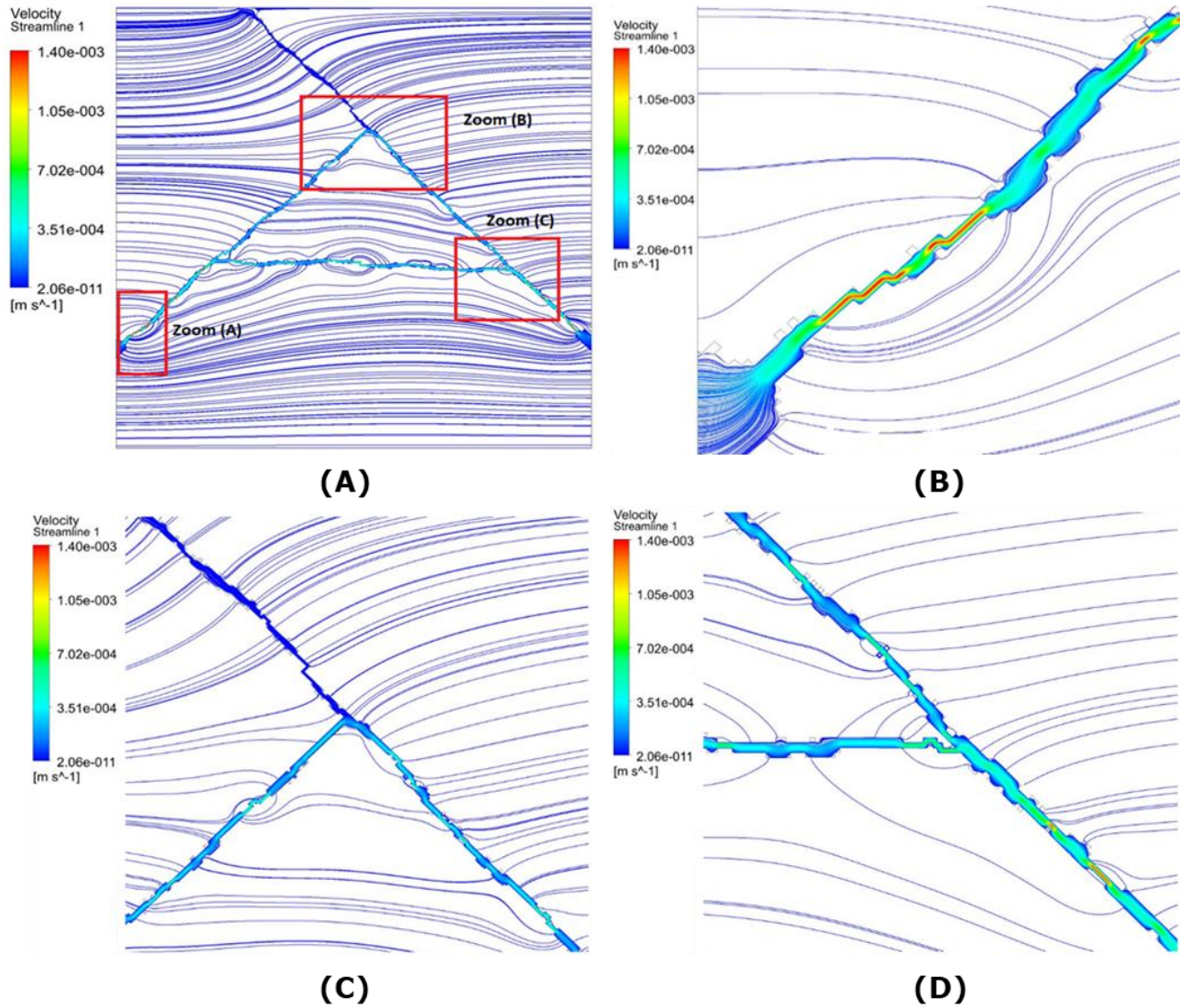


Figure 6.8 Fracture network 1 velocity streamlines, $P=5$ Pa isotropic matrix permeability (K_x & $K_y=2000$ mD), with fracture surface boundaries set as permeable "Interior faces"

A. Zooms on three random locations between fracture and matrix; B. Velocity streamlines on location (A); C. Velocity streamlines on location (B); and D. Velocity streamlines on location (C)

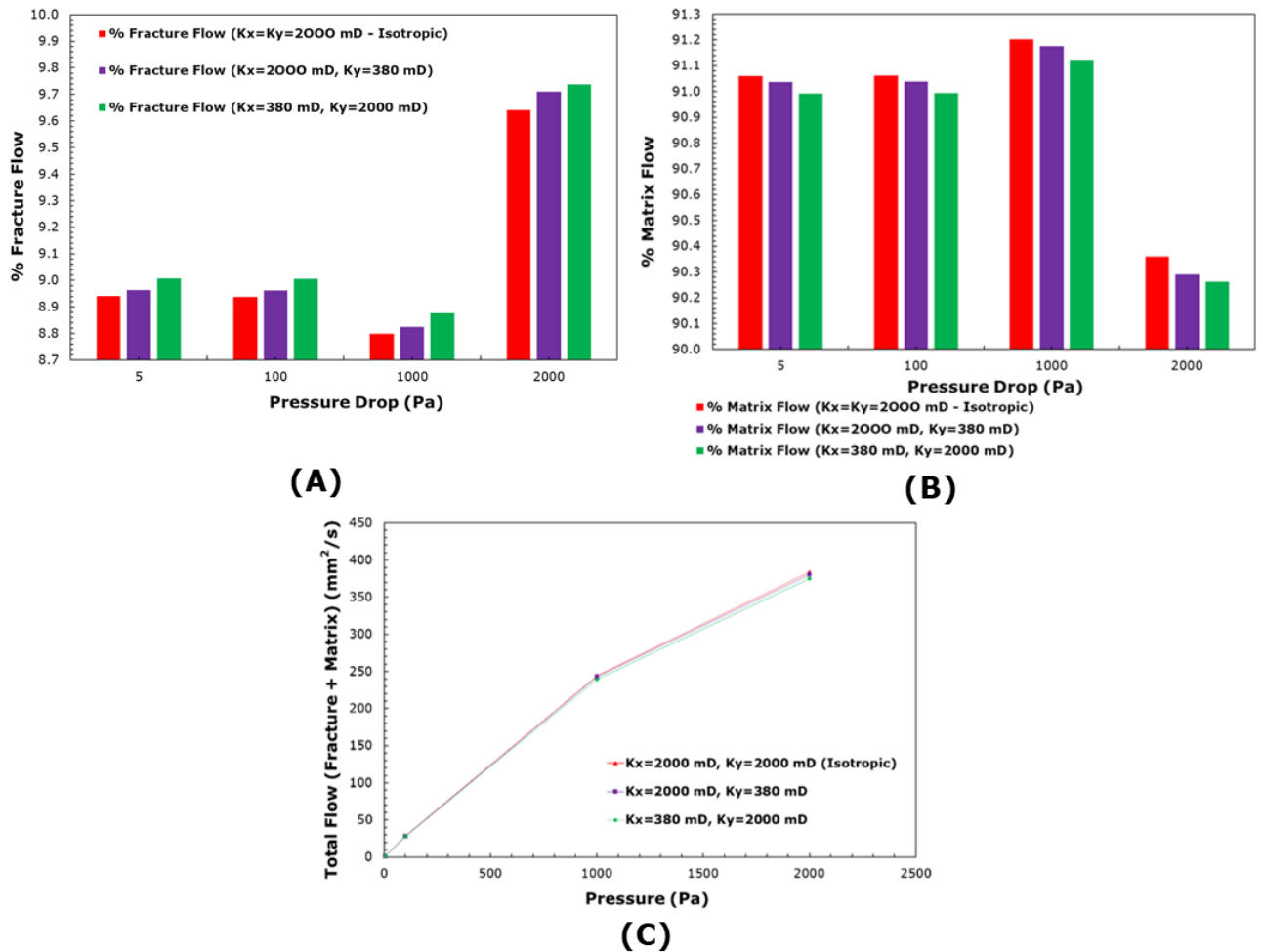


Figure 6.9 Comparisons of fracture network 1 flow percentages in fractures and matrix; as well, total flow (fracture + matrix) between isotropic and anisotropic permeability models

A. % Fracture flow; B. % Matrix flow; and C. Total flow (mm²/s)

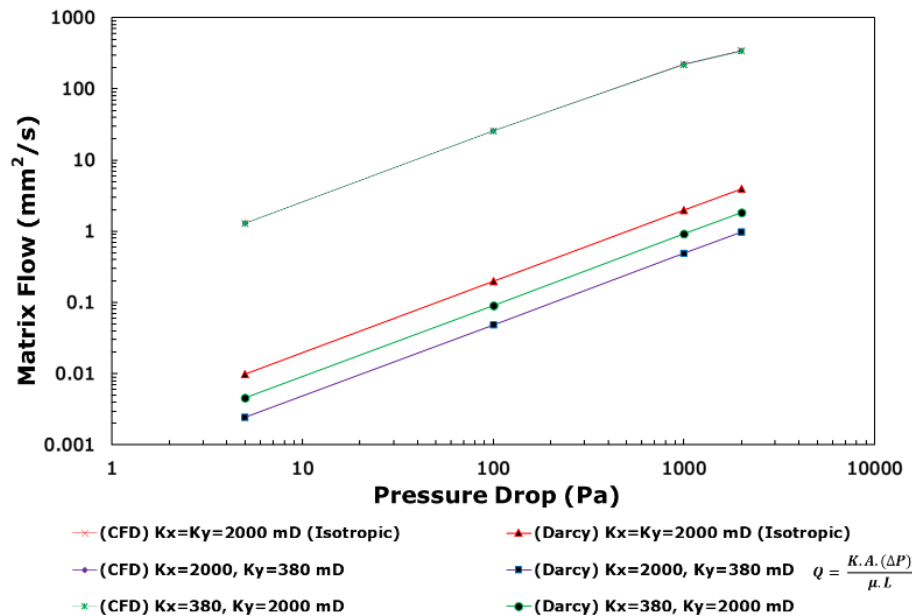


Figure 6.10 Comparison of matrix flow between fracture network 1 ANSYS CFD Fluent FVM models with isotropic and anisotropic matrix permeability scenarios, & Darcy equation

6.3.6.2 Fracture network 2 simulation results

This network had no fracture outlets as the fractures continued only inside the matrix before an outlet with dead end. As well, the reading line of the total domain passed through matrix only without fracture outlet; therefore, in this network, the total flow of the domain represented only matrix flow at the outlet. The models with isotropic and two anisotropic matrix permeability scenarios were compared and the results were that the total flow (flow in matrix only) decreased 11.6% and 110% respectively for the second and third anisotropic matrix scenarios in average difference value (ADV). Figure 6.13C clarifies this.

As the total flow represented the matrix flow only at the outlet, therefore, it was compared with Darcy flow equation 2.3, and for anisotropic permeability scenarios, effective permeability ($K_{\text{effective}}$) was calculated as equation 5.11, then applied in Darcy law. The matrix flow increased 120%, 174% and 86% respectively for the first, second and third matrix of ANSYS CFD Fluent FVM model scenarios in ADV. Figure 6.14 clarifies this, which shows that Darcy formula underestimated matrix flow in this network even without fracture exitance at the outlet. The fracture and matrix flow were calculated in the vertical section where there were fractures just before the outlet. The average value of % fracture flow of these models were 18.6%, 13.2% and 28.8%, As well, the average value of % matrix flow of these models were 18.4%, 86.8% and 71.2% for the first, second and third scenarios respectively. Figures 6.13A and 6.13B clarify it.

The pressure and velocity contours were presented in [Figures 6.11A and 6.11B](#) respectively, and the pressure contour distribution reflected higher increase between the inlet and the intersection point of fractures at the centre of the network. This reflected unusual pressure distributions in comparison with other networks, therefore, further investigations were conducted as clarified in [Section 6.3.6](#). While velocity contours reflected high velocity at the intersection, and as well, the low velocity of fractures at the dead ends. The velocity streamlines were observed as presented in [Figure 6.12](#) which clarified similar observations approximately as in network 1; all fracture networks reflected high interaction with matrix, and higher velocity inside fractures at intersections that connected with the outlet, which is in this model was fracture/matrix interface layer (fracture surfaces), particularly on the second half of the domain.

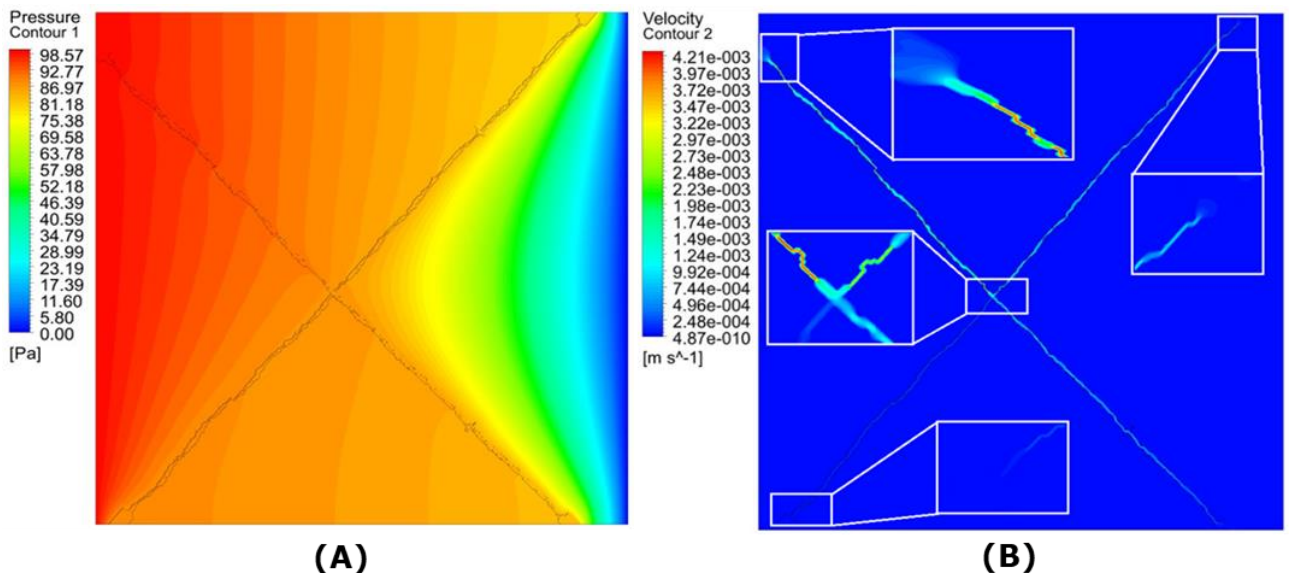


Figure 6.11 Fracture network 2 simulations contours
A. Total pressure at $P=100$ Pa; and B. Velocity contours, with isotropic matrix permeability (K_x & $K_y=2000$ mD), and fracture surface boundaries set as permeable "Interior faces".

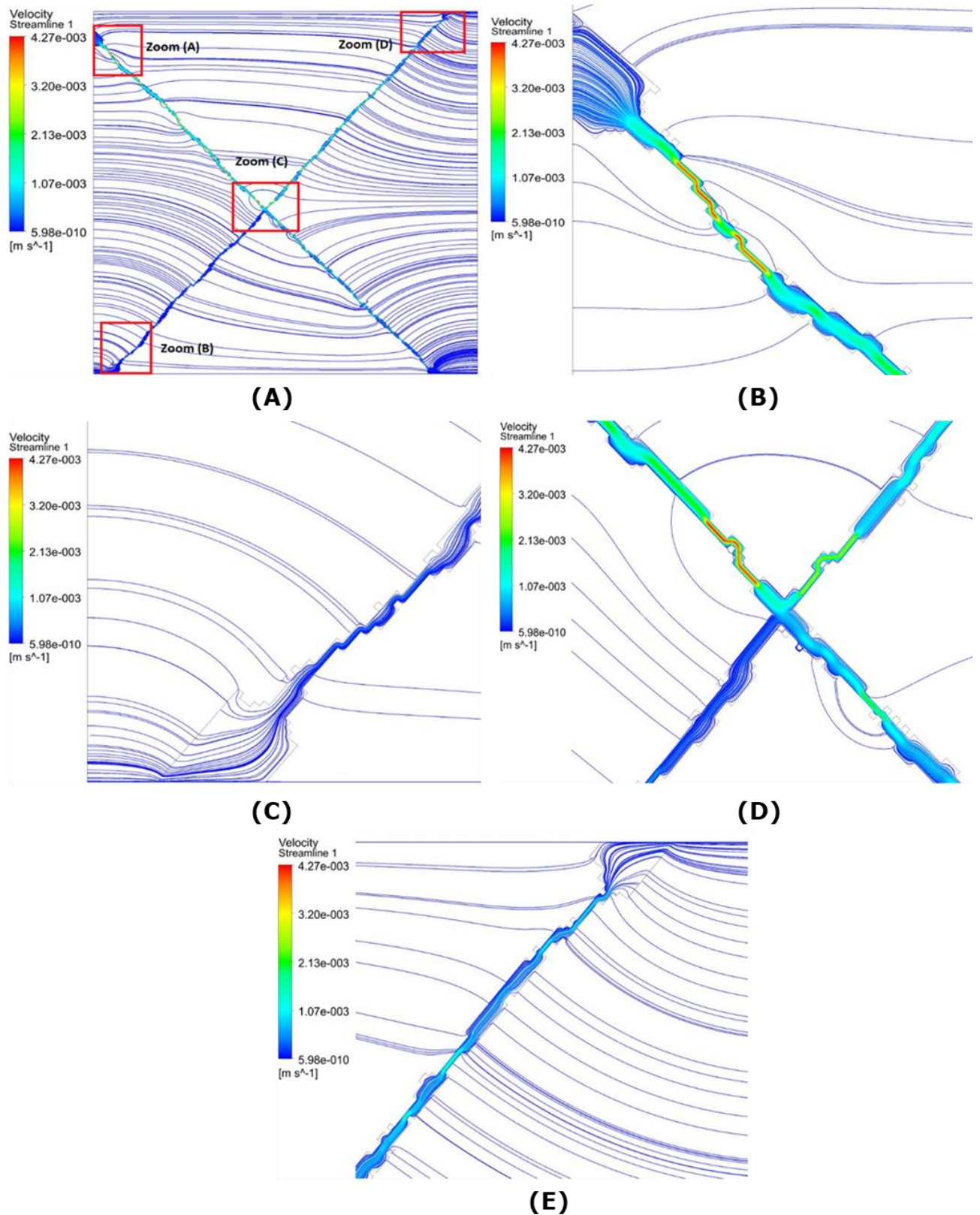


Figure 6.12 Fracture network 2 velocity streamlines, $P=100$ Pa isotropic matrix permeability (K_x & $K_y=2000$ mD), with fracture surface boundaries set as permeable "Interior faces".

A. Zooms on four random locations between fracture and matrix; B, C, D and E. Velocity streamlines on zoom locations (A, B, C, and D) respectively.

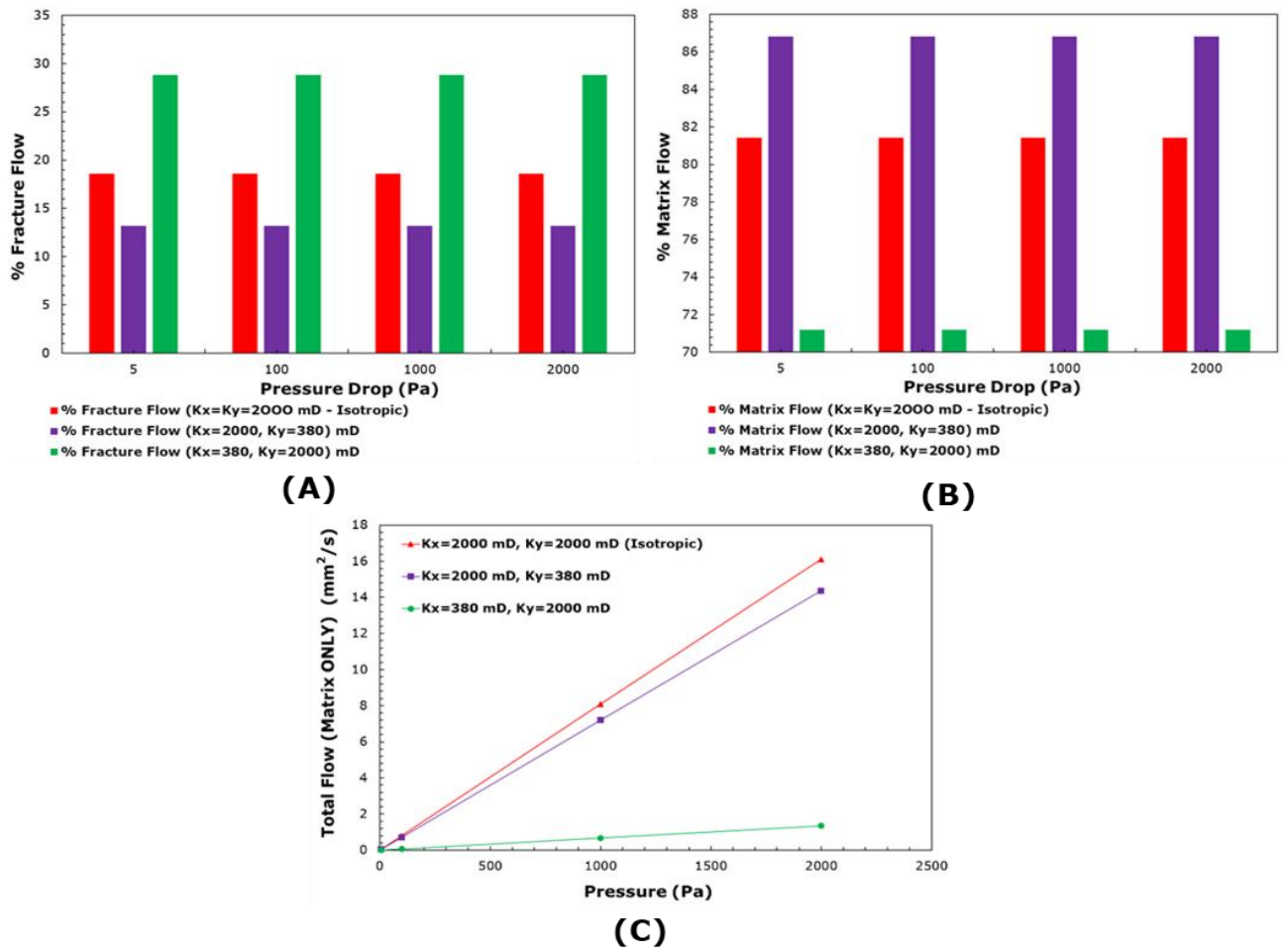


Figure 6.13 Comparisons of fracture network 2 flow percentages in fractures and matrix; as well, total flow (fracture + matrix) between isotropic and anisotropic permeability models

A. % Fracture flow; B. % Matrix flow; and C. Total flow (mm²/s) (matrix flow was the only outlet in this network)

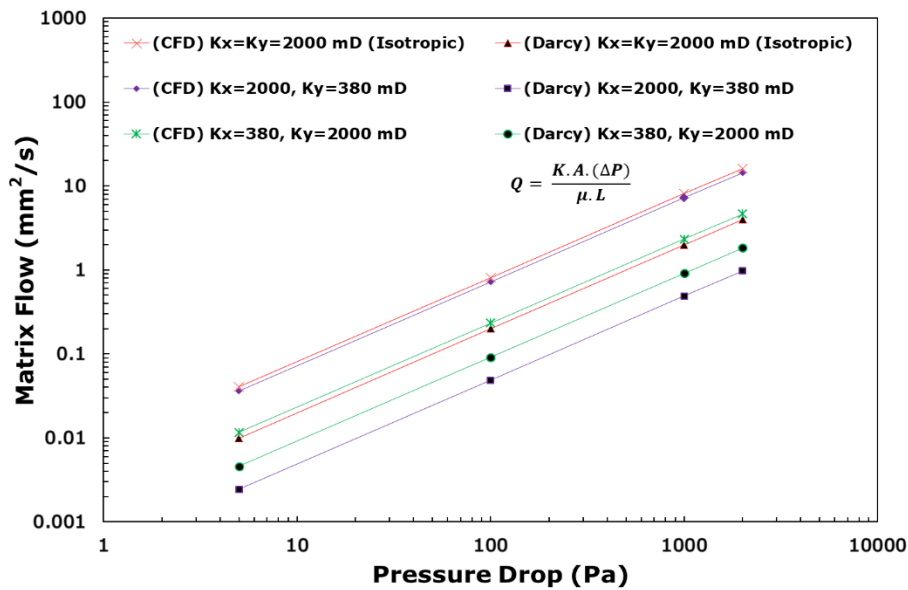


Figure 6.14 Comparison of matrix flow between fracture network 2 ANSYS CFD Fluent FVM models with isotropic and anisotropic matrix permeability scenarios, & Darcy equation

6.3.6.3 Fracture network 3 simulation results

The total flow, fracture flow and matrix flow of the models with isotropic and two anisotropic matrix permeability scenarios were compared. The results were that the total flow decreased 0.44% and 3.68% respectively for the second and third anisotropic matrix scenarios in ADV, [Figure 6.17C](#) clarifies it. The fracture flow decreased 0.33% and 2.9% respectively for the second and third anisotropic matrix scenarios in ADV. The matrix flow decreased 0.46% and 3.8% respectively for the second and third anisotropic matrix scenarios in ADV. In these models of three scenarios of matrix permeability, the average value of % fracture flow in the domain was around 11.5%, and the % matrix flow was 88.5%, [Figures 6.17A and 6.17B](#) present these results. Moreover, the matrix flow was compared with Darcy flow as [equation 2.3](#), and for anisotropic permeability scenarios, effective permeability ($K_{\text{effective}}$) was calculated as [equation 5.11](#), then applied in Darcy law. The flow increased 195%, 199% and 198% respectively for the first, second and third scenarios of ANSYS CFD Fluent FVM models in ADV, which shows that Darcy formula underestimates matrix flow in fracture network 3 with approximately 200%, [Figure 6.18](#) clarifies it. [Figures 6.15A, 6.15B and 6.16](#) present the pressure contours, velocity contours, and velocity streamlines respectively of this model, and all of them have reflected approximately similar behaviours as network 1, with variations due to the different network pattern.

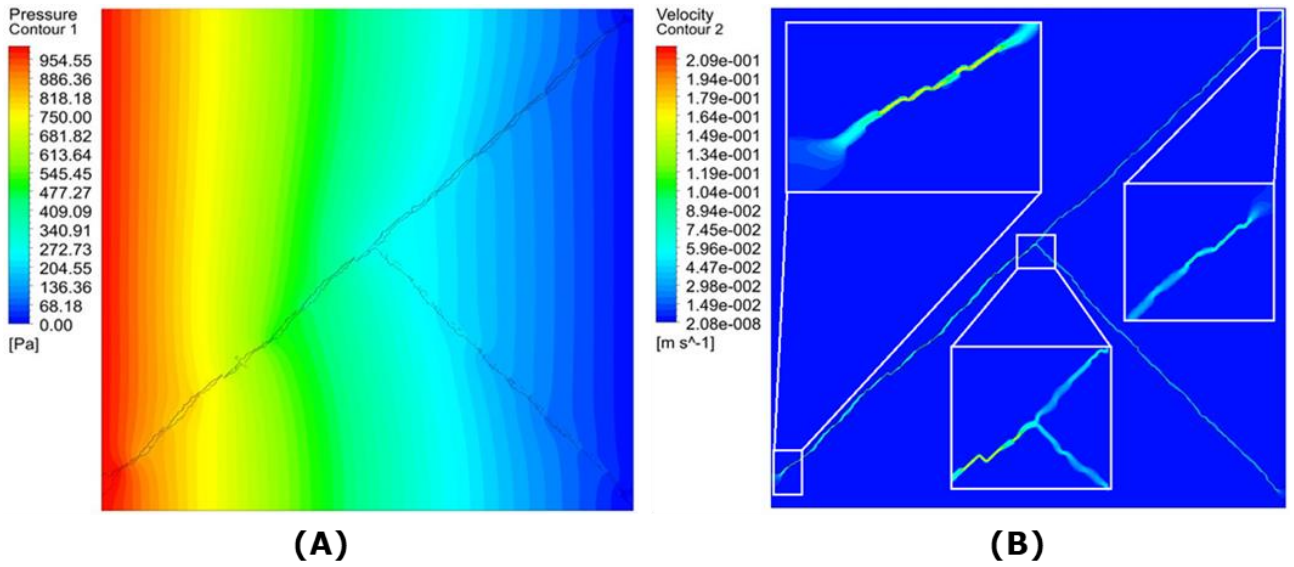


Figure 6.15 Fracture network 3 simulation contours
 A. Total pressure at $P=1000$ Pa; and B. Velocity contours, with isotropic matrix permeability (K_x & $K_y=2000$ mD), and fracture surface boundaries set as permeable "Interior faces"

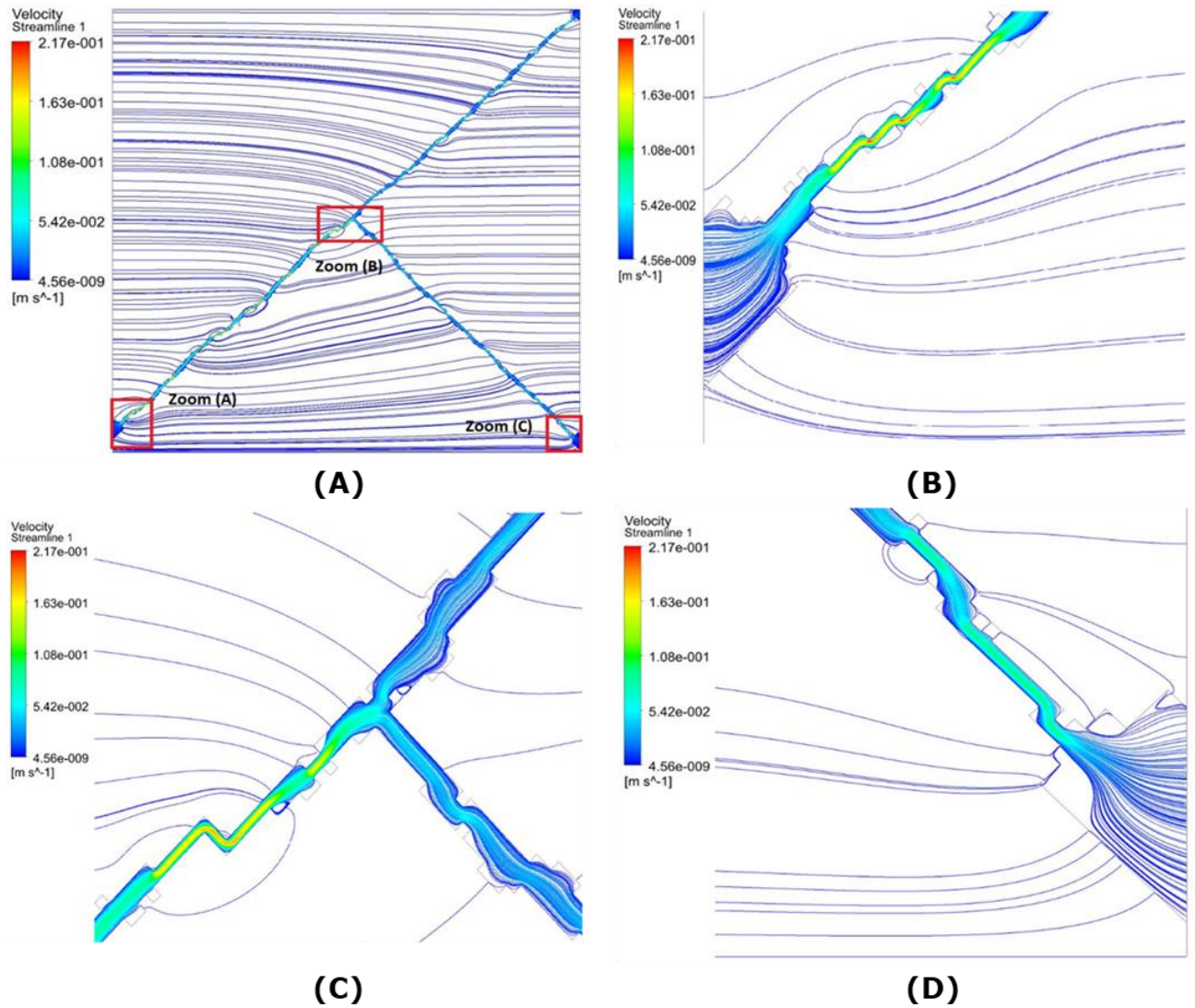


Figure 6.16 Fracture network 3 velocity streamlines $P=1000$ Pa isotropic matrix permeability (K_x & $K_y=2000$ mD), with fracture's surface boundaries set as permeable "Interior faces"

A. Zooms on three random locations between fracture and matrix; B, C, and D, velocity streamlines on zoom locations (A, B, and C) respectively

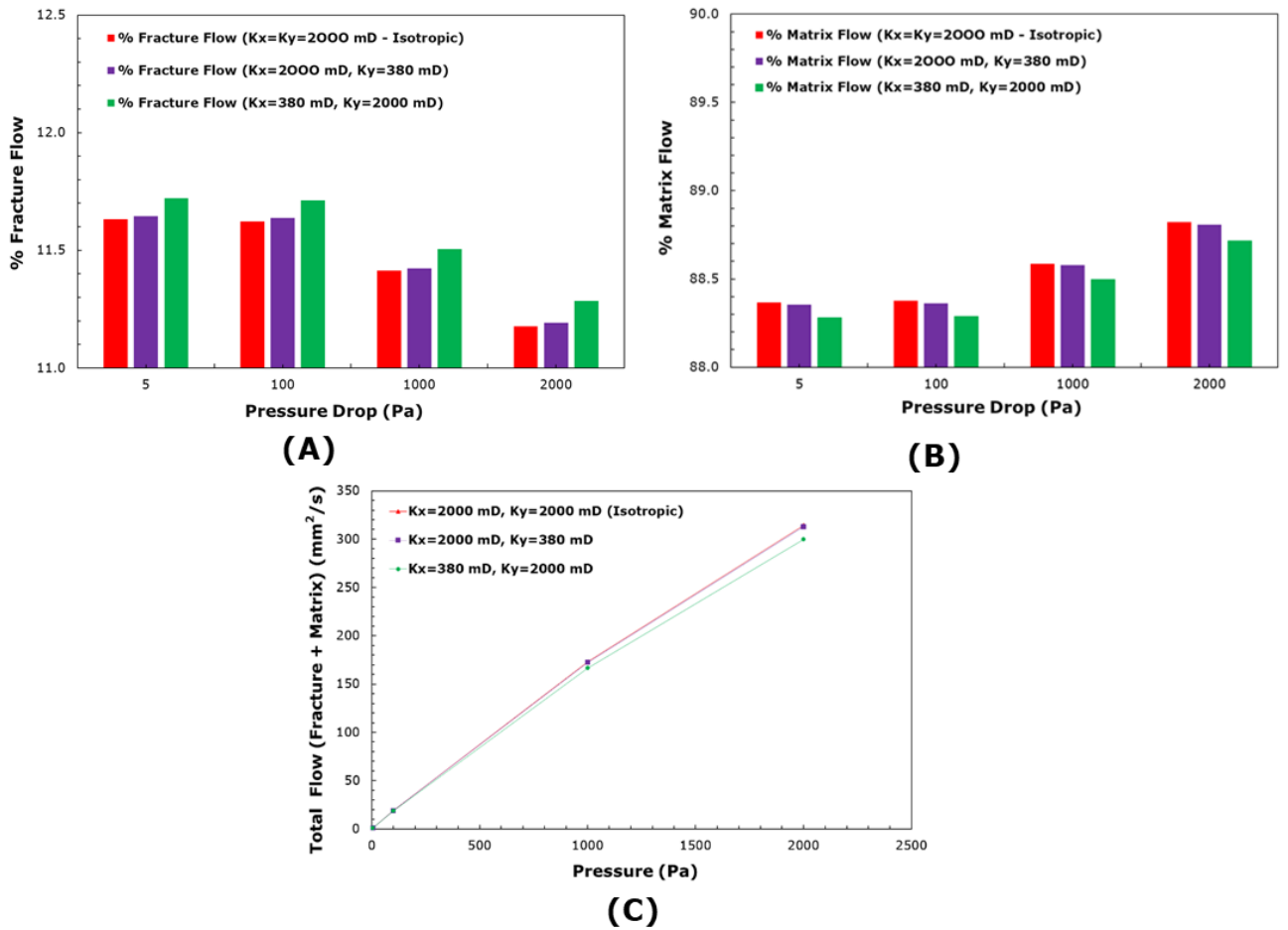


Figure 6.17 Comparisons of fracture network 3 flow percentages in fractures and matrix; as well, total flow between isotropic and anisotropic permeability models A. % Fracture flow; B. % Matrix flow; and C. Total flow (mm²/s)

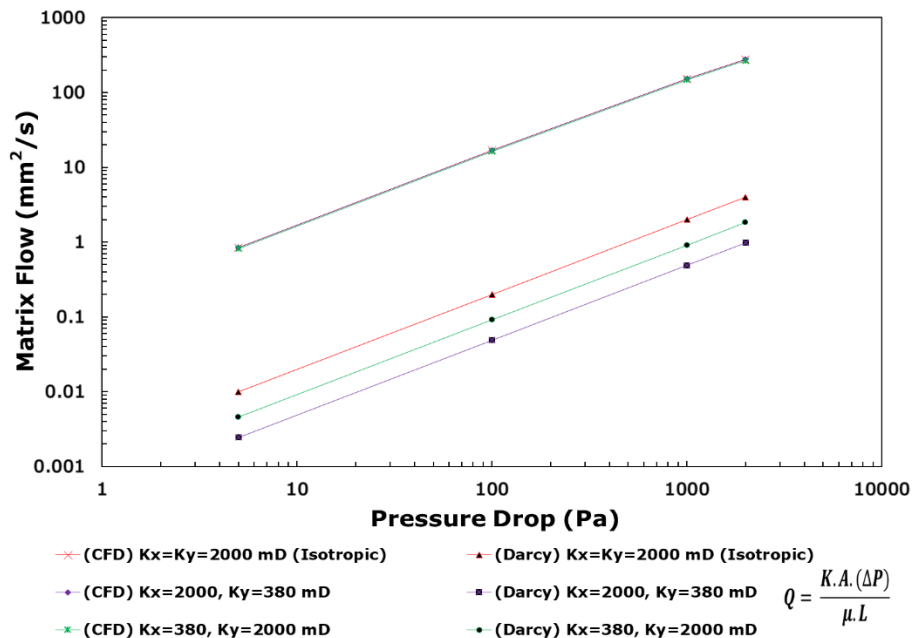


Figure 6.18 Comparison of matrix flow between fracture network 3 ANSYS CFD Fluent FVM models with isotropic and anisotropic matrix permeability scenarios, & Darcy equation

6.3.6.4 Fracture network 4 simulation results

The total flow, fracture flow and matrix flow of the models with isotropic and two anisotropic matrix permeability scenarios were compared. The results were that the total flow increased 0.3% and decreased 0.2% respectively for the second and third anisotropic matrix scenarios in ADV, [Figure 6.21C](#) clarifies it. The fracture flow increased 0.42% and 0.5% respectively for the second and third anisotropic matrix scenarios in ADV. The matrix flow increased 0.3% and decreased 0.3% respectively for the second and third anisotropic matrix scenarios in ADV. In these models of three scenarios of matrix permeability, the average value of % fracture flow in the domain was around 11.7%, and the % matrix flow was 88.3%. [Figures 6.21A and 6.21B](#) present these results. Moreover, the matrix flow were compared with Darcy flow as [equation 2.3](#), and for anisotropic permeability scenarios, effective permeability ($K_{\text{effective}}$) was calculated as [equation 5.11](#), then applied in Darcy law. The flow increased 197.5%, 199.4% and 199% respectively for the first, second and third scenarios of ANSYS CFD Fluent FVM models in average difference value (ADV), which shows that Darcy formula underestimated matrix flow in fracture network 4 with approximately 200%; [Figure 6.22](#) clarifies it.

The pressure and velocity contours were presented in [Figures 6.19A and 6.19B](#) respectively. In addition to the explanation of pressure and velocity contour distribution at network 1, this network represented higher velocity at the horizontal fracture that connected between inlet and outlet boundaries of the domain, which highlighted the effects of “dominant fracture” in fractured networks; as well, the impact of horizontal orientation of fracture on flow proportion and interactions with the matrix. Moreover, the velocity streamlines of this model consolidated these findings and clarified that the higher velocity at the horizontal fracture that connected between inlet and outlet boundaries of the domain has reflected higher fracture/matrix interaction, which highlighted the effects of “dominant fracture” in fractured networks. [Figure 6.20](#) presents it.

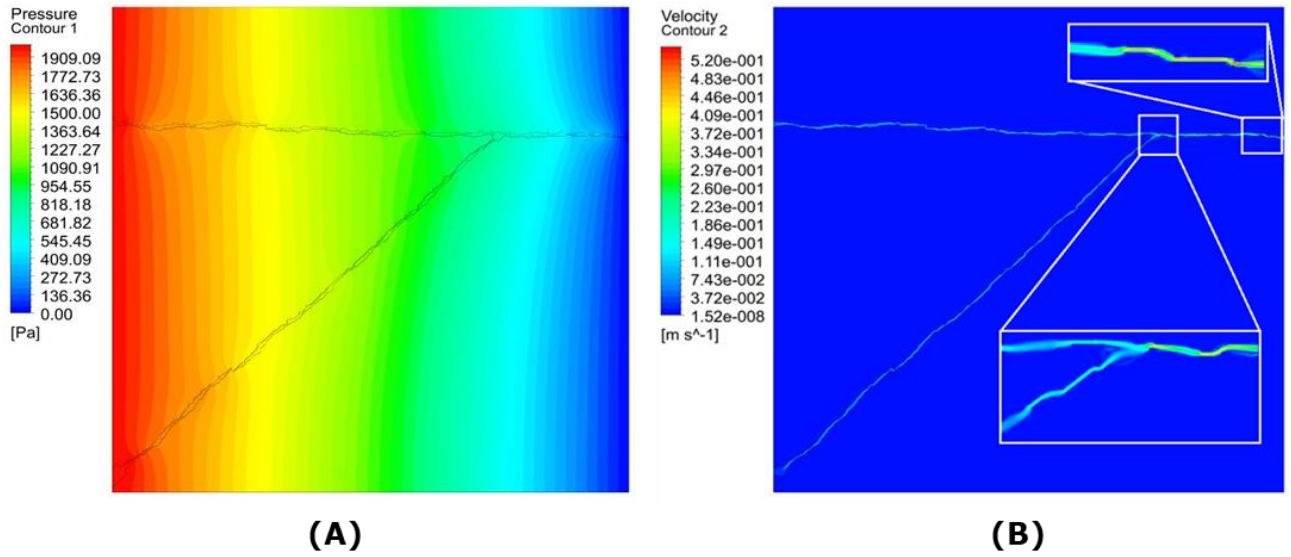


Figure 6.19 Fracture network 4 simulations contours
 A. Total pressure at $P=2000$ Pa; and B. Velocity contours, with isotropic matrix permeability (K_x & $K_y=2000$ mD), and fracture surface boundaries set as permeable "Interior faces".

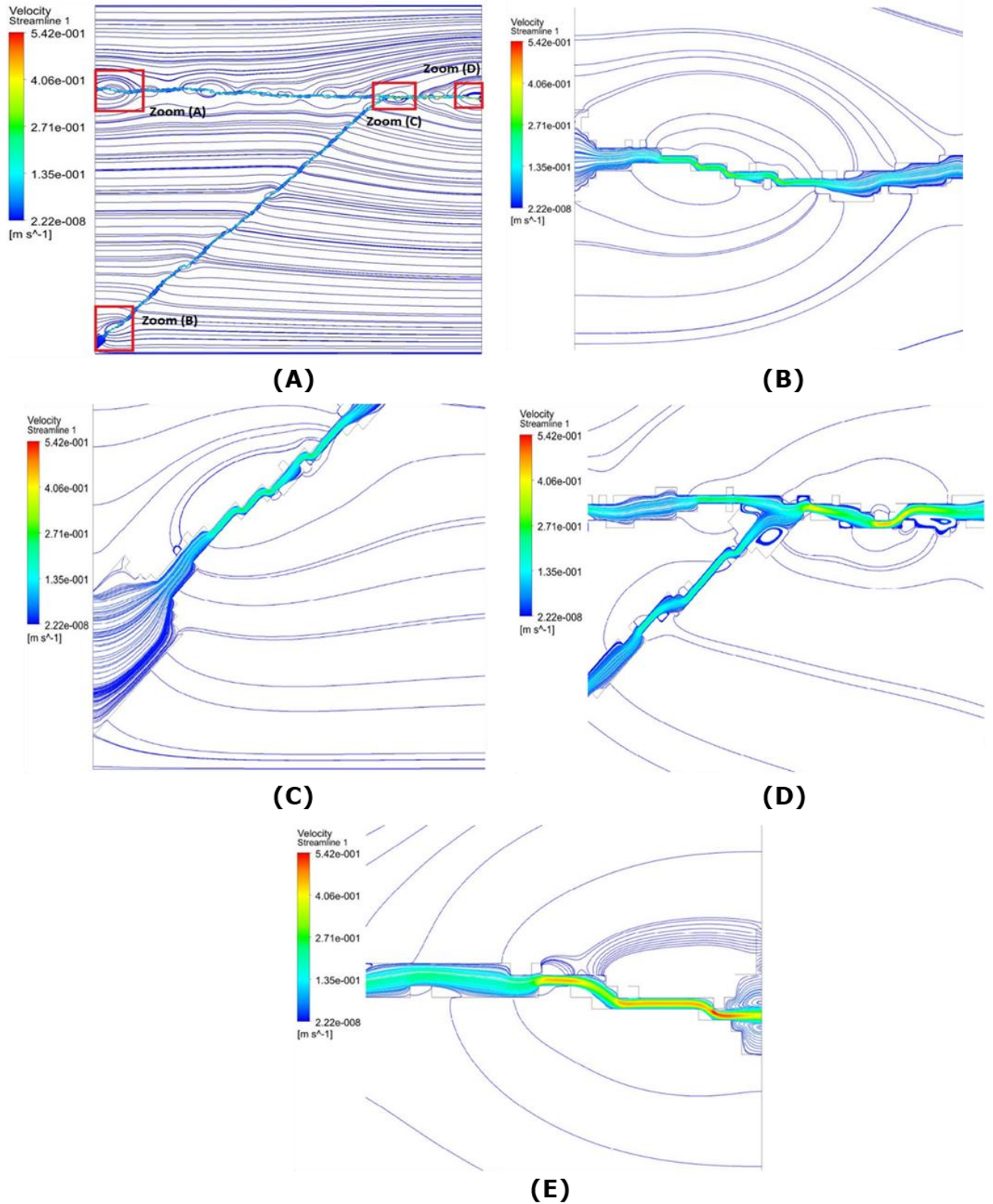


Figure 6.20 Fracture network 4 velocity streamlines $P=2000$ Pa isotropic matrix permeability (K_x & $K_y=2000$ mD), with fracture's surface boundaries set as permeable "Interior faces"

A. Zooms on four random locations between fracture and matrix; B, C, D and E. Velocity streamlines on zoom locations (A, B, C and D) respectively.

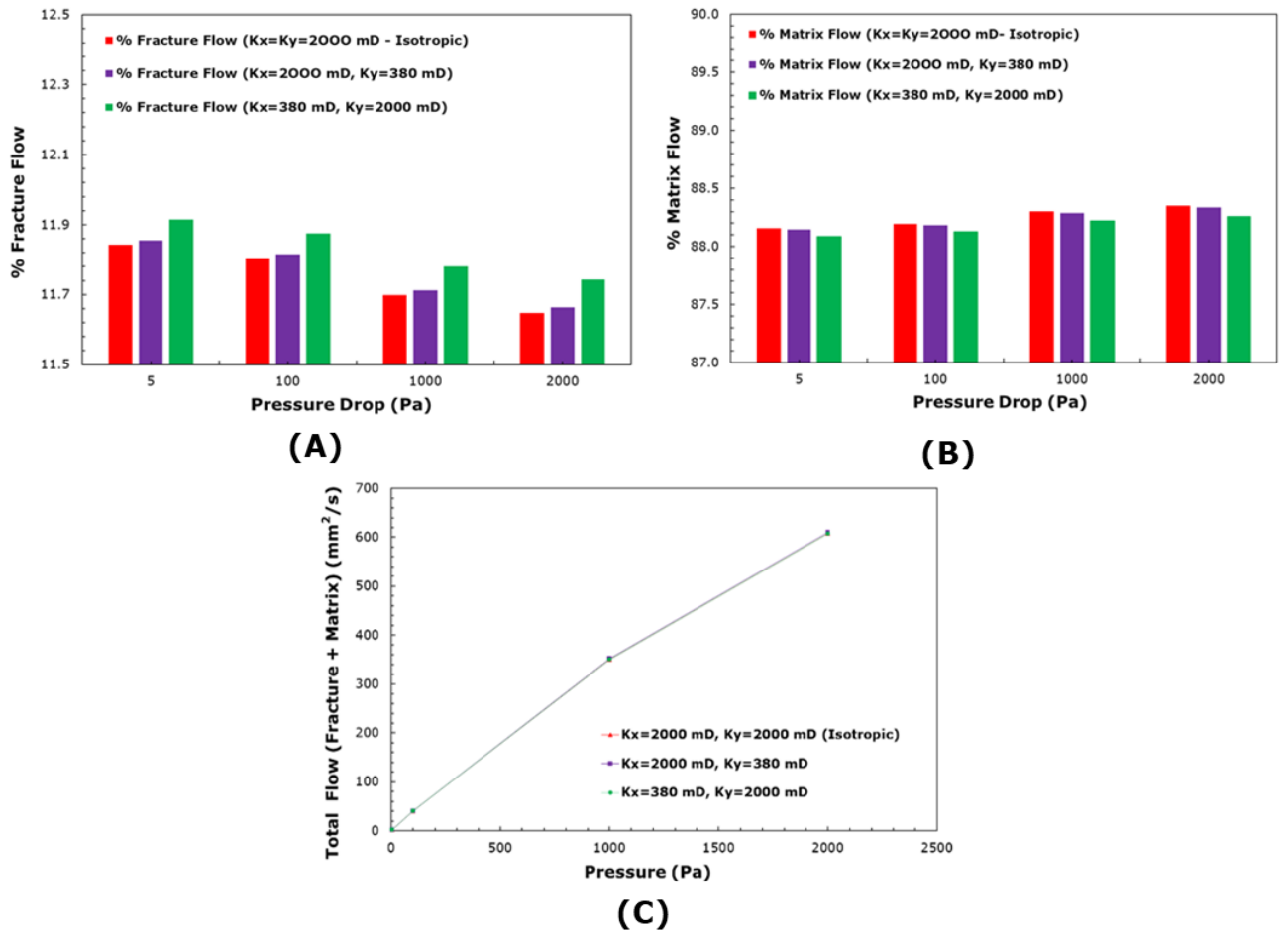


Figure 6.21 Comparisons of fracture network 4 flow percentages in fractures and matrix; as well, total flow between isotropic and anisotropic permeability models A. % Fracture flow; B. % Matrix flow; and C. total flow (mm²/s)

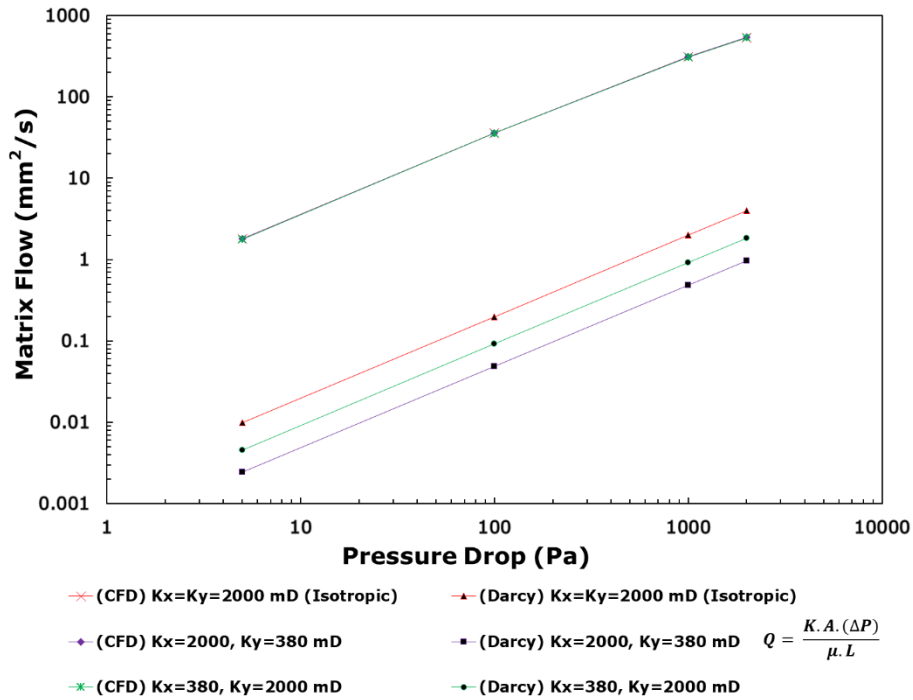


Figure 6.22 Comparison of matrix flow between fracture network 4 ANSYS CFD Fluent FVM models with isotropic and anisotropic matrix permeability scenarios, & Darcy equation

6.3.6.5 Fracture network 5 simulation results

The total flow, fracture flow and matrix flow of the models with isotropic and two anisotropic matrix permeability scenarios were compared. The results were that the total flow decreased 1% and 3.3% respectively for the second and third anisotropic matrix scenarios in ADV, [Figure 6.25C](#) clarifies it. The fracture flow decreased 0.2% and 2.01% respectively for the second and third anisotropic matrix scenarios in ADV. The matrix flow decreased 1.03% and 3.4% respectively for the second and third anisotropic matrix scenarios in ADV. In these models of three scenarios of matrix permeability the average value of % fracture flow in the domain was around 6.7%, and the % matrix flow was 93.3%. [Figures 6.25A and 6.25B](#) present these results. Moreover, the matrix flow was compared with Darcy flow as [equation 2.3](#), and for anisotropic permeability scenarios, effective permeability ($K_{\text{effective}}$) was calculated as [equation 5.11](#), then applied in Darcy law. The flow increased 196%, 199% and 198% respectively for the first, second and third scenarios of ANSYS CFD Fluent FVM models in ADV, which shows that Darcy formula underestimated matrix flow in fracture network 5 with approximately 200%. [Figure 6.26](#) clarifies it.

Figures 6.23A, 6.23B and 6.24 present the pressure contours, velocity contours, and velocity streamlines respectively of this model, and all of them have reflected approximately similar behaviours as network 1, with variations due to the different network pattern. In addition, it has stressed the effect of branch fractures “dead end fractures” which were connected with the dominant fractures, which still have low velocity as zoom A and B in figures 6.24B and 6.24C, in comparison with the dominant fractures that were connected between inlet and outlet of the domain.

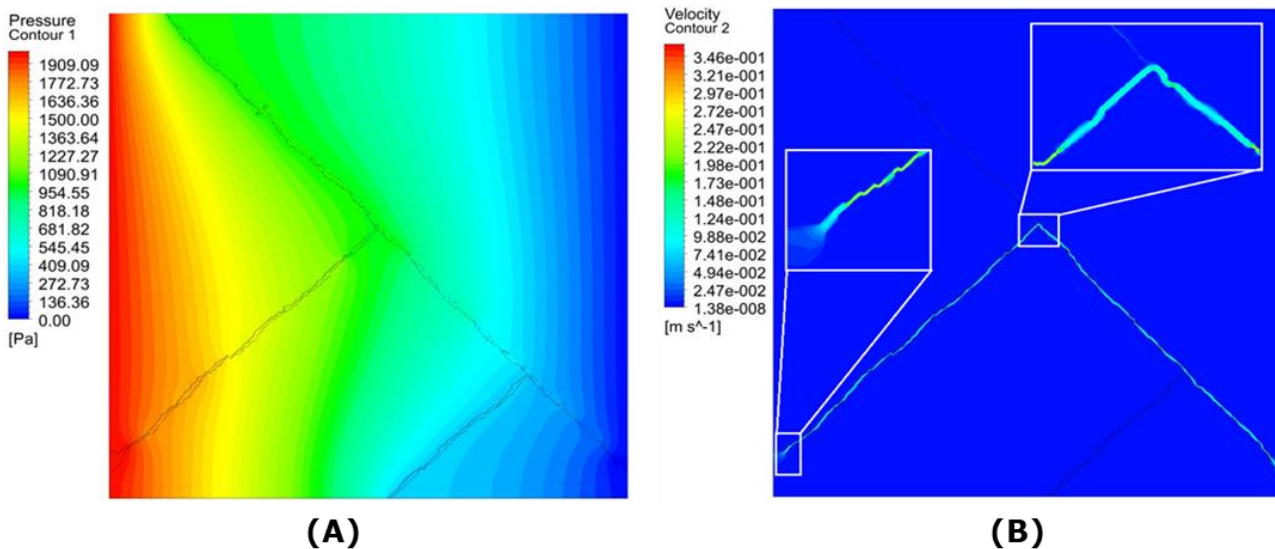


Figure 6.23 Fracture network 5 simulation contours
 A. Total pressure at $P=2000$ Pa; and B. Velocity contours, with isotropic matrix permeability (K_x & $K_y=2000$ mD), and fracture surface boundaries set as permeable “Interior faces”

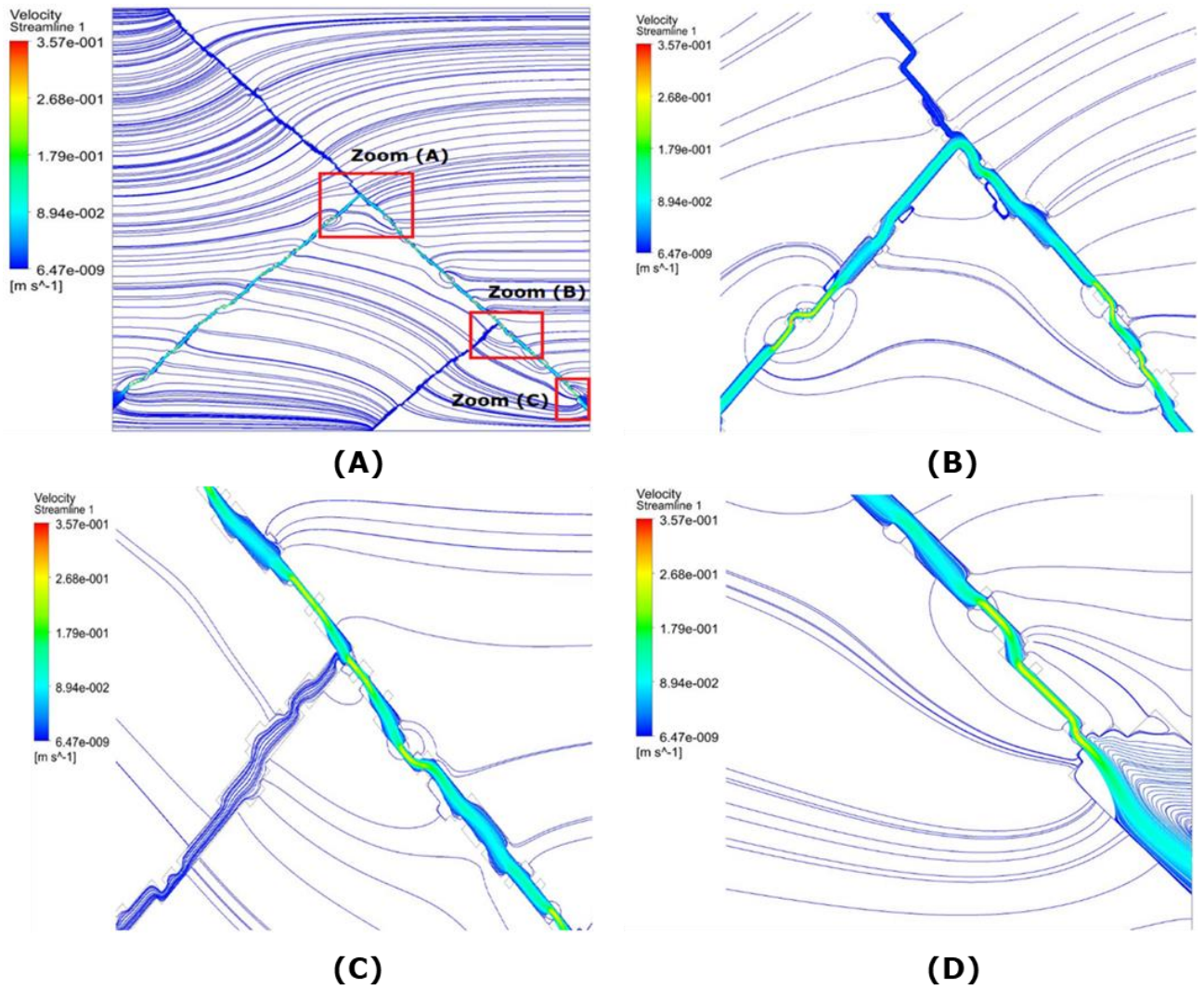


Figure 6.24 Fracture network 5 velocity streamlines $P=2000$ Pa, isotropic matrix permeability (K_x & $K_y=2000$ mD), with fracture's surface boundaries set as permeable "Interior faces"

A. Zooms on three random locations between fracture and matrix; B, C, and D, Velocity streamlines on zoom locations (A, B, and C) respectively.

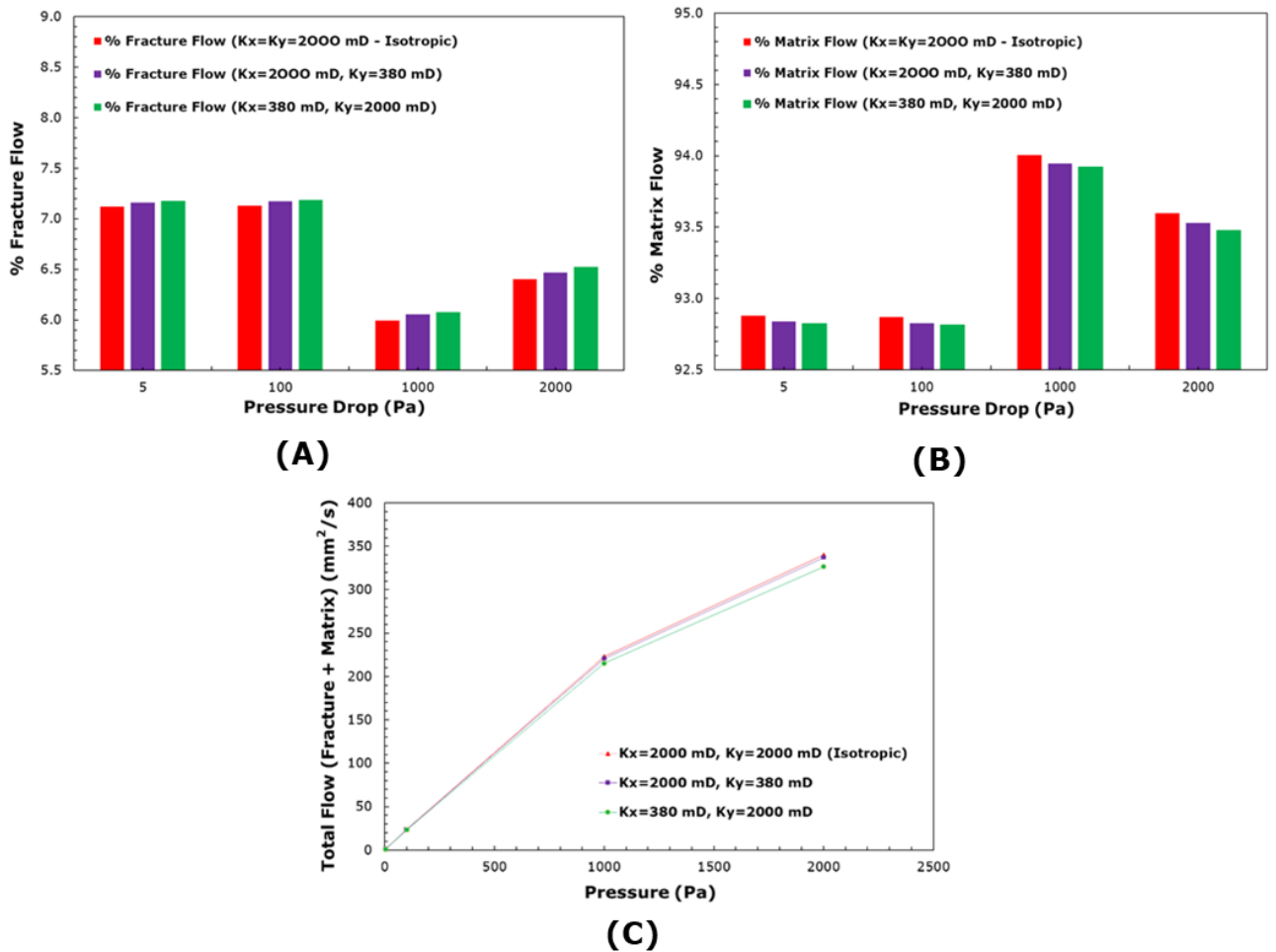


Figure 6.25 Comparisons of fracture network 5 flow percentages in fractures and matrix; as well, total flow between isotropic and anisotropic permeability models
 A. % Fracture flow ; B. % Matrix flow; and C. total flow (mm^2/s)

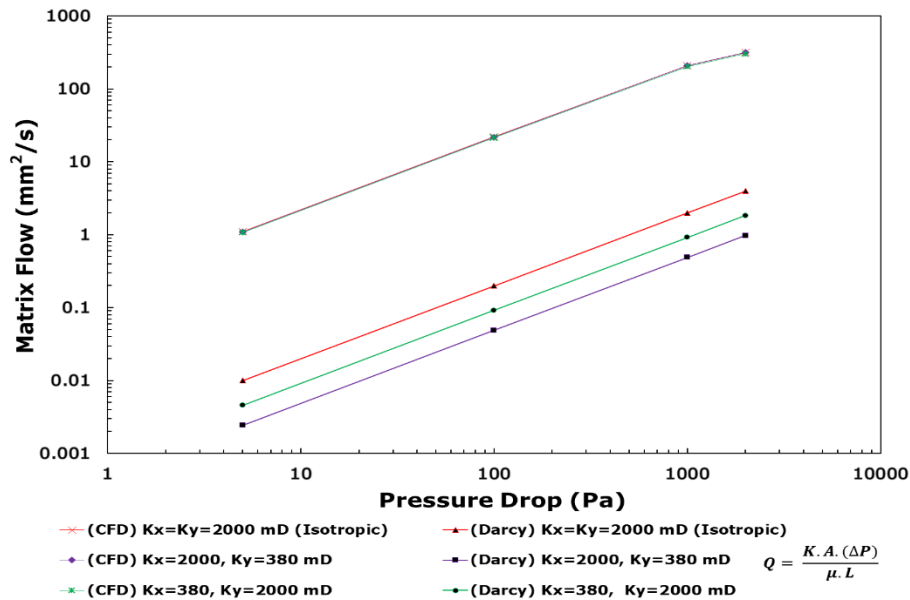


Figure 6.26 Comparison of matrix flow between fracture network 5 ANSYS CFD Fluent FVM models with isotropic and anisotropic matrix permeability scenarios, & Darcy equation (Darcy formula underestimated matrix flow in fracture network 5 by approximately 200%)

6.3.7 Investigating fracture network 2 model

As stated in section 6.3.5.2, fracture network 2 had reflected an unusual pressure distribution inside the domain between the first and second half along the flow length in comparison with the other fracture network models, as clarified in the total pressure contours Figure 6.11A. Therefore, it was necessary to investigate it further to clarify the cause of this unusual pressure distribution. It's good to stress here that this network pattern was the only network for which the fractures inside the domain had no outlet, at the outlet side of the domain; in other words, there were no fractures allowing fluids to flow directly from inlet towards outlet in the domain, due to the fractures' orientation pattern ending inside the matrix only. Thus, this network was investigated further with two approaches, as clarified below.

6.3.7.1 First Approach

The model of Network 2 was further investigated by simulating it with 3 different boundary conditions. All the three models were isotropic $K_x=K_y=2000$ mD, permeable fracture surfaces with the matrix "interior faces boundary" and pressure inlet $P=1000$ Pa, pressure outlet zero. The X-Velocity profile was extracted in each

model of the total domain to calculate the total flow by observing the reading line inside the domain FLUENT (called Reading line of the total domain). It's good to note that the X-Velocity inside the fractures were not extracted for these comparisons. The three boundary conditions were changed at the far side (top and bottom) of the matrix, and the boundaries set-up of these models were: first, fracture Y-outlets and symmetry edges were assigned with non-porous "walls" boundary condition only; second, fracture Y-outlets were assigned with non-porous "walls" boundary condition only, and the rest were assigned with Symmetry conditions; and third, fractures Y-outlets and the adjacent surfaces were assigned with Symmetry conditions only. [Figure 6.27](#) illustrates these set-ups and the static pressure contours of three boundaries, and [Figure 6.28](#) illustrates X-velocity profiles. The average value of X-Velocity in each section was calculated, then compared with the initial simulation values of fracture network 2. The outcome of the comparisons was that ADV were very small, and the highest ADV was in the first set-up with 0.27%, see [Table 6.5](#) below.

The comparisons among these profiles were very small (%), and the static pressure contours from ANSYS CFD Fluent FVM had not reflected any changes inside the domain of these three scenarios. Therefore, the same ANSYS CFD Fluent FVM models were read by ANSYS CFD Fluent FVM -POST, to read the static pressure distribution inside the domain. Reading the pressure contours inside ANSYS CFD Fluent FVM -POST gave a more accurate visualization of the contours as it gave the opportunity to increase the number of contour lines inside the domain. The result was that the pressure contours of the domain had similar behaviour to these 3 models' set-ups, but the clarity of the contour was much better, and it showed clear interaction between the fractures and the matrix. [Figure 6.29](#) below clarifies it.

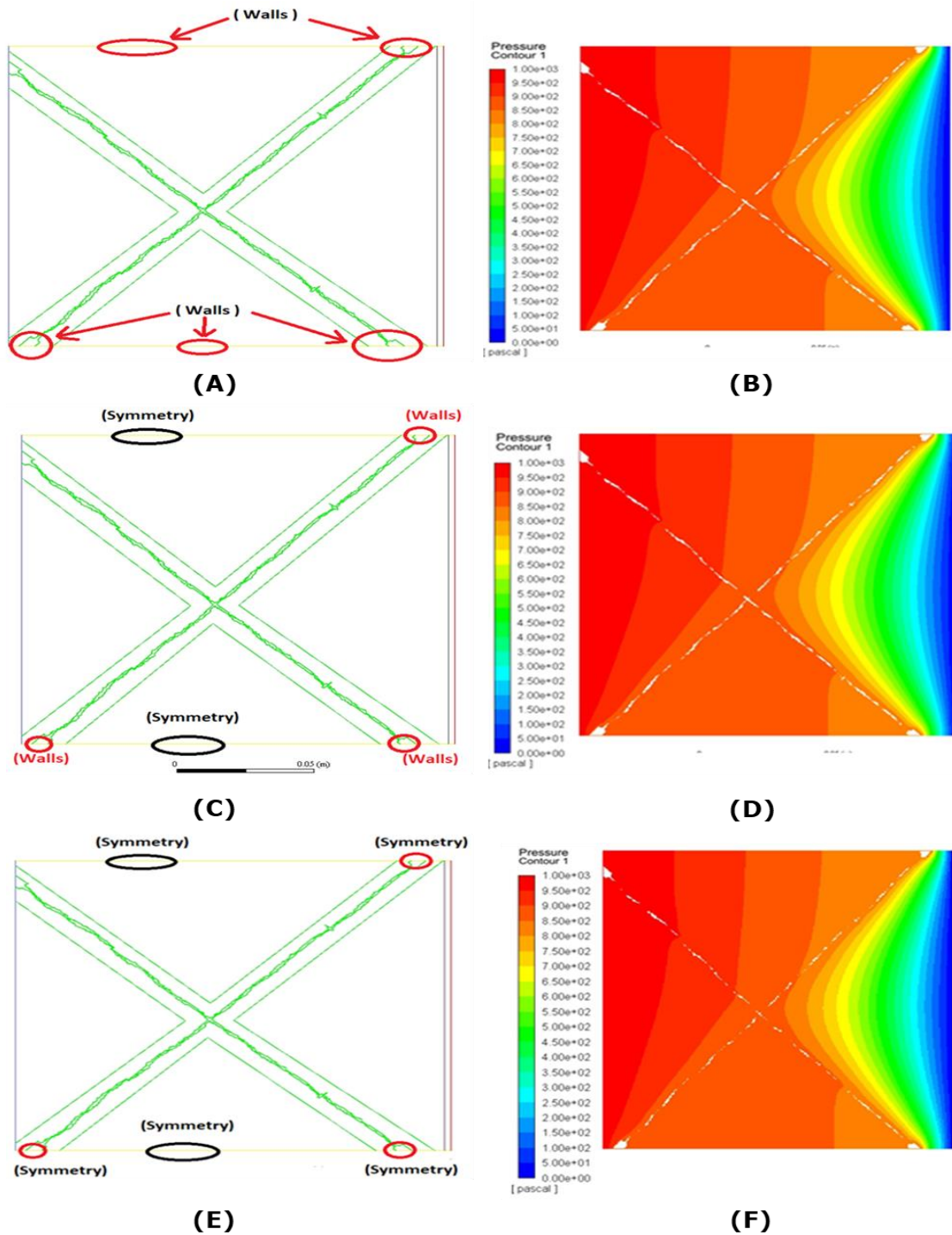


Figure 6.27 Clarifies 3 boundary conditions of network 2, which were changed at the far side (top and bottom) of the matrix, and the static pressure contours of these models

A. C. and E.: the first, second and third boundary set-ups respectively. B. D. F.: static pressure contours of three boundary models respectively

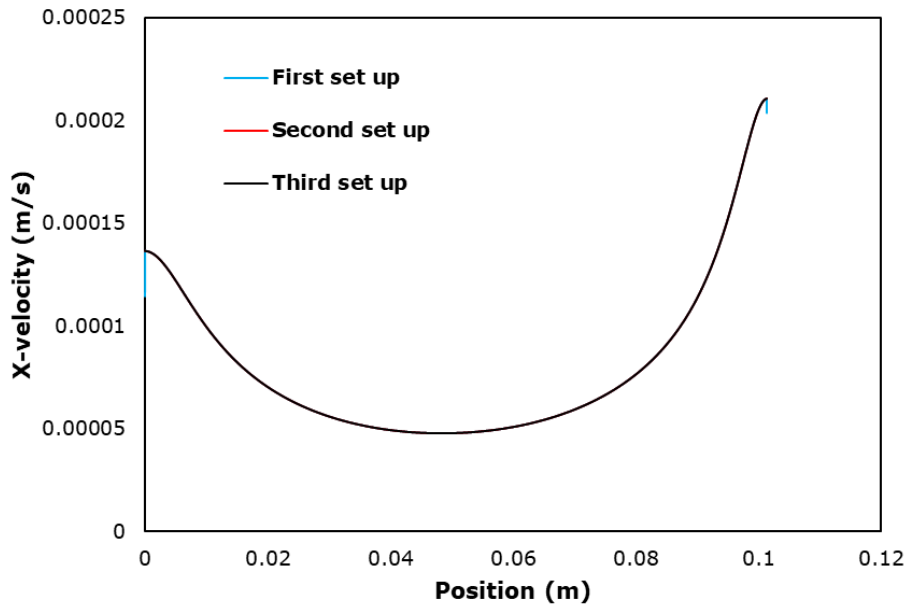


Figure 6.28 X-Velocity profiles of the total domain of the three set-ups of boundaries in network model 2, the reading lines of the total domain (all profiles almost matched)

Table 6.5 ADV of X-velocity comparisons between the three boundary condition set-ups and initial model of network 2

Fracture Network 2	The First Simulation (the initial model)	First Boundary Condition Set-up	Second Boundary Condition Set-up	Third Boundary Condition Set-up
X-Velocity profile (average) (m/S)	7.97444E-05	7.9532E-05	7.97424E-05	7.97442E-05
(%) Average difference value (ADV)		0.267	0.00253	0.000221

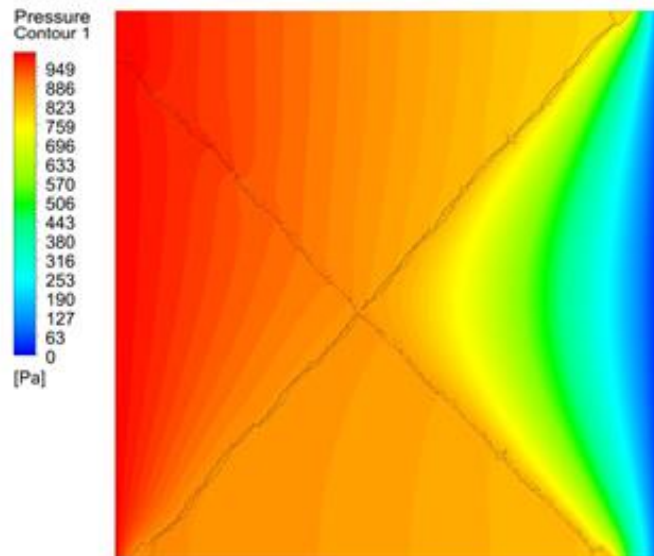


Figure 6.29 Static pressure contours from ANSYS CFD Fluent FVM -POST network 2

6.3.7.2 Second Approach

As the first approach had not reflected any changes in the pressure value and the distribution of the contours, therefore further investigation was conducted to check the pressure changing behaviour inside the domain from inlet towards outlet of the domain. This case was investigated further by using the same initial ANSYS CFD Fluent FVM model with the Third set-up (fracture Y-outlets and the adjacent surfaces (top and bottom side of far matrix) were assigned with Symmetry condition only) and simulated, but with the time Transient set-up instead of Steady set-up, in order to investigate the pressure changing inside the domain with different time steps.

Thus, two time steps were used: first, **0.025 seconds** and divided into 5 steps; and second, **0.02 seconds** and divided into 10 steps. Then, static pressure contours were read in each step, and as well, these steps were recorded as videos to visualize the pressure changes. It's good to note that the reason to choose these two times was because the first-time steps were large and unable to check for more focused variations of the pressures in the domain; therefore, the second time was used with smaller time steps. The outcome of these transient simulations was that the pressure contours of the domain were changing along the domain due to the pressure drop, and the final pressure distribution was due to the effect of the fracture network geometry pattern. [Figure 6.30](#) below illustrates transient static pressures contours with these time steps. These pressure changes were not detected during the Steady set-up simulations, as it gave the final distribution inside the domain.

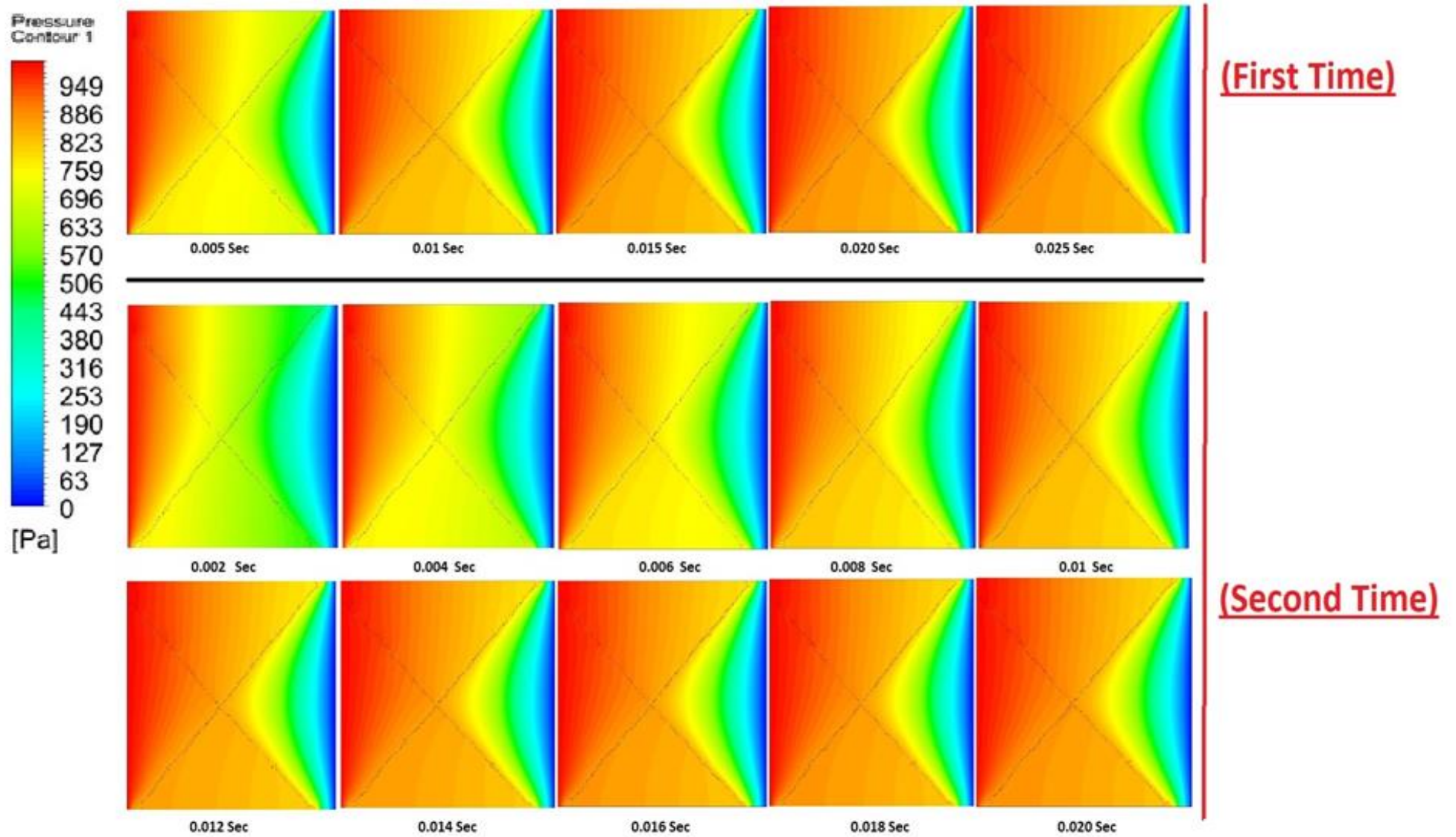


Figure 6.30 Static pressure transient with two different time steps

6.3.7.3 Analysis of pressure contours distribution in Network 2

The analysis for the pressure distribution in this model followed this reasoning. The fracture was not passing through the entire domain (from inlet toward outlet) and there was no flow exit of the fracture outlets; in other words, it was ending inside the matrix domain. The total flow from the inlet toward domain outlet, passed through fracture permeable surfaces (fracture/matrix interface layer). In the first half, matrix flow was affected by the fracture barrier, and had to pass fracture/matrix interface layer, and at the same time, fracture flow had no outlet, which led both fracture and matrix flow to pass the other end of the fracture interface permeable layer. As well, the matrix domain between the first and second half of the domain was surrounded with inclined fractures from both sides. This caused pressure build up in the first half, so the flow was choked between the inlet and the first half of the domain in X-axis of the Cartesian axis. In the second half of the domain, the pressure started to take the normal reduction along the flow length in the domain: particularly after passing the fracture, as flow was then passed through matrix only towards the domain outlet without fracture barrier. [Figure 6.31](#) below clarifies this.

This process of pressure build of this network clarified the outcomes of previous researchers in the literature, that consider fractures in fractured formations can represent a barrier or facilitator of fluid flow, based on various factors; for example, when fractures have varied orientation angles, and are not ordinated with flow axis, higher resistance is present with an increase of inclination angle ([Li et al. 2021](#); [Zhu et al. 2020](#); [Ahmadi et al. 2018](#); [Sahimi 2011](#); [Sarkar, Toksöz and Burns 2004](#); [Tiab and Donaldson 2004](#); [Nelson 2001 pp. 12, 217](#); [Sen 1995](#)). Also, the location of pressure drawdown in relation to fractures' orientations inside fractured formations plays a major role in fracture / matrix effects on domain flow ([Luo et al. 2020](#); [Popov et al. 2009 pp. 226-227, 230](#)), and if fractures are not connected between inlet and outlet inside fractured formations, connectivity among the fracture network leads flow distribution in the fractured domain to be varied and uneven ([Li et al. 2021](#); [Luo, Tang and Zhou 2019](#); [Berkowitz 2002](#); [Zimmerman and Yeo 2000 p. 864](#); [Nordqvist et al. 1992](#)). As fracture connectivity is weak in this case, the matrix is the main fluid transporter in the domain, and matrix permeability will increase fracture connections and affect total domain flow ([Li et al. 2021](#); [Ahmadi et al. 2018](#); [Yi and Xing 2018](#); [Spence et al. 2014](#); [Ishibashi et al. 2012](#); [Narr, Schechter and Thompson 2006](#)). Moreover, as fractures in this network had no outlet, only fluid could pass through interface layers between

matrix and fracture, which led to increased capillary pressure of interface layer, and the results increased pore pressure, and accordingly, fluid flow proportions increased from fracture interface layer toward matrix. This was because capillary pressure drives fluid inside the matrix, which works against viscosity that drives fluids toward more permeable spaces (ie. fracture) from the matrix (Yin et al. 2017; Hughes and Blunt 2001; Sen 1995 pp. 111, 309; McDonald et al. 1991; Pruess and Tsang 1990). As well, the fracture/matrix capillary number is altered by increasing pressure inside the fracture open space domain (Tiab and Donaldson 2004), and varies along a fracture due to varied fracture apertures from point to point, and surface roughness of a fracture (Sahimi 2011 pp. 18, 244; Jahn, Cook and Graham 2008; Tiab and Donaldson 2004; Wagner et al. 2001). This operation of percolation of interface layer is affected by many factors such as: the proportion of the fracture contact area with matrix (Zimmerman and Bodvarsson 1996 pp. 44-45); fracture density; size distribution; fractures' orientations; and fracture special distribution (Narr 2011 p. 374; Narr, Schechter and Thompson 2006). This model confirmed this effect, as matrix flow in ANSYS CFD Fluent FVM model scenarios ($K_x=K_y=2000$ mD), ($K_x=2000$ $K_y=380$ mD) & ($K_x=380$ $K_y=2000$ mD) increased 120%, 174% and 86% respectively in ADV, in comparison with Darcy flow equation. This has clarified percolation theory effects in such a network pattern.

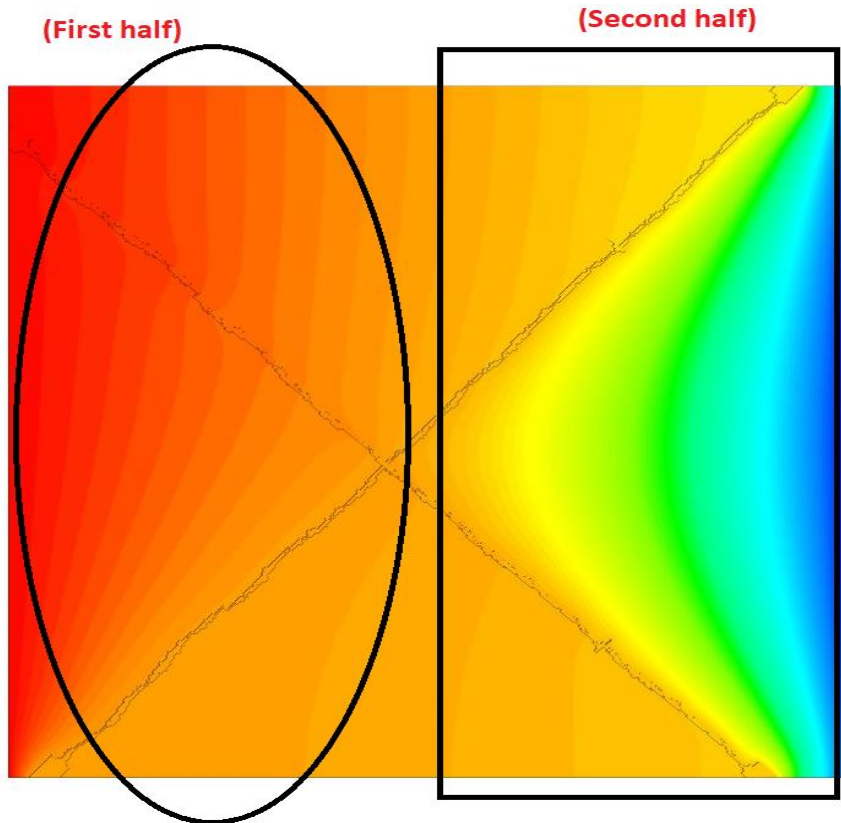


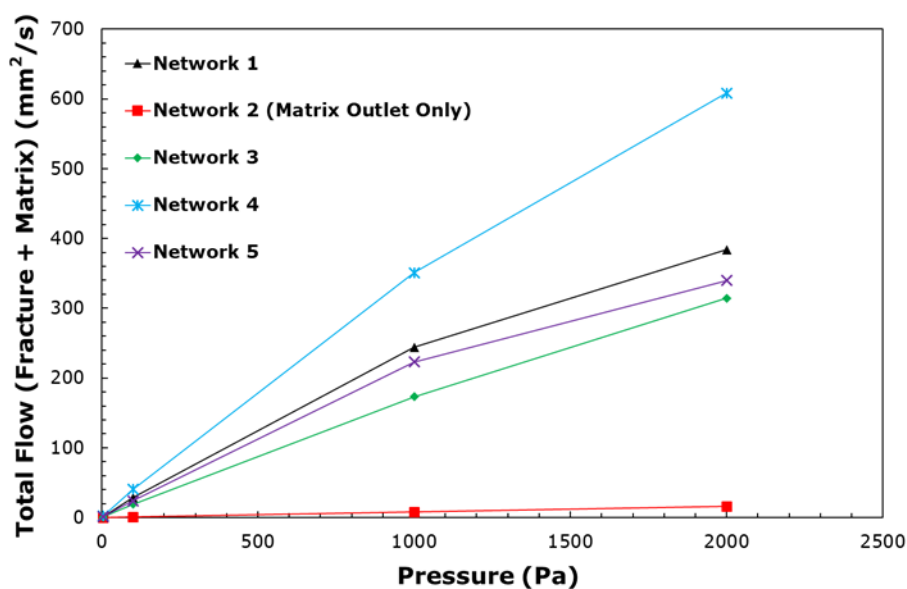
Figure 6.31 Clarifies fracture network 2 - two behaviours of static pressure contour in the same domain

6.4 Comparisons Among Fracture Network Models

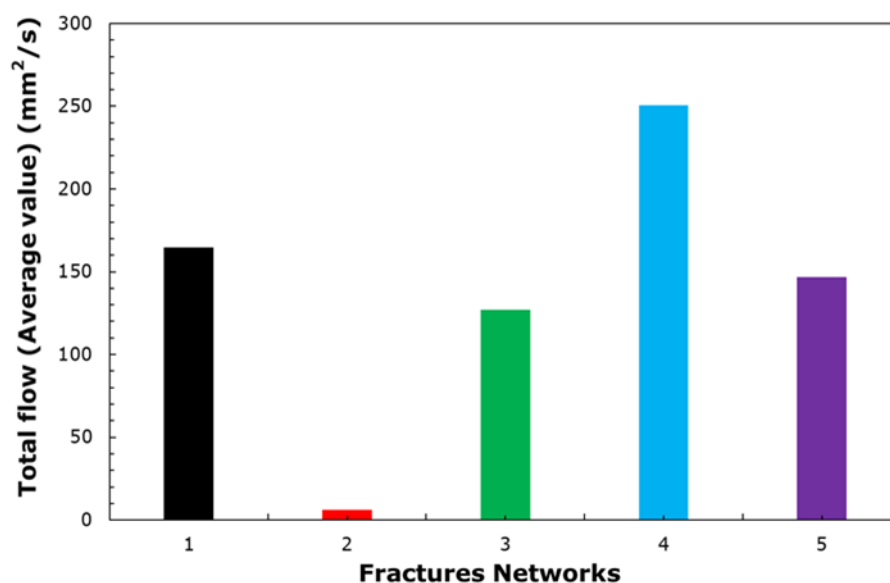
To investigate the effect of fracture network geometry patterns, that have different fracture network orientations inside the fractured media, on the total fractured media, consisting of both fractures and matrix, it was mandatory to conduct comparisons of flow in these models for fractures and matrix. Thus, the flow rates of total, fracture and matrix were compared among the five fracture network models, with isotropic matrix permeability $K_x=K_y=2000$ mD and four pressure drop (5, 100, 1000, 2000) Pa, zero pressure outlet; all fracture surfaces were permeable and interacting with the matrix “interior face boundary”.

The results of the total flow rate comparison of these five models were: fracture network 4 was the highest flow rate 250 mm²/s in average value, while the lowest was in fracture network 2 with 6.26 mm²/s in average value. [Figure 6.32](#) presents these results. The results of the matrix flow rate comparison of these five models were: fracture network 4 had the highest flow rate 221.2 mm²/s in average value,

while the lowest was in fracture network 2 with 6.26 mm²/s in average value. Figure 6.33 presents these results. Similarly, fracture flow rate of network 4 had the highest rate with 29.2 mm²/s in average value, and the lowest was in network 2 with 1.16 mm²/s in average value. Figure 6.34 clarifies this.

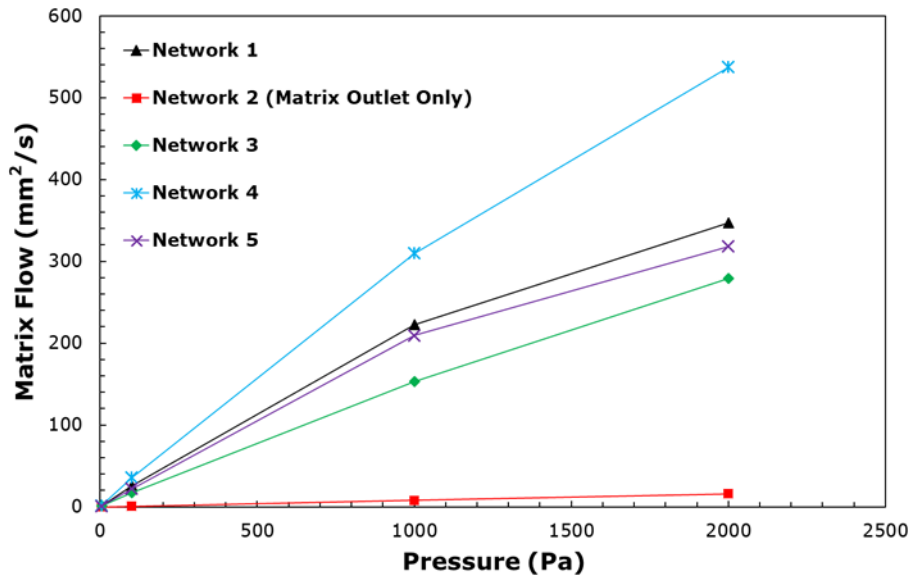


(A)

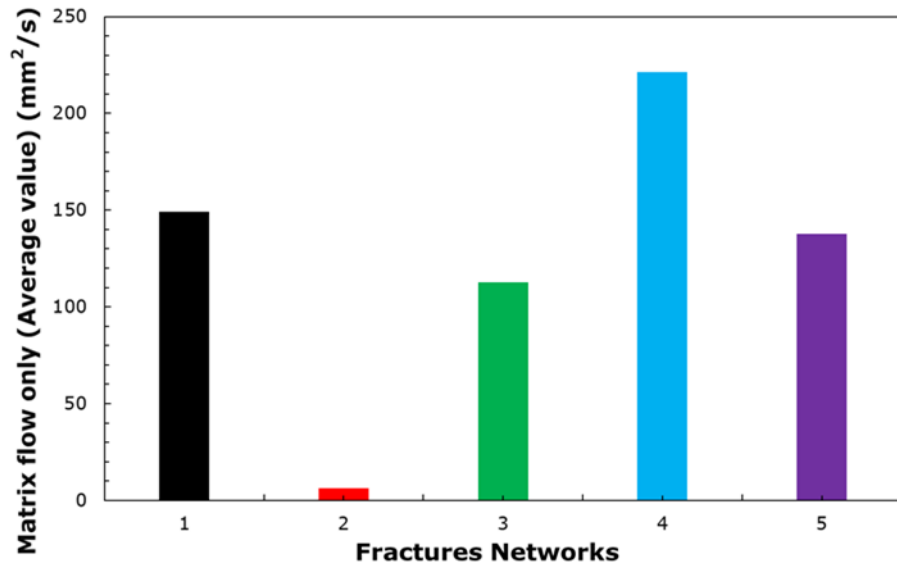


(B)

Figure 6.32 A. Total flow (mm²/s) comparisons of 5 fracture networks with K_x=K_y=2000, B. Average value of total flow (mm²/s) comparisons of all fracture networks with K_x=K_y=2000 mD, in four pressure drops models (5,100, 1000, 2000) Pa , zero pressure outlet, with permeable fracture surfaces "interior face boundary"

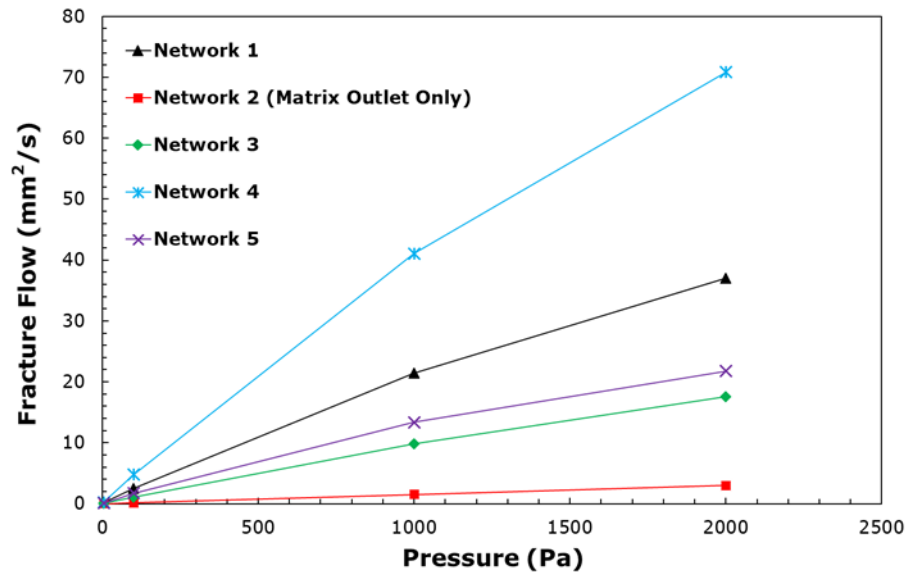


(A)

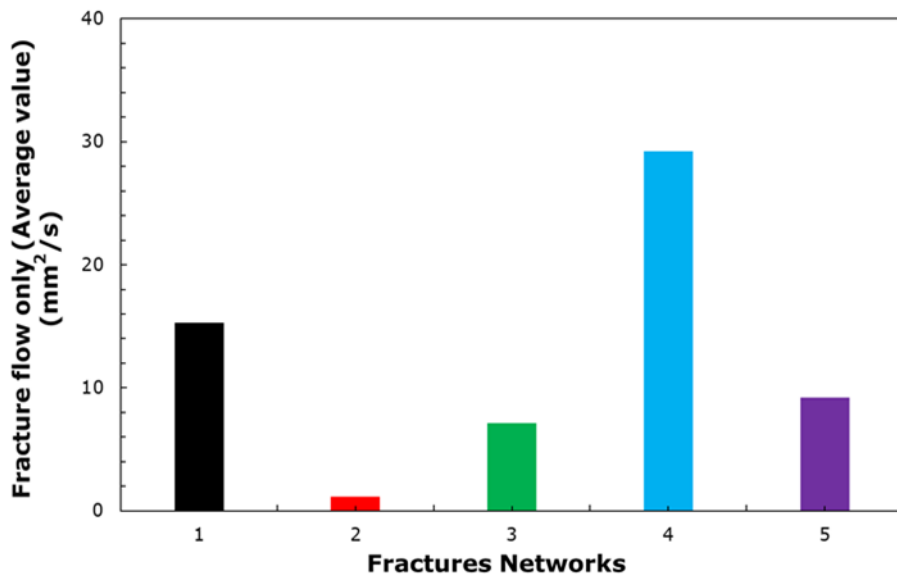


(B)

Figure 6.33 A. Matrix flow (mm^2/s) comparisons of 5 fracture networks with $K_x=K_y=2000$; B. Average value of matrix flow (mm^2/s) comparisons of all fracture networks with $K_x=K_y=2000$ mD, in four pressure drops models (5,100, 1000, 2000) Pa, zero pressure outlet, with permeable fracture surfaces "interior face boundary"



(A)



(B)

Figure 6.34 A. Fracture flow (mm^2/s) comparisons of 5 fracture networks with $K_x=K_y=2000$, B. Average value of fracture flow (mm^2/s) comparisons of all fracture networks with $K_x=K_y=2000$ mD, in four pressure drops models (5,100, 1000, 2000) Pa, zero pressure outlet, with permeable fracture surfaces "interior face boundary"

6.4.1 Results analysis

The results of these comparisons among the fracture network models flow reflected interesting results, summarised as follows:

1. From highest to lowest flow of fracture network models, fracture network 4 had the highest total flow, then network 1, network 5, network 3 and network 2 was the lowest in all pressure drops, with all matrix permeability scenarios isotropic and anisotropic. Fracture and matrix flow had the same behaviour. This confirmed the effects of many factors on fracture network flow, such as: network patterns and fractures' orientations on fractured domain flow, which play a crucial role in fluid flow distribution inside fractured domains; fracture/matrix interactions on each other during flow and fluid movements among these media, as both share the same physical locations; fracture locations and angles in relation with flow directions; fracture intersection nodes' effect on pressure behaviour of the domain, and the effect of fracture connectivity; and the effect of surrounding matrix properties, such as permeability, on flow percentage in the fractured domain (Li et al. 2021; Luo et al. 2020; Zhu et al. 2020; Yang et al. 2019; Luo, Tang and Zhou 2019; Wu et al. 2019; Ahmadi et al. 2018; Zou, Jing and Cvetkovic 2017; Liu, Li and Jiang 2016; Ishibashi et al. 2012; Sahimi 2011 p. 45; Popov et al. 2009; Nordqvist et al. 1992).

Moreover, it was seen that fractures have highest flow rate when there is a fracture in the network that connects between inlet and outlet of domain boundaries, as it is considered as the least resistant fluid flow path which will carry a higher proportion of the network's flow, even with a small inclination angle with respect to the pressure gradient axis (Sarkar, Toksöz and Burns 2004). This was observed in Network 4 which reflected highest flow in fracture and matrix domains, due to the horizontal fracture orientations which were parallel to flow direction in X Cartesian axis, that connected between inlet and outlet boundaries of the fractured domain. Similar behaviour was observed in network 1 as there was one fracture with horizontal orientation that connected in the middle of the domain between the two angled inlet and outlet boundary fractures, and altered domain flow. Similarly, other networks 5 and 3 followed

this argument, except network 2 as there was no fracture outlet in the domain. This has clarified that as the fracture connections between inlet and outlet boundaries are eased, and have less resistance to flow with angles, this will increase fracture network flow. This case has clarified the findings of [Li et al. \(2021\)](#) and [Wu et al. \(2019\)](#); in the case that a fracture of any network is connected directly between the inlet and outlet in the domain, it will be called a “dominant channel”, as the velocity and flow is much larger than other network branches. The pattern of network 4 pattern in this research reflected this effect, with highest flow proportion in comparison with the other networks. Fracture network pattern shapes play a major role, whether easing or obstructing fracture network flow; as well, if a fracture network has a simple pattern it eases flow more than a network with a more complicated fracture pattern ([Li et al. 2021](#); [Zimmerman and Yeo 2000](#)). As in the case of networks 1, 3, and 5, fluid flow went from highest to lowest respectively here due to the fact that the fracture patterns got more complicated with branches, creating more distance of flow inside fractures between inlet and outlet domain boundaries, and fracture orientation angles.

In addition, it was observed, when fracture flow was high, this meant higher velocity inside the fracture, which meant matrix flow proportions increased as well. This was due to higher fluid movement proportions between the fracture and surrounding matrix. This interaction was increased with rough fracture networks, because the percolation limit relies on many factors such as: local capillary pressure relies on interfacial tension, fracture aperture, and contact angle ([Prues and Tsang 1990](#)); matrix and fracture rely on pressure differences between both media ([Sen 1995 pp. 111, 309](#)); inner surfaces of fractures are varied, with different roughnesses which consist of different curvature shapes (the pores in this roughness represent the cluster gateways of fluid flow between matrix and fracture ([Sahimi 2011 pp. 15, 18, 45, 244](#)); critical value of inner fracture contact areas with matrix ([Zimmerman and Bodvarsson 1996 p. 44-45](#)); fracture density; size distribution; fracture orientations; and fracture special distribution, which is related to fractures’ intersection and relates to increase fractures’ length spanning ([Luo, Tang and Zhou 2019](#); [Narr 2011 p. 374](#); [Narr, Schechter and Thompson 2006](#)).

2. In fracture networks, the interesting finding was that matrix flow % out of the total flow was much higher than the fracture flow %. This finding introduced

the importance of matrix flow in rough fractured networks, in comparison with some beliefs in the previous literature, where fractures were considered the main conductor of fractured media flow, even excluding matrix flow contribution to fractured media in some cases (Luo et al. 2020; Tiab and Donaldson 2004; Toksöz and Burns 2004; Nelson 2001). In this research, matrix flow in fracture network models was compared with Darcy flow (equation 2.3). All the networks reflected an increase in flow approximately 200% (ADV), except fracture network 2 which reflected varied matrix flow increases around 120%, 174% and 86% with permeability scenarios ($K_x=K_y=2000$ mD), ($K_x=2000$ $K_y=380$ mD) & ($K_x=380$ $K_y=2000$ mD) respectively. Network 2 was the only network where the fracture domain did not pass to the outlet of the domain. These results confirmed the findings of Spence et al. (2014); Ishibashi et al. (2012) and Narr, Schechter and Thompson (2006) that fluid flow prediction and movements in naturally fractured reservoirs are highly related to fracture networks' transmissivity and interactions with the surrounding matrix, and that matrix flow contribution is highly significant in the fractured domain. Moreover, Li et al. (2021); Yang et al. (2019); Zou, Jing and Cvetkovic (2017); Dippenaar and Van Rooy (2016); Ishibashi et al. (2012); Popov et al. (2009) pp. 226-227, 230) and Sen (1995) pp. 111, 309) clarified that the existence of a fracture in fractured media influences the effective permeability of the total domain, and accordingly will affect the domain's overall flow substantially. This is due to the tangential forces inside fracture surfaces, different flow velocities between fracture and matrix along rough fractures, and varied pressures from point to point inside a fracture. These can each cause fluid movements and interactions between matrix and fracture to be more active, which leads to increased matrix flow in proportion with non-linear in the fractured domain.

3. Fracture networks 3 and 4 had the same average aperture value 609 micrometre and standard deviation (332), and the fracture area % inside the domains was 1.33% and 1.27% respectively. However, although the fracture area % in network 4 was less, the total flow rate and matrix flow rate of fracture network 4 increased 65.46% and 65.1% respectively in ADV. This case reflected the effects of fracture orientation inside the domain, because both fracture network models had similar fracture lengths and standard deviations, with marginal difference in fracture area percentage in both domains, only 6%.

The main difference was the fracture orientations; in fracture network 4 there was one horizontal fracture in the network that connected between inlet and outlet boundaries "dominant fracture", while in fracture network 3 both fractures were inclined with 45° angles as clarified in point 1. This case confirmed the effects of angled fractures in comparison with a dominant channel in fractured networks. As stated by [Li et al. \(2021\)](#) and [Zhu et al. \(2020\)](#), in fracture networks, fracture orientation angles have an important effect on a fracture network's flow, fracture permeability and seepage characteristics of a fracture network. In comparison between fracture networks with the same fracture porosity but with different dip angles, therefore, as the dip angle increased, the fracture network's permeability decreased. The reason for this permeability decrease is due to the increase of fluid flow resistance, and the maximum dip angle effect is with 45° . Similar findings were made by [Sarkar, Toksöz and Burns \(2004\)](#), but the model only considered impermeable fracture network surfaces with single aperture parallel plates model, and stated that the angled fracture was effected by $(\cos \theta)$ value, which meant adding more length to fracture length in comparison with horizontal orientation fractures.

4. Fracture networks 2 and 4 had a very similar value of average apertures, 610 and 609 micrometres respectively, and the percentage of fracture area inside the domains was 1.75% and 1.27% respectively, which meant fracture network 2 had 0.48% bigger fracture area than fracture network 4. However, ADV of the total flow rate and matrix flow rate increased 190.24% and 189% respectively in fracture network 4. The fracture network differences between the two were: fracture network 2 had no fracture outlets, as the fractures ended before the domain outlet boundary; and as well, network 2 fractures had orientations with inclined angles 45° , while half of the fracture area in fracture network 4 was with horizontal orientation "dominant fracture". This case reflected the effect of fractures on flow percentages of fracture and matrix in fractured domain as clarified in point 1 and 2. As well, although network 2 had no fracture at the outlet boundary, matrix flow in comparison with Darcy flow was increased with 120%, 174% and 86% with permeability scenarios ($K_x=K_y=2000$ mD), ($K_x=2000$ $K_y=380$ mD) & ($K_x=380$ $K_y=2000$ mD) respectively. This clarifies fracture networks' transmissivity and interactions with the surrounding matrix, and the non-linearity of matrix flow, as discussed in point 2.

5. For fracture networks 1 and 5, the percentage of fracture area inside the domains was 1.60% and 1.49% respectively, which meant fracture network 1 had 0.11% bigger fracture area than fracture network 5. ADV of the total flow rate, fracture flow rate and matrix flow rate increased 11.25%, 50% and 8% respectively in fracture network 1. The pattern descriptions of these networks were that both networks had one fracture inlet and one fracture outlet with angled fractures with 45° . However, network 5 had more fracture branches and its fractures were all inclined by 45° , while network 1 had an extra benefit which altered the flow proportions: one horizontal fracture branch with zero angle in Cartesian X-axis that connected between inlet and outlet inclined fractures. This comparison further clarifies point 1, as fracture networks with simple patterns (network 1) are more eased to flow than a network with more connected fractures pattern (network 2); as well, this demonstrates the effects of angles on network fractures (Li et al. 2021; Zhu et al. 2020; Zimmerman and Yeo 2000).
6. For networks 1, 2, 3, 4 and 5, % fracture flow average value with pressure drops 5, 100, 1000, and 2000 Pa, was approximately 9%, 18.6%, 11.46%, 11.75% and 6.66%. % matrix flow average values were 90.9%, 81.42%, 88.54%, 88.25% and 93.34%, respectively. As can be seen, the matrix flow percentages were much higher than fracture flow percentages in all the fracture networks which showed the matrix domain does work as a main fluid provider and conductor, as clarified in point 2. However, each network model reflected approximately similar values of fracture and matrix flow percentages with changing pressures between 5, 100, 1000 and 2000 Pa. Few of these networks with different patterns reflected very small change in percentages of fracture and matrix flow (fluctuations less than 1% only) in each network with increasing pressure. Figures 6.35 and 6.36 below present an example of isotropic scenario models ($K_x=K_y=2000$ mD) of all five networks. As well, effective permeability ($K_{\text{effective}}$) was calculated as equation 5.11 for all matrix permeability scenarios, then, average value of % matrix flow comparisons were made of all fracture networks in four pressure drops models (5,100, 1000, 2000) Pa, zero pressure outlet, with permeable fracture surfaces "interior face boundary". Figure 6.37 presents this. This small change of networks' matrix and fracture flow percentages is clarified below:

- a) Fracture network 1, on pressures 5 and 100 Pa, reflected similar behaviour of fracture and matrix flow percentages. However, at 1000 Pa % fracture flow decreased, and % matrix flow increased, and at 2000 Pa, fracture flow % increased and matrix flow % decreased. Thus, between 1000 and 2000 Pa these percentages swung between increase and decrease; similar behaviour was observed in fracture network 5, but with different fluctuation values with a range of 1% change only.
- b) Fracture network 3, on pressure 5 and 100 Pa, reflected similar behaviour of fracture and matrix flow percentages. However, at 1000 and 2000 Pa, fracture flow % continued to decrease with increasing the pressure, and matrix flow % continued to increase with increasing pressure, in the same ranges of 1% change only.
- c) Fracture network 4, fracture flow % reflected steady and slight decrease by increasing pressure between 5 and 2000 Pa respectively, while matrix flow % increased steadily and slightly by increasing pressure, in the same ranges of 1% change only.
- d) Fracture network 2, reflected similar behaviour of fracture and matrix flow percentages with all pressures.

To analyse this fluctuation of fracture and matrix percentages' slight change with pressure (fluctuations less than 1% only), it was important to explain each network pattern and condition as below:

- For network 2, flow of matrix and fracture percentages had similar behaviour with pressure changes due to the reason that the fracture did not pass through the outlet boundary in fractured domain, and flow only passed between fracture to matrix through fracture interface layer. This meant increasing pressure increased fluid movements between fractures and matrix, but with the same percentages as clarified in points 2 and 4.
- Fracture networks 1, 3, and 5 were all affected with higher pressures 1000 and 2000 Pa, the main reason for this was that higher-pressure inlet improved flow in the matrix, in comparison with a lower pressure drop, due to the pressure effect on fluid particles that were trapped in pores of the matrix ([Suri et al. 2020](#)). As well, these fracture networks had different patterns which had an important effect on fracture network's flow, fracture permeability, and seepage characteristics of the fracture network, as clarified in points 1,2, and 3. Fracture network patterns get more complex when branches have highest angle effect 45° ([Li et al. 2021](#); [Zhu et al.](#)

2020; Zimmerman and Yeo 2000), and more intersection angles among fracture networks at nodes have an effect on pressure behaviour of the domain, and the effect of fracture connectivity (Luo, Tang and Zhou 2019; Hyman et al. 2015). This causes more distance of fluid flow inside fractures between inlet and outlet domain boundaries, and varied % fracture areas of each network, and varied contact areas of fracture surfaces with matrix, which affects capillary pressure of fractures in these networks (Hughes and Blunt 2001; Wagner et al. 2001; Berkowitz and Ewing 1998; Stauffer and Aharony 1992). Also, pore structure plays an important role in adsorption of fluids in formations (Andersen and Zhou 2020; Yin et al. 2017). These factors led to these small fluctuations, of less than 1%, of fracture and matrix flow percentages among these networks with either increase or decrease in pressure. In addition, by increasing pressure, fluid momentum inside fractures was increased, which led to increase % fracture flow and overcome fractures' roughness resistance (Briggs, Karney and Sleep 2017; Dippenaar and Van Rooy 2016; Briggs, Karney and Sleep 2014).

- Fracture network 4 was affected between pressures 5 to 2000 Pa. This change reflected similar factor effects as above of networks 1, 3, and 5. However, due to the existence of a dominant fracture, that was connected directly between the inlet and outlet in the domain and had higher effects on the network domain, and another fracture with 45° angle, this led to increase the flow interactions with surrounding matrix. More fluids moved from fractures towards matrix, due to effects of capillary pressure in fracture/matrix interface layer, by increasing fracture flow rate, and more fluids moved into matrix (Yin et al. 2017; Hughes and Blunt 2001), and as clarified in detail in points 1,2,3 and 4.

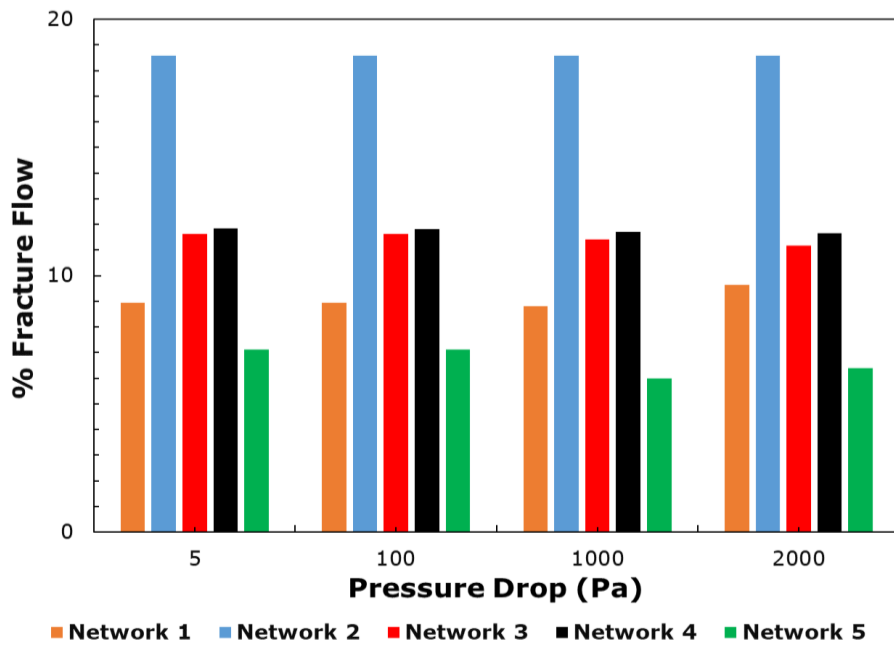


Figure 6.35 % Fracture flow only of fracture networks with isotropic matrix permeability ($K_x=K_y=2000$ mD)
 (% Fracture flow in some networks reflected minor change of 1% with pressure changing (network 4) or only higher pressures 1000 and 2000 Pa (networks 1, 3, and 5))

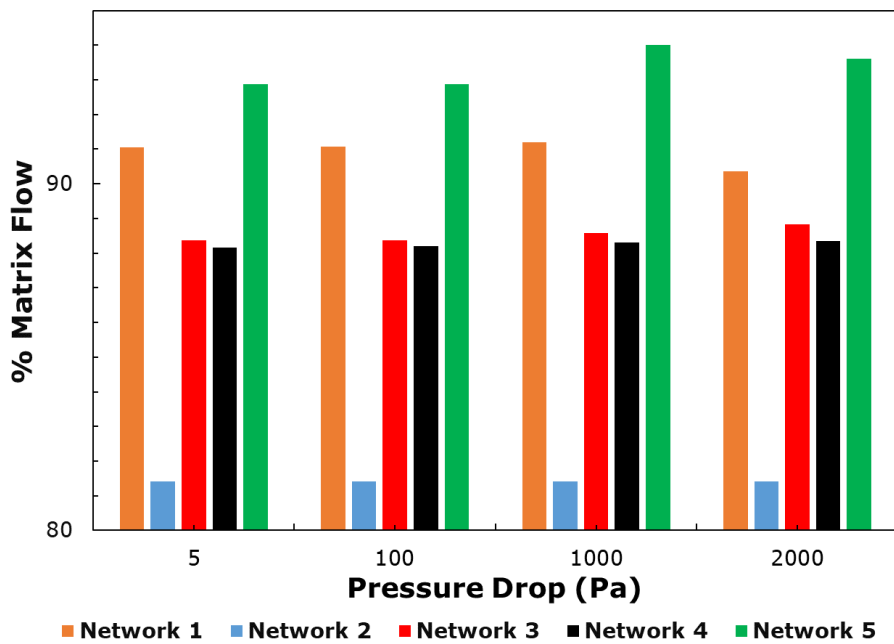


Figure 6.36 % Matrix flow only of fracture networks with isotropic matrix permeability ($K_x=K_y=2000$ mD)
 (% Matrix flow in some networks reflected minor change with 1% with pressure changing (network 4) or only higher pressures 1000 and 2000 Pa (networks 1, 3, and 5))

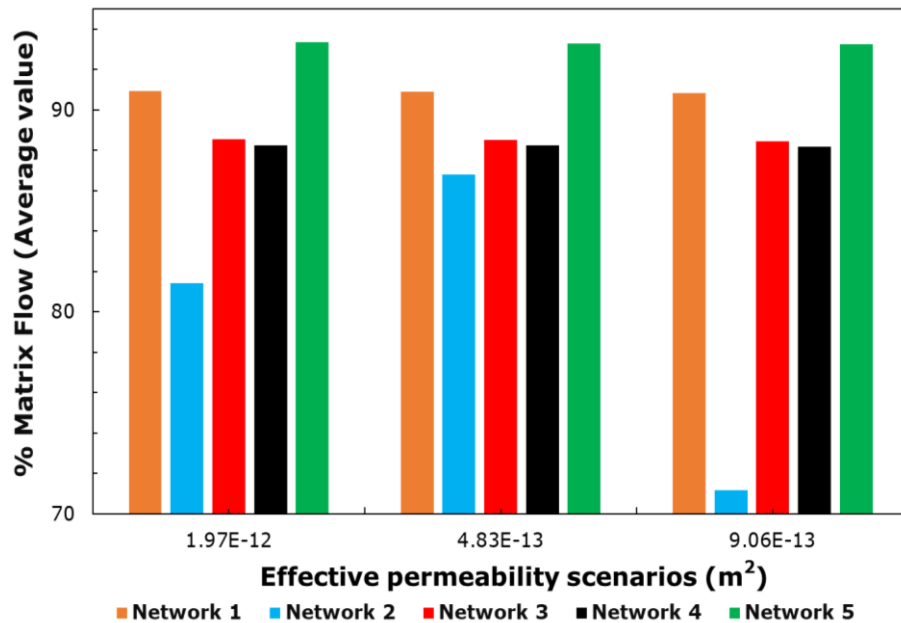


Figure 6.37 % Matrix flow comparisons average value of all fracture networks in four pressure drops models (5,100, 1000, 2000) Pa, zero pressure outlet, with permeable fracture surfaces “interior face boundary”, with effective permeabilities of all matrix scenarios

6.5 Comparisons Of Ten Sections Inside Fracture Network Models

Each fracture network had a distinguished pattern inside the fracture domain, that consisted of fractures and the surrounding matrix. In each vertical section inside the domain, there was a different percentage of the fracture and matrix areas, and each one had a different flow contribution into the total flow of the domain at that particular point. Therefore, to investigate the flow along the fractured network domain, ten vertical sections were considered by creating ten vertical reading lines in ANSYS CFD Fluent FVM to observe X-velocity and calculate the total flow in each model. The X-distance among these lines were equal and based on 0.01m increments. All these lines had the same height which was 0.10152m, to cover the total domain height. The main goal of this investigation was to understand the flow variations along the fractured network domains, where the fracture/matrix area percentages were varied in each section of each fracture network model. Thus, five models were chosen, one from each network. All the five models had the same isotropic matrix permeability ($K_x=K_y=2000$ mD), and the same inlet pressures

($P=1000$) pa and outlet pressure (zero) pa, fracture surfaces were set as permeable "interior face boundary". The total number of sections was 50; [Figure 6.38 and 6.39](#) clarify the sections and pressure contours of the networks, and [Figures 6.40 and 6.41](#) present the total flow of the sections.

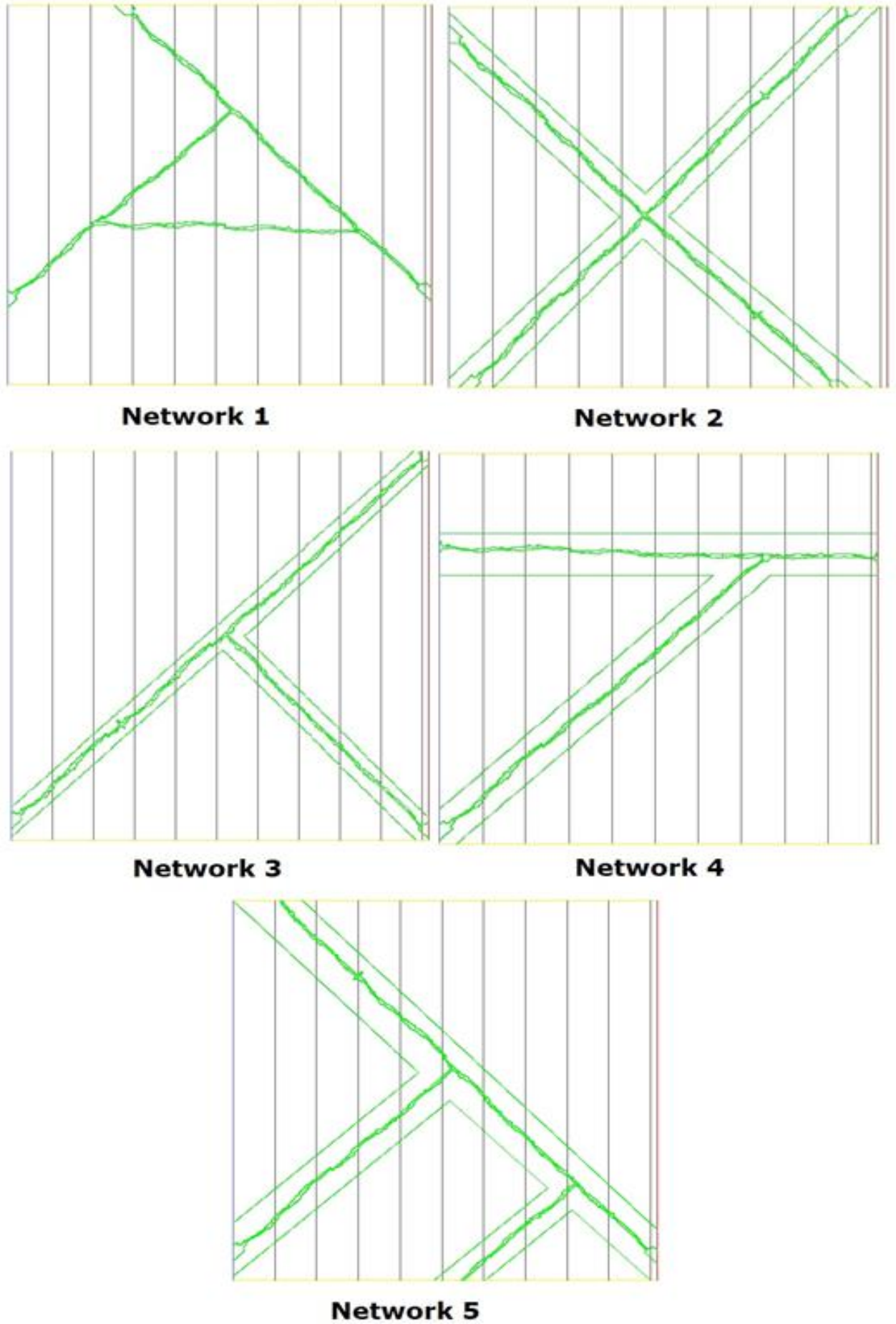


Figure 6.38 Ten sections inside fracture network models

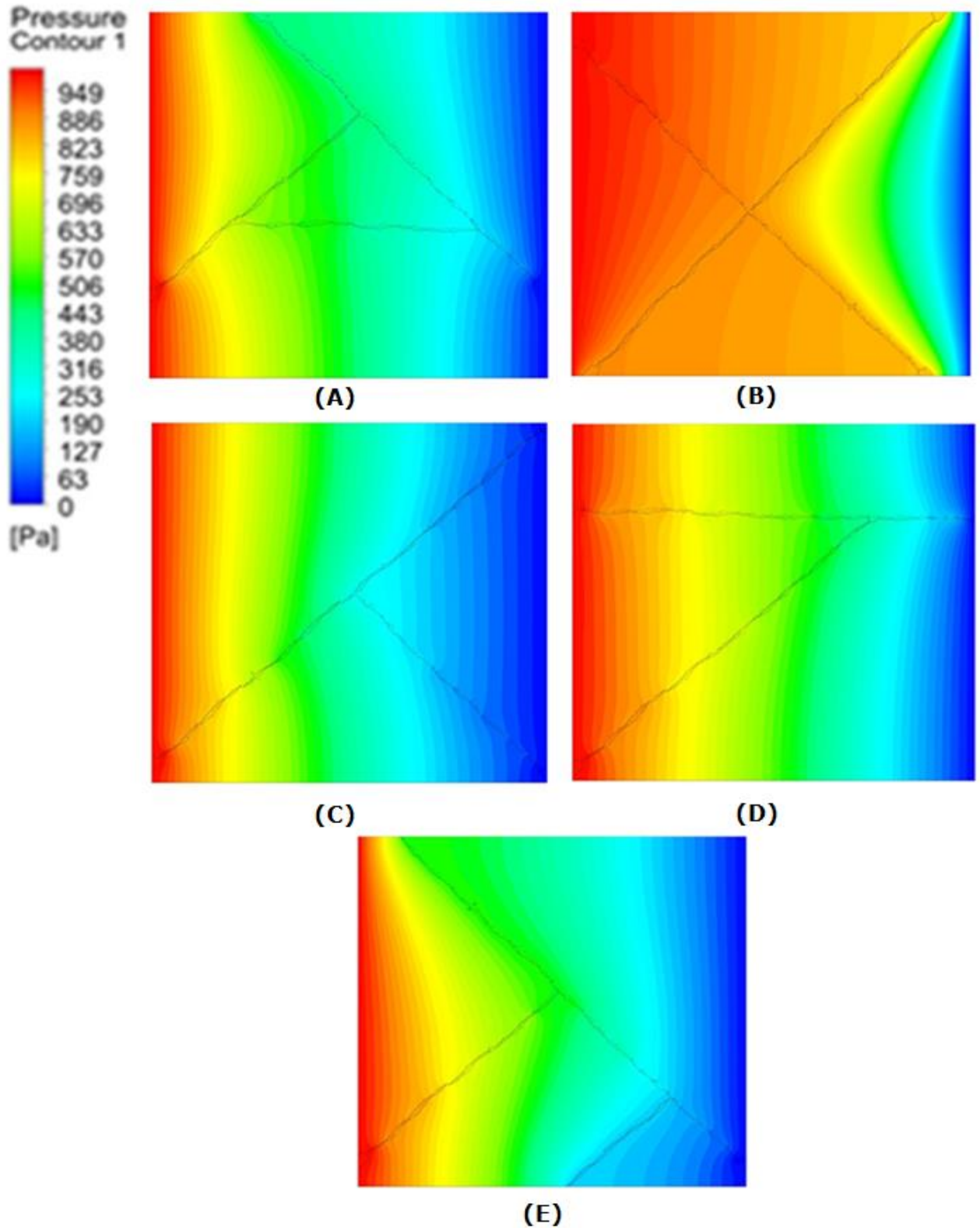


Figure 6.39 Total pressure contours of five fractured network ANSYS CFD Fluent FVM models with $K_x=K_y=2000$ mD, $P=1000$ Pa
 A. B. C. D. and E.: fracture networks 1, 2, 3, 4 and 5, respectively

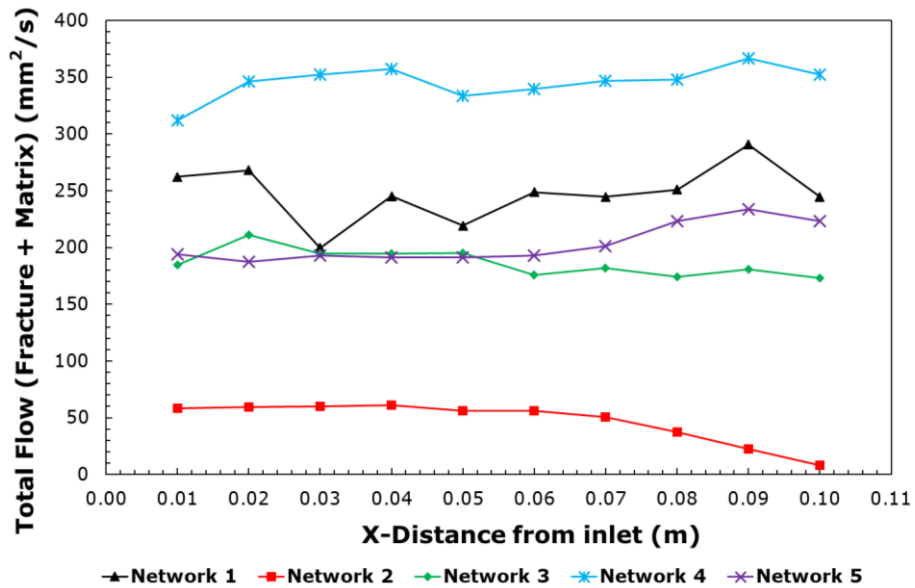


Figure 6.40 The total flow trends of fracture network models' sections with $K_x=K_y=2000$ mD, $P=1000$ Pa

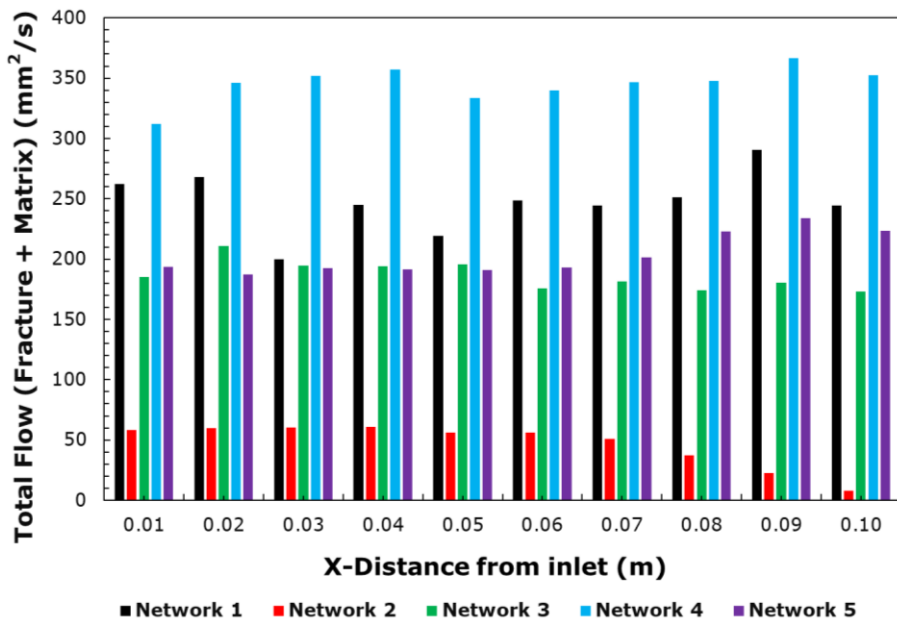


Figure 6.41 The total flow histograms of fractured network model sections with $K_x=K_y=2000$ mD, $P=1000$ Pa

6.5.1 Results analysis

The total flow comparisons of these 50 sections reflected that the flow of total domain kept varying along the flow, but the average values of one model still matched with the total flow, from the highest to lowest fracture networks 4, 1, 5, 3 and 2, as presented in [Figures 6.40 and 6.41](#). Thus, fracture network 4 had the highest total flow discharge and fracture network 2 (no fracture outlet) had the lowest total flow discharge, but the interesting finding was that fracture networks 1, 5 and 3, at the same section 0.03m in X-distance, had approximate values of total flow, as presented in [Figure 6.40](#) of their total flow trends. For fracture networks 5 and 3, at section 0.01m, network 5 had the highest flow while network 3 started with less flow. At the following section 0.02 the scenarios were vice versa, then, between section 0.03 and 0.05 they had close values of total flow; lastly, after 0.05m network 5 continued to steadily increase while network 3 continued to steadily decrease.

This investigation reflected that media flow in fractures changes from section to section, relying on many factors such as: fracture and matrix areas in section, as each one has different flow contributions; fracture orientation, whether with angle or horizontal incorporation of flow direction; and matrix/fracture properties such matrix permeability, and fractures' tortuosity. As can be seen, the total flow for network 1 in average value was higher than for networks 5 and 3 respectively, however, at x-distance section 0.03 m, all of them had approximate values of total flow. As well at this section, networks 1 and 3 had one inclined fracture with 45° , while network 5 had two inclined fractures with 45° ; however, one of these was a branch fracture which didn't connect between inlet and outlet boundaries of the domain, therefore the contribution of this fracture was low as clarified by [Li et al. \(2021\)](#) and [Wu et al. \(2019\)](#), who have analysed the effects of dominant fractures in fracture networks. This comparison highlights the importance of fracture network patterns, fracture angles, fracture/matrix percentage areas in each location, and fracture connectivity between the inlet and outlet boundaries in fractured network domains, as discussed in [Section 6.4.1](#). As well, it has proved that choosing the right point to draw a well in fractured formations is crucial to increase fracture networks' flow efficiency and functionality, by considering the factors that were highlighted in [Section 6.4.1](#) such as fractures' orientations, fractures' angles, and fractures' connectivity between pressure drops or draw down pressure points.

6.6 Flow Comparisons Between Rough Fracture Network And Single Horizontal Rough Fracture

To have a better vision about fracture networks' effect on fractured domains, a comparison was conducted between a rough fracture with horizontal angle orientation, that was modelled and used in Chapters 4 and 5, with one of the fracture networks that had closest fracture network fractal properties, as Table 6.2 above. Fracture network 4 was chosen, and the difference between these two models is clarified in Table 6.6 below. These two fractured domains had small differences in average aperture, but the fracture area proportions in network 4 had 100% increase.

Table 6.6 Fractal properties comparison between fracture network 4 and single rough fracture

Fractured media type	Number of Sections	Average Aperture (μ) (micron)	The standard deviation (σ)	Fracture area (m^2)	Matrix area (m^2)	(%) Fracture area
Rough Fracture (single)	185	581	230.8	0.000060499	0.01024581	0.59
Fracture Network 4	376	609	322	0.00012884	0.010177	1.27

Both were modelled in ANSYS CFD Fluent FVM, with isotropic matrix permeability ($K_x=K_y=2000$ mD), fracture surfaces were set as permeable boundary with the surrounding matrix "interior face boundary", and the same pressure drops applied in each (5, 100, 1000, 2000) Pa and zero pressure outlets. Both models had the same total domain area (10.15 X 10.15) cm, but the difference was the fracture open area percentage, which was approximately 0.6% in the single fracture and 1.27% in network 4 (approximately 100% increase of area in network 4). Then, comparisons were conducted of total flow, and % fracture and matrix flow, in these two fractured media.

The comparisons reflected interesting findings; despite total flow of fracture network 4 having a higher flow rate due to the higher fracture porosity: approximately ten times the single rough fracture in average values of pressure drops (5, 100, 1000, 2000) Pa. However, the importance is in % of fracture and matrix flow in each domain, as % of fracture and % matrix flow proportions in each domain were very different: in the single rough horizontal fracture model, % fracture flow was 82% in average value and % matrix flow 17% in average value,

while in network 4 it was 11.7% fracture flow percentage and 88.2% matrix flow percentage in average values. [Figures 6.42, 6.43 and 6.44](#) below illustrate these results. This comparison has indicated that a rough fracture in horizontal angle orientation is totally different to a rough network fracture with angled fractures; although the total domain areas were similar (10.15 X 10.15) cm, the flow proportions of fracture and matrix were totally opposite. In other words, in network 4, % of matrix flow percentage was 88.2% and 11.7% fracture flow percentage, which clarifies that the matrix was the main fluid conductor and provider; this was a totally different observation to that from flow in a single rough fracture with horizontal inclination. This has indicated that flow investigation in real conditions with angled network fractures is mandatory and crucial, in order to optimise fluid flow calculations in fractured media. This result has confirmed the clarifications of [Yin et al. \(2017\)](#) and [Sahimi \(2011\)](#), which stressed that a fracture network represents real fractured media flow, as the inner surfaces of fractures/voids are different, with different roughness which consists of different curvature shapes. The pores in this roughness represent the cluster gateways of fluid flow between matrix and fracture. As stated by [Zhu et al. \(2020\)](#); [Narr \(2011\) p. 374](#); [Narr, Schechter and Thompson \(2006\)](#) and [Sen \(1995\)](#), these show the effects of percolation on fracture network flow, due to the effect of fractures' orientation on fractured domain flow and accordingly on percolation, which is affected by fractures' lengths and orientations as important factors to be considered in fractured network modeling. As well, this has confirmed the findings of [Ahmadi et al. \(2018\)](#); [Yi and Xing \(2018\)](#); [Zou, Jing and Cvetkovic \(2017\)](#); [Spence et al. \(2014\)](#); [Ishibashi et al. \(2012\)](#); [Rasouli and Rasouli \(2012\)](#); [Popov et al. \(2009\)](#); [Narr, Schechter and Thompson \(2006\)](#); [Dietrich et al. \(2005\)](#) and [Hughes and Blunt \(2001\)](#), which stated that fluid flow prediction and movements in naturally fractured reservoirs are highly related to fracture networks' transmissivity and interactions with the surrounding matrix, and matrices' effects and importance to the domain flow contribution. Particularly, in fractured formations with good matrix permeability, as when overburden stresses are high and fracture apertures reduce significantly, then, most fluid will be immigrated through the matrix. Moreover, the results of this comparison have confirmed the finding of [Lu et al. \(2017\)](#), which stressed that a single fracture couldn't represent reservoir flow conditions. More detailed analyses of fractured network media with angles, and the effects of fracture angles and interaction with surrounding matrix, was clarified in [Section 6.4.1](#).

The comparison results of both fractured media types: rough fracture network and single rough fracture, have provided more evidence against previous research in the literature, which assumed the fracture as main fluid conductor and matrix as only fluid provider to fractures, or excluded matrix effects and flow contributions from the models and considered only fracture flow without matrix existence in the domain, as reported by [Luo et al. \(2020\)](#); [Zou, Jing and Cvetkovic \(2017\)](#); [Dippenaar and Van Rooy \(2016\)](#); [Liu, Li and Jiang \(2016\)](#); [Hyman et al. \(2015\)](#); [Sahimi \(2011\)](#); [Sarkar, Toksöz and Burns \(2004\)](#); [Tiab and Donaldson \(2004\)](#); [Nelson \(2001\)](#); [Golf-Racht \(1982\)](#) and [Snow \(1969\)](#).

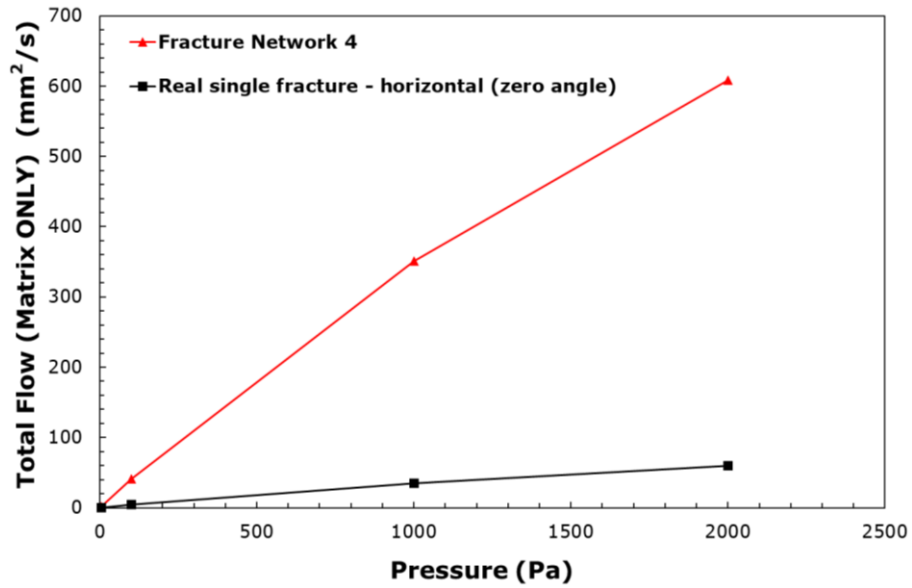


Figure 6.42 Total flow comparison between rough fracture network 4 and single rough horizontal fracture ($K_x=K_y=2000$ mD), average values of pressure drops (5, 100, 1000, 2000) Pa

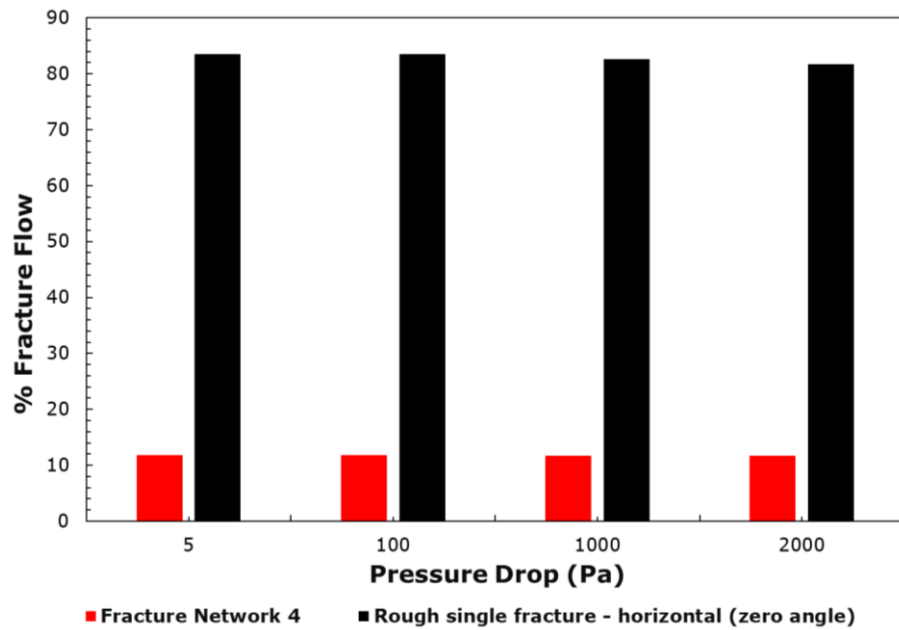


Figure 6.43 % Fracture flow only, comparison between rough fracture network 4 and single rough horizontal fracture ($K_x=K_y=2000$ mD)

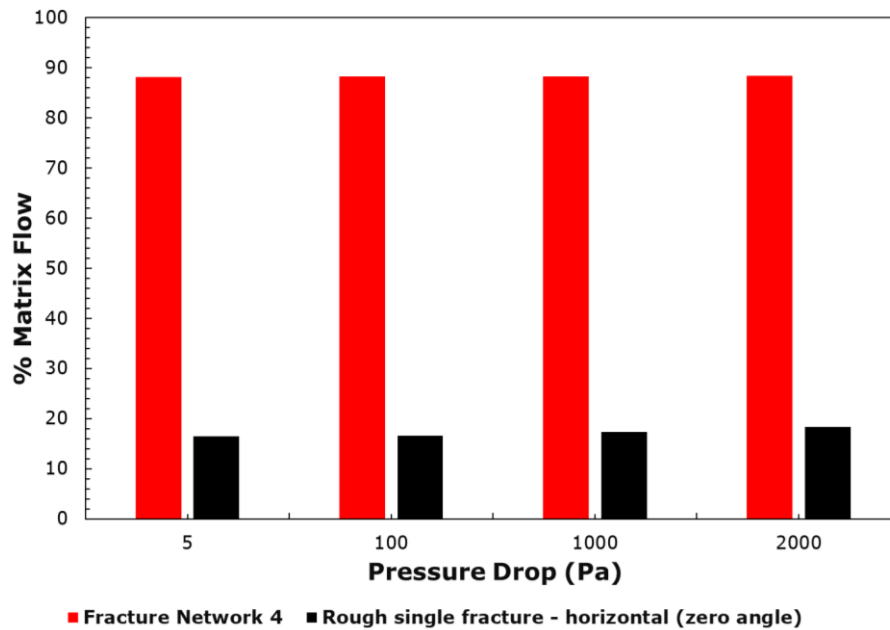


Figure 6.44 % Matrix flow only, comparison between rough network fracture 4 and single rough horizontal fracture ($K_x=K_y=2000$ mD)

6.7 Flow Comparisons Between Fracture Network Models And Literature Flow Models

To the best findings of this research, as detailed in Chapter 2, many of the previous works considered fractures as non-permeable with surrounding matrix; as well, in some of these studies, estimated geometry of a parallel plates fracture with a single height was used as reported by [Luo et al. \(2020\)](#); [Zou, Jing and Cvetkovic \(2017\)](#); [Dippenaar and Van Rooy \(2016\)](#); [Liu, Li and Jiang \(2016\)](#); [Hyman et al. \(2015\)](#); [Sahimi \(2011\)](#); [Sarkar, Toksöz and Burns \(2004\)](#); [Tiab and Donaldson \(2004\)](#); [Nelson \(2001\)](#); [Golf-Racht \(1982\)](#) and [Snow \(1969\)](#). Therefore, to compare the research results of these fracture networks with the previous research in the literature was somewhat of a challenge. Therefore, one of the previous works which had a close vision to this research was done by [Sarkar, Toksöz and Burns \(2004\) p. 11](#), was chosen, which had introduced an empirical formula of calculating flow in parallel plate inclined single height fractures network with non-permeable surfaces with matrix (no matrix effect inclusion), and fracture apertures will be average value as equivalent aperture ' h_{eq} ' of all network, as [equation 2.30](#) in chapter 2 ([Section 2.5.4](#)).

In this research, the above formula was compared with fracture flow in fracture network ANSYS CFD Fluent FVM models, and used “h” as “heq” which was equivalent average apertures height. Fracture flow of five fracture networks with pressure drops (5, 100, 1000, 2000) Pa were observed, then, [Sarkar, Toksöz and Burns \(2004\)](#)’s formula was applied, and average values of each network were calculated in both. [Figure 6.45](#) and [Table 6.7](#) below clarify the results. ADV was calculated too between ANSYS CFD Fluent FVM results and [Sarkar, Toksöz and Burns \(2004\)](#)’s equation, to compare the results. As can be seen, [Sarkar, Toksöz and Burns \(2004\)](#)’s formula reflected slight changes of fracture flow in each network, while the ANSYS CFD Fluent FVM network models reflected massive change in fracture flow, based on the fracture network orientation, fractal properties in each model, fracture/matrix interactions and fluid flow movements. The highest ADV was in network 2 with 196%, while the lowest ADV was in network 4 with 88% difference. This comparison shows that using [Sarkar, Toksöz and Burns \(2004\)](#)’s formula overestimated fracture flow and would mislead fracture flow calculations. Thus, this comparison shows further evidence to the analysis of [Section 6.4.1](#) that investigation of fractured formation flow without including matrix effect, rough fracture profile, and fracture network’s orientations pattern will highly mislead flow calculations of any fractured formation.

Table 6.7 Average value of fracture flow with pressure drops (5, 100, 1000, 2000) Pa of ANSYS CFD Fluent FVM fracture networks and [Sarkar, Toksöz and Burns \(2004\)](#)’s formula

Fracture flow (Average Value)	Fracture Flow Network 1 (mm ² /s)	Fracture Flow Network 2 (mm ² /s)	Fracture Flow Network 3 (mm ² /s)	Fracture Flow Network 4 (mm ² /s)	Fracture Flow Network 5 (mm ² /s)
Networks-CFD	15.2896	1.1630	7.1558	29.2327	9.2271
Sarkar et al. 2004's equation	69.2539	75.7650	75.3930	75.3930	73.1865

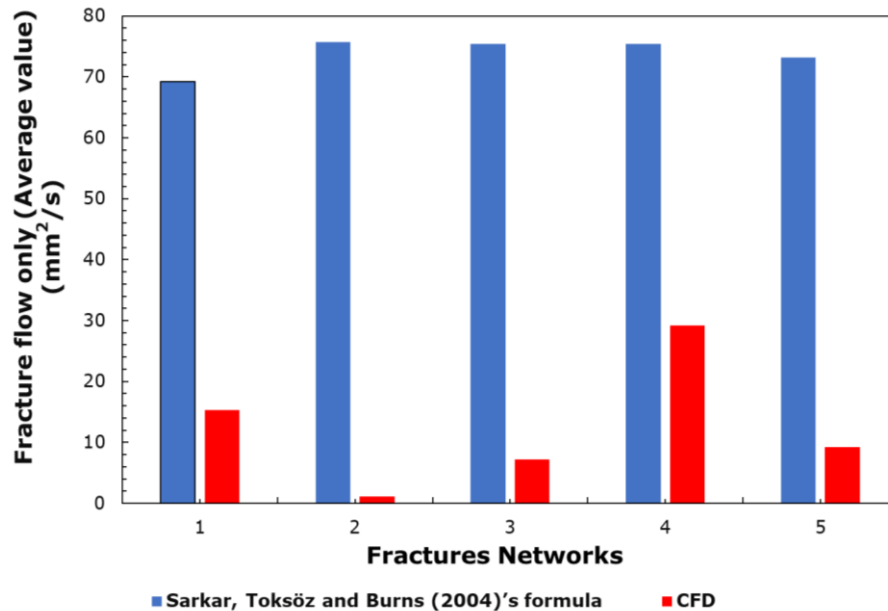


Figure 6.45 Comparisons of fracture networks - fracture flow only (average value) (mm^2/s) with $K_x=K_y=2000$ mD, ($P=5, 100, 1000, 2000$) Pa

6.8 Conclusions

In this chapter, fracture network models were created and investigated in ANSYS CFD Fluent FVM, with the pattern of each network taken from a referenced fracture network image. The goal of these models was to investigate fluid flow in models which most mimicked the main conditions of real fractured media, such as: including fracture networks with varied patterns, rough fractures, fracture networks with varied orientations (horizontal and inclined), and isotropic and anisotropic matrix permeability. The outcomes of these fractured network models have reflected totally different results than those for single horizontal fractures, also different to some beliefs in the previous literature about flow in fractured media. These outcomes can be summarised as follows:

- a) The percentage of fracture flow in fractured media has been overestimated in the previous literature. As the models of this study's calculations presented, that fracture networks with orientations either horizontal or with 45° (scenario with worst angle effect on flow) of Cartesian axis, and with either isotropic and anisotropic matrix permeability, have low % fracture flow contribution in fractured domain, at approximately 12% fracture flow percentage in this research's model conditions.

- b) The percentage of matrix flow in fractured media is much underestimated, which has led many researchers in the previous literature to exclude the matrix from the calculations. The models of this study's calculations have presented that matrix flow is actually much higher, with all the patterns and heterogeneity scenarios, at approximately 88% matrix flow contribution in fractured domain, and this percentage could vary based on matrix permeability, but still the % matrix flow rate will be higher than expected previously based on this research's results. [Karpyn and Piri \(2007\) p. 1](#) stated that "fractures control the overall conductivity of the rock while the porous matrix provides fluid storage capacity". This concept was adopted by many of the previous works in the literature to consider assumed flow conditions in fractured media such as: fracture surfaces impermeable with surrounding matrix; fracture geometry consisting of smooth parallel plates fractures with single height instead of rough fracture, which has least interaction with the matrix; fractures are the main fluid conductors and matrix fluid providers only as double porosity reservoirs concept; and consideration only of single fractures with either horizontal or inclined angle in Cartesian axis in fractured domain, instead of networks of connected fractures. These assumptions have been reported by [Luo et al. \(2020\)](#); [Wang et al. \(2020\)](#); [Su et al. \(2019\)](#); [Luo et al. \(2018\)](#); [Briggs, Karney and Sleep \(2017\)](#); [Zou, Jing and Cvetkovic \(2017\)](#); [Dippenaar and Van Rooy \(2016\)](#); [Liu, Li and Jiang \(2016\)](#); [Hyman et al. \(2015\)](#); [Briggs, Karney and Sleep \(2014\)](#); [Sahimi \(2011\)](#); [Popov et al. \(2009\)](#); [Sarkar, Toksöz and Burns \(2004\)](#); [Tiab and Donaldson \(2004\)](#); [Nelson \(2001\)](#); [Yamatomi et al. \(2001\)](#); [Golf-Racht \(1982\)](#); [Snow \(1969\)](#); and [Warren and Root \(1963\)](#). The results and findings of this research have totally disproved these assumptions in the previous literature, particularly in fracture networks, because the matrix flow contribution has been shown in fact to be much higher than for fractures' open spaces in the domain, and can be considered as main fluid conductor instead of fractures when there is good matrix permeability value surrounding fractures. It's good to note that most fracture formations consist of fracture networks, except for some types of fractures, which have unconnected fractures as fracture formation classification by [Tiab and Donaldson \(2004\)](#) and [Nelson \(1987\)](#).
- c) Fracture/matrix interaction is very active and has been shown to play a crucial role in fracture networks with angled rough fractures, as matrix flow is much increased due to fluid movements from fractures to matrix domain.

As well, matrix flow reflected non-linear increase, approximately 200%, in comparison with Darcy law in this research's models' conditions.

- d) Fractures in fractured formations which do not pass through the outlet boundary or discharge point of flow, have affected the total flow of the fractured domain, and decreased flow in high percentage. This case reflects that the easy path of fluid in fractured media has affected the surrounding matrix flow by supplying the fluid from the fracture into the matrix and vice versa, and increased fractured domain connectivity, which leads to high increase of flow percentage in fracture and matrix. Although the flow decrease in fractured domain due to fractures did not pass to outlet, it reflected a high increase of flow through the matrix. Thus, matrix flow in fracture networks reflected non-linear increase in comparison with the Darcy equation.
- e) If a fracture does not pass through the domain, then fractures in fractured media can represent barriers of flow in domains instead of facilitators, as they increase pressure drops in the fractured domain. However, as mentioned in point 4, there is still an increase calculated in the matrix flow due to the effect of fracture/matrix interaction and fluid movement between the two domains.
- f) Fractures' rough geometry and network pattern has a key impact on the flow percentage of the fractured network domain. Simple network patterns has better connectivity than complicated fracture network patterns with more fracture branches.
- g) Dominant fracture existence in a fracture network, connected between inlet and outlet boundaries, plays a significant role in increasing fractured network domain flow in matrix and fractures.
- h) Assuming impermeable fracture surfaces will overestimate fracture flow, and also will exclude the matrix flow effect and contribution to flow percentages as clarified in points 1, 2 and 3. It has been proven in this research investigation that matrix flow contribution is significant, and a main fluid conductor in fractured domains.
- i) A single fracture, horizontal or with angle in Cartesian axis, cannot represent flow in fractured domain conditions. This is because it will mislead flow calculation in fractured formations, and will massively reduce the effects of interaction between fractures and surrounding matrix. This has confirmed the previous findings of [Lu et al. \(2017\)](#).

7 Conclusions And Future Work

7.1 Conclusions

Fractured formations' characteristics and parameters were reviewed, such as: permeability; porosity; single fracture flow (parallel plates and rough fractures); flow in a network of fractures; imbibition and percolation; and fracture friction factor. This review was begun with theories, then with other development works to review both understanding and progress to date. The majority of previous studies relied on simplification assumptions, that aided understanding of the flow, and at the same time provided, as much as possible, realistic models which could visualize and approximate flow as in real fractured media in subsurface layers of the earth's crust. Therefore, there were many gaps in understanding and modelling fractured media flow. Thus, in this research, investigations were conducted on fractured media using Computational Fluid Dynamic tool ANSYS CFD Fluent FVM to investigate fluid flow in different kinds of fractured media, from the simple and widely used geometries to more complex ones: parallel plates fractures with single apertures; rough fractures; and rough fracture network patterns, respectively. As well, this research investigated multiple fracture surface conditions such as inclusion and exclusion of the matrix effect on a fracture's flow and a matrix's flow, and a matrix with anisotropic permeability's effects on flow. Validations and comparisons were conducted among these fracture models. This study reflected very interesting findings, and the outcomes are very promising. Many points came up after the results of these models as new knowledge, which have not yet been approached until now. These are summarised below.

1. The Computational Fluid Dynamic tool FLUENT FVM was used in modelling fractured media types, and was validated with the previous works and theories from the literature. It was proven that the analysis results of this tool have the ability to provide the qualitative and quantitative data, criterion identification, and accurate estimate of flow, in fractured media components such as open fractures and surrounding matrices.

2. It was shown that a parallel plates fracture with single aperture height does not represent the reality of flow in fractured media, and can mislead analysis outcomes significantly, despite it being widely used in industry for simplicity, because it will not account for the effect of changing fluid velocity/pressure along the flow in the fractured domain, which will overestimate % fracture flow and underestimate % matrix flow in case matrix effect was included in fractured domain modelling.
3. Considering rough fracture geometry with varied apertures along the flow will reflect more accurate estimation of flow in fractured media in subsurface layers of earth crust and reservoirs. This mimics real conditions of flow as in fractured formations more rigorously, such as: rough fracture flow resistance, matrix/fracture interaction, and eddies/vortices' creation and effects on fracture bulk flow and matrix flow.
4. Matrix interaction with rough fracture is very important; therefore, it's vital to be included in fractured media flow calculations, as the interaction between matrix and fracture is high and very active.
5. One of the very interesting findings was that the well-known Darcy formula of fluid flow in matrix can underpredict matrix flow of fractured formations, and the matrix flow reflected non-linearity increase in fractured media models.
6. Anisotropic matrix permeability effects of in-plane (K_x) permeability and through plane (K_y) permeability were investigated in both types of fractured media: parallel plates and rough fracture. K_x and K_y reflected two visions in these two types of fractures, either similar or different effects based on different percentages of fracture and matrix flow. As stressed in point 2 that using parallel plates fractures will mislead flow calculation, therefore, anisotropic permeability effects in rough fracture only are highlighted here. Thus, if both in-plane K_x and through plane K_y permeabilities are changing at the same time, then K_x had highest effect on fractured domain flow. However, if one of the permeabilities (K_x or K_y) is changing, then through plane K_y had highest effect on fractured domain flow, as it had a proven increase in fracture flow and significantly in matrix flow too, with the same pressure gradient values and directions. These findings are very significant, as it gives evidence that through plane (K_y) permeability is important in fractured formations, not only in-plane (K_x) permeability.
7. As stressed in point 2 that parallel plates fractures mislead flow calculations, therefore friction factor values were extracted and investigated in rough

fracture geometry only by ANSYS CFD Fluent FVM fracture models. As well, many conditions were applied, such as: impermeable and permeable fracture surfaces to consider fracture/matrix interaction and fluid movement effects; and isotropic and anisotropic matrix permeability with many different scenarios. The outcomes were that fracture/matrix interaction, with consideration of anisotropic matrix permeability in both directions in-plane K_x and through plane K_y had significant effects on rough fracture friction factor values. This has led to a conclusion that considering mimicked conditions of subsurface flow in fracture modelling will result in the most optimised results calculations of fracture friction factor.

8. Two new proposed rough fracture friction factor models were developed and introduced to industry; the analytical model was applicable until Reynolds number values equal or less (≤ 10) and numerical model was suitable to be used until Reynolds number value 3000. Both models account for: permeable fracture surfaces; anisotropic matrix permeability along the fracture flow with different matrix layers, and varied matrix permeability in-plane (K_x) permeability and through plane (K_y) permeability in Cartesian directions in the same layer; fracture roughness; and tortuosity.
9. Fracture network models were created and investigated in ANSYS CFD Fluent FVM, and the pattern of each network was taken from a referenced fracture network image. The goal of these models was to investigate fluid flow in models which most mimicked the main conditions of real fractured media, such as: varied fracture network patterns, rough fractures, fracture networks with varied orientations (horizontal and inclined), fracture/matrix interactions and fluid movements, and isotropic and anisotropic matrix permeability scenarios. The outcomes of these fractured network models reflected totally different results than those for single horizontal fractures, and contradicted some beliefs in the previous literature about flow in fractured media. Therefore, considering rough fractured networks is essential to get most optimised flow results, due to the following reasons:
 - a) The percentage of fracture flow in fractured media has been overestimated in the previous literature. These models of rough fractured network calculations have shown that fracture networks with pattern orientations either horizontal or with 45° (worst angle for effect on flow in scenario) of Cartesian axis, and with either isotropic and

anisotropic matrix permeability, have a low % fracture flow contribution in fractured domain: approximately 12% fracture flow, in this research's models' setup.

- b) The percentage of matrix flow in fractured media has been much underestimated; the rough fractured network models of this study's calculations have presented that matrix flow is actually much higher, with all the patterns and anisotropic matrix permeability scenarios, at approximately 88% matrix flow contribution in the fractured domain, in this research's models' setup. [Karpyn and Piri \(2007\) p. 1](#) stated that "fractures control the overall conductivity of the rock while the porous matrix provides fluid storage capacity". As well, [Berkowitz \(2002\) p. 867](#) stated that "fractures' conductivity differences are expected to be minimal when they are embedded in permeable or impermeable host rocks". The results and findings of this research have totally disapproved these assumptions in the previous literature, particularly in fracture networks, because flow contribution from the matrices surrounding fractures is in fact much higher than fractures' open spaces in the domain, and can be considered as a main fluid conductor when matrix permeability has reasonable leakage value. Fracture/matrix interaction is very active and plays a crucial role in fracture networks with angled fractures, as matrix flow is very much increased due to fluid movement from fractures to matrix domain. As well, matrix flow in fractured networks reflected non-linear increase, approximately 200%, in comparison with Darcy law in the fractured domain in this research's models' setup. Thus, Darcy law was shown to underpredict matrix flow in fractured network formations.
- c) If a fracture does not pass through the domain, then fractures in fractured network media can represent a barrier of flow in domains instead of facilitators, as they increase pressure drops in fractured domain. However, there is still a flow increase calculated in the matrix flow due to the effect of fracture/matrix interaction, and fluid movement between the two domains.
- d) Fractures' rough geometry and network pattern have a key impact on the flow percentage of the fractured network domain. Simple network patterns have better connectivity than complicated fracture network patterns with more fracture branches.

e) Dominant fracture existence in a fracture network, that connects between inlet and outlet boundaries, plays a significant role in increasing fractured network domain flow in matrix and fractures.

10. Thus, comparison of results between a single rough fracture model and fractured network model reflected that a single fracture cannot accurately represent flow in fractured domain conditions. This is because it will mislead flow calculation in fractured formations, and will massively reduce the effects of interaction between fractures and surrounding matrix.

7.2 Recommendations For Future Work

1. Investigate flow in rough fracture networks, with inclusion of the surrounding matrix effect and interaction, but consider multiphase flow (instead of single phase) and account for the effect of the fracture and anisotropic matrix on fluid phase proportions in matrix and fracture.
2. Develop friction factor models for rough fracture network models, that account for heterogeneous properties of fractured formations, such as: rough fracture fractal properties; fracture network pattern in fractured domain; and anisotropic matrix properties, particularly permeability.
3. Investigate fracture/matrix interface layer in rough fracture networks in two zones: first, where the fracture bulk flow occurs; and second, in sharp corners of rough surfaces in fractures. This is in order to envisage fluid flow movements between fracture and matrix due to: varied velocities and pressures; eddies and vortices' effects on fluid movement; and fracture network pattern layout (fractures' orientations, connectivity, dead end fractures or non-dominant fractures) effects.

8 References

- AHMADI, P. et al., 2018. Experimental and CFD Studies on Determination of Injection and Production Wells Location Considering Reservoir Heterogeneity and Capillary Number. *Oil & Gas Science and Technology - Revue de l'IFP*, 74.
- AL-YOUSEF, H., 2005. Permeability Anisotropy Measurement on Whole Cores B Analytical Solution and Application. Kingdom of Bahrain: Society of Petroleum Engineers.
- ANDERSEN, P.Ø. and ZHOU, Y., 2020. Steady state relative permeability experiments with capillary end effects: Analytical solutions including derivation of the intercept method. *Journal of Petroleum Science and Engineering*, 192, 107249.
- ANSYS, 2011. ANSYS FLUENT User's Guide. 14th ed. Canonsburg, USA: ANSYS, Inc.
- ANSYS, 2013. ANSYS Fluent Theory Guide. 15th ed. Canonsburg, USA: ANSYS, Inc.
- ANSYS UDF Manual, 2013. ANSYS Fluent UDF Manual. 15th ed. Canonsburg, USA: ANSYS, Inc.
- ARTHUR, J., 2018. Porous Media Flow Transitioning into the Forchheimer Regime: a PIV Study. *Journal of Applied Fluid Mechanics*, 11, pp. 297-307.
- AURADOU, H. et al., 2005. Permeability anisotropy induced by the shear displacement of rough fracture walls. *Water Resources Research*, 41(9).
- BARTON, N. and CHOUBEY, V., 1977. The shear strength of rock joints in theory and practice. *Rock mechanics*, 10(1), pp. 1-54.
- BEAR, J., 1972. *Dynamics of fluids in porous media*. American Elsevier.
- BEAR, J. and BUCHLIN, J.M., 1991. *Modelling and Applications of Transport Phenomena in Porous Media*. Springer Netherlands.
- BERKOWITZ, B., 2002. Characterizing flow and transport in fractured geological media: A review. *Advances in Water Resources*, 25(8), p. 861.

- BERKOWITZ, B. and EWING, R.P., 1998. Percolation Theory and Network Modeling Applications in Soil Physics. *Surveys in Geophysics*, 19(1), pp. 23-72.
- BO, C. et al., 2014. *A case Study of Hydraulic Fractures Optimization in Heavy Oil*. SPE-172849-MS ed. Society of Petroleum Engineers.
- BOURBIAUX, B. et al., 2002. *An Integrated Workflow to Account for Multi-Scale Fractures in Reservoir Simulation Models: Implementation and Benefits*. Society of Petroleum Engineers.
- BOURDET, D., 1985. *Pressure Behavior of Layered Reservoirs With Crossflow*. Bakersfield, California: Society of Petroleum Engineers.
- BRIGGS, S., KARNEY, B.W. and SLEEP, B.E., 2014. Numerical modelling of flow and transport in rough fractures. *Journal of Rock Mechanics and Geotechnical Engineering*, 6(6), pp. 535-545.
- BRIGGS, S., KARNEY, B.W. and SLEEP, B.E., 2017. Numerical modeling of the effects of roughness on flow and eddy formation in fractures. *Journal of Rock Mechanics and Geotechnical Engineering*, 9(1), pp. 105-115.
- BROWN, S.R., 1995. Simple mathematical model of a rough fracture. *Journal Geophysical Research*, 100(B4), pp. 5941–5952.
- BROWN, G.O., 2002. Henry Darcy and the making of a law. *Water Resources Research*, 38(7), pp. 1-12.
- CHEN, Z. et al., 2017. Effect of roughness on water flow through a synthetic single rough fracture. *Environmental Earth Sciences*, 76(4), pp. 186.
- CHERY, L. and DE MARSILY, G., 2007. *Aquifer Systems Management*. Taylor & Francis.
- CHUNG, T.J., 2010. *Computational Fluid Dynamics*. 2nd Edition ed. University of Alabama: Huntsville.
- CRANDALL, D., AHMADI, G. and SMITH, D.H., 2010. Computational Modeling of Fluid Flow through a Fracture in Permeable Rock. *Transport in Porous Media*, 84(2), pp. 493-510.
- CRANDALL, D., BROMHAL, G. and KARPYN, Z.T., 2010. Numerical simulations examining the relationship between wall-roughness and fluid flow in rock fractures. *International Journal of Rock Mechanics and Mining Sciences*, 47(5), pp. 784-796.

- CRANDALL, D., BROMHAL, G. and SMITH, D.H., 2009. *Conversion of a Micro-CT Scanned Rock Fracture Into a Useful Model; ASME 2009 Fluids Engineering Division Summer Meeting.*
- DAKE, L.P., 1978. *Fundamentals of Reservoir Engineering.* Elsevier Scientific Publishing Company.
- DEVOLD, H., 2006. *Oil And Gas Production Handbook.* Edition 1.3 ed. Oslo: ABB ATPA Oil and Gas.
- DI FRATTA, C. et al., 2016. Characterization of anisotropic permeability from flow front angle measurements. *Polymer Composites*, 37(7), pp. 2037-2052.
- DICMAN, A., PUTRA, E. and SCHECHTER, D.S., 2004. *Modeling Fluid Flow Through Single Fractures Using Experimental, Stochastic and Simulation Approaches.* Society of Petroleum Engineers.
- DIETRICH, P. et al., eds. 2005. *Flow and Transport in Fractured Porous Media.* Springer.
- DIPPENAAR, M.A. and VAN ROOY, J.L., 2016. On the cubic law and variably saturated flow through discrete open rough-walled discontinuities. *International Journal of Rock Mechanics and Mining Sciences*, 89, pp. 200-211.
- DONALDSON, E.C. and TIAB, D., 2004. *Petrophysics: Theory and Practice of Measuring Reservoir Rock and Fluid Transport Properties.* Elsevier Science.
- DOUGLAS, J.F. et al., 2005. *Fluid Mechanics.* Pearson/Prentice Hall.
- DULLIEN, F.A.L., 1992a. *Porous Media Fluid Transport and Pore Structure.* First Edition ed. San Diego, California: Academic Press, Inc.
- DULLIEN, F.A.L., 1992b. *Porous Media: Fluid Transport and Pore Structure .* Second Edition ed. California: Academic Press.
- EARLOUGHER, R.C., 1977. *Advances in Well Test Analysis.* Henry L. Doherty Memorial Fund of AIME.
- ESKINAZI, S., 1968. *Principles of Fluid Mechanics.* Allyn and Bacon.
- EVANS, R.D. and CIVAN, F., 1994. *Characterization of non-Darcy multiphase flow in petroleum bearing formation. Final report; Sponsor Org.: USDOE, Washington, DC (United States).* United States.

- GAO, C. and DEANS, H.A., 1988. Pressure Transients and Crossflow Caused by Diffusivities In Multilayer Reservoirs. *SPE Formation Evaluation*, 3(02), pp. 438-448.
- GEERTSMA, J., 1974. Estimating the Coefficient of Inertial Resistance in Fluid Flow Through Porous Media. *Society of Petroleum Engineers Journal*, 14(05), pp. 445-450.
- GEIGER, S., SCHMID, K.S. and ZARETSKIY, Y., 2012. Mathematical analysis and numerical simulation of multi-phase multi-component flow in heterogeneous porous media. *Current Opinion in Colloid & Interface Science*, 17(3), pp. 147-155.
- GIDASPOW, D., LI, F. and HUANG, J., 2013. A CFD simulator for multiphase flow in reservoirs and pipes. *Powder Technology*, 242, pp. 2-12.
- GLOVER, P.W.J. and HAYASHI, K., 1997. Modelling fluid flow in rough fractures: Application to the Hachimantai geothermal HDR test site. *Physics and Chemistry of the Earth*, 22(1), pp. 5-11.
- GOLF-RACHT, T.V.V., 1982. *Fundamentals of Fractured Reservoir Engineering*. Developments in Petroleum Science, 12 ed. Netherlands -Amsterdam: Elsevier Scientific Publishing Company.
- GONZALEZ-GARCIA, R. et al., 2000. Three-dimensional characterization of a fractured granite and transport properties. *Journal of Geophysical Research: Solid Earth*, 105(B9), pp. 21387-21401.
- GU, T. et al., 2009. Experimental and CFD studies of fluid dynamic gauging in duct flows. *Chemical Engineering Science*, 64(2), pp. 219-227.
- GUSTAFSSON, A.-., WESTERLUND, L. and HELLSTRÖM, G., 2010. CFD-modelling of natural convection in a groundwater-filled borehole heat exchanger. *Applied Thermal Engineering*, 30(6-7), pp. 683-691.
- HE, L. et al., 2014. Complex relationship between porosity and permeability of carbonate reservoirs and its controlling factors: A case study of platform facies in Pre-Caspian Basin. *Petroleum Exploration and Development*, 41(2), pp. 225-234.
- HIDAYATI, D.T., CHEN, H. and TEUFEL, L.W., 2000. *The Reliability of Permeability-Anisotropy Estimation From Interference Testing of Naturally Fractured Reservoirs*. Villahermosa, Mexico: Society of Petroleum Engineers.

- HOLSTEIN, E.D., 2007. *Reservoir Engineering and Petrophysics - Volume V*. Texas -USA: Society of Petroleum Engineers.
- HOSSEINIAN, A., 2011. *Numerical simulations of fluid flow through a single rough walled fracture*. [online] PhD thesis, Curtin University of Technology. Available from: <https://espace.curtin.edu.au/handle/20.500.11937/1764> [Accessed 25 June 2020].
- HUGHES, R.G. and BLUNT, M.J., 2001. Pore-Scale Modeling of Multiphase Flow in Fractures and Matrix/Fracture Transfer. (SPE 71297-PA).
- HUSSAIN, D.M. , April 2016. CFD supervisory weekly meeting.
- HUTCHINSON, C.A., J., DODGE, C.F. and POLASEK, T.L., 1961. Identification, Classification and Prediction of Reservoir Nonuniformities Affecting Production Operations. *Journal of Petroleum Technology*, 13(03), pp. 223-230.
- HYMAN, J.D. et al., 2015. dfnWorks: A discrete fracture network framework for modeling subsurface flow and transport. *Computers & Geosciences*, 84, pp. 10-19.
- INGHAM, D.B. and POP, I., 2005. *Transport Phenomena in Porous Media III*. Elsevier Science.
- ISHIBASHI, T. et al., 2012. GeoFlow: A novel model simulator for prediction of the 3-D channeling flow in a rock fracture network. *Water Resources Research*, 48(7).
- JAHANI, N., HAUGEN, B. and BERGE, G., 2015. Coupled fluid flow and elasto-plastic damage analysis for fractured porous chalk with induced wormhole. *International Journal of Rock Mechanics and Mining Sciences*, 80, pp. 129-136.
- JAHN, F., COOK, M. and GRAHAM, M., 2008. *Hydrocarbon Exploration and Production* 2nd Edition ed. Oxford, UK: Elsevier.
- JAMBHEKAR, V., 2011. *Forchheimer Porous-media Flow Models - Numerical Investigation and Comparison with Experimental Data*. [online].
- JU, Y. et al., 2019. Evaluation of water permeability of rough fractures based on a self-affine fractal model and optimized segmentation algorithm. *Advances in Water Resources*, 129, pp. 99-111.
- KALDOR, M., KARL, T.L. and SAID, Y., 2007. *Oil Wars*. First ed. London: Pluto Press.

- KARIMZADE, E. et al., 2019. Modelling of Flow–Shear Coupling Process in Rough Rock Fractures Using Three-Dimensional Finite Volume Approach. *Rock Mechanics and Rock Engineering*, 52(11), pp. 4693-4713.
- KARPYN, Z. and PIRI, M., 2007. Prediction of fluid occupancy in fractures using network modeling and X-Ray microtomography. I: Data conditioning and model description. *Physical review.E, Statistical, nonlinear, and soft matter physics*, 76, 016315.
- KARPYN, Z.T., GRADER, A.S. and HALLECK, P.M., 2007. Visualization of fluid occupancy in a rough fracture using micro-tomography. *Journal of colloid and interface science*, 307(1), pp. 181.
- KAZEMI, H. et al., December 1967. Numerical Simulation of Water-Oil Flowing Naturally Fractured Reservoirs. SPE (317).
- KELLER, A.A., ROBERTS, P.V. and BLUNT, M.J., 1999. Effect of fracture aperture variations on the dispersion of contaminants. *Water Resources Research*, 35(1), pp. 55-63.
- KOYAMA, T. et al., 2009. Numerical modelling of fluid flow tests in a rock fracture with a special algorithm for contact areas. *Computers and Geotechnics*, 36(1), pp. 291-303.
- KULATILAKE, P.H.S.W. et al., 2008. Quantification of Aperture and Relations Between Aperture, Normal Stress and Fluid Flow for Natural Single Rock Fractures. *Geotechnical and Geological Engineering*, 26(3), pp. 269-281.
- LANG, P., PALUSZNY, A. and ZIMMERMAN, R., 2014. Permeability tensor of three-dimensional fractured porous rock and a comparison to trace map predictions. *Journal of Geophysical Research: Solid Earth*, 119.
- LEI, G. et al., 2015. *Calculation of full permeability tensor for fractured anisotropic media*. Berlin] : Springer.
- LESPINASSE, M.S., J., 2000. Quantification of fluid flow: hydro-mechanical behaviour of different natural rough fractures. *Journal of Geochemical Exploration*, (69–70), pp. 483–486.
- LI, Q. et al., 2021. Effects of natural micro-fracture morphology, temperature and pressure on fluid flow in coals through fractal theory combined with lattice Boltzmann method. *Fuel*, 286, 119468.

- LIU, R., LI, B. and JIANG, Y., 2016. Critical hydraulic gradient for nonlinear flow through rock fracture networks: The roles of aperture, surface roughness, and number of intersections. *Advances in Water Resources*, 88, pp. 53-65.
- LOUIS, C., 1969. *A Study of Groundwater Flow in Jointed Rock and Its Influence on the Stability of Rock Masses*. Imperial College of Science and Technology.
- LU, C. et al., 2017. Transient pressure analysis of a volume fracturing well in fractured tight oil reservoirs. *Journal of Geophysics and Engineering*, 14(6), pp. 1509-1520.
- LUO, W., TANG, C. and ZHOU, Y., 2019. A New Fracture-Unit Model and Its Application to a Z-Fold Fracture. *SPE Journal*, 24(01), pp. 319-333.
- LUO, W. et al., 2018. A new semi-analytical method for calculating well productivity near discrete fractures. *Journal of Natural Gas Science and Engineering*, 57, pp. 216-223.
- LUO, W. et al., 2020. An Alternative BEM for Simulating the Flow Behavior of a Leaky Confined Fractured Aquifer With the Use of the Semianalytical Approach. *Water Resources Research*, 56(5), e2019WR026581.
- MA, D. et al., 2018. Experimental Investigation on Hydraulic Properties of Granular Sandstone and Mudstone Mixtures. *Geofluids*, 2018, 9216578.
- MASCIOPINTO, C., 1999. Particles' transport in a single fracture under variable flow regimes. *Advances in Engineering Software*, 30(5), p. 327.
- MCDONALD, A.E. et al., 1991. *Some Important Considerations in the Simulation of Naturally Fractured Reservoirs*. Society of Petroleum Engineers.
- MERIAM, J.L. and HENDERSON, J.M., 1992. *Engineering Mechanics*. Wiley.
- MORENO, L. et al., 1988. Flow and tracer transport in a single fracture: A stochastic model and its relation to some field observations. *Water Resources Research*, 24(12), pp. 2033-2048.
- NARR, W., 2011. *Characterization of Naturally Fractured Reservoirs*. Richardson, USA: Society of Petroleum Engineers.
- NARR, W., SCHECHTER, D.S. and THOMPSON, L.B., 2006. *Naturally Fractured Reservoir Characterization*. Society of Petroleum Engineers.

NAZRIDOUST, K., AHMADI, G. and SMITH, D.H., 2006. A new friction factor correlation for laminar, single-phase flows through rock fractures. *Journal of Hydrology*, 329(1-2), pp. 315-328.

NELSON, R.A., 1987. Fractured Reservoirs: Turning Knowledge into Practice. *Journal of Petroleum Technology* (SPE-16470-PA).

NELSON, R.A., 2001. *Geologic Analysis of Naturally Fractured Reservoirs*. Gulf Professional Pub.

NORDQVIST, A.W. et al., 1992. A variable aperture fracture network model for flow and transport in fractured rocks. *Water Resources Research*, 28(6), pp. 1703-1713.

OLAREWAJU, J.S. and LEE, W.J., 1990. Rate Performance of a Layered Reservoir With Unsteady-State Interlayer Crossflow. *SPE Formation Evaluation*, 5(01), pp. 46-52.

ORON, A. and BERKOWITZ, B., 1998. Flow in rock fractures: The local cubic law assumption reexamined. *Water Resources Research - WATER RESOUR RES*, 34, pp. 2811-2825.

PARSONS, R.W., 1966. Permeability of Idealized Fractured Rock. *Society of Petroleum Engineers Journal*, 6(02), pp. 126-136.

PASCAL, H. and QUILLIAN, R.G., 1980. *Analysis Of Vertical Fracture Length And Non-Darcy Flow Coefficient Using Variable Rate Tests*. Dallas, Texas: Society of Petroleum Engineers.

PETCHSINGTO, T., 2008. *Numerical Study of Fracture Aperture Characteristics and their impact on Single-Phase flow and Capillary-Dominated Displacement* [online] Doctor of Philosophy thesis, The Pennsylvania State University. Available from: <https://etda.libraries.psu.edu/catalog/8195>.

PETCHSINGTO, T. and KARPYN, Z., 2009. Deterministic Modeling of Fluid Flow through a CT-scanned Fracture Using Computational Fluid Dynamics. *Energy Sources Part A-recovery Utilization and Environmental Effects*, 31, pp. 897-905.

PIRI, M. and KARPYN, Z., 2007. Prediction of fluid occupancy in fractures using network modeling and X-ray microtomography. II: Results. *Physical review.E, Statistical, nonlinear, and soft matter physics*, 76, 016316.

- POPOV, P. et al., 2009. Multiphysics and Multiscale Methods for Modeling Fluid Flow Through Naturally Fractured Carbonate Karst Reservoirs. *SPE Reservoir Evaluation & Engineering*, 12(02), pp. 218-231.
- PREUSS, K. AND TSANG, Y.W., 1990. On Two-Phase Relative Permeability and Capillary Pressure of Rough-Walled Rock Fractures. *Water Resources Research*, 26(No.9), pp. 1915- 1926.
- QIAN, J. et al., 2011. Experimental study of the effect of roughness and Reynolds number on fluid flow in rough-walled single fractures: a check of local cubic law. *Hydrological Processes*, 25(4), pp. 614-622.
- RASOULI, A. and RASOULI, V., 2012. *Simulations of Fluid Flow Through a Porous Formation With a Single Rough Fracture Plane*. Stockholm, Sweden: International Society for Rock Mechanics and Rock Engineering.
- RASOULI, V. and HOSSEINIAN, A., 2011. Correlations Developed for Estimation of Hydraulic Parameters of Rough Fractures Through the Simulation of JRC Flow Channels. *Rock Mechanics and Rock Engineering*, 44(4), pp. 447-461.
- REITSMA, S. AND KUEPER, B.H, 1994. Laboratory Measurement of Capillary Pressure-Saturation Relationships in a Rock Fracture. *Water Resources Research*, 30(No.4), pp. 865- 878.
- ROSLIN, A. et al., 2020. 3D pore system reconstruction using nano-scale 2D SEM images and pore size distribution analysis for intermediate rank coal matrix. *Fuel*, 275, pp. 117934.
- ROSLIN, A., POKRAJAC, D. and ZHOU, Y., 2019. Cleat structure analysis and permeability simulation of coal samples based on micro-computed tomography (micro-CT) and scan electron microscopy (SEM) technology. *Fuel*, 254, pp. 115579.
- RUHLAND, M. M., 1973. Méthode d'étude de la fracturation naturelle des roches associée à divers modèles structuraux [English translation: Study method of natural fracturing of rocks associated with various structural models]. *Sciences Géologiques, bulletins et mémoires [Geological Sciences, Bulletin]* 26 (No. 2-3), pp. 91-113.
- RUINA, A.L. and PRATAP, R., 2008. *Introduction to Statics and Dynamics*. Pre-print for Oxford University Press.

- RUSSELL, D.G. and PRATS, M., 1962. The Practical Aspects of Interlayer Crossflow. *Journal of Petroleum Technology*, 14(06), pp. 589-594.
- SAHIMI, M., 2011. *Flow and transport in porous media and fractured rock : from classical methods to modern approaches*. Second, revised and enlarged edition. ed. Weinheim: Wiley-VCH.
- SAIDI, A.M., 1987. *Reservoir Engineering of Fractured Reservoirs: Fundamental and Practical Aspects*. Total.
- SALMAGUND, P.I., 2017. *Fractures pattern*. [online] Available from: <https://photosalmagundi.wordpress.com/tag/fracture-patterns/page/2/> [Accessed 05/05 2017].
- SARKAR, S., TOKSÖZ, M. and BURNS, D., 2004. *Fluid Flow Modeling in Fractures*. (<http://hdl.handle.net/1721.1/68616>). Massachusetts Institute of Technology. Earth Resources Laboratory.
- SARKAR, S., TOKSÖZ, M. and BURNS, D., 2011. Fluid Flow Simulation in Fractured Reservoirs.
- SCHAFRIK, S. and MILLAR, D.L., 2015. Verification of a CFD code use for air flow simulations of fractured and broken rock. *Applied Thermal Engineering*, 90, pp. 1131-1143.
- SCHEIDEGGER, A.E., 1963. *The Physics of Flow Through Porous Media*. University of Toronto Press.
- SCHRAUF, T.W. and EVANS, D.D., 1986. Laboratory Studies of Gas Flow Through a Single Natural Fracture. *Water Resources Research*, 22(7), pp. 1038-1050.
- SEN, Z., 1995. *Applied Hydrogeology for Scientists and Engineers*. First ed. Boca Raton , Florida: CRC Press, Inc.
- SIMMONS, C.T., 2008. Henry Darcy (1803–1858): Immortalised by his scientific legacy. *Hydrogeology Journal*, 16(6), pp. 1023-1028.
- SINGH, K., SINGH, D. and PATHEGAMA, R., 2014. Laboratory Simulation of Flow through Single Fractured Granite. *Rock Mechanics and Rock Engineering*, 48.
- SNOW, D.T., 1969. Anisotropic Permeability of Fractured Media. *Water Resources Research*, 5(6), pp. 1273-1289.

- SOBIESKI, W. and TRYKOZKO, A., 2014. Darcy's and Forchheimer's laws in practice. Part 1. The experiment. *Technical Sciences / University of Warmia and Mazury in Olsztyn*, nr 17(4), pp. 321-335.
- SOBIESKI, W. and TRYKOZKO, A., 2011. Sensitivity Aspects of Forchheimer's Approximation. *Transport in Porous Media - TRANS POROUS MEDIA*, 89, pp. 155-164.
- SPENCE, G.H. et al., 2014. *Advances in the Study of Fractured Reservoirs*. Geological Society.
- STAUFFER, D. AND AHARONY, A., 1992. *Introduction to Percolation Theory*. London: Taylor and Francis.
- SU, X. et al., 2019. Experimental and Numerical Modelling of Nonlinear Flow Behavior in Single Fractured Granite. *Geofluids*, 2019, 8623035.
- SURI, Y. et al., 2020. Numerical fluid flow modelling in multiple fractured porous reservoirs. *Fluid Dynamics and Materials Processing*, 16(2), pp. 245-266.
- SWANSON, W.M., 1970. *Fluid Mechanics*. Holt, Rinehart, and Winston.
- TAKHANOV, D., 2011. *Forchheimer Model for Non-Darcy Flow in Porous Media and Fractures*. [online] MSc thesis, Imperial College London. Available from: <https://spiral.imperial.ac.uk/bitstream/10044/1/24389/2/Takhanov-D-2011-Pet-Eng-MSc-thesis.pdf> [Accessed 20/09/2020].
- TIAB, D. and DONALDSON, E.C., 2004. *Petrophysics : Theory and Practice of Measuring Reservoir Rock and Fluid Transport Properties*. Second edition ed. Burlington - USA: Elsevier Science.
- TSANG, Y.W., 1984. The Effect of Tortuosity on Fluid Flow Through a Single Fracture. *Water Resources Research*, 20(No. 9), pp. 1209-1215.
- TSANG, Y.W.T., C.F., 1987. Channel model of flow through fractured media. *Water Resources Research*, 23(3), pp. 467-479.
- TSE, R. and CRUDEN, D.M., 1979. Estimating joint roughness coefficients. *International Journal of Rock Mechanics and Mining Sciences & Geomechanics Abstracts*, 16(5), pp. 303-307.

- VAN GENUCHTEN, M.T., 1980. A Closed-Form Equation for Predicting the Hydraulic Conductivity of Unsaturated Soils. *Soil Science of America Journal*, 44, pp. 892-898.
- VERSTEEG, H.K.M., W., 1995. *An Introduction to Computational Fluid Dynamics*. First Edition ed. New York: Longman Group Ltd.
- VERSTEEG, H.K. and MALALASEKERA, W., 2007. *An Introduction to Computational Fluid Dynamics: The Finite Volume Method*. Pearson Education Limited.
- WANG, C. et al., 2020. A New Method for Pore Structure Quantification and Pore Network Extraction from SEM Images. *Energy Fuels*, 34(1), pp. 82-94.
- WARREN, J.E. and PRICE, H.S., 1961. Flow in Heterogeneous Porous Media. *Society of Petroleum Engineers Journal*, 1(03), pp. 153-169.
- WARREN, J.E. and ROOT, P.J., 1963. The Behavior of Naturally Fractured Reservoirs. (SPE 426-PA).
- WHITE, F.M., 2003. *Fluid Mechanics*. Fifth Edition ed. New York: McGraw-Hill.
- WHITE, F.M., 2011. *Fluid Mechanics*. New York: McGraw-Hill.
- WINTERTON, R.H.S., 2014. *Thermal Design of Nuclear Reactors*. Elsevier Science.
- WITHERSPOON, P.A. et al., 1980. Validity of Cubic Law for fluid flow in a deformable rock fracture. *Water Resources Research*, 16(6), pp. 1016-1024.
- WU, H. et al., 2019. Imaged based fractal characterization of micro-fracture structure in coal. *Fuel*, 239, pp. 53-62.
- WU, Y. and PRUESS, K., 2000. Numerical simulation of non-isothermal multiphase tracer transport in heterogeneous fractured porous media. *Advances in Water Resources*, 23(7), pp. 699-723.
- YAMATOMI, J. et al., 2001. *Modeling and analysis of fluid flows through a rock fracture with wall roughness*. Washington, D.C.: American Rock Mechanics Association.
- YANG, S. et al., 2019. A new fracture permeability model of CBM reservoir with high-dip angle in the southern Junggar Basin, NW China. *Energy Exploration & Exploitation*, 37(1), pp. 125-143.

- YI, J. and XING, H., 2018. Finite element lattice Boltzmann method for fluid flow through complex fractured media with permeable matrix. *Advances in Water Resources*, 119, pp. 28-40.
- ZABALETA, A.D.J.G., 2007. *Computational Fluid Dynamics Studies in Heat and Mass Transfer Phenomena in Packed Bed Extraction and Reaction Equipment: Special Attention to Supercritical Fluids Technology*. [online] Ph.D. thesis thesis, Universitat Politècnica de Catalunya. Available from: <https://upcommons.upc.edu/handle/2117/93766?locale-attribute=en> .
- ZHANG, Z. and NEMCIK, J., 2013. Friction Factor of Water Flow Through Rough Rock Fractures. *Rock Mechanics and Rock Engineering*, 46(5), pp. 1125-1134.
- ZHONG, W. et al., 2018. Determination of Permeability and Inertial Coefficients of Sintered Metal Porous Media Using an Isothermal Chamber. *Applied Sciences*, 8, p. 1670.
- ZHOU, J. et al., 2016. The Friction Factor in the Forchheimer Equation for Rock Fractures. *Rock Mechanics and Rock Engineering*, 49.
- ZHU, X. et al., 2020. A Complex Network Model for Analysis of Fractured Rock Permeability. *Advances in Civil Engineering*, 2020, 8824082.
- ZIMMERMAN, R.W. and BODVARSSON, G.S., 1996. Hydraulic conductivity of rock fractures. *Transport in Porous Media*, 23(1), pp. 1-30.
- ZIMMERMAN, R.W. and YEO, I., 2000. Fluid Flow in Rock Fractures: From the Navier-Stokes Equations to the Cubic Law. In: B FAYBISHENKO, P.A. WITHERSPOON and S BENSON, eds. *Dynamics of Fluids in Fractured Rock*, Vol 122. Washington: American Geophysical Union.
- ZOU, L., JING, L. and CVETKOVIC, V., 2017. Modeling of flow and mixing in 3D rough-walled rock fracture intersections. *Advances in Water Resources*, 107, pp. 1-9.

9 Appendix 1 – Recreating Rough Fracture From A Fracture Image

To create a geometry that had the same properties of the previous models, such as standard deviation, fracture aperture frequency and aperture normal distribution, was a challenging step. It required the same (X, Y) Cartesian coordinates that previous models had used at each point on the fracture, to be used in the DesignModeler of the ANSYS-Fluent; however, these were not available for this research. Therefore, to overcome this challenge, a different approach was considered in this research to get (X, Y) Cartesian coordinates of the previous fracture geometry, detailed as follows. In the beginning, one of the fracture images was chosen from the [Nazridoust, Ahmadi and Smith \(2006\)](#) paper, which was the same in [Crandall Ahmadi and Smith \(2010\)](#)'s paper; this fracture is fracture (d) in [Nazridoust, Ahmadi and Smith \(2006\)](#)'s paper figure 2 p 318.

To get a high resolution of the image, the image was zoomed and divided into three separate equal lengths by Paint software, to enable getting very accurate coordinates and resolution. Then the image was saved as a JPEG file type, and applied into image digitizer online software. The challenges of this method were as follows. Due to the zooming effect and transferral of the images through different software (Pdf into Paint software then into the online image digitizer software), this affected the image pixels, and it was difficult to get sharp and clear lines of the fracture surfaces. In addition, the shadow lines beside the fracture surfaces were visible as a result. [Figure 9.1](#) highlights the shadow lines on one of the zoomed images. Finally, the image dimensions were not to scale in the [Nazridoust, Ahmadi and Smith \(2006\)](#) paper and had been cropped to fit the paper size.

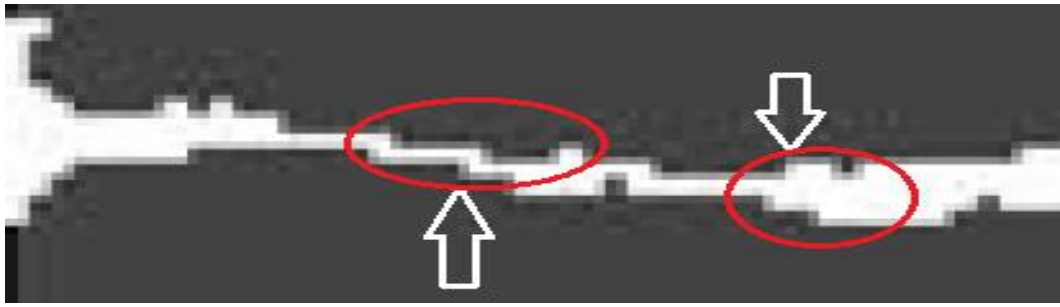


Figure 9.1 Shadow lines parallel to the fracture surface

Therefore, to overcome these difficulties, some modifications were considered in the method. Firstly, as the X-direction length of the fracture from the given data was known, 10.15cm, therefore, the log-in data in the image digitizer would be a more efficient method to get accurate coordinates of X-direction. Secondly, the Y-direction of the image dimension was not clear because it was a cropped section; therefore, it was not clear how to determine the log-in data of Y-direction inside the image digitizer online software! To tackle this issue, an approximation method was considered, which involved applying the X-length scale into Y-scale of the image (because the X-length was known), then examining the results coordinates. However, the results were totally wrong coordinates of Y-direction, and the fracture surfaces crossed and intersected each other between the top and the bottom fracture surfaces. To solve this challenge, another approach was applied which was comparison of the given data in the paper and the image digitizing to get the best outcome, then re-adjusting the coordinates manually by EXCEL software. Following this, the outcomes of Y-coordinates were accurate and gave an accurate result. This method was therefore adopted here, and the sequence of these steps is summarised below for more clarity:

First step: the fracture was divided into three equal parts as mentioned above; the total fracture length was 10.15cm and a third of the fracture length was 3.383cm. The images below ([Figure 9.2](#)) illustrate the divided sections of the fracture. For the Y-coordinates, a scale was calculated manually of the image by relying on the smallest fracture apertures height as given by the paper, which was 240 micrometre.

Second step: each of the sections was uploaded separately in the image digitizer online software, and given the length in both coordinates X and Y; then, the desired points were chosen. For this stage it was very important to click on the corner of each fracture with complete precision, which was very time consuming, in order to get coordinates as accurate as possible of the points for the top and bottom

fracture's walls. Then the coordinates X and Y could be downloaded as an EXCEL file.

Third step: the points that were observed from the image digitizer software were then drawn in an EXCEL file, to check the profile of the fracture; [Figure 9.3](#) below illustrates the fracture. As can be seen in the generated fracture profile, the profile was very poor, due to the reasons mentioned above which affected image pixels, and therefore affected the image's clarity.

Fourth step: the information from the EXCEL file of coordinates, from the image digitizer, was combined with the given data in the papers of [Nazridoust, Ahmadi and Smith \(2006\)](#); and [Crandall, Ahmadi and Smith \(2010\)](#).

[Nazridoust, Ahmadi and Smith \(2006\) p. 317](#) stated that "in the sections shown of fractures, which were selected for flow analysis, the minimum aperture is 240 μm ", and [Crandall, Ahmadi and Smith \(2010\)](#) clarified the fracture in geometry by stating:

The aperture height varied by increments of 240 μm within the fracture profiles. The frequency distributions of these fracture apertures from 240 to 1, 680 μm . As can be seen, these profiles are completely Open (no zero apertures) ([Crandall Ahmadi and Smith 2010 p. 497](#)).

Thus, based on the given data in these two papers, all the (X, Y) coordinates that were generated by the image digitizer software were modified manually in order to get the minimum apertures with 240 microns; every increment made 240 microns for the apertures and in X-direction lengths of each segment. This method considered the approximate values that were close to matching the increments of 240 micrometre; for instance, if the length between two points was 700 micrometre, then it was approximated into 720 micrometre, which is 3 times of 240- micrometre increments. [Table 9.1](#) below clarifies part of this method.

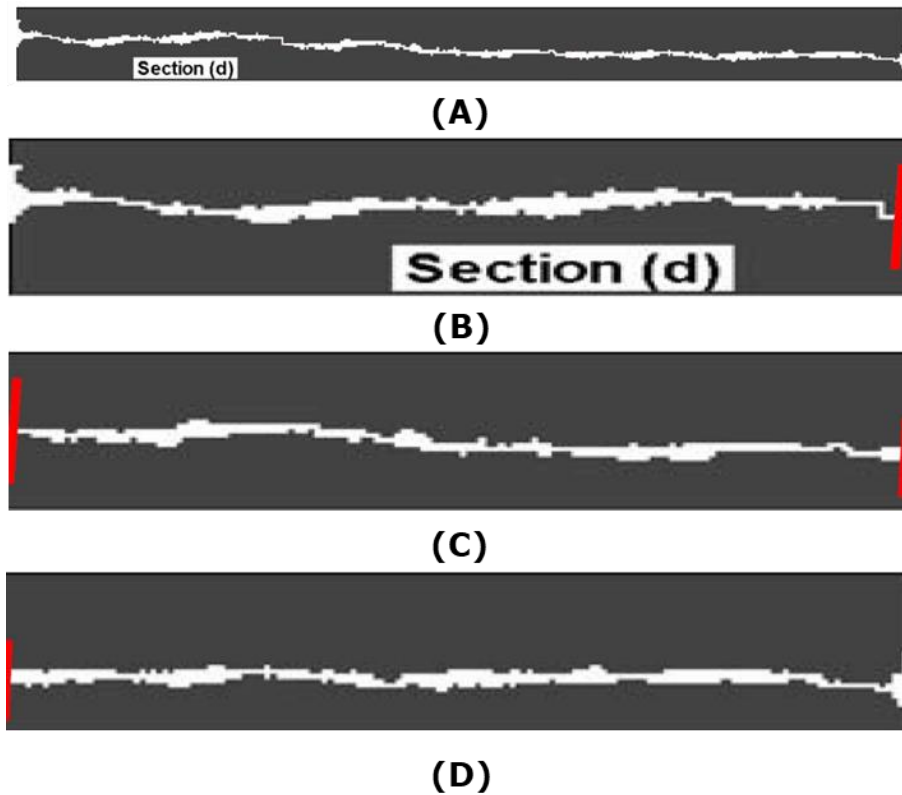


Figure 9.2 Rough fracture geometry, original and divided into three sections
 A. Rough fracture (d) from [Nazridoust, Ahmadi and Smith \(2006\)](#)'s paper, [figure 2 p318 \(permission for academic reuse from Elsevier Number: 4755041107899\)](#).
 B. C. and D.: First, second and third sections respectively of full fracture

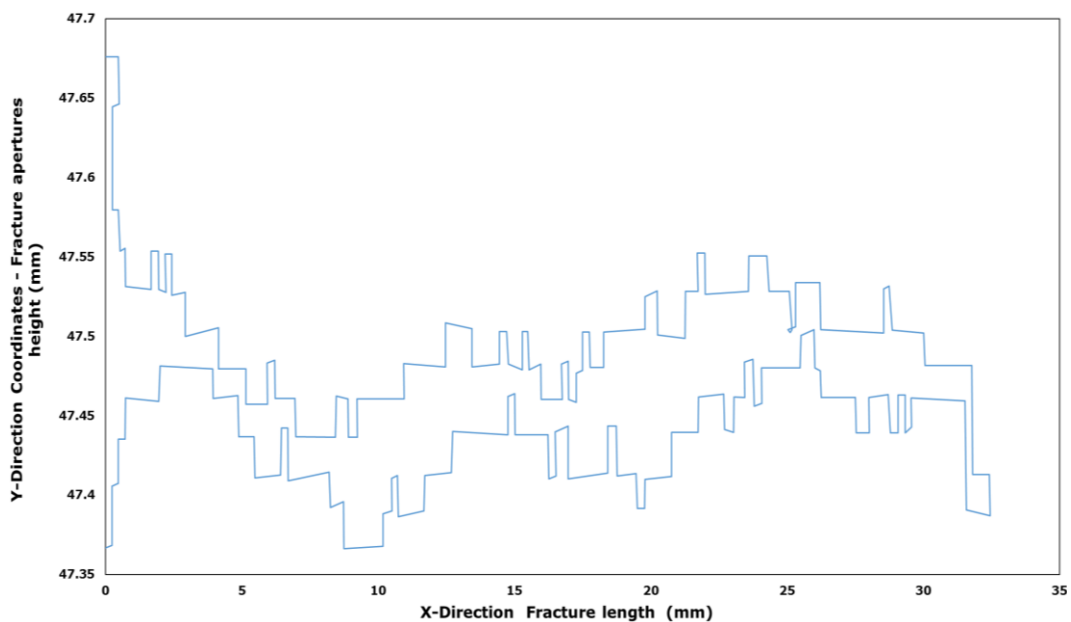


Figure 9.3 Fracture profile that was created from the image digitizer coordinates

Table 9.1 Section of the manually amended image digitizer (X, Y) coordinates table by EXCEL

X-Value (Initial)	X1-X2	X-Value (Modified)	Y-Value (Initial)	Y1-Y2 (Initial)	Y-Value (Modified) 240 micron increments	Y1-Y2 (Modified)
8.99	0	0	1750	0	1750	0
234	225.01	240	1750	0	1750	0
247	13	240	1950	200	2230	480
459	212	480	1950	0	2230	0
472	13	480	2060	110	2470	240
683	211	720	2070	10	2470	0
696	13	720	2170	100	2710	240
1870	1174	1920	2180	10	2710	0
1870	0	1920	2270	90	2950	240
3740	1870	3840	2280	10	2950	0
3750	10	3840	2170	-110	2710	-240
4680	930	4800	2170	0	2710	0
4680	0	4800	2060	-110	2470	-240
5230	550	5280	2050	-10	2470	0
5230	0	5280	1940	-110	2230	-240
6170	940	6240	1950	10	2230	0
6170	0	6240	2070	120	2470	240
6380	210	6480	2070	0	2470	0
6410	30	6480	1950	-120	2230	-240
7800	1390	7920	1950	0	2230	0
7800	0	7920	1830	-120	1990	-240
8270	470	8400	1830	0	1990	0
8260	-10	8400	1730	-100	1750	-240
9780	1520	9840	1740	10	1750	0
9780	0	9840	1840	100	1990	240
10000	220	10080	1840	0	1990	0
10000	0	10080	1960	120	2230	240
10200	200	10320	1960	0	2230	0
10200	0	10320	1830	-130	1990	-240
11200	1000	11280	1840	10	1990	0
11200	0	11280	1960	120	2230	240
12100	900	12240	1950	-10	2230	0
12100	0	12240	2060	110	2470	240
14100	2000	14160	2060	0	2470	0
14100	0	14160	2170	110	2710	240

After modifying the data, a new fracture was drawn by EXCEL to check the new profile. The new modified fracture profile had a good match with the profile of fracture that was used in [Nazridoust, Ahmadi and Smith \(2006\)](#); and [Crandall Ahmadi and Smith \(2010\)](#). Similar processes were applied for the second and third section. The images below ([Figures 9.4 and 9.5](#)) illustrate the modified fracture profile of the first section and the entire fracture.

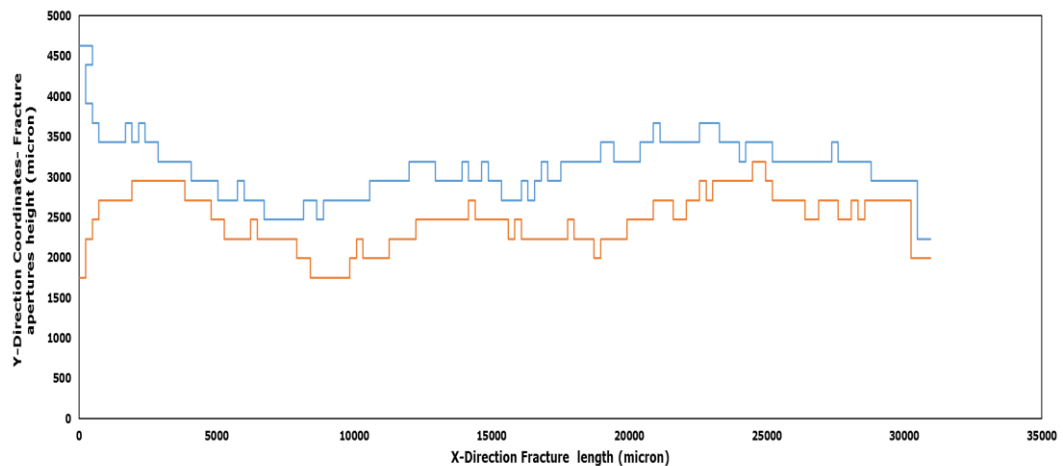


Figure 9.4 The amended fracture's profile of the first section

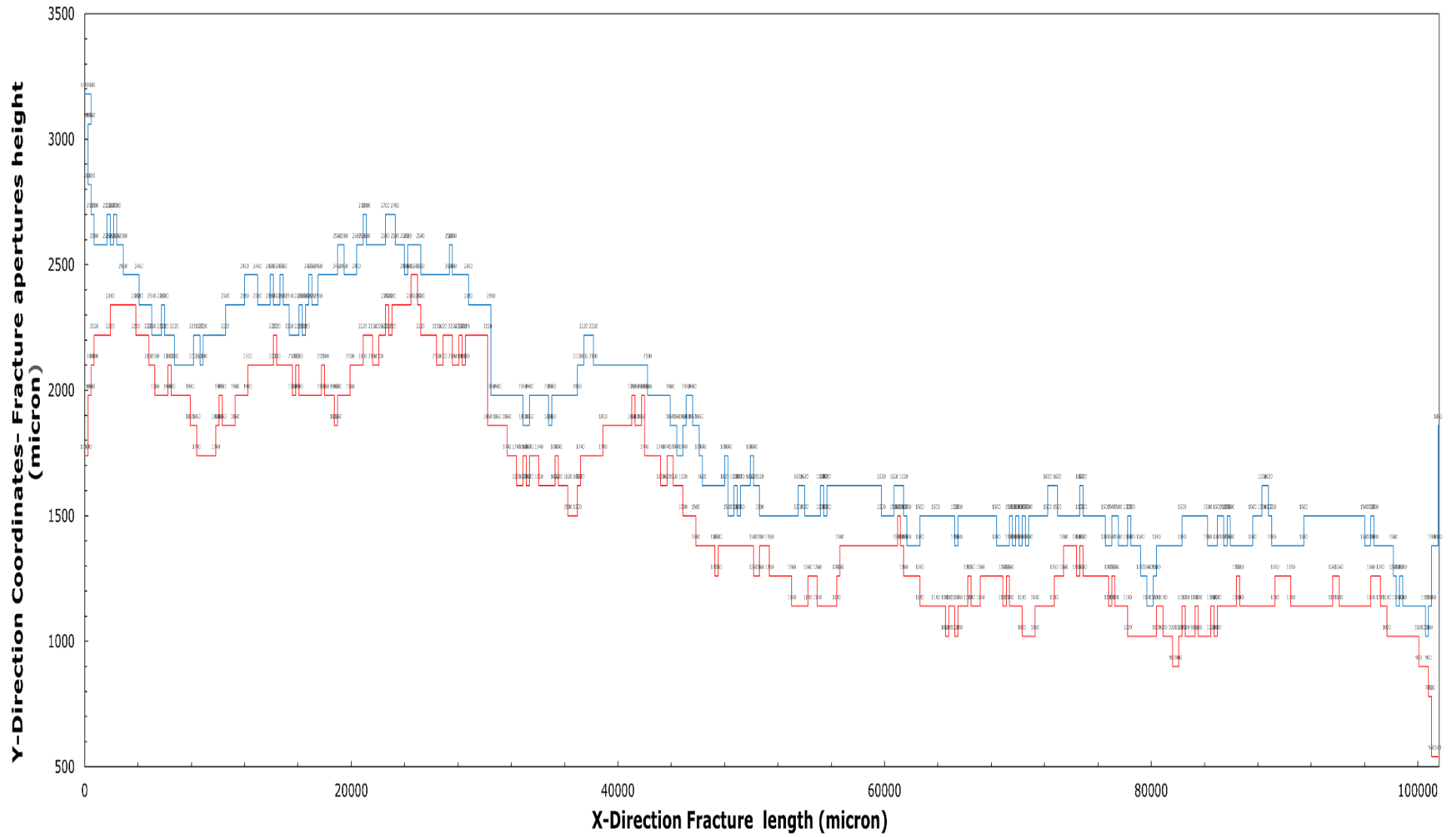


Figure 9.5 The amended fracture's profile of the entire fracture profile

9.1 Rough Fracture Geometry Validation

After creating the fracture profile, it was vital to check that the new fracture geometry matched with the geometry used in [Nazridoust, Ahmadi and Smith \(2006\)](#); and [Crandall et al. \(2010\)](#)'s models. This was in order to get accurate results of simulations, which would enable this research to validate its results against their models. Thus, there were some steps which were considered in order to validate the new fracture profile and properties, to be sure they were accurate and matching, so that the new fracture geometry had the same fracture properties that were used in the previous models of these two papers. These steps are clarified below:

First step: simply, the profile matching along the fracture was checked by comparing the new fracture's profile with [Nazridoust, Ahmadi and Smith \(2006\)](#)'s fracture's profile, to ensure both fracture profiles matched with the length of each segment and the apertures' heights. The result was that both fractures had the same profile. [Figure 9.6](#) below illustrates the case of matching top fracture surfaces in all sections.

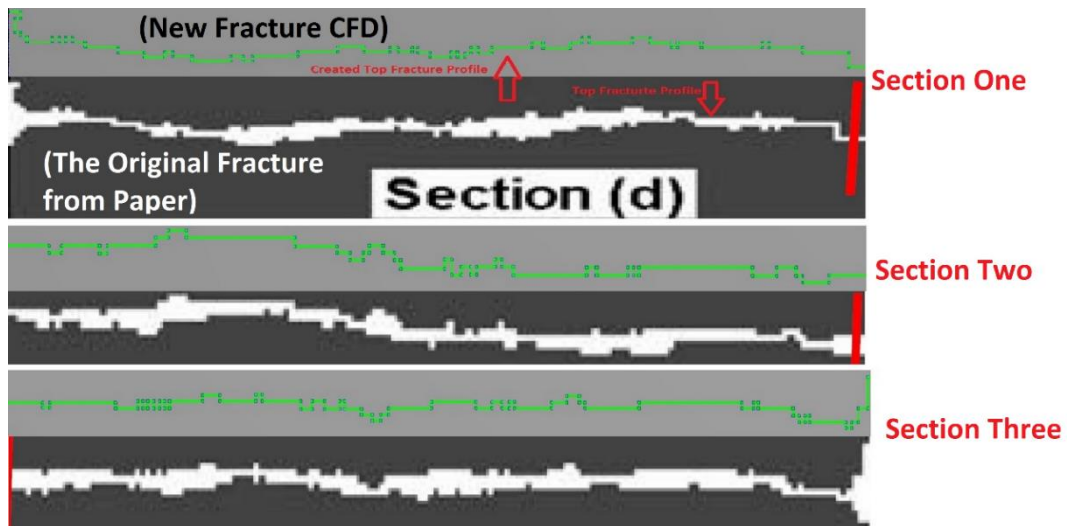


Figure 9.6 Matching the new fracture profile with [Nazridoust, Ahmadi and Smith \(2006\)](#)'s fracture's profile

Second step: the properties of the new fracture were checked with the properties of the [Nazridoust, Ahmadi and Smith \(2006\)](#) fracture, to authenticate the similarity of both fractures. The properties that were considered were similar to the properties which were in the papers of [Nazridoust, Ahmadi and Smith \(2006\)](#); and [Crandall et al. \(2010\)](#), called "the statistical features of fracture aperture". These

properties were: fracture aperture frequency, standard deviation and normal distribution, and tortuosity. Each one of these properties had a different method for observation in the result, and are clarified below.

Fracture aperture frequency: this was to calculate the percentage of fracture aperture frequency and compare it with Nazridoust, Ahmadi and Smith (2006)'s fracture's frequency. The method was firstly to calculate the section numbers along the fracture and classify the data under aperture height groups, which were (240, 480, 720, 960, 1200, 1440) micron. The next step was to calculate the total number of sections, and finally to divide each group by the total number of sections to get the frequency of each fractures' group. The total number of sections in this fracture that was considered was 185 sections. As well, the same method was applied to calculate the frequency of fracture (D) from Nazridoust, Ahmadi and Smith (2006)'s paper; Tables 9.2 and 9.3 and Figure 9.7 below clarify the method. The result of this comparison was that the new fracture profile had a good agreement with Nazridoust, Ahmadi and Smith (2006)'s fracture.

Table 9.2 Calculations of fracture aperture height frequency of Nazridoust, Ahmadi and Smith (2006)'s fracture – section D

Fracture Height (micron)	Frequency (Number of Sections)	% Frequency
240	80	19
480	149	35
720	128	31
960	58	13
1200	2	0.5
1440	0	0
	416	
	(Total Sections)	

Table 9.3 Comparison of fracture aperture height frequency of this research's fracture with Nazridoust, Ahmadi and Smith (2006)'s fracture

Fracture Height (micron)	Frequency (number of sections in my fracture)	(Frequency/ Total sections) my fracture	% Frequency (my fracture)	% Frequency (Nazridoust's fracture)
240	35	0.189	18.9	19
480	64	0.346	34.6	35
720	60	0.324	32.4	31
960	25	0.135	13.5	13
1200	1	0.005	0.5	0.5
1440	0	0.000	0.0	0
	185			
	(Total Sections)			

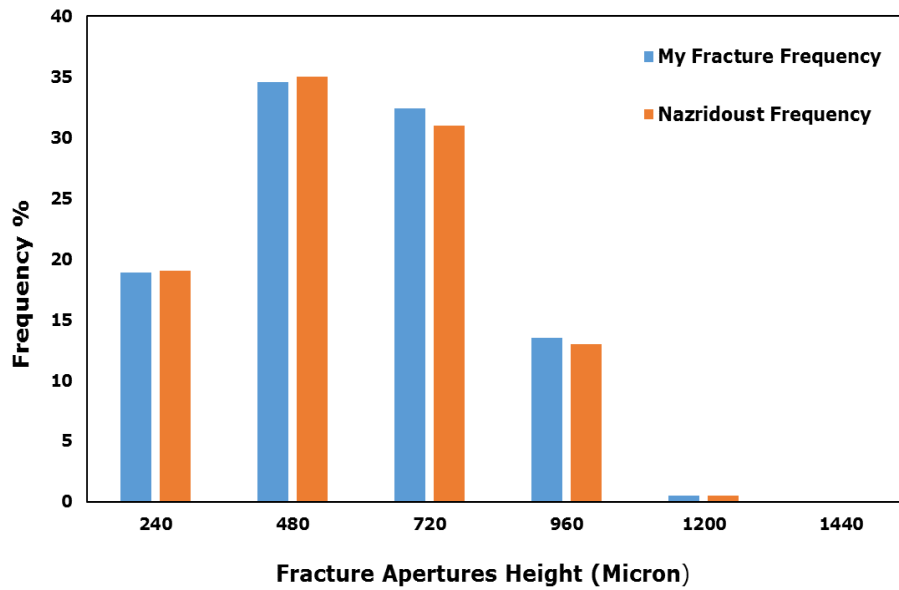


Figure 9.7 Comparisons of this research's fracture aperture height frequency with Nazridoust, Ahmadi and Smith (2006)'s fracture

Standard Deviation (σ): this is a measure that was used to quantify the amount of variation of data values. This value can indicate whether data is close to or far from the mean value of data (μ). Low standard deviation value indicates that a set of data are close to mean value, while a high value indicates that the data set is distributed over a wide range from the mean value. Thus, it's been widely used in matching fracture aperture data, and is considered one of the factors that helps to recognise the similarity among fractures' profiles. Standard deviation can be calculated as equation 9.1.

$$\sigma = \sqrt{\frac{1}{N} \sum_{i=1}^N (X_i - \mu)^2} \quad (9.1)$$

To compare this fracture's geometry and Nazridoust, Ahmadi and Smith (2006)'s fracture, it was mandatory to calculate both values and draw the standard deviation values, then calculate the normal distribution curves of these two fractures and observe the bell shape of both fractures' curves. In this research's fracture, 185 sections were considered. Tables 9.4 and 9.5, and figure 9.8 below illustrate the case. In figure 9.8 it can be seen from the bell shape that the standard deviation of both fractures had a small deviation. The reason that both curves did not match fully was due to the number of sections that were considered in each calculation, as Nazridoust, Ahmadi and Smith (2006) considered around 416 sections along the fracture.

Table 9.4 Standard deviation calculations of this research's fracture

Fracture Height (Xi)	Frequency (N) (Number of Sections)	Sum of Fracture Apertures Heights to get Average Aperture	Average Aperture (μ) (micron)	(Xi- μ) ²	[(Xi- μ) ² *Frequency]	The standard deviation
240	35	8400	581.1891892	116410.0628	4074352.199	$\sigma = \sqrt{\frac{1}{N} \sum_{i=1}^N (X_i - \mu)^2}$
480	64	30720	581.1891892	10239.25201	655312.1286	
720	60	43200	581.1891892	19268.4412	1156106.472	
960	25	24000	581.1891892	143497.6304	3587440.76	
1200	1	1200	581.1891892	382926.8196	382926.8196	
1440	0	0	581.1891892	737556.0088	0	
	185	107520			9856138.378	230.817
	(Total Sections)					

Table 9.5 Normal distribution calculation of this research's fracture and Nazridoust, Ahmadi and Smith (2006)'s fracture

μ	Normal distribution of my Fracture	Normal distribution of Nazridoust's Fracture
-2	6.60285E-17	1.0385E-10
-1.5	1.00749E-09	2.7725E-06
-1	0.000136245	0.004023772
-0.5	0.163292612	0.317460849
0	1.734531654	1.361577749
0.5	0.163292612	0.317460849
1	0.000136245	0.004023772
1.5	1.00749E-09	2.7725E-06
2	6.60285E-17	1.0385E-10

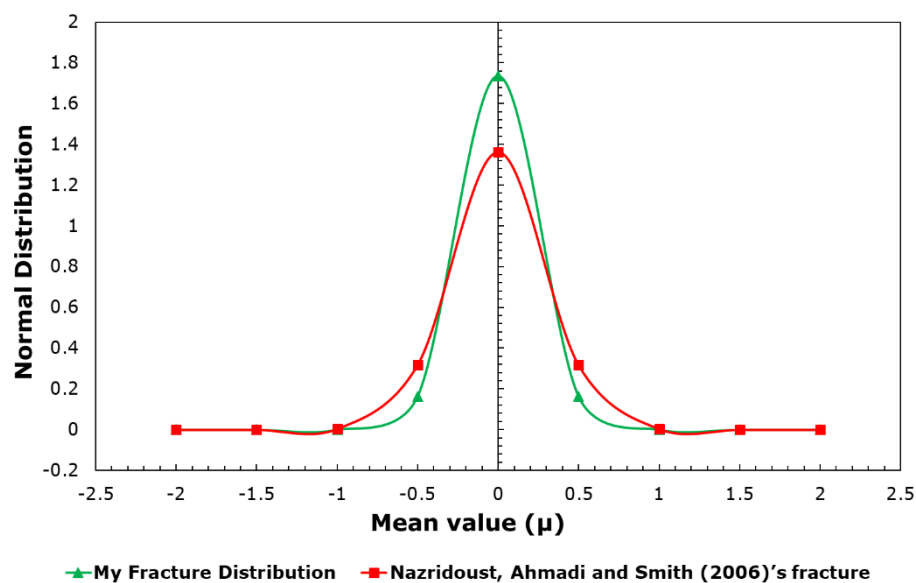


Figure 9.8 Normal distribution of this research's fracture compared with Nazridoust, Ahmadi and Smith (2006)'s fracture

Tortuosity: this value represents the actual distance fluid flow travels through a fracture in comparison with a fracture's length. To calculate fluid travel inside fractures with varied fracture segments and heights was somewhat challenging. Therefore, an estimate method was considered which could be applied by unfolding lengths of a fracture's segments, and considering it as the length of the fracture's surface. The average values of both top and bottom surfaces of the fracture were considered as the fluid's travel distance inside the fracture (L_e). The [equation 9.2](#) and [Table 9.6](#) below illustrate the calculations. The result of my fracture tortuosity was that it does match exactly with [Nazridoust, Ahmadi and Smith \(2006\)](#)'s fracture tortuosity value.

$$\theta = \frac{L_e}{L} - 1 \quad (9.2)$$

Where: L_e = fluid travel (equal to the average value of fracture surfaces length),
 L = fracture domain length

Table 9.6 Calculation of tortuosity value of this research's fracture geometry

Top Fracture wall	0.13368 m
Bottom Fracture wall	0.13189 m
$L_e = \left(\frac{0.13368 + 0.13189}{2} \right)$	0.132785
Entire Fracture domain length	0.10152 m
$\theta = \left(\frac{0.132785}{0.10152} \right) - 1$	$\theta = 0.308$ The same value of Nazridoust, Ahmadi and Smith (2006)'s fracture

To conclude, after checking the values of the statistical features of fracture apertures of my model fracture, all of them were well-matched with [Nazridoust, Ahmadi and Smith \(2006\)](#)'s fracture's statistical features. Thus, this fracture profile

was authenticated, and could be considered as a similar fracture to [Nazridoust, Ahmadi and Smith \(2006\)](#), and was therefore used in the models of this research.

10 Appendix 2 - Post-processing FLUENT Solver Of Fracture Networks

The meshed fracture network geometries with named boundaries were transferred into the FLUENT solver. At this stage, many processes needed to be completed, which were: assigning physics set-up of the model; choosing fluid type; assigning values of the boundary conditions (either pressure/velocity) base; selecting the simulation iterations residuals; and starting the simulations. Each step is clarified below. These conditions were created similar to the conditions of the models in Chapter 4 and this research, to enable us to compare these models' results with a single fracture with horizontal fracture orientations (flow parallel to the fracture).

10.1 Fluent set-up

Models:

The model conditions that were considered were Viscous Laminar-Single phase fluid model, because the targeted goals of this research focused on laminar flow in fractured porous media. This was due to the low Reynolds number of flow in fractured media that were reported in the literature of the majority of the cases.

Materials:

A single-phase fluid flow was modelled, and water was considered as the fluid flow in the fracture and the matrix. The properties of water that were used in the simulations of this research were loaded from the materials database of FLUENT, which were: density 998.2 kg/m³, viscosity 0.001003 kg/m.s and chemical formula H₂O.

Cell Zone Conditions:

The model was divided into two main geometry zones (fractures and matrix); each one had different conditions, but both zones' materials were water. The fracture

network zones were considered as an open space with liquid water. The matrix zones were considered a porous zone surrounding the open fracture, filled with water fluid material. A porous zone is a permeable medium; many properties had to be assigned here which were:

- The fluid direction of water fluid flow, which was in-plane X-direction of Cartesian axis.
- Matrix permeability of each direction of X and Y axis; this could be different for each flow direction in the case of (anisotropic permeability) or the same for X and Y directions in the case of (isotropic permeability), and the permeability unit was (m^2) instead of Darcy units.
- Matrix porosity was logged-in as fluid porosity, which was considered 20% in my models.

Boundary Conditions:

The conditions of the domain boundaries were set at this stage. The inlet was set to be "pressure inlet" instead of velocity inlet; this was to mimic the real conditions in subsurface layers of the earth's crust and to represent pressure as the main drive mechanism of fluids in fractured porous media. This interpreted the differential pressure force losses along the matrix, and as well, that flow was horizontal with the X-Cartesian axis. The domain outlet was set to be "pressure outlet" and kept with zero value, to allow pressure to build inside the domain between the inlet and outlet. The upper and lower boundaries of the matrix were set to be symmetrical, to mimic the conditions of matrix continuous outstretching in Y-direction of the Cartesian axis. The matrix and the fracture were set up as interior domains. The fracture surfaces were set up as "Interior face boundary". This was because the "Interiors" set-up allowed interaction between the fracture network domain and the matrix domain, which was the best option to investigate fracture network effects on the flow, due to the varied patterns of fracture networks in these models. [Figure 10.1](#) below clarifies these boundaries for some networks, and other networks were similar.

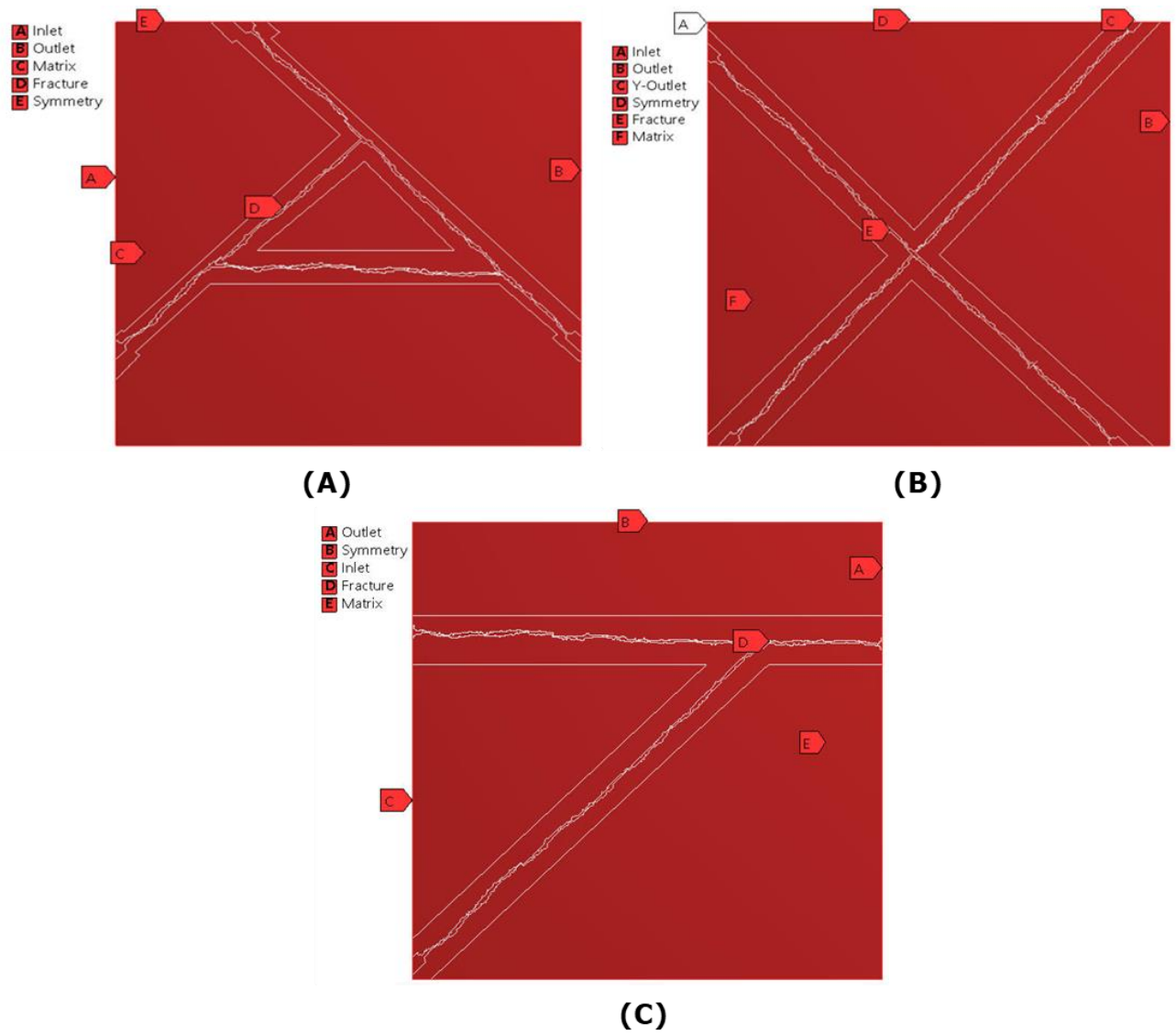


Figure 10.1 Examples of fracture network boundaries in some of the networks **A.** **B.** and **C.:** Fracture networks 1, 2, and 4, respectively.

10.1.1 Solution

Similar solution set ups as stated in parallel plates and rough fracture [chapter 3 section 3.5.1.3.](#)